NASA Contractor Report 3994

On the Modeling of Low-Reynolds-Number Turbulence

Ronald M. C. So and G. J. Yoo

GRANT NAG3-167
JULY 1986

NASA

NASA Contractor Report 3994

On the Modeling of Low-Reynolds-Number Turbulence

Ronald M. C. So and G. J. Yoo
Arizona State University
Tempe, Arizona

Prepared for
Lewis Research Center
under Grant NAG3-167

National Aeronautics
and Space Administration

Scientific and Technical Information Branch

1986

This Page Intentionally Left Blank

Table of Contents

This Page Intentionally Left Blank

Notation

English Letters

C_1, C_2, C_3, C_4, C_5	model constants, specified in Table 1.
C_{1w}, C_{2w}	model constants introduced by wall correction, specified in Table 1.
C_μ	model constant associated with ν_t, specified in Table 1.
C_s	model constant associated with diffusion model, specified in Table 1.
$C_{\epsilon 1}$, $C_{\epsilon 2}$	model constants associated with ϵ-equation, specified in Table 1.
D	pipe diameter
f_1, f_2, f_3	damping functions, specified in Table 1.
h_i	grid spacing
J = 0 or 1	index denoting two-dimensional or axisymmetric flows.
$k = \frac{1}{2}(\overline{u^2} + \overline{v^2} + \overline{w^2})$	turbulent kinetic energy
p	fluctuating pressure
r	radial coordinate
R	pipe radius
$Re = u_* R/\nu$	turbulent Reynolds number
$R_D = U_o D/\nu$	pipe Reynolds number
u	fluctuating velocity along x-direction
u_*	friction velocity
U	mean velocity along x-direction
U_o	mean velocity at pipe center
v	fluctuating velocity along r-direction
w	fluctuating velocity along θ-direction
W	mean velocity along θ-direction
x	axial coordinate
$Y^+ = (R-r)u_*/\nu$	normalized r-coordinate

Greek Letters

$\alpha = 1/\kappa$	log-law slope
β	constant in law-of-the-wall
α_1, β_1, γ_1	model constants associated with redistribution model, specified in Table 1.
ϵ	dissipation rate of k
θ	circumferential coordinate
κ	von Karman constant
ν	fluid kinematic viscosity
ν_t	turbulent diffusivity
ρ	fluid density
σ_ϵ	model constant associated with ϵ-equation, specified in Table 1.
ψ_i	normalized dependent variables
Ω	angular velocity

Abstract

A full Reynolds-stress closure that is capable of describing the flow all the way to the wall has been formulated for turbulent flow through circular pipes. Since viscosity does not appear explicitly in the pressure redistribution terms, conventional high-Reynolds-number models for these terms are found to be applicable. However, the models for turbulent diffusion and viscous dissipation have to be modified to account for viscous diffusion near a wall. Thus modified, viscous dissipation in the flow is no longer isotropic as postulated by Kolmogorov for high-Reynolds-number turbulence. Two redistribution and two diffusion models are investigated for their effects on the model calculations. Wall correction to pressure redistribution modelling is also examined. Diffusion effects on calculated turbulent properties are further investigated by simplifying the transport equations to algebraic equations for the Reynolds stresses. Two approximations are explored. These are the equilibrium and non-equilibrium turbulence assumptions. Finally, the two-equation closure is also used to calculate the flow in question and the results compared with all the other model calculations.

Fully-developed pipe flows at two moderate Reynolds numbers are used to validate these model calculations. They are chosen because detailed turbulence measurements near the wall are available. The calculations show that all closure models give good agreement with measurements of mean velocity, shear stress, turbulent kinetic energy and dissipation rate near a wall.

However, the slope of the logarithmic law-of-the-wall recovered from these calculations varies from one closure model to another. Some closure model predicts the correct behavior of the log-law constant as a function of Reynolds number, while others provide the wrong trend. Wall correction is found to have little effect on the model calculations. Mean-strain effects on redistribution modelling are found to give rise to an adverse influence on the calculated log-law, in the case of non-equilibrium algebraic stress closure. All closure models examined fail to predict the steep rise of turbulence intensities near a wall correctly. Also, they fail to reproduce the isotropic behaviour of the normal stresses at the pipe center. Overall, the best model prediction is given by the full Reynolds-stress closure incorporating a non-isotropic gradient diffusion model and the Launder et al. (1975) model for pressure redistribution.

1. Introduction

1.1 Motivation

The flow inside a practical combustor, such as gas turbine or solid fuel ramjet combustor, is usually very complicated, especially at the combustor wall. Besides geometry effects, cooling and dilution air through the combustor wall, fuel sublimation from the solid fuel grain and rotation of the combustor further complicate the wall boundary-layer flow. Conventional modelling of combustor flow is to assume high-Reynolds number turbulence, since the flow Reynolds number is normally very high inside the combustor. The wall boundary conditions are satisfied indirectly by specifying some empirical functions, such as the logarithmic law-of-the-wall for mean velocity and equilibrium turbulence for the turbulence field, to link the conditions at the wall to the first calculation point away from the wall. Consequently, the effects of viscosity and conductivity near the combustor wall cannot be resolved correctly and hence their influence on the flow outside the near wall region cannot be assessed. Therefore, this presents a difficult problem for the calculation of flow inside practical combustor because the complicated boundary conditions render the simple law-of-the-wall and equilibrium turbulence assumptions near the wall invalid. It is clear that conventional high-Reynolds-number turbulent closure models need to be modified to account for viscosity and conductivity effects near a wall before they can be applied with confidence to calculate the flow inside practical combustors.

Some work along this direction has been carried out by previous researchers (e.g. Jones and Launder 1972b; Hanjalic and Launder 1976; Chien 1980). These studies will be reviewed in the next section and further improvements will be identified. Therefore, based on this review, the objectives of the present study are formulated in Section 1.3.

1.2 Brief Discussion of Previous Work

Reynolds-stress closure+ of turbulence applied to turbulent flow calculations was first examined by Hanjalic and Launder (1972). In their model, certain assumptions concerning the structure parameters, $\overline{u_i u_i}/k$, (i not summed), where u_i is the i^{th} component of the fluctuating velocity and $2k = \overline{u_i u_i}$ (summation over i) is the turbulent kinetic energy, were invoked to simplify the four Reynolds-stress transport equations for two-dimensional thin shear layers to two equations for turbulent shear stress and k. These were then solved with the mean flow equations and an equation governing the transport of ϵ, the dissipation rate of k. The closure was arrived at by assuming the flow Reynolds number to be very large and that $\overline{u_i u_i}/k$ = constant throughout the shear layer with the constants given by plane shear flow measurements. In view of these approximations, the boundary conditions cannot be applied at the wall. Rather, they were applied near the wall. In particular, the mean flow velocity was matched to the logarithmic law-of-the-wall, the gradient of k was set equal to

+ The term "Reynolds-stress closure" is used to denote closure schemes that solves the full set of Reynolds-stress transport equations as well as models that solve the Reynolds shear stress and k equations alone (e.g. Hanjalic and Launder 1972, 1976).

zero, the shear stress was determined from the mean momentum equation with the convection terms neglected and ϵ was set equal to the turbulence generation rate. The model gave good comparison with measurements away from the wall for a wide variety of thin shear layers. However, detailed flow modelling near a wall remained unattainable, just as in the case of the mixing-length model where the same equilibrium turbulence arguments were used to determine the behaviour of the mixing length near a wall.

In view of the initial success of the Reynolds-stress closure model, later researchers (e.g. Launder et al. 1972; Mellor and Herring 1973; Mellor and Yamada 1974; Irwin and Smith 1975; Launder et al. 1976; Gibson and Rodi 1981) relaxed the assumption, $\overline{u_i u_i}/k$ = constant throughout the shear layer, and solved the full set of Reynolds-stress transport equations. However, the large-Reynolds-number assumptions were retained in the modelling of the turbulent diffusion, redistribution and energy dissipation rate terms in the Reynolds-stress transport equations. Consequently, the boundary-layer flow very near the wall had to be handled in the same manner as that proposed by Hanjalic and Launder (1972). The boundary conditions for $\overline{u_i u_i}$ near a wall, however, required special attention. In general, either a slip condition for $\overline{u_i u_i}$ was imposed (Irwin and Smith 1975) or the Neuman boundary conditions were specified (Mellor and Yamada 1974). The amount of slip specified for $\overline{u_i u_i}$ depended to a great extent on the type of flow considered. As a result, the closure model was problem dependent and, in spite of the

improvement, it still could not provide an accurate description of the flow very near the wall. This, in turn, means that the Reynolds-stress closure cannot be used to estimate the Reynolds number effects on turbulent flows, because in the immediate vicinity of a wall viscous effects have to be important (Mellor and Herring 1973).

The logarithmic law-of-the-wall assumption was generally applicable for a wide class of simple turbulent flows. However, it failed to provide a reasonably accurate estimate of the near wall mean velocity in separating flows, in relaminarizing flows and in complex turbulent flows (e.g. Stratford 1959; Jones and Launder 1972a; Bissonnette and Mellor 1974). In order to remedy this unsatisfactory boundary condition, Jones and Launder (1972b) proposed to modify the two-equation model of turbulence, i.e. the $k-\epsilon$ model, for Reynolds-number effects. The shear stress, $-\overline{u_1 u_2}$, was then calculated by assuming $-\overline{u_1 u_2} = \nu_t (\partial U_1/\partial x_2)$, where $\nu_t = C_\mu k^2/\epsilon$, U_1 was the local mean flow and x_2 was the coordinate normal to the wall. With suitable modification to ϵ near a wall to account for viscosity effects, they found that the modified $k-\epsilon$ equations can be integrated with the boundary conditions, $U_1 = 0$, $k=0$ and $\epsilon=0$, applied at the wall. This allowed the near wall flow to be calculated directly from the governing equations, and good agreement with relaminarizing flow measurements (Jones and Launder 1972a) was obtained. Furthermore, the logarithmic behaviour of the near wall flow was recovered when the flow Reynolds number was sufficiently large. Later, Hanjalic and Launder (1976) applied the arguments of Jones

and Launder (1972b) to modify their (Hanjalic and Launder 1972) Reynolds-stress closure model to account for viscosity effects near a wall. In their new closure model, they relaxed the assumption $\overline{u_i u_i}/k$ = constant. Instead, they assumed $(3/4)(\overline{u_1^2} + \overline{u_2^2}) = k$ and $\overline{u_2^2} \simeq 4(\overline{u_1 u_2})^2/k$ based on the pipe and channel flow measurements of Laufer (1954) and Eckelman (1970). This way, the near wall behaviour of $\overline{u_2^2}/k$, i.e. $\overline{u_2^2}/k \to 0$ as $x_2 \to 0$, was satisfied. Their calculated mean velocity and shear stress results were in excellent agreement with the channel flow measurements of Patel and Head (1968) and Eckelman (1970) and the relaminarizing flow data of Jones and Launder (1972a). In spite of these successes, the near wall behaviour of $\overline{u_i u_i}/k$ cannot be calculated. To do this, one needs to resort to a full Reynolds-stress closure model where all the transport equations for $\overline{u_i u_j}$ are solved rather than the equations for k and $\overline{u_1 u_2}$ alone.

1.3 Present Objectives

The primary objective of this study is to formulate a full Reynolds-stress closure model so that the calculations can be carried all the way to the wall and satisfy the boundary conditions at the wall for U_i, $\overline{u_i u_j}$ and ϵ. Validation of the model is carried out by comparing the calculated results with fully-developed turbulent pipe flow data at two moderate Reynolds number. By selecting fully-developed turbulent pipe flows, the complexity involved in solving the transport equations can be greatly reduced because the governing equations simplify to second-order, non-linear ordinary differential equations. This, in turn, allows the various modelling assumptions to be assessed

easily. A secondary objective, is to investigate the effects of redistribution and diffusion models on the modelled flow. To this end, the models of Rotta (1951) and Launder et al. (1975) for pressure redistributions are examined in detail together with a non-isotropic and an isotropic gradient diffusion model for turbulent diffusion. The effects of diffusion modelling are further investigated by simplifying the transport terms in the Reynolds-stress equations according to the suggestion of Rodi (1976). This results in a set of algebraic equations for the Reynolds stresses and can be solved with the low-Reynolds-number form of the $k-\epsilon$ equations (Jones and Launder 1972b; Chien 1980). The final objective, then, is to compare all the above model calculations with the results obtained from the basic two-equation model and to identify a model that performs the best in pipe flow calculations.

2. Low-Reynolds-Number Closures

For an incompressible flow, the transport equations for the Reynolds stresses $\overline{u_i u_j}$ can be concisely expressed in Cartesian tensor as

$$\frac{D\,\overline{u_i u_j}}{Dt} = \frac{\partial}{\partial x_k}\left[-\overline{u_i u_j u_k} - \overline{\frac{p}{\rho}(\delta_{ik}u_j + \delta_{jk}u_i)} + \nu\,\frac{\partial\,\overline{u_i u_j}}{\partial x_k}\right] - \left[\overline{u_j u_k}\frac{\partial U_i}{\partial x_k} + \overline{u_i u_k}\frac{\partial U_j}{\partial x_k}\right] + \overline{\frac{p}{\rho}\left(\frac{\partial u_i}{\partial x_j} + \frac{\partial u_j}{\partial x_i}\right)} - 2\nu\,\overline{\frac{\partial u_i}{\partial x_k}\frac{\partial u_j}{\partial x_k}}\,. \qquad (1)$$

Here, lower and upper case u's denote fluctuating and time-averaged velocity components, respectively, and overbars imply the usual time averaging of the correlations in question.

The terms in (1), from left to right, in general, can be interpreted as the convection, diffusion, production, redistribution and viscous dissipation of $\overline{u_i u_j}$, respectively. Of these five groups of terms, the convection and production terms are exact and do not need modelling. In the past, only high-Reynolds-number models have been proposed for the diffusion, redistribution and dissipation terms. Consequently, the resultant closure model is not valid for flows near a wall (Mellor and Herring 1973). Although some advances toward this direction have been made by Hanjalic and Launder (1976), a full Reynolds-stress closure for low-Reynolds-number turbulence is still not available. In the next section, an attempt will be made to close (1) so that the resultant transport equations are valid for low as well as high-Reynolds-number flows. At least two different models are proposed for each of the three terms

that required modelling. The relative merits of these models will be investigated. Diffusion modelling is further examined by greatly simplifying the transport equations into algebraic equations for the Reynolds stresses. Two approximations will be investigated; one is the equilibrium turbulence assumption and another is Rodi's (1976) approximation. A discussion of these algebraic stress closures is given in Section 2.2. Finally, the two-equation closure model of Chien (1980) for low-Reynolds-number turbulence is included in Section 2.3 for the sake of completeness.

2.1 Full Reynolds-Stress Closures

In order to model (1) for low-Reynolds-number turbulence, appropriate models for the redistribution, diffusion and dissipation terms have to be formulated. The subsequent sections provide a first attempt for this endeavour.

2.1.1 Redistribution Models

Since the term

$$\overline{\frac{p}{\rho}\left(\frac{\partial u_i}{\partial x_j} + \frac{\partial u_j}{\partial x_i}\right)}$$

has a zero trace for an incompressible flow, it acts to diminish the difference between the normal-stress components (Hinze 1959). Therefore, it neither produces nor destroys turbulence energy. Furthermore, p satisfies the equation

$$\frac{1}{\rho}\frac{\partial^2 p}{\partial x_i \partial x_i} = -\left[\frac{\partial^2 (u_i u_j - \overline{u_i u_j})}{\partial x_i \partial x_j} + 2\frac{\partial u_i}{\partial x_j}\frac{\partial U_j}{\partial x_i}\right], \qquad (2)$$

obtained by taking the divergence of the equation for u_i. Since ν does not appear explicitly in (2), this suggests that, to first order, any high-Reynolds-number model for this term can be adopted for the present study. Specifically, the redistribution model proposed by Launder et al. (1975) is adopted. This can be written as

$$\overline{\frac{p}{\rho}\left(\frac{\partial u_i}{\partial x_j} + \frac{\partial u_j}{\partial x_i}\right)} = - C_1 \frac{\epsilon}{k} \left(\overline{u_i u_j} - \frac{2}{3}\delta_{ij} k\right) - \alpha_1 \left(P_{ij} - \frac{2}{3}\delta_{ij} P\right) - \beta_1 \left(D_{ij} - \frac{2}{3}\delta_{ij} P\right) - \gamma_1 k S_{ij} , \qquad (3)$$

where

$$P_{ij} = - \left[\overline{u_j u_k} \frac{\partial U_i}{\partial x_k} + \overline{u_i u_k} \frac{\partial U_j}{\partial x_k} \right],$$

$$D_{ij} = - \left[\overline{u_i u_k} \frac{\partial U_k}{\partial x_j} + \overline{u_j u_k} \frac{\partial U_k}{\partial x_i} \right],$$

$$S_{ij} = \frac{\partial U_i}{\partial x_j} + \frac{\partial U_j}{\partial x_i} ,$$

$$P = - \overline{u_i u_k} \frac{\partial U_i}{\partial x_k}$$

and C_1, α_1, β_1, and γ_1, are model constants. According to Launder et al. (1975), α_1, β_1, and γ_1 are not independent constants. Rather, they are related to one constant C_2. These and other model constants are listed in Table 1 for reference.

Launder et al.'s model includes both the symmetric and antisymmetric mean-strain effects on redistribution modelling. However, their influence on near wall flow calculations has not been clearly demonstrated. In order to evaluate the effects of mean-strain modelling on the flow near a wall, Rotta's (1951) simple return-to-isotropy model for the redistribution terms will

also be examined in the present investigation. The model is given by (3) by setting $\alpha_1 = \beta_1 = \gamma_1 = 0$.

2.1.2 Wall Correction to Redistribution Modelling

Since the presence of a rigid wall affects the pressure field, thus impeding the transfer of turbulence energy from the streamwise direction to that normal to the wall, Launder et al. (1975) propose a wall correction to the pressure redistribution model to account for this wall effect. The correction is designed specifically to model the decrease of turbulence energy transfer to the normal direction. Since then, the wall correction has been used by Irwin and Smith (1975) to model curved shear flow and by Gibson and Launder (1978) to model atmospheric boundary layers. However, in these calculations, the near wall flow is not resolved directly. Therefore, the value of wall correction in pressure redistribution modelling has not been clearly demonstrated. The present approach allows the near wall flow to be calculated directly and, thus, provides a good opportunity to assess the relative merits of the wall correction.

In view of this, the wall correction proposed by Launder et al. (1975) will also be investigated. When this correction term is included in the pressure redistribution modelling, the complete model becomes

$$\overline{\frac{p}{\rho}\left(\frac{\partial u_i}{\partial x_j} + \frac{\partial u_j}{\partial x_i}\right)} = -C_1 \frac{\epsilon}{k}\left(\overline{u_i u_j} - \frac{2}{3}\delta_{ij}k\right)$$

$$- \alpha_1\left(P_{ij} - \frac{2}{3}\delta_{ij}P\right) - \beta_1\left(D_{ij} - \frac{2}{3}\delta_{ij}P\right)$$

$$- \gamma_1 \, k \, S_{ij}$$

$$+ \frac{k^{3/2}}{\epsilon x_2}\left[C_{1w}\frac{\epsilon}{k}\left(\overline{u_i u_j} - \frac{2}{3}\delta_{ij}P\right)\right.$$

$$\left. + C_{2w}\left(P_{ij} - D_{ij}\right)\right] , \qquad (4)$$

where x_2 is measured normal to the wall and the model constants C_{1w} and C_{2w} are specified in Table 1.

2.1.3 Diffusion Models

The other terms in (1) that need modelling are the diffusion and viscous dissipation terms. Since these terms involve ν explicitly, their high-Reynolds-number models (Launder et al. 1975; Kolmogovor 1941) have to be modified to account for viscosity effects. This can be easily carried out for the diffusion model by including the term $\nu(\partial\overline{u_i u_j}/\partial x_k)$ in the final diffusion model for low-Reynolds-number flows just as Hanjalic and Launder (1976) have done. If pressure diffusion is neglected, as suggested by Hanjalic and Launder (1976), the model for the diffusion term becomes

$$\frac{\partial}{\partial x_k}\left[-\overline{u_i u_j u_k} + \nu\frac{\partial\overline{u_i u_j}}{\partial x_k} + \overline{\frac{p}{\rho}\left(\delta_{jk}u_i + \delta_{ik}u_j\right)}\right]$$

$$= \frac{\partial}{\partial x_k}\left[\nu\frac{\partial\overline{u_i u_j}}{\partial x_k} + C_s\frac{k}{\epsilon}\left(\overline{u_k u_l}\frac{\partial\overline{u_i u_j}}{\partial x_l} + \overline{u_j u_l}\frac{\partial\overline{u_k u_i}}{\partial x_l}\right.\right.$$

$$\left.\left. + \overline{u_i u_l}\frac{\partial\overline{u_j u_k}}{\partial x_l}\right)\right] . \qquad (5)$$

This model is based on the gradient diffusion assumption and is tensorially correct. Also, it gives a non-isotropic diffusivity. On the other hand, past researchers (e.g. Mellor and Yamada 1974) have found that a much simpler isotropic diffusivity model for high-Reynolds-number turbulence works equally well as the non-isotropic one, even though the model is tensorially inconsistent. Whether this also holds true for low-Reynolds-number turbulence will again be examined in the present investigation. To this end, the simpler isotropic gradient diffusion model given by

$$\frac{\partial}{\partial x_k}\left[-\overline{u_i u_j u_k} + \nu\frac{\partial\overline{u_i u_j}}{\partial x_k} + \overline{\frac{p}{\rho}(\delta_{jk}u_i + \delta_{ik}u_j)}\right]$$

$$= \frac{\partial}{\partial x_k}\left[(\nu + \nu_t)\frac{\partial\overline{u_i u_j}}{\partial x_k}\right], \qquad (6)$$

where ν_t is defined as

$$\nu_t = C_\mu \frac{k^2}{\epsilon} f_2 , \qquad (7)$$

and f_2 is a damping function specified in Table 1, is also investigated. It should be pointed out that inherent in this model is the assumption that pressure diffusion is not important and can be neglected. A comparison of these two models will, therefore, provide a clear indication on which gradient diffusion model is more appropriate for low-Reynolds-number turbulence closure.

2.1.4 Dissipation Models

For high-Reynolds-number turbulence, Kolmogorov (1941) assumed viscous dissipation to be isotropic. However, near a

wall this assumption is no longer valid because the turbulent flow Reynolds number in this region is not large. To see how Kolmogorov's dissipation model should be modified to account for Reynolds-number effects, the Reynolds-stress equations (1) are examined for near wall behaviour with the proposed diffusion models (5) and (6).

When (5) is used in conjunction with the Reynolds-stress closure of Hanjalic and Launder (1976), good results for channel (or two-dimensional) flows are obtained. However, when it is used in conjunction with the full Reynolds-stress closure for axisymmetric flows, the following difficulty would appear at the wall. The difficulty is associated with the term $(\partial/\partial x_k)(\nu\partial\overline{u_i u_j}/\partial x_k)$. If cylindrical coordinates (x, r, θ) are used to expand this term for fully-developed pipe flows, then at the wall, the leading term becomes

$$\frac{1}{r^J}\frac{\partial}{\partial r}\left(r^J \nu \frac{\partial \overline{u_i u_j}}{\partial r}\right) = \frac{\partial}{\partial r}\left(\nu \frac{\partial \overline{u_i u_j}}{\partial r}\right) + \frac{J\nu}{r}\frac{\partial \overline{u_i u_j}}{\partial r} , \qquad (8)$$

where J = 0 or 1 for two-dimensional or axisymmetric flows, respectively. At the wall, $\overline{u_i u_j} = a_{ij}y^N + b_{ij}y^{N+1} + \cdots$ (Mellor and Herring 1973), where $N \geq 2$, a_{ij}, b_{ij}, --- are constants to be determined, and $y = R - r$. Substituting this expansion into (8) gives

$$\frac{1}{r^J}\frac{\partial}{\partial r}\left(r^J \nu \frac{\partial \overline{u_i u_j}}{\partial r}\right) = (N-1)Na_{ij}\nu y^{N-2}$$

$$+ \left[N(N+1)b_{ij}\nu - \frac{JNa_{ij}\nu}{R-y}\right]y^{N-1} + O(y^N) . \qquad (9)$$

Therefore, for N=2, all the terms on the right hand side of (9), except the first term, vanish at y = 0, and this is true for all

near wall flows, be it two-dimensional or axisymmetric. This means that molecular diffusion is finite at the wall. Since the term $(\partial/\partial x_k)(\nu\partial\overline{u_i u_j}/\partial x_k)$ does not need modelling and ν does not appear in other diffusion terms; additional terms are required in the modelling of the dissipation function, $2\nu\overline{(\partial u_i/\partial x_k)(\partial u_j/\partial x_k)}$, in order to balance the finite molecular diffusion at the wall. The foregoing arguments, therefore, suggests that the Kolmogorov (1941) high-Reynolds-number model for the dissipation function should be modified to give,

$$2\nu\overline{\frac{\partial u_i}{\partial x_k}\frac{\partial u_j}{\partial x_k}} = \frac{2}{3}\delta_{ij}\epsilon + \frac{2\nu\delta_{il}\delta_{jm}\overline{u_l u_m}}{(\delta_{2k}x_k)^2}\ , \qquad (10)$$

for low-Reynolds-number flows.

The dissipation model (10) is not isotropic when the Reynolds-number is finite. However, at very large Reynolds number (10) approaches Kolmogorov's model asymptotically and the correct limiting behaviour is recovered.

2.2 Algebraic Stress (ASM) Closures

Less sophisticated closure models for high-Reynolds-number turbulence have also been put forward by various researchers. Specific assumptions are put forward to simplify the Reynolds-stress equations (1) so that the equations are reduced to algebraic equations for the Reynolds stresses. The equilibrium turbulence assumption is used by So (1975, 1977) and So and Mellor (1978) to calculate curved shear flows, rotating and swirling flows. On the other hand, Rodi (1976) proposes to approximate the transport (convective and diffusive) terms in (1)

by the stress ratios $\overline{u_i u_j}/k$. Since then, this non-equilibrium turbulence scheme has been used by Gibson (1978), Gibson and Launder (1978) and Leschziner and Rodi (1981) to calculate a wide variety of turbulent shear flows. These closure models will also be extended to low-Reynolds-number turbulence and their performance compared with the full-Reynolds-stress models to further identify the effects of diffusion modelling.

In the course of modelling (1) taking the algebraic stress closure approach, the solution of two more transport equations are required (Gibson 1978). Normally, the k and ϵ equations are solved in addition to the mean flow equations. Therefore, the modifications of these closure models for low-Reynolds-number turbulence can be achieved via two different approaches. One is to modify the basic equations for k and ϵ and another is to modify both the k-ϵ equations and the models for pressure redistribution and dissipation. In Section 2.1, it has been shown that the high-Reynolds-number form of the pressure redistribution models is also applicable to low-Reynolds-number flows. However, the dissipation model has to be modified for low-Reynolds-number turbulence. In algebraic stress closures, turbulent diffusion is either neglected or approximated by the stress ratios via Rodi's approximation. If the dissipation model is modified to account for viscosity effects, then it can be shown that, under the assumption of equilibrium ASM, the resultant algebraic stress equations are not balanced at the wall. On the other hand, under Rodi's approximation, the additional dissipation term would cancel out with the extra

dissipation term introduced by Chien (1980) in the k equation. Consequently, the approach taken here is to modify the k-ϵ equations alone. The modified forms of the k-ϵ equations are given in Section 2.3, while the simplified forms of the Reynolds-stress equations needed for the equilibrium and non-equilibrium algebraic stress closures are specified in the following two sections.

2.2.1 Equilibrium Assumption

If the equilibrium turbulence assumption is invoked, production of turbulence energy is equal to its dissipation rate. The Reynolds-stress equations (1) simplify to

$$0 \simeq -\left[\overline{u_j u_k}\frac{\partial U_i}{\partial x_k} + \overline{u_i u_k}\frac{\partial U_i}{\partial x_k}\right] + \overline{\frac{p}{\rho}\left(\frac{\partial u_i}{\partial x_j} + \frac{\partial u_j}{\partial x_i}\right)} - 2\nu\,\overline{\frac{\partial u_i}{\partial x_k}\frac{\partial u_j}{\partial x_k}} \quad . \tag{11}$$

The high-Reynolds-number models for the pressure redistribution and dissipation terms are used to close (11). These are given by (3) and the Kolmogorov isotropic dissipation model, or

$$2\nu\overline{\frac{\partial u_i}{\partial x_k}\frac{\partial u_j}{\partial x_k}} = \frac{2}{3}\delta_{ij}\epsilon \quad . \tag{12}$$

Again, Rotta's return-to-isotropy model is obtained from (3) by setting $\alpha_1 = \beta_1 = \gamma_1 = 0$. Both Rotta's and Launder et al.'s models will be investigated and the results compared with the full Reynolds-stress models.

2.2.2 Non-Equilibrium Assumption

In this case, the transport terms in (1) are approximated by Rodi's (1976) assumption and (1) is reduced to

$$\frac{\overline{u_i u_i}}{k}(P - \epsilon) \tilde{=} - \left[\overline{u_j u_k}\frac{\partial U_i}{\partial x_k} + \overline{u_i u_k}\frac{\partial U_j}{\partial x_k}\right]$$

$$+ \overline{\frac{p}{\rho}\left(\frac{\partial u_i}{\partial x_k} + \frac{\partial u_j}{\partial x_k}\right)} - 2\nu\overline{\frac{\partial u_i}{\partial x_k}\frac{\partial u_j}{\partial x_k}} \quad . \tag{13}$$

If (3) and (12) are used to model the last two terms in (13), algebraic equations for $\overline{u_i u_j}$ can be derived from (13). It is now clear that if (10) is used to model the dissipation term, ϵ in (13) will have to be replaced by $\epsilon + 2\nu k/x_2^2$ (see eq. (14)). The net result is again equivalent to (13) with the dissipation function given by (12).

2.3 Two-Equation Closure

Equation (1) can now be expressed in terms of $\overline{u_i u_j}$, U_i, k, ϵ and their gradients. Transport equations are, therefore, available for all unknowns except ϵ. Two options are available for ϵ. Either the equation proposed by Jones and Launder (1972b) or the equation modified by Chien (1980) for low-Reynolds-number turbulence can be used. Since the k equation obtained by contracting (1) using the proposed models is similar to that proposed by Chien (1980), it is decided that Chien's ϵ-equation would be more appropriate for the present full Reynolds-stress closure. Also, (12) and (13) can be expressed in terms of $\overline{u_i u_j}$, U_i, k, ϵ and the gradients of U_i. To complete the definition of k and ϵ in the flow field, two equations governing the transport of k and ϵ are required. Since the ϵ-equation modified by Chien

(1980) is used in the full Reynolds-stress closure it would be appropriate to also use the k-equation modified by Chien for low-Reynolds-number turbulence rather than by contracting (1) with models given by (3), (5) and (10). These two equations are:

$$\frac{Dk}{Dt} = \frac{\partial}{\partial x_k}\left[(\nu + \nu_t)\frac{\partial k}{\partial x_k}\right] + P - \epsilon - \frac{2\nu k}{x_2^2} , \tag{14}$$

$$\frac{D\epsilon}{Dt} = \frac{\partial}{\partial x_k}\left[(\nu + \frac{\nu_t}{\sigma_\epsilon})\frac{\partial \epsilon}{\partial x_k}\right] + C_{\epsilon 1}\frac{\epsilon}{k}P - C_{\epsilon 2} f_1 \frac{\epsilon^2}{k}$$

$$- \frac{2\nu\epsilon}{x_2^2} e^{-C_4 x_2 u_* / \nu} , \tag{15}$$

where x_2 is measured normal from the wall and the model constants $C_{\epsilon 1}$, $C_{\epsilon 2}$, C_4, σ_ϵ and damping function f_1 are specified in Table 1. The diffusivity ν_t is again taken to be given by (7). Therefore, the two-equation closure is given by solving (14) and (15) together with the mean flow equations. It should be pointed out that, in the full Reynolds-stress and algebraic stress closures, an assumption for the turbulent stresses, $\overline{u_i u_j}$, is not required. For the two-equation closure, a gradient transport model for $\overline{u_i u_j}$ is invoked, such that

$$-\overline{u_i u_j} = \nu_t\left(\frac{\partial U_i}{\partial x_j} + \frac{\partial U_i}{\partial x_i}\right) - \frac{2}{3}\delta_{ij}k . \tag{16}$$

3. Fully-Developed Pipe Flows at Moderate Reynolds Numbers

Fully-developed turbulent pipe flows at moderate Reynolds numbers are used to validate the full Reynolds-stress and algebraic stress models. If models (4), (5) and (10) are substituted into (1) and the component equations are written in cylindrical coordinates (x, r, θ) with mean and fluctuating velocities given by (U, 0, 0) and (u, v, w), respectively, then the governing equations including the simplified mean flow (Laufer 1954) and ϵ equations are:

$$\nu\frac{dU}{dr} - \overline{uv} + \frac{u_*^2 r}{R} = 0 \ , \tag{17}$$

$$\frac{1}{r}\frac{d}{dr}\left[r\left(\nu + \frac{\nu_t}{\sigma_\epsilon}\right)\frac{d\epsilon}{dr}\right] - C_{1}\frac{\epsilon}{k}\overline{uv}\left(\frac{dU}{dr}\right)$$

$$- C_{2}f_1\frac{\epsilon^2}{k} - \frac{2\nu\epsilon}{(R-r)^2}\, e^{-C_4(R-r)u_*/\nu} = 0 \ , \tag{18}$$

$$\frac{1}{r}\frac{d}{dr}\left[r\left(\nu + C_s\frac{k}{\epsilon}\overline{v^2}\right)\frac{d\overline{u^2}}{dr}\right] + \frac{1}{r}\frac{d}{dr}\left[2C_s r\,\frac{k}{\epsilon}\,\overline{uv}\frac{d\overline{uv}}{dr}\right]$$

$$- \left[C_1 - C_{1w}\frac{k^{3/2}}{\epsilon(R-r)}\right]\frac{\epsilon}{k}\left(\overline{u^2} - \frac{2}{3}k\right)$$

$$- 2\left[1 - \frac{2}{3}\alpha_1 + \frac{1}{3}\beta_1 + C_{2w}\frac{k^{3/2}}{\epsilon(R-r)}\right]\overline{uv}\,\frac{dU}{dr} - \frac{2}{3}\epsilon$$

$$- \frac{2\nu\overline{u^2}}{(R-r)^2} = 0 \ , \tag{19}$$

$$\frac{1}{r}\frac{d}{dr}\left[r(\nu + 3C_s\frac{k}{\epsilon}\overline{v^2})\frac{d\overline{v^2}}{dr}\right] - \frac{2C_s}{r}\frac{k}{\epsilon}\overline{v^2}\frac{d\overline{w^2}}{dr}$$

$$- \frac{4C_s}{r}\frac{k}{\epsilon}\overline{w^2}\frac{(\overline{v^2} - \overline{w^2})}{r} - \left[C_1 - C_{1w}\frac{k^{3/2}}{\epsilon(R-r)}\right]\frac{\epsilon}{k}(\overline{v^2} - \frac{2}{3}k)$$

$$- 2\left[\frac{\alpha_1}{3} - \frac{2\beta_1}{3} - C_{2w}\frac{k^{3/2}}{\epsilon(R-r)}\right]\overline{uv}\frac{dU}{dr}$$

$$- \frac{2}{3}\epsilon - \frac{2\nu\overline{v^2}}{(R-r)^2} - 2\nu\frac{\overline{v^2} - \overline{w^2}}{r^2} = 0 \quad , \tag{20}$$

$$\frac{1}{r}\frac{d}{dr}\left[r(\nu + C_s\frac{k}{\epsilon}\overline{v^2})\frac{d\overline{w^2}}{dr}\right] + \frac{4C_s}{r}\frac{k}{\epsilon}\overline{w^2}\frac{(\overline{v^2} - \overline{w^2})}{r}$$

$$+ \frac{1}{r}\frac{d}{dr}\left[\frac{2C_s rk}{\epsilon}\overline{w^2}\frac{(\overline{v^2} - \overline{w^2})}{r}\right] + \frac{2C_s}{r}\frac{k}{\epsilon}\overline{v^2}\frac{d\overline{w^2}}{dr}$$

$$- \left[C_1 - C_{1w}\frac{k^{3/2}}{\epsilon(R-r)}\right]\frac{\epsilon}{k}(\overline{w^2} - \frac{2}{3}k) - \frac{2}{3}(\alpha_1 + \beta_1)\overline{uv}\frac{dU}{dr}$$

$$- \frac{2}{3}\epsilon - \frac{2\nu\overline{w^2}}{(R-r)^2} + 2\nu\frac{\overline{v^2} - \overline{w^2}}{r^2} = 0 \quad , \tag{21}$$

$$\frac{1}{r}\frac{d}{dr}\left[r(\nu + 2C_s\frac{k}{\epsilon}\overline{v^2})\frac{d\overline{uv}}{dr}\right] - \frac{2C_s}{r}\frac{k}{\epsilon}\overline{w^2}\frac{\overline{uv}}{r}$$

$$+ \frac{1}{r}\frac{d}{dr}\left[rC_s\frac{k}{\epsilon}\overline{uv}\frac{d\overline{v^2}}{dr}\right] - \frac{C_s}{r}\frac{k}{\epsilon}\overline{uv}\frac{d\overline{w^2}}{dr}$$

$$- \left[C_1 - C_{1w}\frac{k^{3/2}}{\epsilon(R-r)}\right]\frac{\epsilon}{k}\overline{uv} -$$

$$- f_3\left[(1 - \alpha_1 + C_{2w}\frac{k^{3/2}}{\epsilon(R-r)})\overline{v^2} - (\beta_1 + C_{2w}\frac{k^{3/2}}{\epsilon(R-r)})\overline{u^2} + \frac{\gamma_1}{2}k\right]\frac{dU}{dr}$$

$$- \frac{2\nu\overline{uv}}{(R-r)^2} - \nu\frac{\overline{uv}}{r^2} = 0 \tag{22}$$

In writing down these equations, a damping factor f_3 specified in Table 1 and suggested by Hanjalic and Launder (1976) is included in the stress production term of (22). This damping factor is found to be necessary in the course of solving (17)-(22), because

without it shear production near a wall is found to be over-predicted. Similarly, turbulent diffusivities near a wall are found to be way over-predicted if C_s is taken to be a true constant. In all subsequent calculations, C_s is damped by a factor f_2 similar to that specified in (7). These and other model constants are specified in Table 1 and are consistent with those recommended by various researchers (Rotta 1951; Launder et al. 1975; Chien 1980).

Boundary conditions are specified at the wall and at the symmetry plane. These are given by:

$$U = \epsilon = \overline{u^2} = \overline{v^2} = \overline{w^2} = \overline{uv} = 0 \qquad \text{at } r = R \text{ (wall)}, \tag{23}$$

$$\left.\begin{aligned} \frac{d\epsilon}{dr} = \frac{d\overline{u^2}}{dr} = \frac{d\overline{v^2}}{dr} = \frac{d\overline{w^2}}{dr} = 0 \\ \overline{uv} = 0 \end{aligned}\right\} \quad \text{at } r = 0 . \tag{24}$$

Only one boundary condition is specified for U, since the symmetry condition for U has been utilized to evaluate the integration constant when the mean momentum equation is integrated to give (17).

Similarly, component equations for (1) using (4) and (6) for closure can also be written down. However, for brevity's sake, they are not included here. As before, it is found necessary to damp the shear production term in the equation for $\overline{uv}$ by the factor f_3. Rotta's model is given by the same set of equations with $\alpha_1 = \beta_1 = \gamma_1 = C_{1w} = C_{2w} = 0$. If no wall correction is required, C_{1w} and C_{2w} should be set equal to zero.

For algebraic stress and two-equation closures, the transport equations to be solved are (17), (18) and a corresponding k-equation which can be written as

$$\frac{1}{r}\frac{d}{dr}\left[(\nu + \nu_t)\frac{dk}{dr}\right] - \overline{uv}\left(\frac{dU}{dr}\right) - \epsilon - \frac{2\nu k}{(R-r)^2} = 0 \ . \tag{25}$$

In the case of algebraic stress closures, the stresses $\overline{u_i u_j}$ are provided by (11) or (13) which can be written out in their component forms. For two-equation closure, $-\overline{uv}$ is provided by (16) which reduces to

$$-\overline{uv} = \nu_t \left(\frac{\partial U}{\partial r}\right) \ . \tag{26}$$

The boundary conditions for k are:

$$\left.\begin{aligned} k &= 0 \qquad \text{at} \quad r = R, \\ \frac{dk}{dr} &= 0 \qquad \text{at} \quad r = 0 \ . \end{aligned}\right\} \tag{27}$$

4. Method of Solution

The set of equations (17)-(22) with boundary conditions (23) and (24) are solved numerically by the Newton iteration scheme (Na 1979). First, normalization of the dependent variables U by u_*, $\overline{u_i u_j}$ by u_*^2 and ϵ by u_*^3/R are carried out, while the independent variable r is made non-dimensional by u_*/ν, so that $Y^+ = u_*(R-r)/\nu$ is the new dimensionless coordinate. Therefore, the integration from the pipe wall to the centerline is now carried out from $Y^+ = 0$ to $Y^+ = Re$, where $Re = u_* R/\nu$ is the turbulent Reynolds number to be specified. Re is related to the pipe flow Reynolds number $R_D = U_0 D/\nu$ by $Re = (u_*/2U_0)R_D$. Therefore, once R_D and the pressure drop along the pipe are known, Re can be determined and it becomes the only input parameter to the problem.

Next, the six first- and second-order ordinary differential equations are written into eleven first-order equations by defining new variables for $d(\overline{u_i u_j}/u_*^2)/dY^+$ and $d(\epsilon R/u_*^3)/dY^+$. If these eleven variables are denoted by ψ_i, i = 1, ... 11, such that $\psi_1 = U/u_*$, $\psi_2 = \epsilon R/u_*^3$, $\psi_3 = \overline{u^2}/u_*^2$, $\psi_4 = \overline{v^2}/u_*^2$, $\psi_5 = \overline{w^2}/u_*^2$, $\psi_6 = \overline{uv}/u_*^2$, $\psi_7 = d\psi_2/dY^+$, $\psi_8 = d\psi_3/dY^+$, $\psi_9 = d\psi_4/dY^+$, $\psi_{10} = d\psi_5/dY^+$, $\psi_{11} = d\psi_6/dY^+$, then their derivatives can be approximated by centered-difference gradients and averages centered at the midpoints of the grid, defined by

$$Y_0^+ = 0;\ Y^+_j = Y^+_{j-1} + h_j\ ,\ j = 1, 2, \ldots, M;\ Y^+_M = Re; \tag{28}$$

$$\frac{d\psi_i}{dY^+} = \frac{(\psi_i)_j - (\psi_i)_{j-1}}{h_j}\ . \tag{29}$$

The resultant equations are nonlinear algebraic equations. Therefore, they have to be linearized before the factorization scheme can be used. Newton's linearization scheme is used so that the Newton (k+1) iterates for $(\psi_i)_j$ can be written as

$$(\psi_i)_j^{(k+1)} = (\psi_i)_j^{(k)} + \delta(\psi_i)_j^{(k)} \quad . \tag{30}$$

These are then substituted into the eleven first-order differential equations. If quadratic and higher-order terms in $\delta(\psi_i)_j^{(k)}$ are neglected, the resultant linear algebraic equations can be put into vector-matrix form as

$$[\underline{A}]\ [\underline{\delta}] = [\underline{\Psi}] \ , \tag{31}$$

where $[\underline{A}]$ is the coefficient matrix of order MxM and its elements are matrices of order 11x11. The matrix $[\underline{A}]$ is of the tridiagonal form, while the matrix $[\underline{\Psi}]$ is a column matrix of $(\psi_i)_j$ and $(\psi_i)_{j-1}$. The boundary conditions are:

$$\begin{aligned} &\delta(\psi_i)_0 = 0 \ ; \qquad i = 1, \ldots, 6 \ ; \\ &\delta(\psi_6)_M = 0 \ ; \\ &\delta(\psi_i)_M = 0 \ ; \qquad i = 7, \ldots, \ldots, 10 \ . \end{aligned} \tag{32}$$

Once the equations are put into the form (31) and (32), they can be solved interatively using any matrix inversion technique. Iteration is carried out until $[\underline{\delta}]$ meets certain accuracy criterion. For the present study, the accuracy criterion is chosen as

$$\left| \frac{\delta(\psi_i)_j^{(k)} - \delta(\psi_i)_j^{(k-1)}}{\delta(\psi_i)_j^{(k)}} \right| \leq 10^{-4} \ . \tag{33}$$

A non-uniform grid is used to carry out the calculations. Typically, five grid points are specified between $Y^+ = 0$ and $Y^+ = 5$. This is followed by 15 grid points between $Y^+ = 5$ and $Y^+ = 65$. The rest of the region $65 \leq Y^+ \leq Re$ is then divided into 30-50 grid points depending on the problem considered. In general, this system of grid spacing is sufficient to give convergent solution after ~1500 iterations.

The equations for the other closure models can be similarly solved. However, for brevity's sake, they are not outlined in detail here. Anyway, once a solution scheme has been developed for the more complex set of equations (17)-(22), the same scheme can be easily adapted to solve a set of simpler equations.

5. Presentation of Results

Fully-developed pipe flows at two different Reynolds numbers are selected for comparison with the model calculations. These are the detailed measurements of Laufer (1954) at R_D = 50,000, and of Schildknecht et al. (1979) at R_D = 21,750. They are chosen for their careful measurements of the turbulence field near the wall. Consequently, they would provide accurate data for the evaluation of the full Reynolds-stress model for low-Reynolds-number turbulence. The input parameter for these two calculations is Re = 1052 and 489, respectively, for Laufer's and Schildknecht et al.'s experiments. Calculations are carried out to compare the performance of different redistribution and diffusion models. The redistribution models examined are Rotta's (1951) return-to-isotropy model and Launder et al.'s models including mean-strain and wall effects. As for diffusion, two models are investigated; one is Launder et al.'s model given in (5) and another is an isotropic model given in (6). The effects of diffusion modelling are further examined by considering less sophisticated closure models such as algebraic stress closures. Again, redistribution modelling effects are studied by comparing the Rotta and Launder et al. models. Finally, these model calculations are compared with the simple two-equation closure results.

In view of the large number of calculated results and their close similarities, the comparisons with data are presented separately rather than together in one figure for each flow property. Although this involves many more figures to be

presented, it will give a clearer comparison of each closure model with measurements. Altogether eleven model calculations are made for each experiment. These are organized for presentation in the following manner. With the exception of the k-ϵ model calculation, each set of comparison consists of eight figures where the model calculations of both experiments are presented. These eight figures, numbered a through h, show the comparisons of U/u_* in semi-log plot, U/U_o, $\overline{uv}/u_*^2$, k/u_*^2, $\epsilon R/u_*^3$, $\overline{u_i u_i}/u_*^2$, $\overline{u_i u_i}/k$ and $\overline{uv}/k$ versus $1-2r/D$ in the sequence given. The comparisons of the near wall behavior are shown as insets in each figure, and the coordinate used is the normalized wall coordinate Y^+. Only five figures are presented for the k-ϵ model calculations. These are U/u_* in semi-log plot, U/U_o, $\overline{uv}/u_*^2$, k/u_*^2 and $\epsilon R/u_*^3$ versus $1-2r/D$.

The results for the full Reynolds-stress closure using (5) for diffusion modelling are presented in Figures 1-3. Rotta's model results are given in Figure 1a-1h, while Launder et al.'s model calculations without and with wall correction are given in Figures 2a-2h and 3a-3h, respectively. Results for full Reynolds-stress closure using (6) for diffusion modelling are shown in Figures 4-6. The first eight figures give the calculated results of Rotta's model and the other figures those of Launder et al.'s model without and with wall correction. Algebraic stress model calculations are presented in Figures 7-10. The first sixteen figures give the results of the equilibrium turbulence calculations using Rotta's and Launder et al.'s model. This is followed by the same calculations

assuming non-equilibrium turbulence. Finally, the k-ϵ results are presented in Figures 11a-11e.

For the sake of clarity, a discussion of these results and their comparisons with measurements is presented in three different sections. These are: (1) effects of mean-strain modelling, (2) effects of diffusion modelling and (3) effects of wall correction on redistribution modelling. Finally, the k-ϵ equation results are presented in Section 5.4.

5.1 Effects of Mean-Strain Modelling

The equations (17)-(22) with boundary conditions (23) and (24) are solved assuming $C_{1w} = C_{2w} = 0$. For each experiment, two calculations are carried out; one with $\alpha_1 = \beta_1 = \gamma_1 = 0$ and another with these constants as given in Table 1. Therefore, a comparison of these two calculations with the measured data would reveal the relative merits of mean-strain modelling. The results are presented in Figures 1 and 2. Other comparisons of the effects of mean-strain modelling, subject to different approximations for turbulent diffusion, are given in Figures 4 and 5 for isotropic diffusion modelling, in Figures 7 and 8 for equilibrium algebraic stress closure and in Figures 9 and 10 for non-equilibrium algebraic stress closure. For ease of reference later on, the set of figures 1, 2; 4, 5; 7, 8 and 9, 10 shall be designated as set A, B, C and D, respectively. Therefore, figure sets A and B give the full Reynolds-stress closure results, while sets C and D show the algebraic stress closure calculations. A comparison of the results within each set will indicate the relative merits of mean-strain modelling given a fixed diffusion

model for closure, while comparisons between different sets will elucidate the effects of diffusion modelling.

In general, both redistribution models give reasonably good results for U, $\overline{uv}$, k and ϵ (Figures a-e of each set of Figures A, B, C, D). However, they fail to replicate correctly the behaviour of the normal stresses near the wall (Figures f-h of each set of Figures A, B, C, D). The calculated mean U is in good agreement with the measured mean U in the near wall region, but shows substantial discrepancy in the pipe core (Figures b of each set of figures), even though the logarithmic behaviour in this region is recovered (Figures a of each set). The measured U can be correlated by a logarithmic law-of-the-wall, such that

$$\frac{U}{u_*} = \alpha \ln Y^+ + \beta \ , \qquad (35)$$

where $\alpha = 1/\kappa$, κ is the von Karman constant and β is parametically dependent on R_D (Afzal and Yajnik 1973). For the experiments of Laufer (1954) and Schildknecht et al. (1979) the constants thus determined are listed in Table 2 together with the quantities U_o/u_*. Likewise, these quantities can also be determined from the calculations. They are also listed in Table 2 for comparison. It can be seen that the measured slope of the log-law is not in agreement with the calculated slopes and that the calculated U_o/u_* are always lower than the measured values. In view of this, it is very difficult to conclude which of the two redistribution models gives a better description of the mean flow.

In order to understand the discrepancy noted between the measured and calculated U, the mean U obtained by integrating (17) using the measured $\overline{uv}$ as input is also shown in Figures a of each set of figures for comparison with the model calculations. The corresponding α, β and U_o/u_* are listed in Table 2. It can be seen that the mean U thus determined is in excellent agreement with that calculated from Rotta's model and the k-ϵ closure. On the other hand, Launder et al.'s model consistently under-predicts the slope and U_o/u_* but over-estimates the constant β. Both models, however, predict an increase in β as R_D is decreased just as in the analysis of Afzal and Yajnik (1973). As for the behaviour of $\overline{uv}$, k and ϵ, the two model calculations are in excellent agreement with measurements, especially near the wall. This demonstrates that the modified dissipation model is valid and can account for the near wall behaviour very well.

The performance of this dissipation model is quite independent of the redistribution model (Figure sets A and B). Therefore, based on the above comparison, it can be concluded that, as far as the mean flow, $\overline{uv}$, k and ϵ behaviours are concerned, the simple return-to-isotropy model of Rotta is just as promising as the more complete model of Launder et al. (1975). The performance of the Launder et al. (1975) model is found to be not as good when used in conjunction with algebraic stress closures (Figure sets C and D). In view of this, mean strain modelling is found to have a negative effect on the overall flow behaviour when turbulent diffusion is improperly modelled (compared figure sets A and B, C and D). A similar conclusion

has also been reached by Yao and So (1985) in their analysis of curved-pipe flow using rapid distortion theory. The present results together with Yao and So's (1985) analysis, therefore, point to the modelling of the turbulent redistribution terms by return-to-isotropy models for fully-developed pipe flows.

Even though different levels of $\overline{v^2}$ and $\overline{w^2}$ are predicted by Launder et al.'s model, their comparison with measured data is slightly better than those obtained from Rotta's model (Figures f of each set). Essentially, both models under-estimate the rise of $\overline{u^2}$ and greatly over-estimate the rise of $\overline{v^2}$ and $\overline{w^2}$ near the wall. They also fail to predict the isotropic behaviour of the turbulence field at the pipe center. As a result, the k distribution in the pipe core is over-predicted (Figures d of each set). A comparison of the stress ratios, $\overline{u_i u_j}/k$, clearly shows the inadequacy of the two models (Figures g and h of each set). Launder et al.'s model gives a better correlation with data for $\overline{uv}/k$ (Figures h of each set); however, it leads to a rather flat variation for $\overline{u_i u_i}/k$ (Figures g of each set). Besides, the limiting values of $\overline{u_i u_i}/k$ at the wall are not predicted correctly. In evaluating the limiting values, the measured data is fitted to the expansions

$$\overline{u_i u_j} = a_{ij}\, y^N + b_{ij}\, y^{N+1} + \ldots$$

near a wall. This allows the a_{ij} and b_{ij} to be determined and hence the values $(\overline{u_i u_i}/k)_w$. For example, experimental values thus determined are: $(\overline{u^2}/k)_w \sim 2$, $(\overline{v^2}/k)_w \equiv 0$ and $(\overline{w^2}/k)_w \sim 0$ for Laufer's data. The corresponding calculated values are $(\overline{u^2}/k)_w \sim .9$, $(\overline{v^2}/k)_w = (\overline{w^2}/k)_w \sim .55$ for Rotta's model and

$(\overline{u^2}/k)_w \sim .9$, $(\overline{v^2}/k)_w \sim .5$ and $(\overline{w^2}/k)_w \sim .6$ for Launder et al.'s model. Therefore, the rapid decrease of $\overline{u^2}/k$ and steep rise of $\overline{v^2}/k$ and $\overline{w^2}/k$ near a wall are not predicted by the models at all (Figures g of each set). Based on these calculations, it seems that the assumption, $\overline{u_i u_i}/k$ are uniform across the flow, is inherent in these closure models. The effects of diffusion modelling on the behaviour of $\overline{u_i u_j}/k$ near a wall will be further examined in Section 5.2.

5.2 Effects of Diffusion Modelling

In order to investigate the effects of diffusion modelling on turbulence closure, another set of calculations is performed with a vastly different diffusion model. This time an isotropic gradient diffusion model for the turbulent stresses is assumed as in (6). The diffusivity ν_t is taken to be given by (7) with the damping function f_2 near a wall included to account for wall proximity effects. Again, calculations are carried out for both the Rotta and Launder et al. models for the redistribution terms. The solution of (17)-(22) is performed assuming C_{1w} and C_{2w} to be identically zero.

The results are also plotted in Figures sets A-D for comparison with the previous calculations. Calculated values for α, β and U_o/u_* are listed in Table 2. It can be seen that Rotta's model now gives rise to over-prediction of α and U_o/u_* and under-estimation of β. However, the parametric dependence of β on R_D is not correctly predicted. On the other hand, Launder et al.'s model also gives an incorrect trend for β. Instead of predicting an increase for β as R_D decreases, it gives

a β that decreases slightly with R_D. Also, the slope, α, increases as R_D decreases. In view of these incorrect trends, it can be concluded that the performance of Launder et al.'s model does not fair well with Rotta's model when an isotropic gradient diffusion model is used to approximate turbulent diffusion.

The near wall behaviours of U, $\overline{uv}$, k and ϵ are again well predicted. This shows that the modelled flow near a wall is essentially governed by the dissipation model and is only slightly dependent on the diffusion and pressure redistribution models. There are small differences in the calculations of $\overline{u_i u_i}/u_*^2$ and $\overline{u_i u_j}/k$ (Figures f-h of each set). However, they are not significant enough to warrant a conclusion that one diffusion model is better than another. Essentially, the shortcomings noted in Section 5.1 for the diffusion model given by (5) are also true for (6). Therefore, the calculations indicate that once a gradient diffusion model is assumed, the results are only slightly dependent on the behaviour of the diffusivity. An isotropic model will give results that are quite similar to those obtained from a non-isotropic one.

5.3 Effects of Wall Correction on Redistribution Modelling

The effects of wall correction on redistribution modelling are assessed by solving (17)-(22) with the wall correction terms included. In the course of solving these equations, it is found that if the C_{1w} and C_{2w} values suggested by Launder et al. (1975) are used convergent solutions to (17)-(22) are not possible. The problem is traced to the coefficient of the terms $(\overline{u_i u_i} - \frac{2}{3}k)$

in (19)-(21). After normalization, the coefficient becomes $[C_1/Re - C_{1w}(\psi_3 + \psi_4 + \psi_5)^{3/2}/2^{3/2}\ \psi_2\eta]$. If $C_{1w} = .125$ is used, as suggested by Launder et al., the coefficient becomes negative over a substantial portion of the pipe. Consequently, these terms $(\overline{u_i u_i} - \frac{2}{3}k)$ change sign and the equations are not balanced. A similar behaviour is also observed in the production term in (20) because C_{2w} is too large. Subsequently, C_{1w} and C_{2w} are slowly decreased until convergent solutions to (17)-(22) are obtained. The values of C_{1w} and C_{2w} thus determined are shown in Table 1. Two sets of model calculations are performed and these are carried out with Launder et al.'s model for the redistribution term and (5) and (6) for the diffusion model.

Actually, convergent solution is possible at some higher values of C_{1w} and C_{2w}. However, the calculated results compare poorly with measurements and they are not shown. Calculations have been made with a series of values for C_{1w} and C_{2w} and they lie in the range $.025 \leq C_{1w} \leq .0625$ and $.003 \leq C_{2w} \leq .0075$. The largest values denote the upper limit for C_{1w} and C_{2w} where convergent solution is possible. In general, the effects of wall corrections are to increase α, β and U_o/u_τ, thus increasing the discrepancies noted between calculations and measurements of the mean flow. Furthermore, the peak value predicted for k increases as C_{1w} and C_{2w} are increased. For example, the calculated peak value for k is more than 20% higher than the measured value when $C_{1w} = .0625$ and $C_{2w} = .0075$ are used. Reduction of these constants to the values given in Table 1 gives the results shown in Figures 3 and 6. Even then, the peak value of k is ~ 10%

higher than measurements and the calculations obtained by neglecting wall corrections (compare Figures 2 and 3, 5 and 6). On the other hand, when C_{1w} = .025 and C_{2w} = .003 are used in the governing equations, the calculated results are essentially indentical to those shown in Figures 2 and 5. If plotted, they practically overlap on top of the curves shown in Figures 2 and 5. Even in the near wall region, little differences are noted. In view of these results, it can be said that if large values of C_{1w} and C_{2w} are specified, wall corrections affect the calculations adversely. However, when small values of C_{1w} and C_{2w} are used for the calculations, wall corrections have little effect on the results.

5.4 Two-Equation Closure Results

The results obtained by solving (14), (15) and (17) together with the appropriate boundary conditions are shown in Figure 11. They display characteristics very similar to those obtained from an equilibrium ASM closure using Rotta's model (Figure 7) and from a full Reynolds-stress closure using (5) for diffusion modelling and Rotta's return-to-isotropy model for pressure redistribution (Figure 1). The calculated α, β and U_o/u_* for these three cases are very similar. However, both the k-ϵ closure and the equilibrium ASM closure fail to predict the correct increase in β as R_D is decreased (Table 1 and Afzal and Yajnik 1973). In view of this, the performance of the two-equation closure is not as good as that of the full Reynolds-stress closure. On the other hand, its prediction of fully-developed turbulent pipe flow properties are better than any ASM

closure models that used the Launder et al. model for pressure redistributions (compare Figure 11 with Figures 8 and 10 and the values of α, β listed in Table 2). Therefore, if only U, uv, k and ϵ information are required in any pipe flow calculation, the k-ϵ equation is a simple closure model to use and will provide reliable results.

6. Application to Fully-Developed Rotating Pipe Flows

One of the objectives of the present study is to develop a closure model for solid fuel ramjet combustor calculation. If the solid fuel ramjet combustor is used to power a projectile fired from a cannon, the whole combustor would spin at a very high rate. As a result of this spin, the flow inside the combustor would also be subject to the influence of a large circumferential velocity which has its maximum value at the combustor wall and decreases rapidly to zero at the combustor centerline. Therefore, the usual logarithmic law-of-the wall may not apply to the flow very near the wall and the high-Reynolds-number closure model may not be applicable to this kind of combustor flow calculation. With the development of the low-Reynolds-number closure models discussed in Section 5, they can then be applied to assess the effects of rotation on the calculated flow field correctly. This section presents the results of such an assessment.

The effects of rotation can be best illustrated by considering a simple model problem where rotation appears as the only additional parameter in the flow field. Such a problem is given by the fully-developed flow through a circular pipe rotating at a constant speed. Since the above results indicate that the equilibrium ASM closure using Rotta's model is just as good as a full Reynolds-stress closure model, the following analysis is carried out with the equilibrium ASM closure model only. In Section 6.1, the governing equations for the rotating

pipe flow problem are specified. The results of this calculation are discussed in Section 6.2

6.1 Governing Equations for Flows Through a Rotating Pipe

Cylindrical coordinates are again used to analyze the flow. The pipe is assumed to rotate at a constant angular speed of Ω, so that the circumferential velocity of the fluid at the pipe wall is $W_o = R\Omega$. When the flow becomes fully-developed and axisymmetric, $\partial/\partial\theta = 0$, $\partial/\partial x = 0$ and $V \equiv 0$. The resultant mean momentum equations reduce to:

$$0 = -\frac{1}{\rho}\frac{dp}{dx} + \frac{1}{r}\frac{d}{dr}(r\nu\frac{dU}{dr}) - \frac{1}{r}\frac{d}{dr}(r\overline{uv}) \ , \tag{35}$$

$$0 = \frac{1}{r^2}\frac{d}{dr}\left[r^2\nu(\frac{dW}{dr} - \frac{W}{r})\right] - \frac{1}{r^2}\frac{d}{dr}(r^2\overline{vw}) \ , \tag{36}$$

and the corresponding k-ϵ equations become

$$0 = \frac{1}{r}\frac{d}{dr}\left[r(\nu + \nu_t)\frac{dk}{dr}\right] - \overline{uv}\frac{dU}{dr} - \overline{vw}(\frac{dW}{dr} - \frac{W}{r}) - \epsilon - \frac{2\nu k}{(R-r)^2} \ , \tag{37}$$

$$0 = \frac{1}{r}\frac{d}{dr}\left[r(\nu + \frac{\nu_t}{\sigma_\epsilon})\frac{d\epsilon}{dr}\right] - C_1\frac{\epsilon}{k}\overline{uv}\frac{dU}{dr} - C_1\frac{\epsilon}{k}\overline{vw}(\frac{dW}{dr} - \frac{W}{r}) - C_2 f_1\frac{\epsilon^2}{k}$$

$$- \frac{2\nu\epsilon}{(R-r)^2}\, e^{-C_4(R-r)u_*/\nu} \ . \tag{38}$$

The boundary conditions are

$$U = k = \epsilon = 0, \ W = W_o \ \text{ at } \ r = R, \tag{39}$$

$$W = 0 \ , \ \frac{dU}{dr} = \frac{dk}{dr} = \frac{d\epsilon}{dr} = 0 \qquad \text{at} \qquad r = 0 \ .$$

If the equilibrium ASM with Rotta's return-to-isotropy model is used to determine $\overline{uv}$ and $\overline{vw}$, then the component equations for $\overline{u_i u_j}$ can be obtained from (11) and are:

$$- C_1\frac{\epsilon}{k}(\overline{u^2} - \frac{2}{3}k) - 2\overline{uv}\frac{dU}{dr} - \frac{2}{3}\epsilon = 0 \ , \tag{40}$$

$$- C_1\frac{\epsilon}{k}(\overline{v^2} - \frac{2}{3}k) + 4\overline{vw}\,\frac{W}{r} - \frac{2}{3}\epsilon = 0 \ , \tag{41}$$

$$- C_1\frac{\epsilon}{k}(\overline{w^2} - \frac{2}{3}k) - 2\overline{vw}(\frac{dW}{dr} - \frac{W}{r}) - 4\overline{vw}\,\frac{W}{r} - \frac{2}{3}\epsilon = 0 \ , \tag{42}$$

$$- C_1\frac{\epsilon}{k}\overline{uv} - \overline{v^2}\frac{dU}{dr} + 2\overline{uw}\,\frac{W}{r} = 0 \ , \tag{43}$$

$$- C_1\frac{\epsilon}{k}\overline{vw} - \overline{v^2}(\frac{dW}{dr} - \frac{W}{r}) + 2(\overline{w^2} - \overline{v^2})\,\frac{W}{r} = 0 \ , \tag{44}$$

$$- C_1\frac{\epsilon}{k}\overline{uw} - \overline{uv}(\frac{dW}{dr} - \frac{W}{r}) - 2\overline{uv}\,\frac{W}{r} - \overline{vw}\frac{dU}{dr} = 0 \ . \tag{45}$$

If it is further assumed that when fully-developed flow is established, a solid-body rotation exists in the fluid, then

$$W = \frac{W_o r}{R} \ , \tag{46}$$

and it follows from (36) that $\overline{vw} \equiv 0$. With these simplifications, (35) can be integrated to give (17) and (37) and (38) reduce to (14) and (15) respectively. The solution of (40) to (45) then gives

$$\overline{v^2} = \overline{w^2} = \frac{C_1 - 1}{C_1}\,\frac{2}{3}k \ , \tag{47}$$

$$\overline{u^2} = \frac{C_1 - 1}{C_1}\,\frac{2}{3}k - \frac{2k}{C_1\epsilon}\,\overline{uv}\frac{dU}{dr} \ , \tag{48}$$

$$- \overline{uw} = \frac{2k}{C_1\epsilon}\,\overline{uv}\frac{W_o}{R} \ , \tag{49}$$

$$- \overline{uv} = \frac{C_1 - 1}{C_1^{\,2}}\,\frac{2}{3}\,\frac{k^2}{\epsilon}\left[\frac{1}{1 + \frac{4k^2}{C_1^{\,2}\epsilon^2}(\frac{W_o}{R})^2}\right]\frac{dU}{dr} \ . \tag{50}$$

Therefore, W_o influences $\overline{uv}$ according to (50) and $\overline{uv}$ in turn affects U, $\overline{u^2}$, k and ϵ. The problem of fully-developed turbulent flow in a rotating pipe is described by equations (14), (15), (17) and (47) - (50). These equations are solved by the same technique discussed in Section 4. The boundary conditions are given by (39) rather than by (23) and (24).

6.2 Results

Since there are no measurements available for comparison with the present calculations, only parametric studies are carried out. In order to evaluate the effects of rotation on the turbulence field, the rotation calculations should be carried out with a known condition for the non-rotating case. Therefore, the Laufer and Schildknecht et al experiments are selected as the known non-rotating case and parametric studies on the effects of rotation are carried out with these cases as the base. Three different calculations are performed. These are $W_o = .105U_o$, $.21U_o$ and $.42U_o$, and the corresponding Ω are 24 RPM, 48 RPM and 96 RPM, respectively. The results are shown in Figure 7 for comparison with the zero rotation case.

In general, rotation has a great influence on the flow even in the fully-developed state. The effects of rotation on the mean flow are clearly evident in the pipe core (Figures 7a and 7b) and it tends to decrease the extent of the log-law region as Ω increases. Also, the turbulent kinetic energy in the pipe core is increased by flow rotation because mixing is being promoted due to the action of the centrifugal forces. At very high rotation, i.e. Ω = 96 RPM, k remains fairly constant in the pipe

core after the maximum value is reached near the pipe wall (Figure 7d). Similar trends are also noted for other turbulence properties (Figures 7e-g). However, since $\overline{uv}$ remains unaffected by Ω in a fully-developed flow (Figure 7c), $\overline{uv}/k$ decreases with rotation (Figure 7h) and the region where $\overline{uv}/k$ is constant disappears once there is rotation in the pipe. This shows that the assumption, $\overline{uv}/k$ = constant over a substantial portion of the pipe, normally invoked by turbulence modellers for simple turbulent flows is not valid for rotating turbulent flows. Finally, the shear stress $\overline{uw}$ is not small, and dependent on Ω, can even be larger than $\overline{uv}$ (Figure 7i). The maximum of $\overline{uw}$ does not occur very near the pipe wall as in the case of $\overline{uv}$. It occurs about half-way between the wall and the pipe center.

7. Conclusions

A low-Reynolds-number turbulence closure for the full set of Reynolds-stress equations is formulated. The formulation is based on a gradient diffusion model for turbulent diffusion, conventional high-Reynolds-number model for pressure redistribution and a modified dissipation model that accounts for viscosity effects near a rigid wall. Validation of the closure model is carried out with fully-developed turbulent pipe flows at two different Reynolds number. In general, the models give good results for U, $\overline{uv}$, k and ϵ, but fails to reproduce the behaviour of the normal turbulent stresses. The failings of the model are even more evident when the structure parameters, $\overline{u_i u_i}/k$, are compared and are especially noticeable in the near wall region. These discrepancies cannot be erased by modifying the redistribution model to account for the reduced turbulence energy transfer from the streamwise direction to that normal to a wall as suggested by Launder et al. (1975). Neither can the correlations between prediction and measurements be improved by the inclusion of mean-strain terms in the modelling of the pressure redistribution terms. Furthermore, it is found that once the gradient diffusion assumption is invoked, the calculated results are only slightly dependent on the diffusivity assumption. An isotropic diffusivity model will give results that are quite similar to those obtained by using a non-isotropic one.

All full-Reynolds-stress closure models examined show the same shortcomings when applied to calculate fully-developed

turbulent pipe flows. They all fail to predict the steep rise of the normal stresses near the pipe wall and the isotropic behaviour of the turbulence field at the pipe center. However, the Launder et al model for pressure redistribution seems to provide better agreement with data concerning the prediction of the mean flow. In view of these results, it can be concluded that a closure model based on the Launder et al. model for the pressure redistribution and a non-isotropic gradient diffusion model gives the best overall results for fully-developed turbulent pipe flow calculations.

The same conclusion cannot be reached when algebraic stress closures are considered, however. Here, Launder et al.'s model gives results that are less appealling than those obtained with Rotta's model. As before, the manner in which turbulent diffusion is modelled has little effect on this overall conclusion; that is,it is true for equilibrium ASM as well as for non-equilibrium ASM. The algebraic stress closures give results that are closely similar to those obtained from full Reynolds-stress closures. Only minor differences appear in the predictions of the stress ratios, $\overline{u_i u_j}/k$. Otherwise the performance of the ASM closures is just as good. The same can also be said of the two-equation closure. Even then, the best overall prediction of the logarithmic law-of-the-wall is provided by the full Reynolds stress model using a non-isotropic diffusion model and the Launder et al. model for pressure redistribution.

Finally, a parametric study of rotation effects on fully-developed turbulent pipe flows reveals that increasing rotation

decreases the extent of the log-law region. Also, rotation tends to increase the overall level of turbulent kinetic energy in the pipe core, as well as other turbulent properties.

References

Afzal, N. and Yajnik, K. 1973 Analysis of turbulent pipe and channel flows at moderately large Reynolds number. J. Fluid Mech. 61, 23-31.

Bissonnette, L. and Mellor, G. L. 1974 Experiments on the behaviour of an axisymmetric turbulent boundary layer with a sudden circumferential strain. J. Fluid Mech. 63, 369-413.

Chien, K. Y. 1980 Predictions of channel and boundary layer flows with a low-Reynolds-number two-equation model of turbulence. AIAA-80-0134.

Eckelman, H. 1970 Experimentelle Untersuchungen in einer turbulumten Kanalstromung mit starken viskosen Wandochichten. Mitt. Max-Planck Inst. f. Stromungsforschung, Gottiugen, No. 48.

Gibson, M. M. and Launder, B.E. 1978 Ground effects on pressure fluctuations in the atmospheric boundary layer. J. Fluid Mech. 86, 491-511.

Gibson, M. M. 1978 An algebraic stress and heat-flux model for turbulent shear flow with streamline curvature. Int. J. Heat Mass Transfer 21, 1609-1617.

Gibson, M. M. and Rodi, W. 1981 A Reynolds-stress closure model of turbulence applied to the calculation of a highly curved mixing layer. J. Fluid Mech. 103, 161-182.

Hanjalic, K. and Launder, B. E. 1972 A Reynolds-stress model of turbulence and its application to thin shear flows. J. Fluid Mech. 52, 609-638.

Hanjalic, K. and Launder, B. E. 1976 Contribution towards a Reynolds-stress closure for low-Reynolds-number turbulence. J. Fluid Mech. 74, 593-610.

Hinze, J. O. 1959 Turbulence. McGraw-Hill Book Co., New York.

Irwin, H. P. A. H. and Smith, P. A. 1975 Prediction of the effect of streamline curvature on turbulence. Phy. Fluids 18, 624-630.

Jones, W. P. and Launder, B. E. 1972a Some properties of sink-flow turbulent boundary layers. J. Fluid Mech. 56, 337-351.

Jones, W. P. and Launder, B. E. 1972b The prediction of laminarization with a two-equation model of turbulence. Int. J. Heat Mass Transfer 15, 301-314.

Kolmogorov, A. N. 1941 The local structure of turbulence in incompressible viscous fluid for very large Reynolds numbers. C. R. Aka. Nank. SSSR 30, 301-305.

Laufer, J. 1954 The structure of turbulence in fully-developed pipe flow. N.A.C.A. Rept. 1174.

Launder, B. E., Morse, A., Rodi, W. and Spalding, D. B. 1972 Prediction of free shear flows - a comparison of the performance of six turbulence models. N.A.S.A. SP-321, 361-426.

Launder, B. E., Reece, G. J. and Rodi, W. 1975 Progress in the development of a Reynolds-stress turbulence closure. J. Fluid Mech. 68, 537-566.

Leschziner, M. A. and Rodi, W. 1981 Calculation of annular and twin parallel jets using various discretization schemes and turbulence-model variations. J. Fluids Eng. 103, 352-360.

Mellor, G. L. and Herring, H. J. 1973 A survey of the mean turbulent field closure models. AIAA J. 11, 590-599.

Mellor, G. L. and Yamada, T. 1974 A hierarchy of turbulence closure models for planetary boundary layers. J. Atmos. Sci. 31, 1791-1806.

Na, T. Y. 1979 Computational Methods in Engineering Boundary Value Problems. Academic Press, New York.

Patel, V. C. and Head, M. C. 1969 Some observations of skin friction and velocity profiles in fully developed pipe and channel flows. J. Fluid Mech. 38, 181-201.

Rodi, W. 1976 A new algebraic relation for calculating the Reynolds stresses. ZAMM 56, 219-221.

Rotta, J. C. 1951 Statistische Theorie Nichthomogener Turbulenz. Zeit. fur Physik 129, 547-572; 131, 51-77.

Schildknecht, M., Miller, J. A. and Meier, G. E. A. 1979 The influence of suction on the structure of turbulence in fully-developed pipe flow. J. Fluid Mech. 90, 67-107.

So, R. M. C. 1975 A turbulence velocity scale for curved shear flows. J. Fluid Mech. 70, 37-57.

So, R. M. C. 1977 Turbulent velocity scales for swirling flows. Turbulence in Internal Flows, edited by S. N. B. Murthy, Hemispheric Publishing Corp., Washington, 347-369.

So, R. M. C. and Mellor, G. L. 1978 Turbulent boundary layers with large streamwise curvature effects. ZAMP 29, 54-74.

Stratford, B. S. 1959 An experimental flow with zero skin friction throughout its region of pressure rise. J. Fluid Mech. 5, 17-35.

Yao, L. S. and So, R. M. C. 1985 Turbulence structure in the entry region of a curved pipe or in a short bend. Submitted to J. Fluid Mech.

Table 1 Model constants and damping functions

Constants or Functions	Redistribution Model	
	Launder et al. (1975)	Rotta (1951)
C_1	1.5	6.22
C_2	.4	--
α_1	$(C_2 + 8)/11$	0
β_1	$(8C_2 - 2)/11$	0
γ_1	$(30C_2 - 2)/55$	0
C_{1w}	.050	0
C_{2w}	.006	0
C_s	$.11f_2$	$.11f_2$
σ_ϵ	1.3	1.3
$C_{\epsilon 1}$	1.35	1.35
$C_{\epsilon 2}$	1.8	1.8
C_μ	.09	.09
C_3	.0115	.0115
C_4	.5	.5
C_5	.008	.01
f_1	$1 - \frac{2}{9} e^{-(k^2/6\nu\epsilon)^2}$	
f_2	$1 - e^{-C_3 u_* (R-r)/\nu}$	
f_3	$1 - e^{-C_5 u_* (R-r)/\nu}$	

Table 2. A Comparison of the Calculated and Measured Constants in the Logarithmic Law-of-the-wall

		Laufer (1954)			Schildknecht et al. (1979)		
		α (κ)	β	U_o/u_*	α (κ)	β	U_o/u_*
Measured U		2.50 (0.40)	5.20	23.76	2.50 (.40)	5.45	22.25
U from measured $\overline{uv}$		2.60 (0.385)	5.00	22.29	2.53 (0.395)	5.90	21.23
Non-isotropic diffusion model	Rotta's model	2.65 (0.377)	5.00	22.69	2.66 (0.378)	5.31	21.08
	Launder et al.'s model	2.46 (0.406)	5.69	22.10	2.48 (0.403)	6.00	20.79
	Launder et al. + wall correction	2.62 (0.382)	5.53	23.04	2.82 (0.355)	4.97	21.65
Isotropic diffusion model	Rotta's model	2.62 (0.382)	5.00	22.60	2.69 (0.372)	5.00	20.79
	Launder et al's model	2.35 (0.426)	6.10	21.70	2.45 (0.408)	5.95	20.43
	Launder et al's + wall correction	2.30 (0.435)	6.97	22.40	2.42 (0.414)	6.72	21.06
Non-equilibrium turbulence	Rotta's model	2.56 (0.391)	6	23.21	2.65 (0.377)	5.81	21.55
	Launder et al.'s model	2.40 (0.417)	6.3	22.04	2.42 (0.413)	6.3	20.45
Equilibrium turbulence	Rotta's model	2.67 (0.375)	5.06	22.77	2.64 (0.379)	5.36	21.15
	Launder et al.'s model	2.47 (0.405)	4.63	21.27	2.51 (0.398)	4.78	19.78
	k-ϵ eq. closure	2.62 (0.382)	5.06	22.76	2.64 (0.379)	5.36	21.15

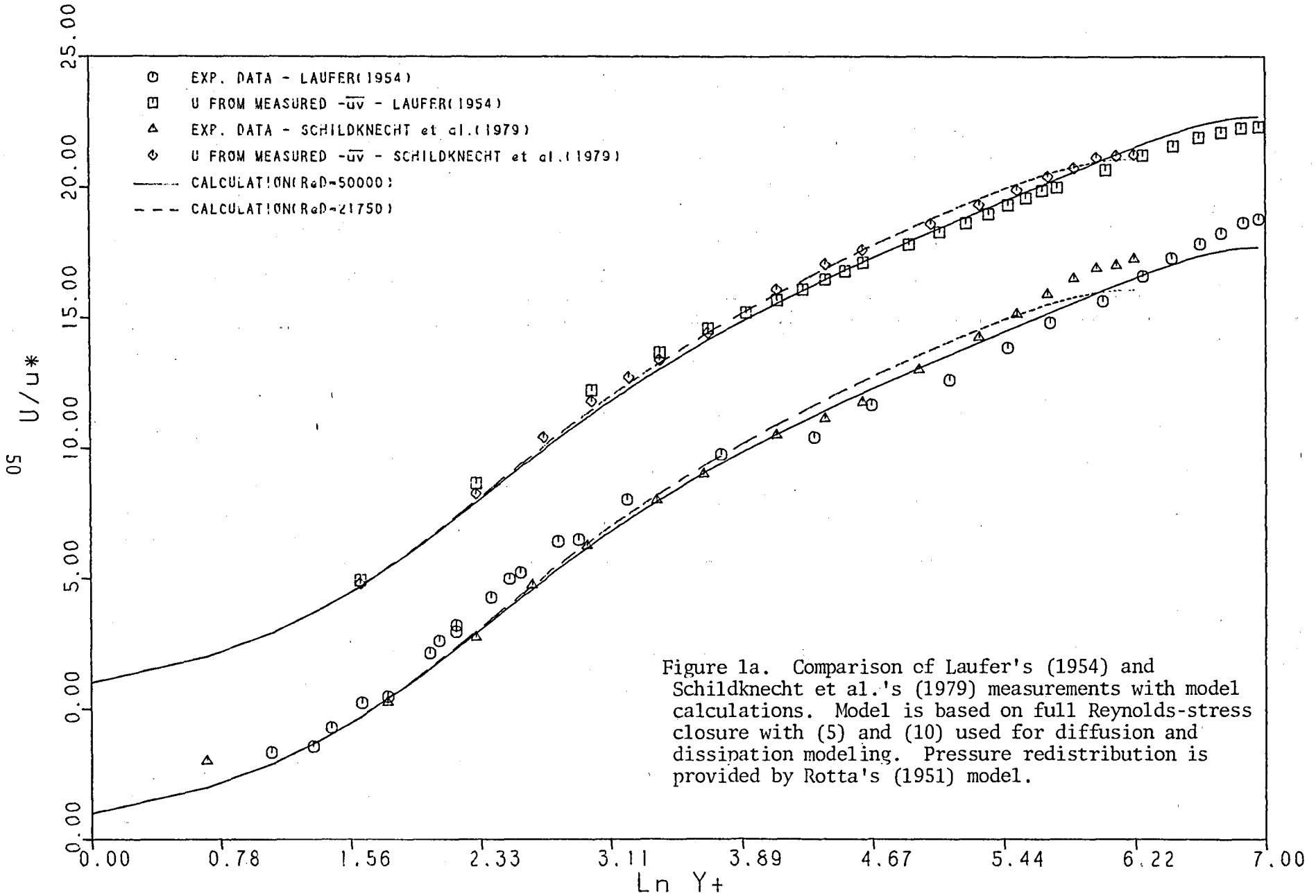

Figure 1a. Comparison of Laufer's (1954) and Schildknecht et al.'s (1979) measurements with model calculations. Model is based on full Reynolds-stress closure with (5) and (10) used for diffusion and dissipation modeling. Pressure redistribution is provided by Rotta's (1951) model.

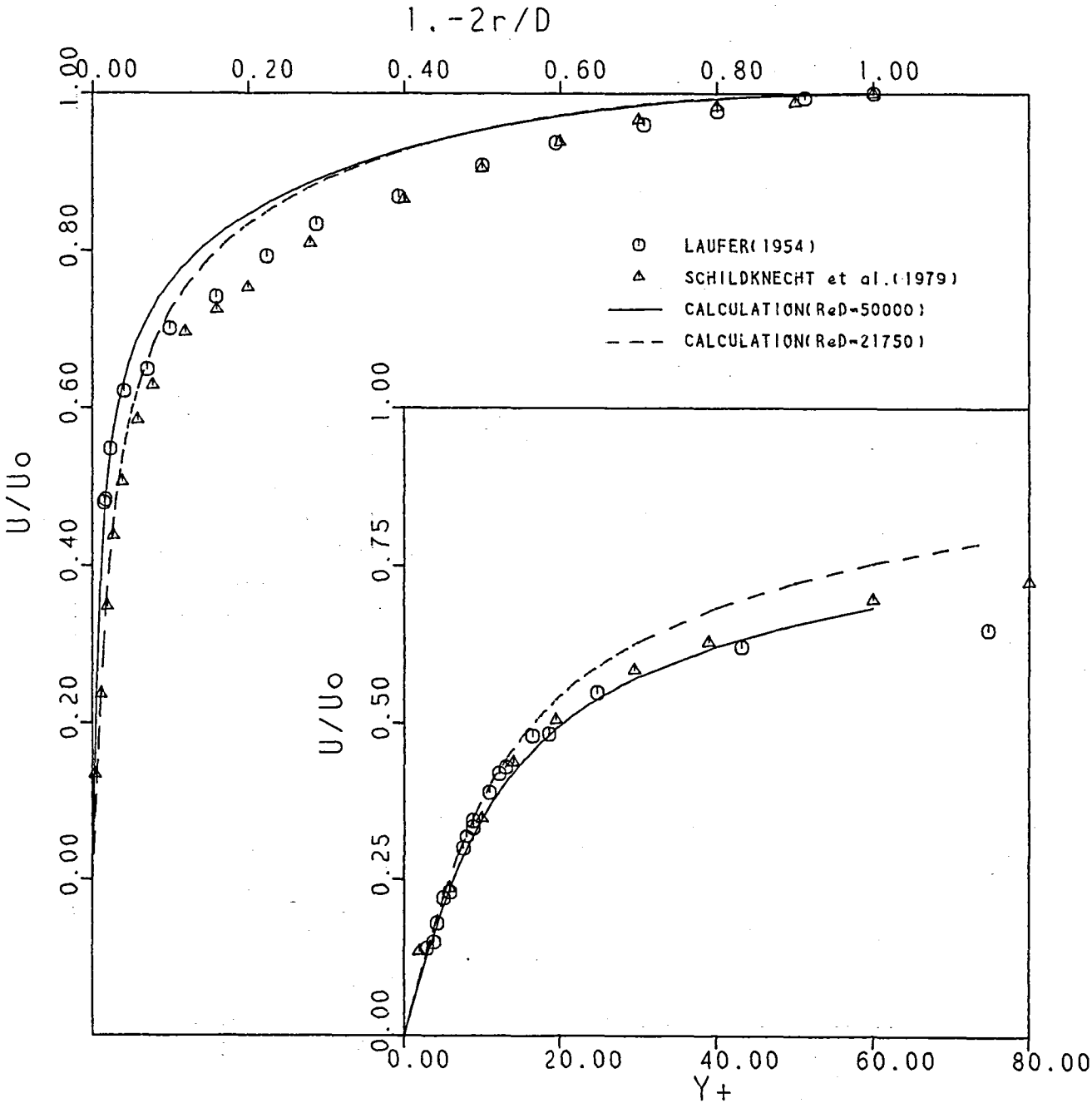
1.-2r/D
0.00
0.20
0.40
0.60
0.80
1.00
U/Uo
LAUFER(1954)
SCHILDKNECHT et al.(1979)
CALCULATION(ReD=50000)
CALCULATION(ReD=21750)
0.00
0.25
0.50
0.75
1.00
20.00
40.00
60.00
80.00
Y+

Figure 1b.

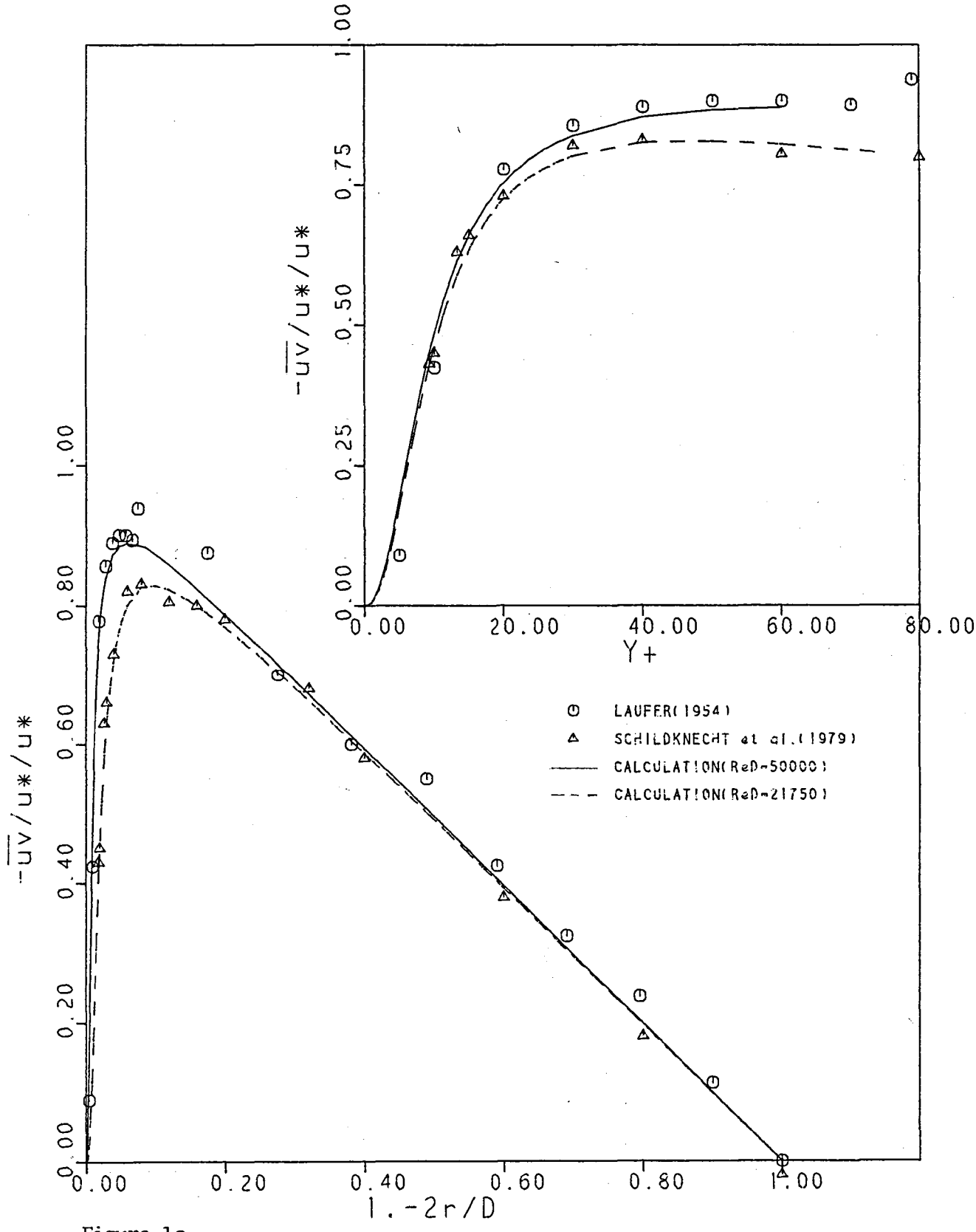
-uv/u*/u*
1.00
0.80
0.60
0.40
0.20
0.00
0.00
0.20
0.40
0.60
0.80
1.00
1.-2r/D
LAUFER(1954)
SCHILDKNECHT et al.(1979)
CALCULATION(ReD=50000)
CALCULATION(ReD=21750)
-uv/u*/u*
1.00
0.75
0.50
0.25
0.00
0.00
20.00
40.00
60.00
80.00
Y+

Figure 1c.

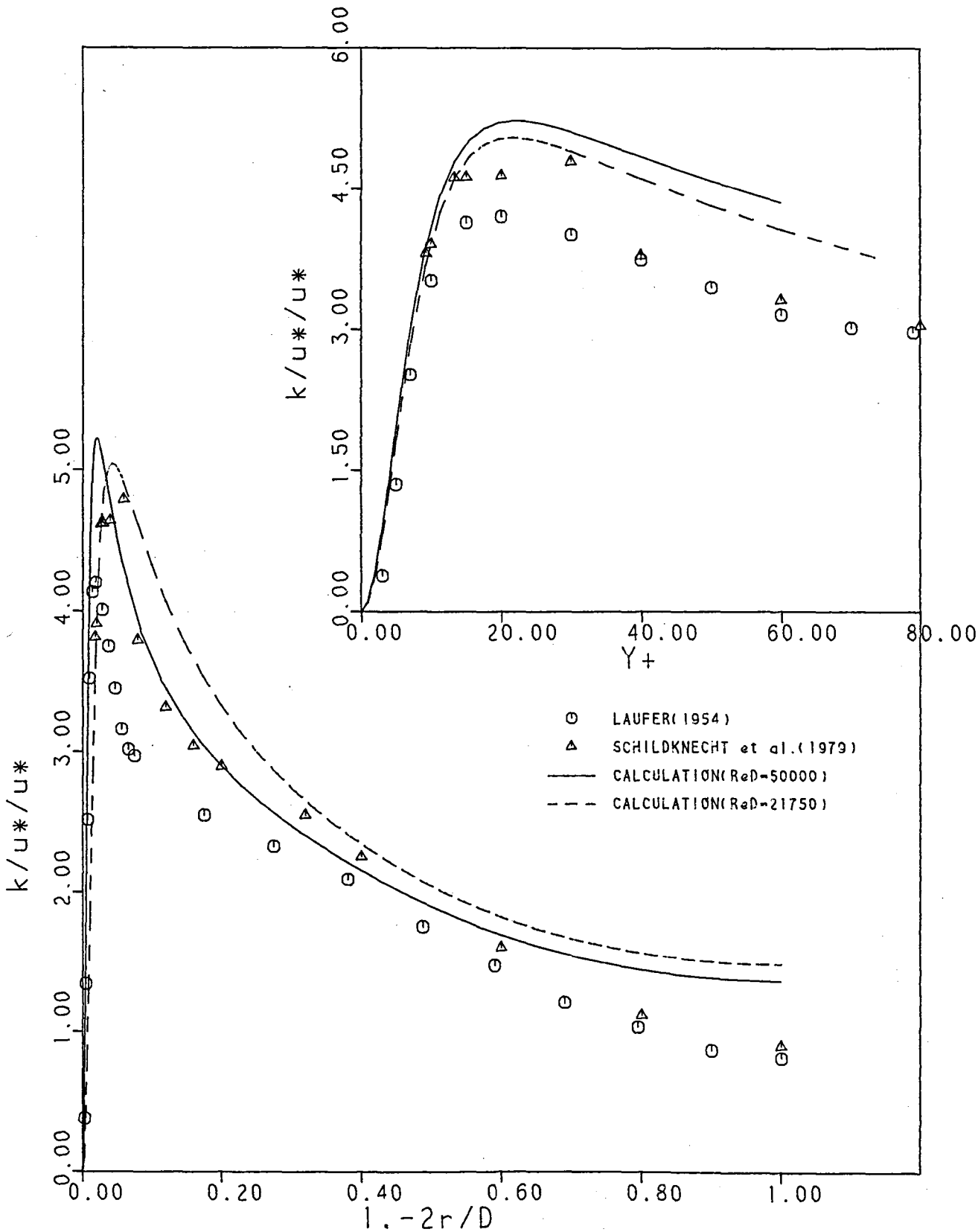
k/u*/u*
1.-2r/D
0.00
1.00
2.00
3.00
4.00
5.00
0.00
0.20
0.40
0.60
0.80
1.00
k/u*/u*
Y+
0.00
1.50
3.00
4.50
6.00
0.00
20.00
40.00
60.00
80.00
LAUFER(1954)
SCHILDKNECHT et al.(1979)
CALCULATION(ReD=50000)
CALCULATION(ReD=21750)

Figure 1d.

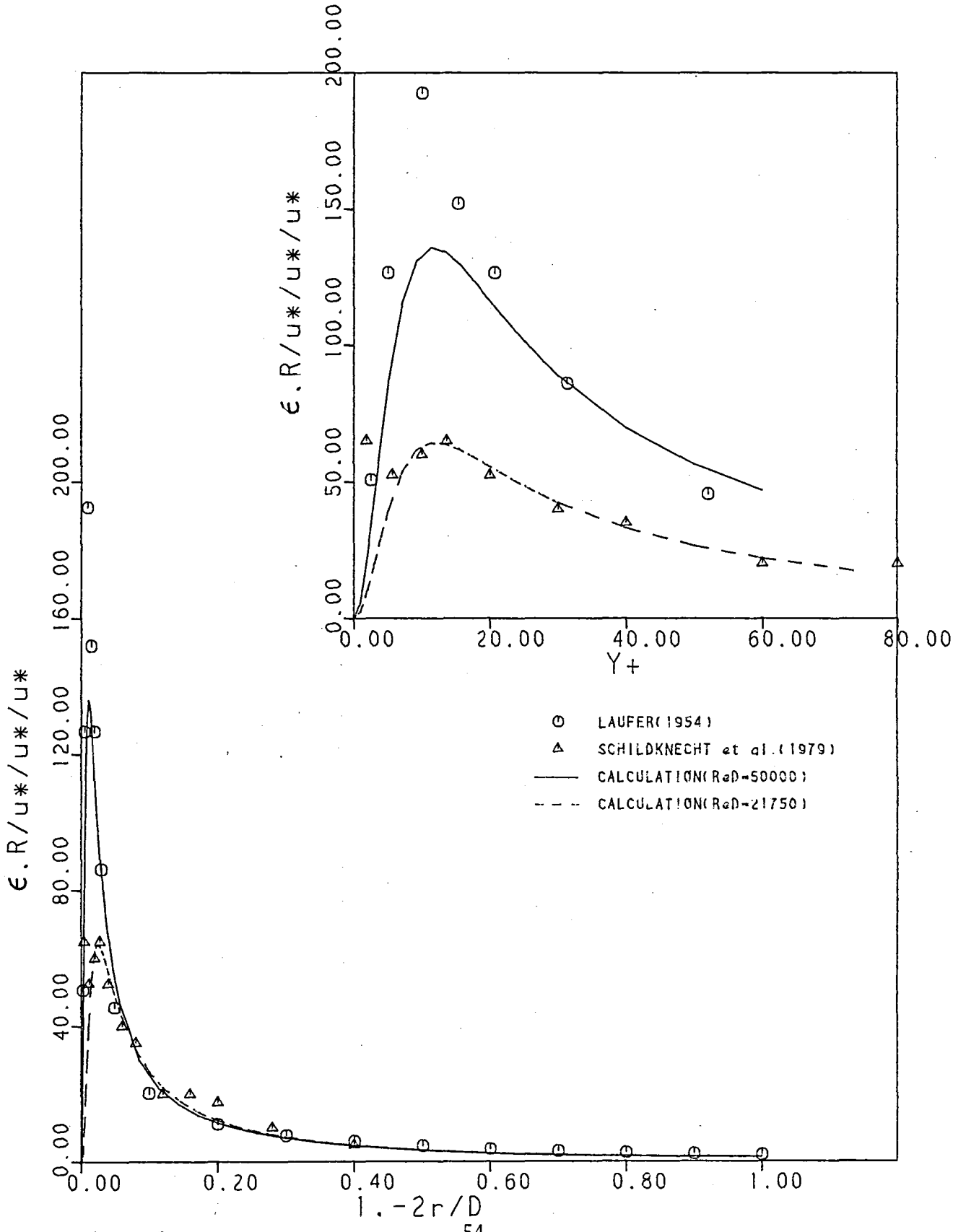
ε.R/u*/u*/u*
200.00
150.00
100.00
50.00
0.00
0.00
20.00
40.00
60.00
80.00
Y+
ε.R/u*/u*/u*
200.00
160.00
120.00
80.00
40.00
0.00
0.00
0.20
0.40
0.60
0.80
1.00
1.-2r/D
LAUFER(1954)
SCHILDKNECHT et al.(1979)
CALCULATION(ReD=50000)
CALCULATION(ReD=21750)

Figure 1e.

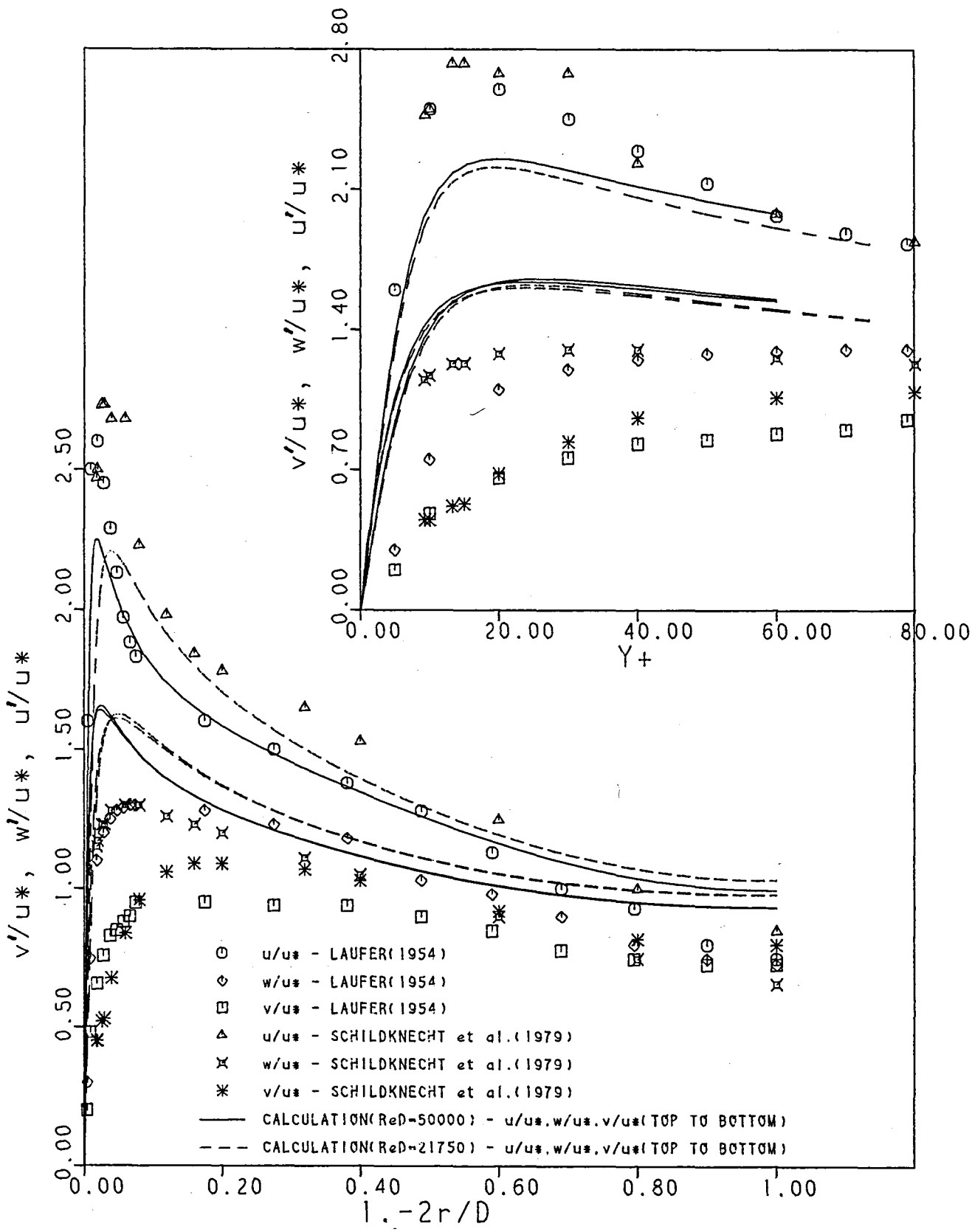
v'/u*, w'/u*, u'/u*
1.-2r/D
0.00
0.20
0.40
0.60
0.80
1.00
0.50
1.00
1.50
2.00
2.50
u/u* - LAUFER(1954)
w/u* - LAUFER(1954)
v/u* - LAUFER(1954)
u/u* - SCHILDKNECHT et al.(1979)
w/u* - SCHILDKNECHT et al.(1979)
v/u* - SCHILDKNECHT et al.(1979)
CALCULATION(ReD=50000) - u/u*,w/u*,v/u*(TOP TO BOTTOM)
CALCULATION(ReD=21750) - u/u*,w/u*,v/u*(TOP TO BOTTOM)
v'/u*, w'/u*, u'/u*
Y+
0.00
20.00
40.00
60.00
80.00
0.70
1.40
2.10
2.80

Figure 1f.

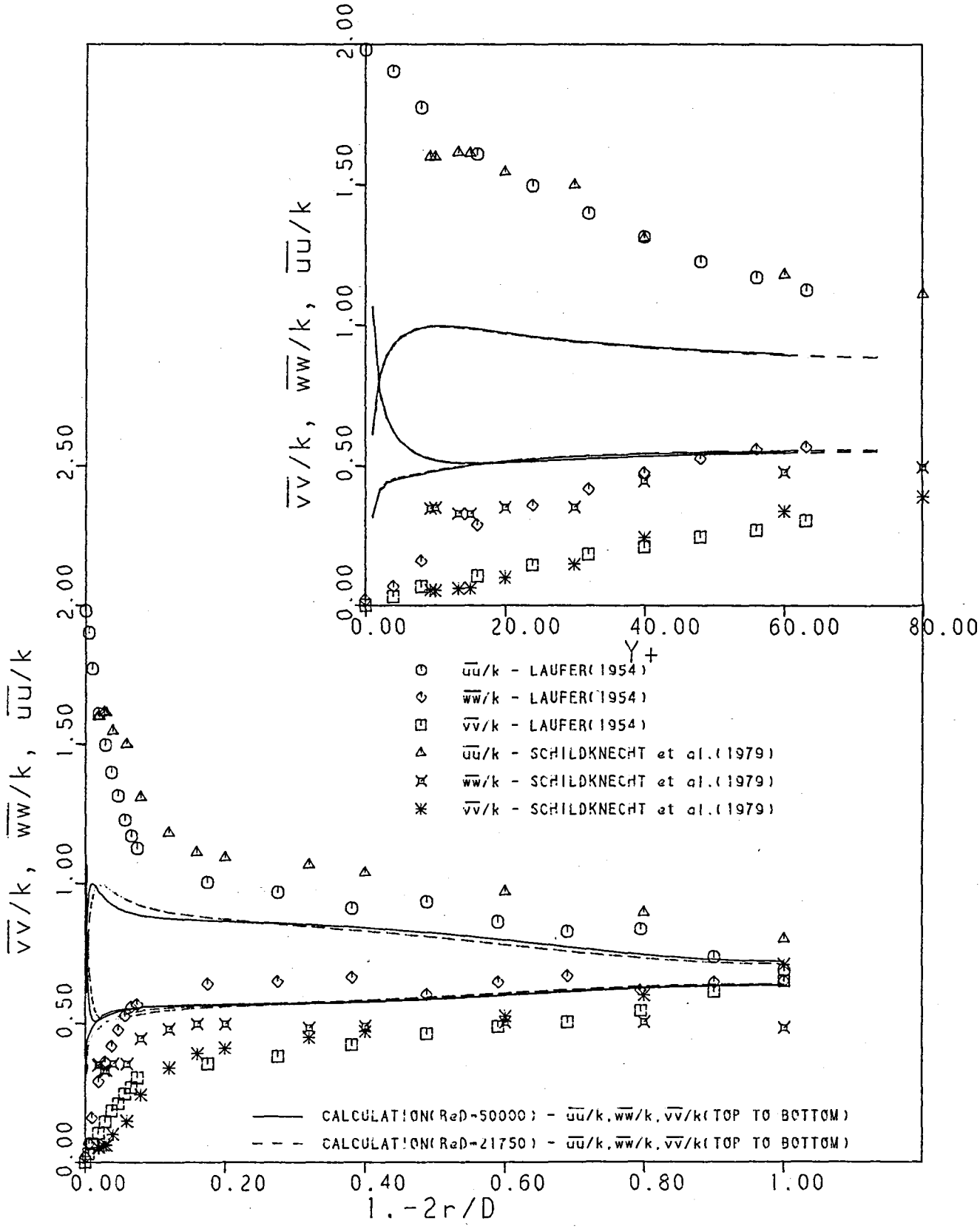
vv/k, ww/k, uu/k
1.-2r/D
0.00
0.20
0.40
0.60
0.80
1.00
0.50
1.00
1.50
2.00
2.50
Y+
0.00
20.00
40.00
60.00
80.00
uu/k - LAUFER(1954)
ww/k - LAUFER(1954)
vv/k - LAUFER(1954)
uu/k - SCHILDKNECHT et al.(1979)
ww/k - SCHILDKNECHT et al.(1979)
vv/k - SCHILDKNECHT et al.(1979)
CALCULATION(ReD=50000) - uu/k, ww/k, vv/k(TOP TO BOTTOM)
CALCULATION(ReD=21750) - uu/k, ww/k, vv/k(TOP TO BOTTOM)

Figure 1g.

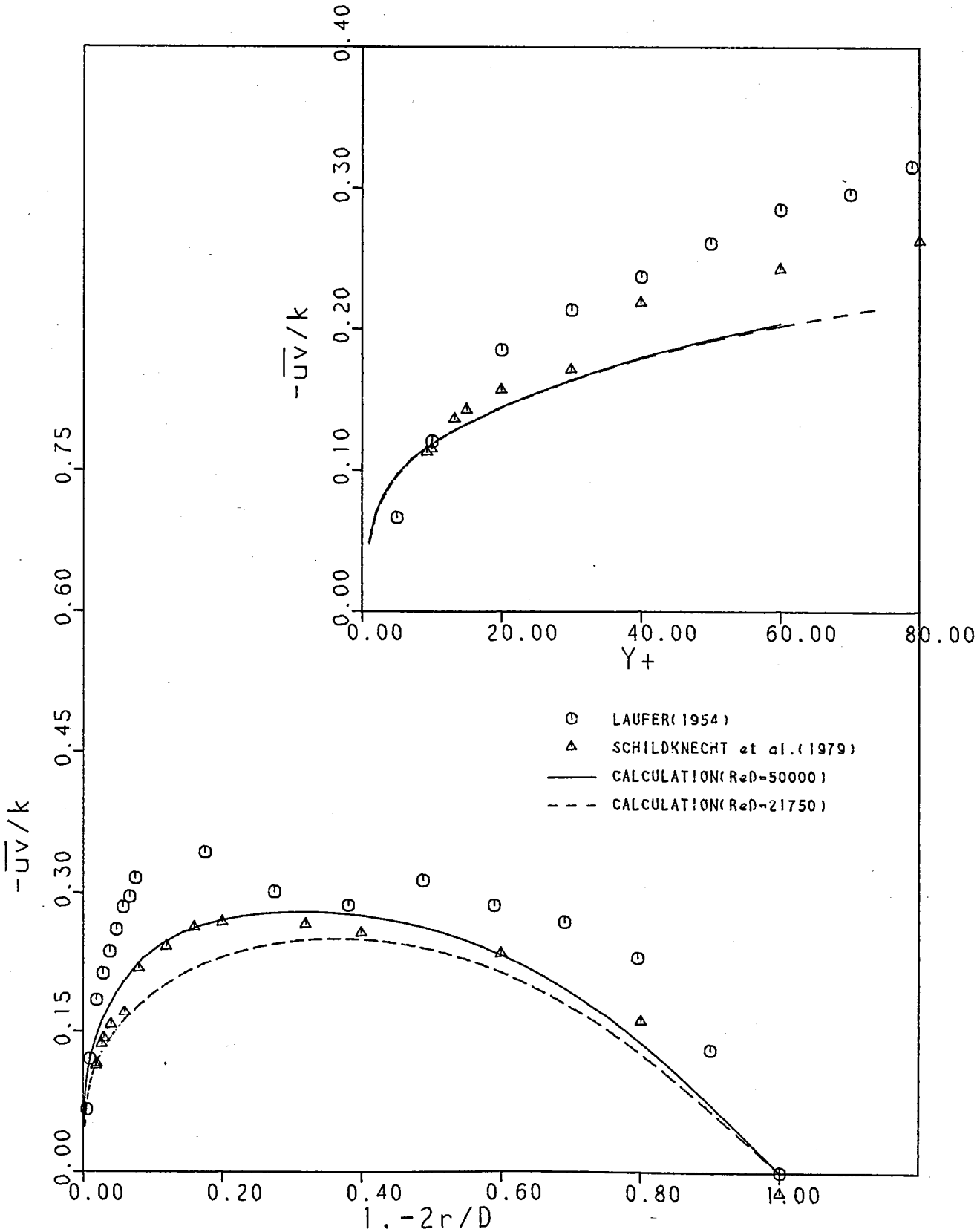
0.40
0.30
0.20
0.10
0.00
$-\overline{uv}/k$
0.00
20.00
40.00
60.00
80.00
Y+
0.75
0.60
0.45
0.30
0.15
0.00
$-\overline{uv}/k$
LAUFER(1954)
SCHILDKNECHT et al.(1979)
CALCULATION(ReD=50000)
CALCULATION(ReD=21750)
0.00
0.20
0.40
0.60
0.80
1.00
1.-2r/D

Figure 1h.

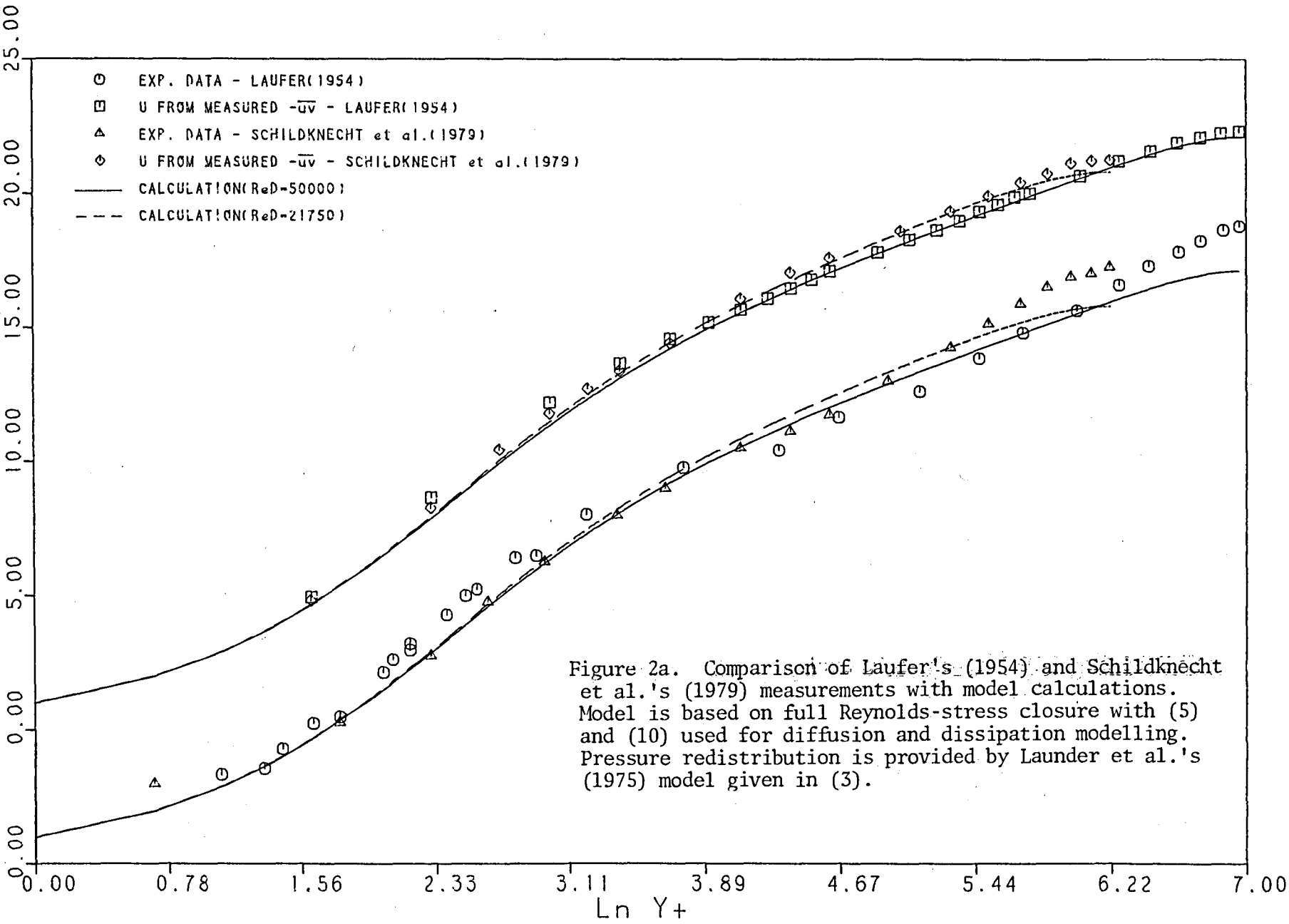

Figure 2a. Comparison of Laufer's (1954) and Schildknecht et al.'s (1979) measurements with model calculations. Model is based on full Reynolds-stress closure with (5) and (10) used for diffusion and dissipation modelling. Pressure redistribution is provided by Launder et al.'s (1975) model given in (3).

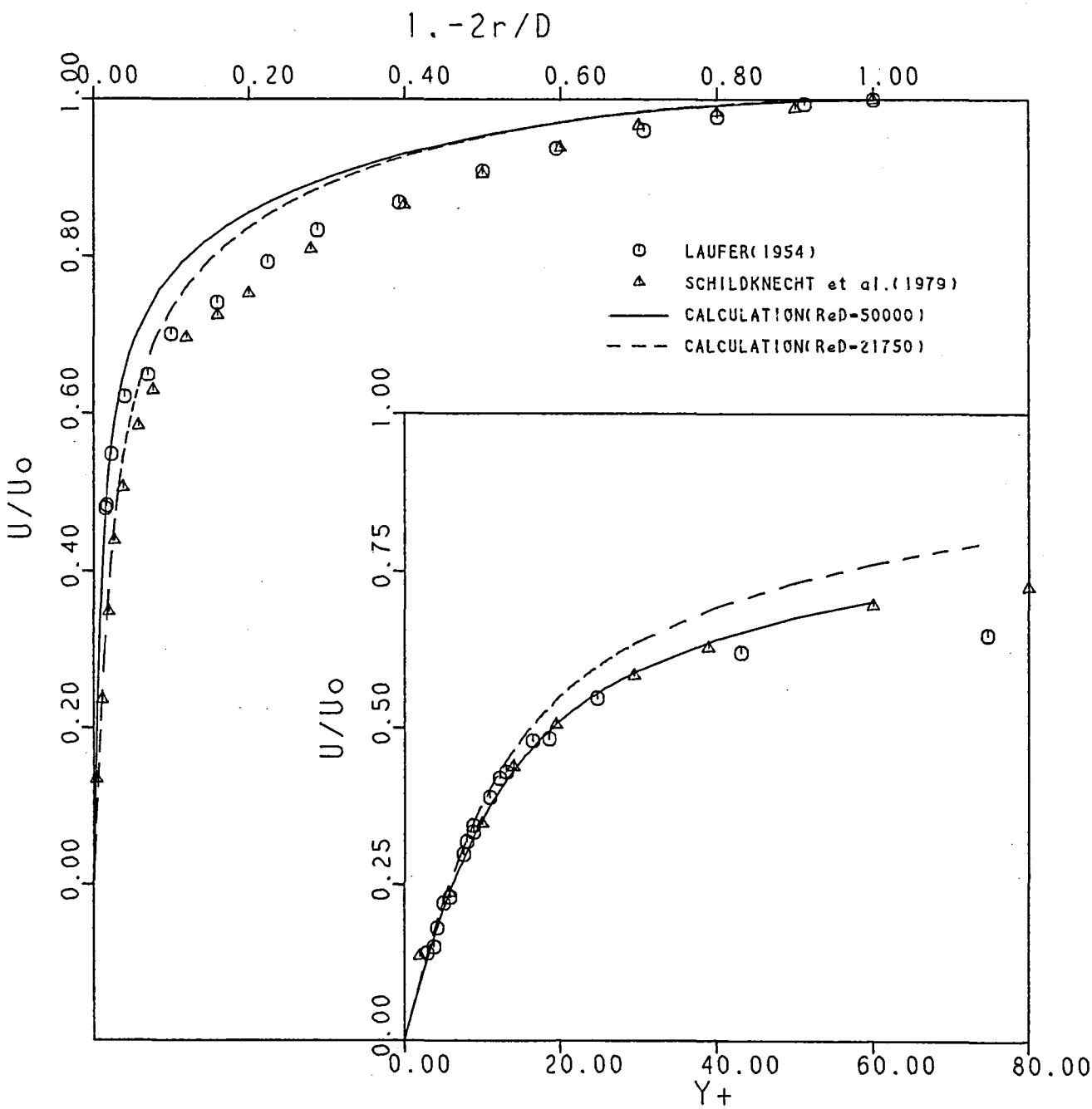
1.-2r/D
0.00
0.20
0.40
0.60
0.80
1.00
U/Uo
LAUFER(1954)
SCHILDKNECHT et al.(1979)
CALCULATION(ReD=50000)
CALCULATION(ReD=21750)
0.00
0.25
0.50
0.75
1.00
20.00
40.00
60.00
80.00
Y+

Figure 2b.

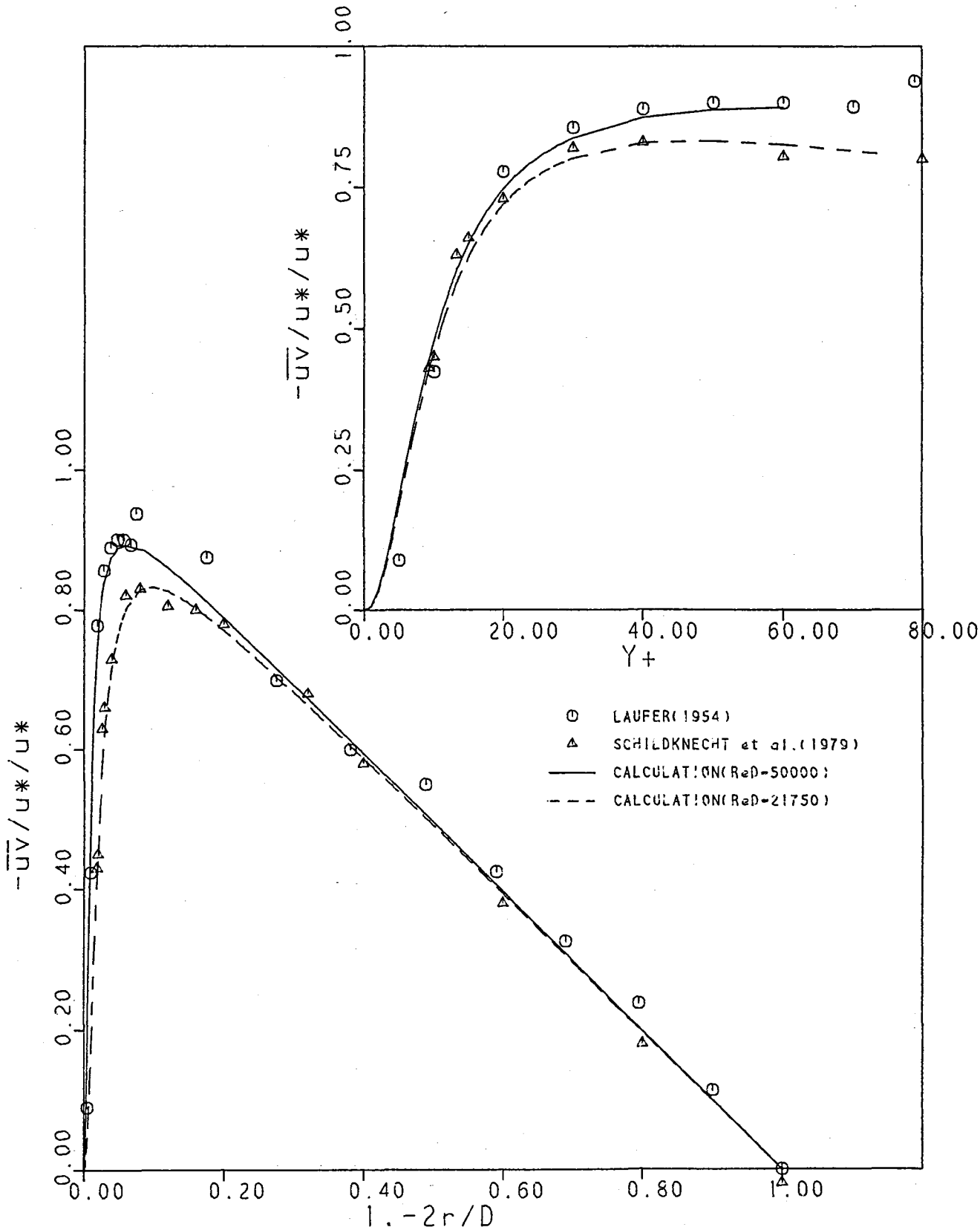
-uv/u*/u*
1.-2r/D
0.00
0.20
0.40
0.60
0.80
1.00
LAUFER(1954)
SCHILDKNECHT et al.(1979)
CALCULATION(ReD=50000)
CALCULATION(ReD=21750)
-uv/u*
Y+
0.00
0.25
0.50
0.75
1.00
20.00
40.00
60.00
80.00

Figure 2c.

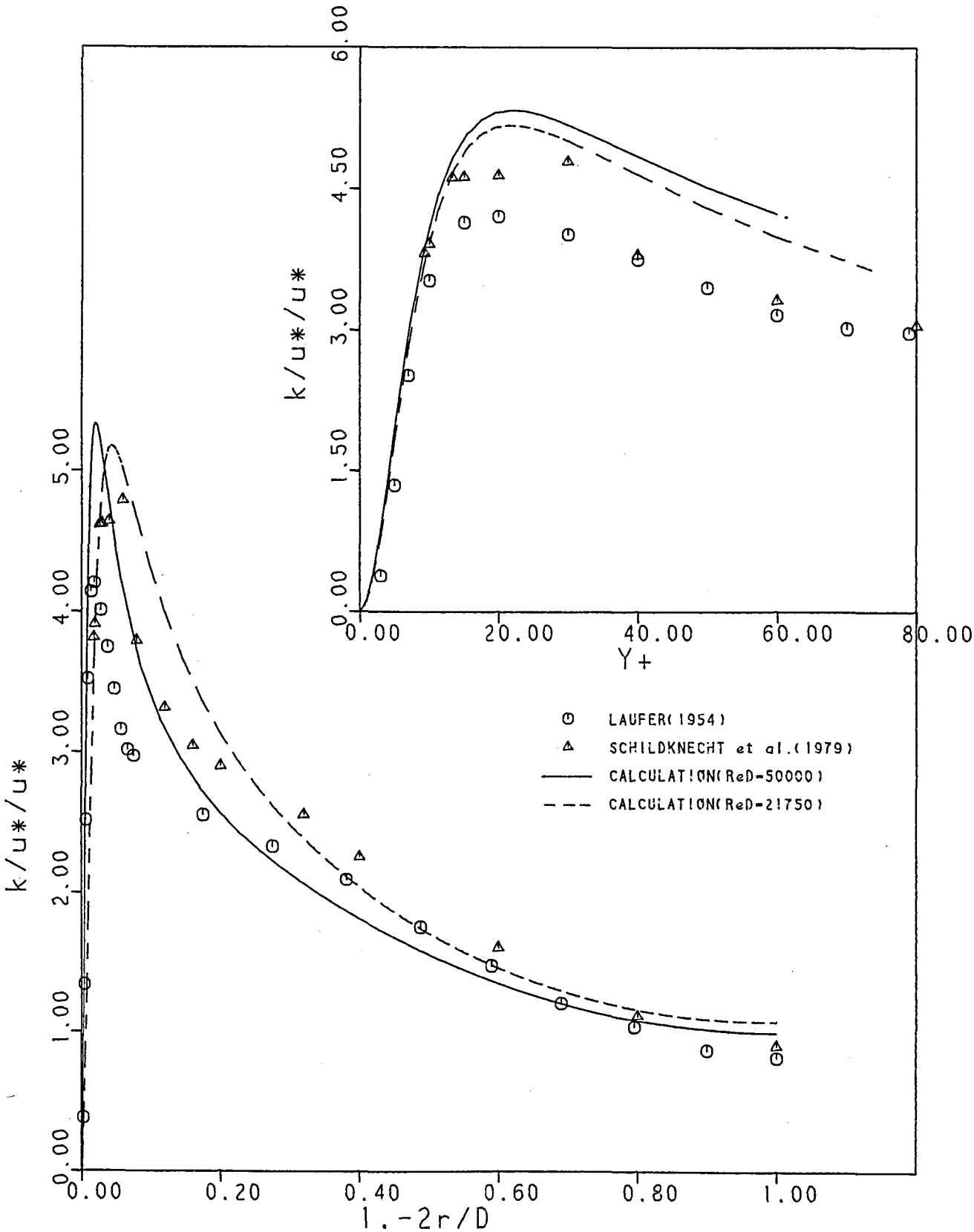
k/u*/u*
1.-2r/D
0.00
0.20
0.40
0.60
0.80
1.00
1.00
2.00
3.00
4.00
5.00
LAUFER(1954)
SCHILDKNECHT et al.(1979)
CALCULATION(ReD=50000)
CALCULATION(ReD=21750)
k/u*/u*
Y+
0.00
20.00
40.00
60.00
80.00
1.50
3.00
4.50
6.00

Figure 2d.

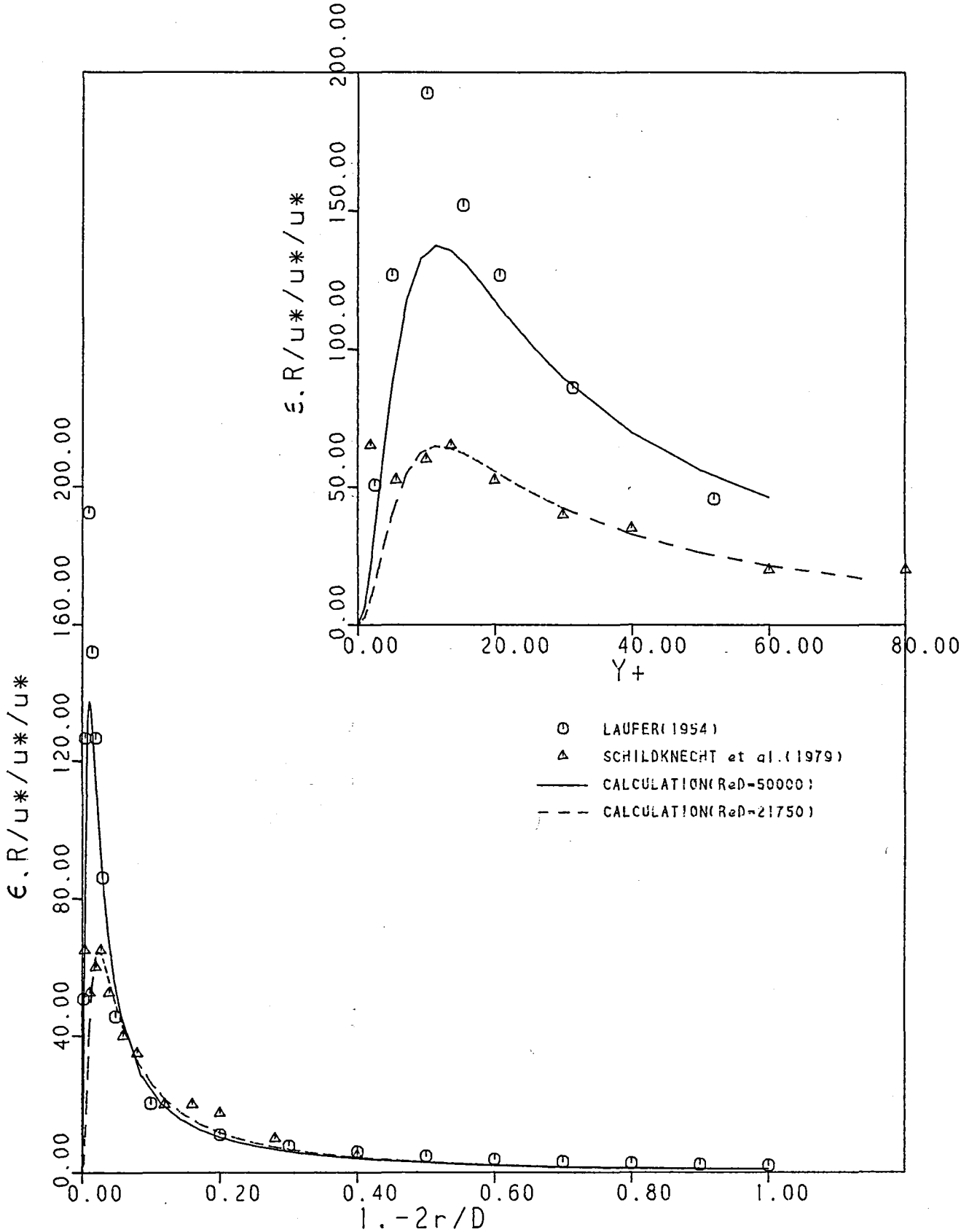
ε.R/u*/u*/u*
0.00
40.00
80.00
120.00
160.00
200.00
0.00
0.20
0.40
0.60
0.80
1.00
1.-2r/D
LAUFER(1954)
SCHILDKNECHT et al.(1979)
CALCULATION(ReD=50000)
CALCULATION(ReD=21750)
ε.R/u*/u*/u*
0.00
50.00
100.00
150.00
200.00
0.00
20.00
40.00
60.00
80.00
Y+

Figure 2e.

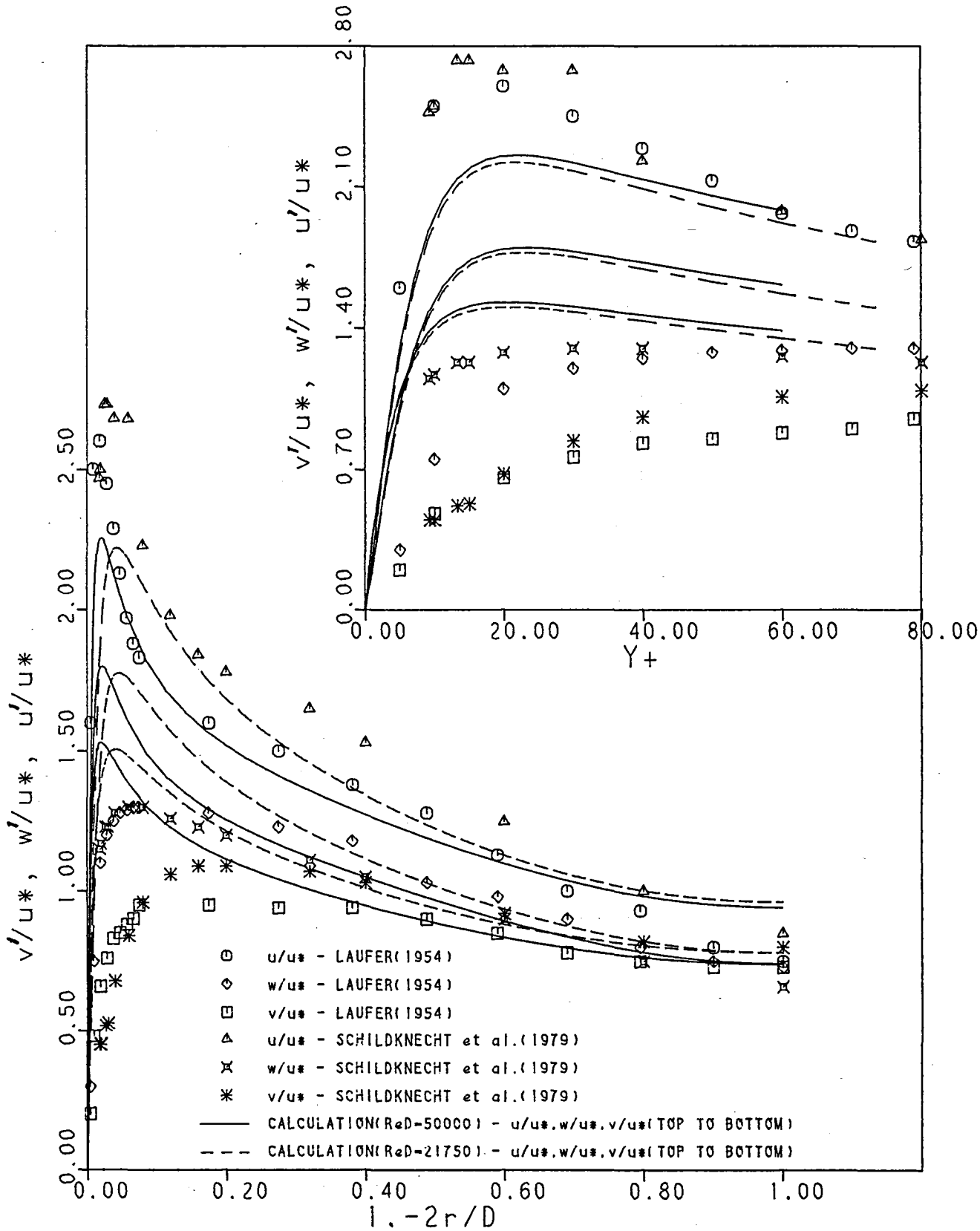
v'/u*, w'/u*, u'/u*
1.-2r/D
0.00
0.20
0.40
0.60
0.80
1.00
0.50
1.00
1.50
2.00
2.50
u/u* - LAUFER(1954)
w/u* - LAUFER(1954)
v/u* - LAUFER(1954)
u/u* - SCHILDKNECHT et al.(1979)
w/u* - SCHILDKNECHT et al.(1979)
v/u* - SCHILDKNECHT et al.(1979)
CALCULATION(ReD=50000) - u/u*,w/u*,v/u*(TOP TO BOTTOM)
CALCULATION(ReD=21750) - u/u*,w/u*,v/u*(TOP TO BOTTOM)
v'/u*, w'/u*, u'/u*
Y+
0.00
20.00
40.00
60.00
80.00
0.70
1.40
2.10
2.80

Figure 2f.

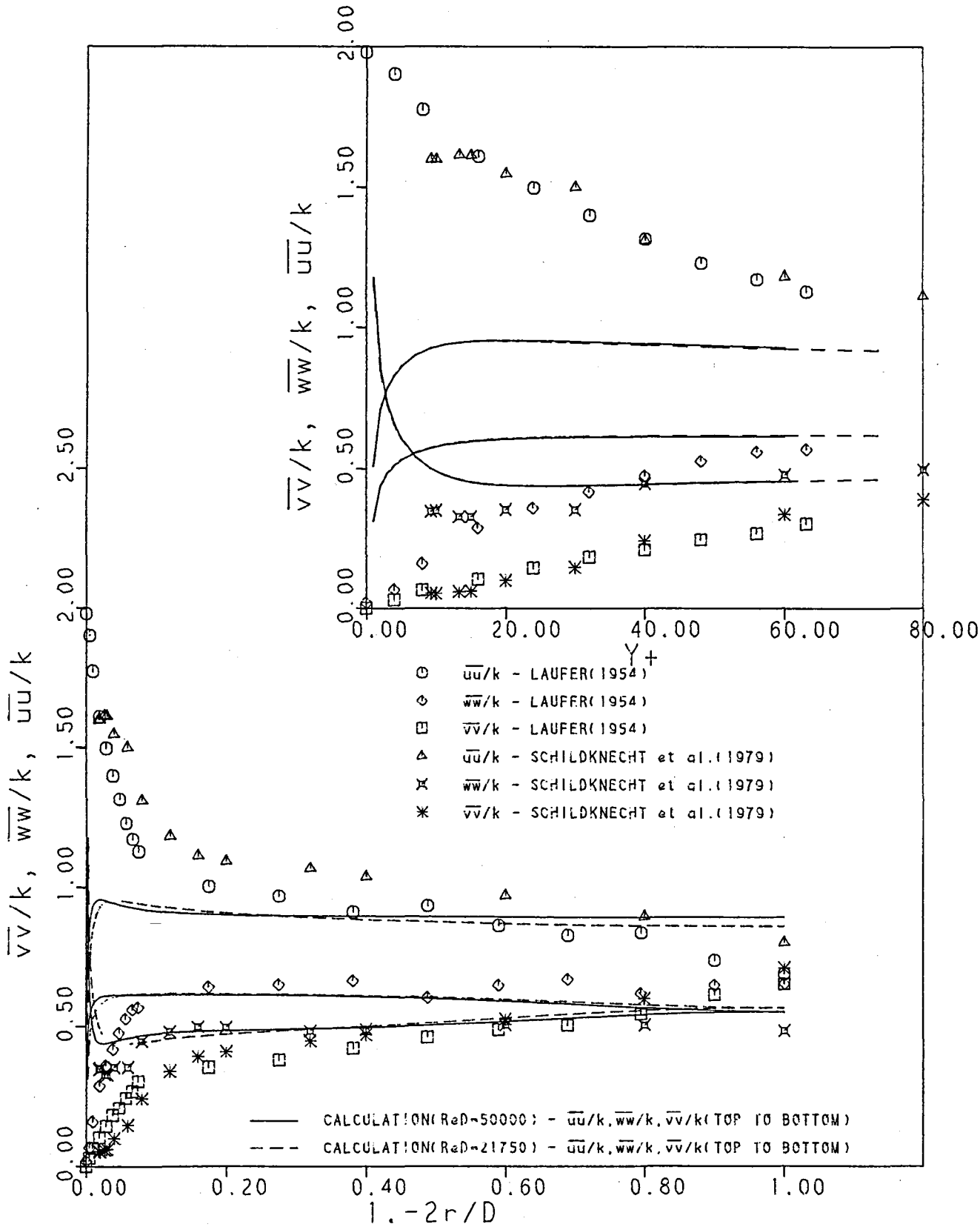
vv/k, ww/k, uu/k
1.-2r/D
0.00
0.20
0.40
0.60
0.80
1.00
0.50
1.00
1.50
2.00
2.50
uu/k - LAUFER(1954)
ww/k - LAUFER(1954)
vv/k - LAUFER(1954)
uu/k - SCHILDKNECHT et al.(1979)
ww/k - SCHILDKNECHT et al.(1979)
vv/k - SCHILDKNECHT et al.(1979)
CALCULATION(ReD=50000) - uu/k,ww/k,vv/k(TOP TO BOTTOM)
CALCULATION(ReD=21750) - uu/k,ww/k,vv/k(TOP TO BOTTOM)
vv/k, ww/k, uu/k
Y+
0.00
20.00
40.00
60.00
80.00
0.00
0.50
1.00
1.50
2.00

Figure 2g.

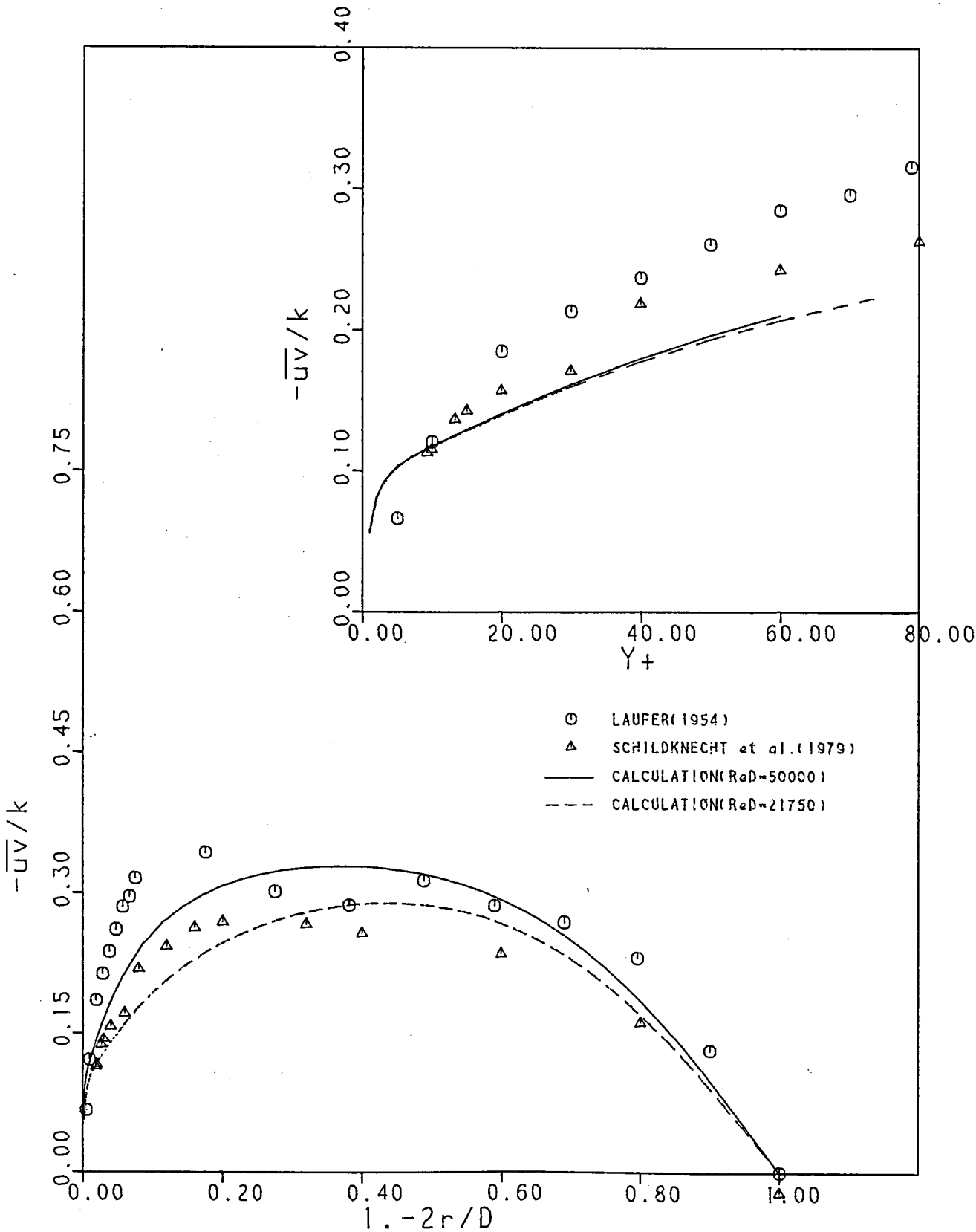
-uv/k
1.-2r/D
0.00
0.15
0.30
0.45
0.60
0.75
0.00
0.20
0.40
0.60
0.80
1.00
LAUFER(1954)
SCHILDKNECHT et al.(1979)
CALCULATION(ReD=50000)
CALCULATION(ReD=21750)
-uv/k
Y+
0.00
0.10
0.20
0.30
0.40
0.00
20.00
40.00
60.00
80.00

Figure 2h.

Figure 3a.

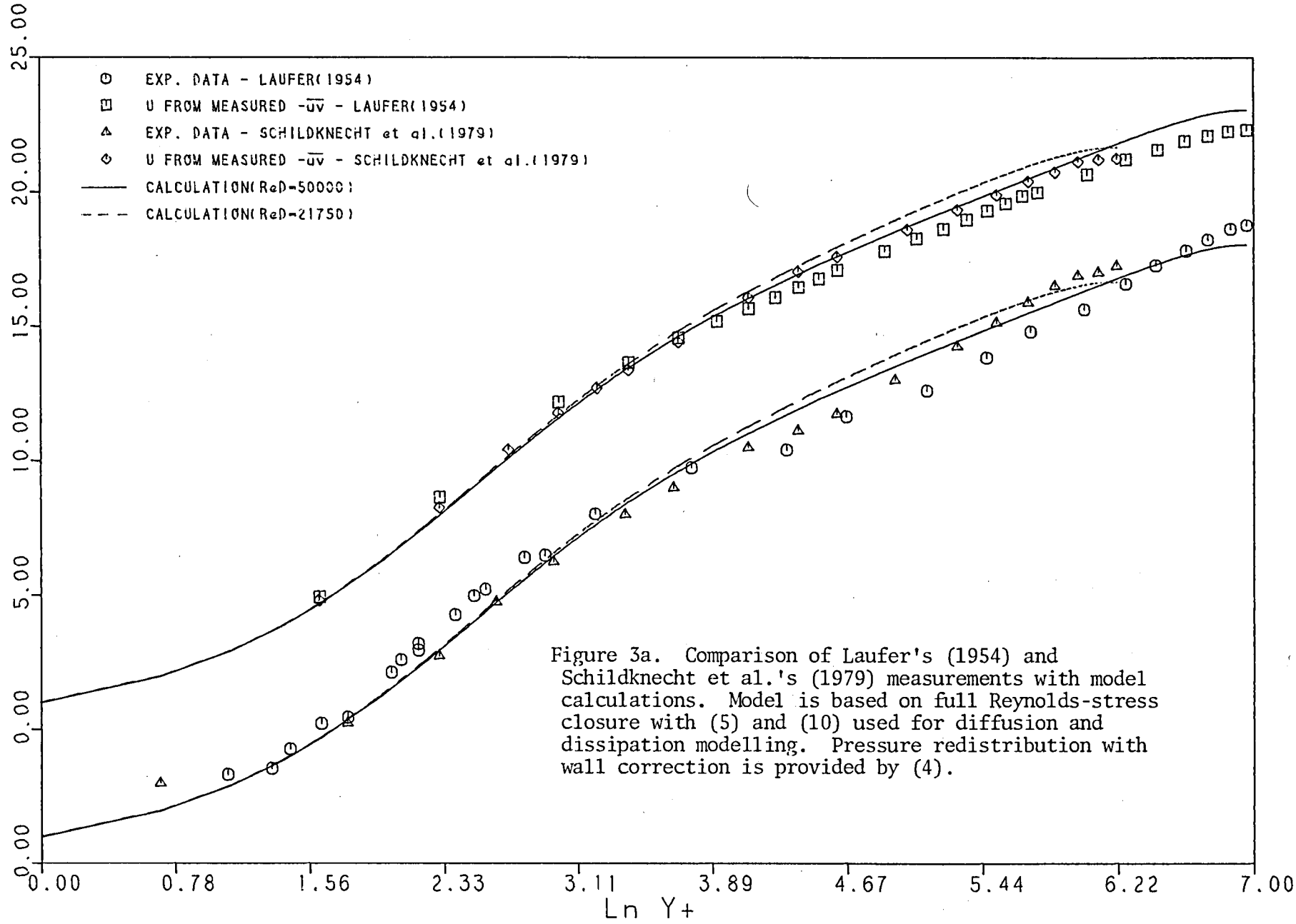

Figure 3a. Comparison of Laufer's (1954) and Schildknecht et al.'s (1979) measurements with model calculations. Model is based on full Reynolds-stress closure with (5) and (10) used for diffusion and dissipation modelling. Pressure redistribution with wall correction is provided by (4).

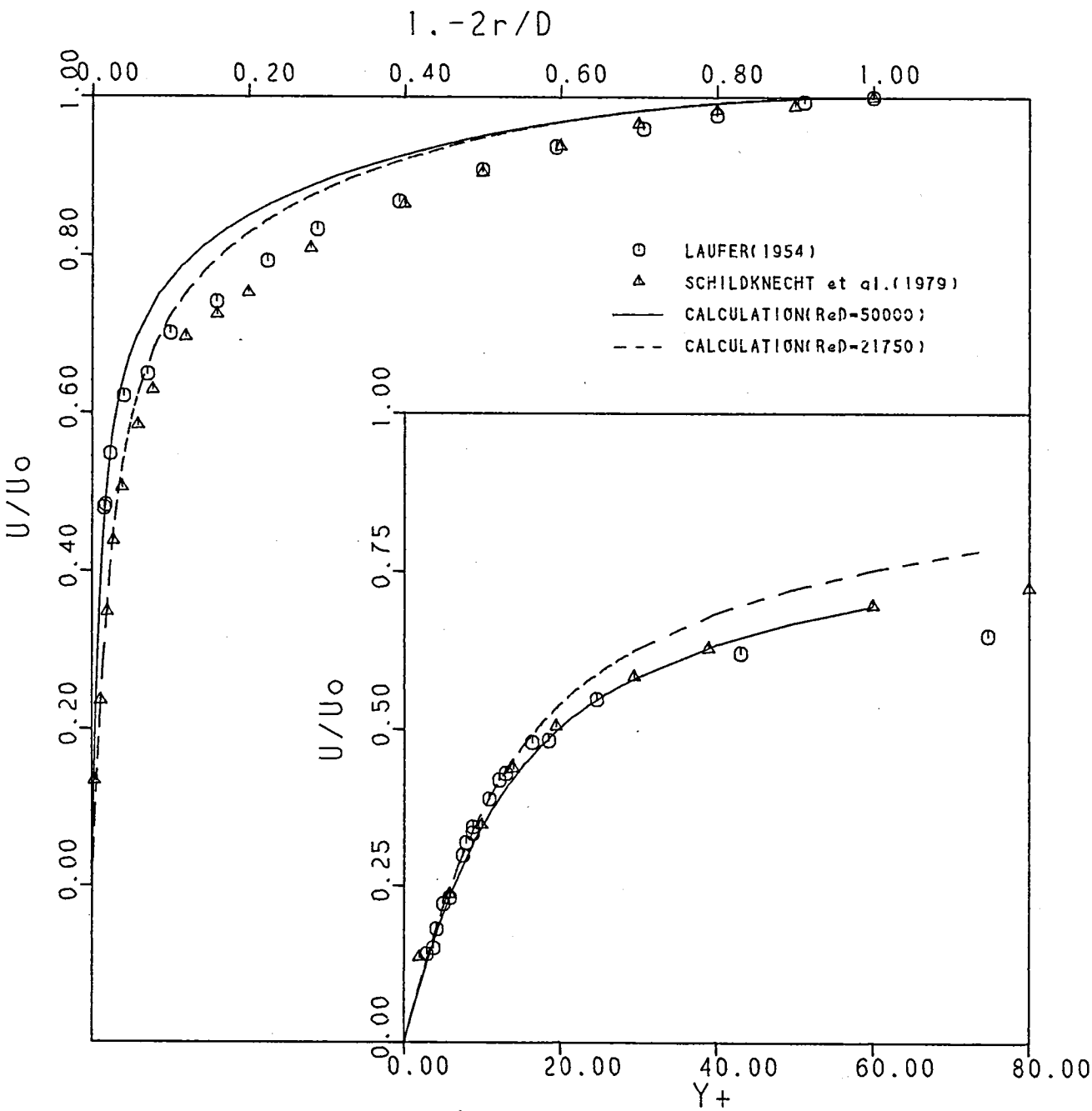
1.-2r/D
0.00
0.20
0.40
0.60
0.80
1.00
U/Uo
LAUFER(1954)
SCHILDKNECHT et al.(1979)
CALCULATION(ReD=50000)
CALCULATION(ReD=21750)
0.00
0.25
0.50
0.75
1.00
20.00
40.00
60.00
80.00
Y+

Figure 3b.

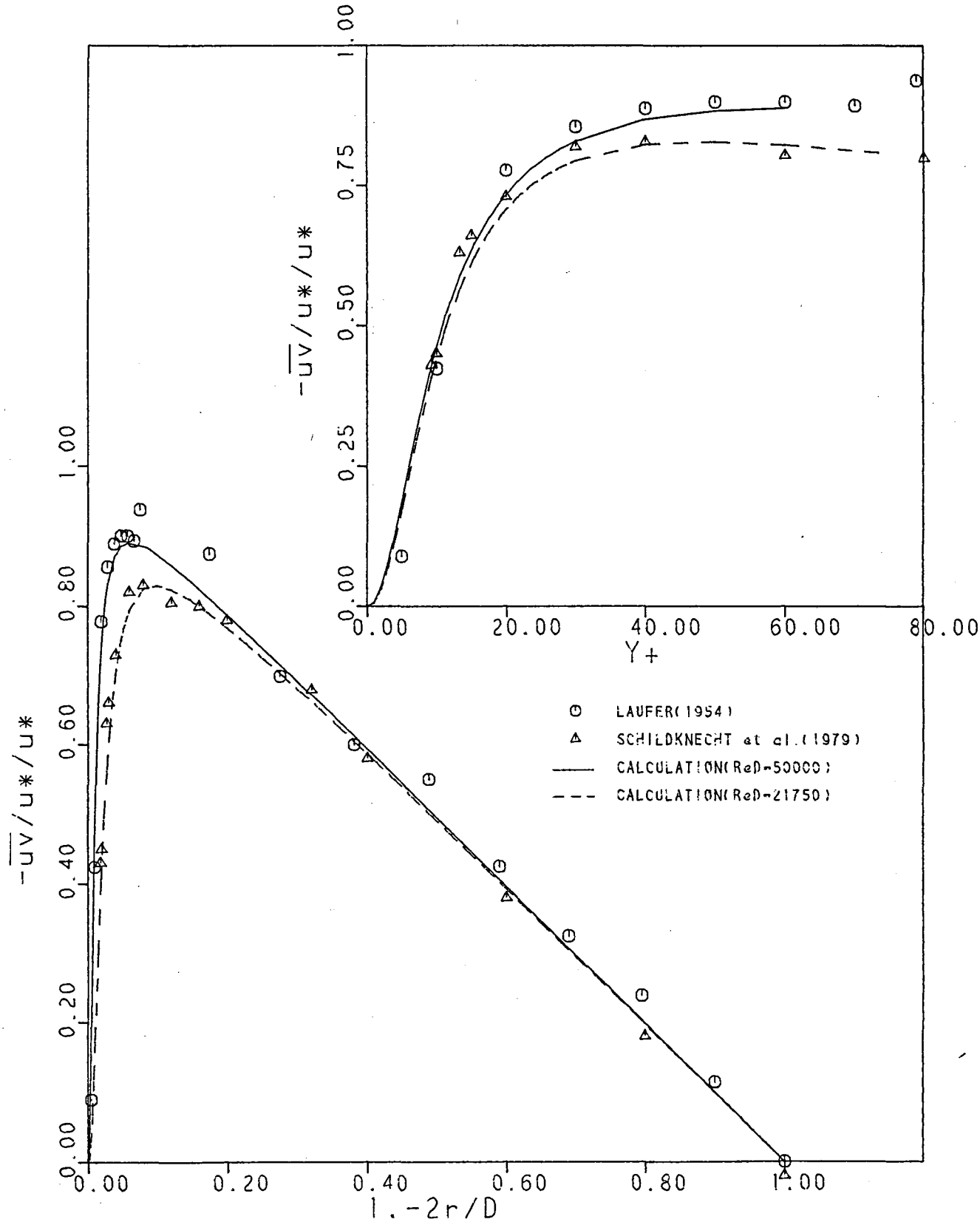
-UV/U*/U*
1.00
0.80
0.60
0.40
0.20
0.00
0.00
0.20
0.40
0.60
0.80
1.00
1.-2r/D
LAUFER(1954)
SCHILDKNECHT et al.(1979)
CALCULATION(ReD=50000)
CALCULATION(ReD=21750)
-UV/U*/U*
1.00
0.75
0.50
0.25
0.00
0.00
20.00
40.00
60.00
80.00
Y+

Figure 3c.

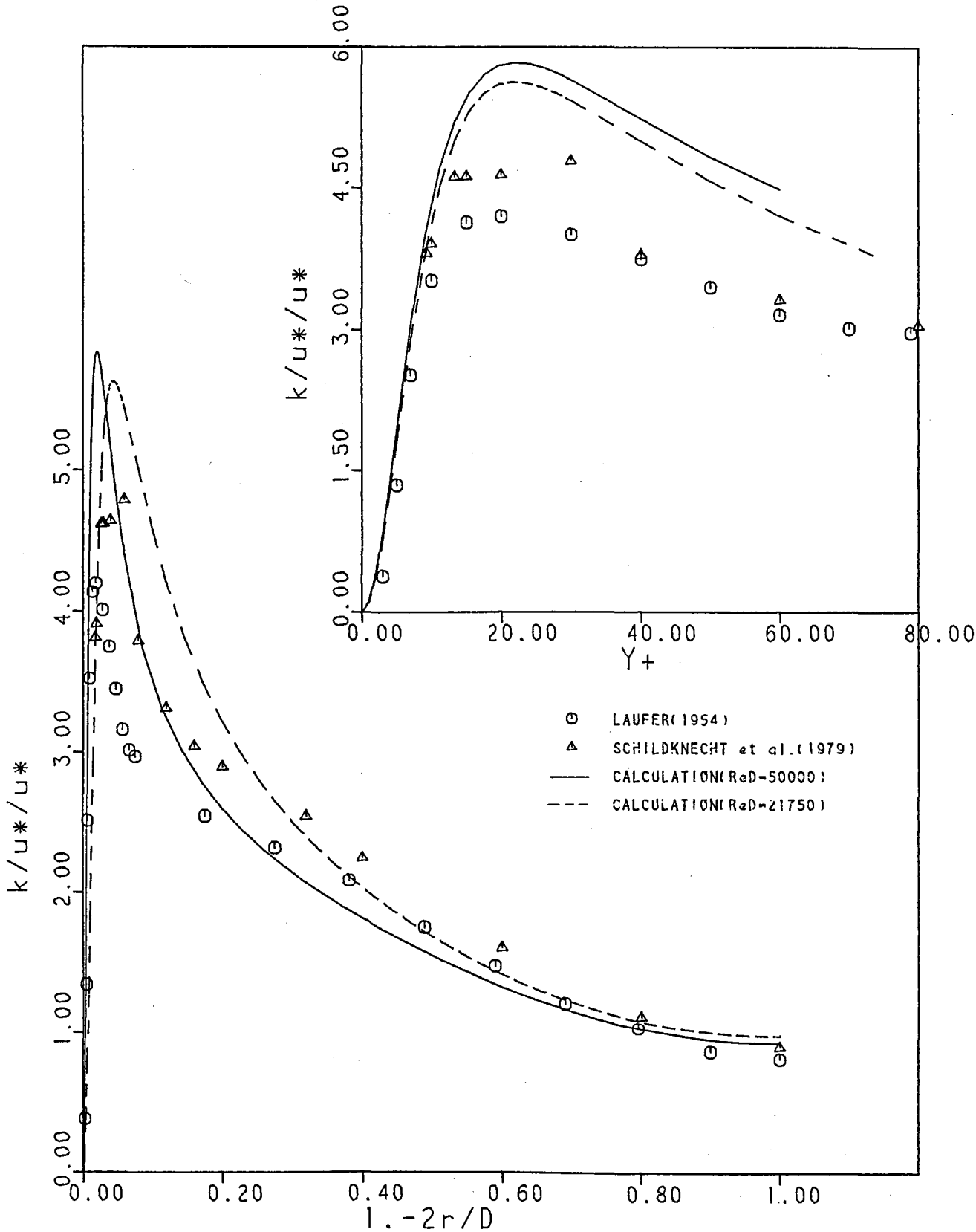
k/u*/u*
1.-2r/D
0.00
1.00
2.00
3.00
4.00
5.00
0.00
0.20
0.40
0.60
0.80
1.00
k/u*/u*
Y+
0.00
1.50
3.00
4.50
6.00
0.00
20.00
40.00
60.00
80.00
LAUFER(1954)
SCHILDKNECHT et al.(1979)
CALCULATION(ReD=50000)
CALCULATION(ReD=21750)

Figure 3d.

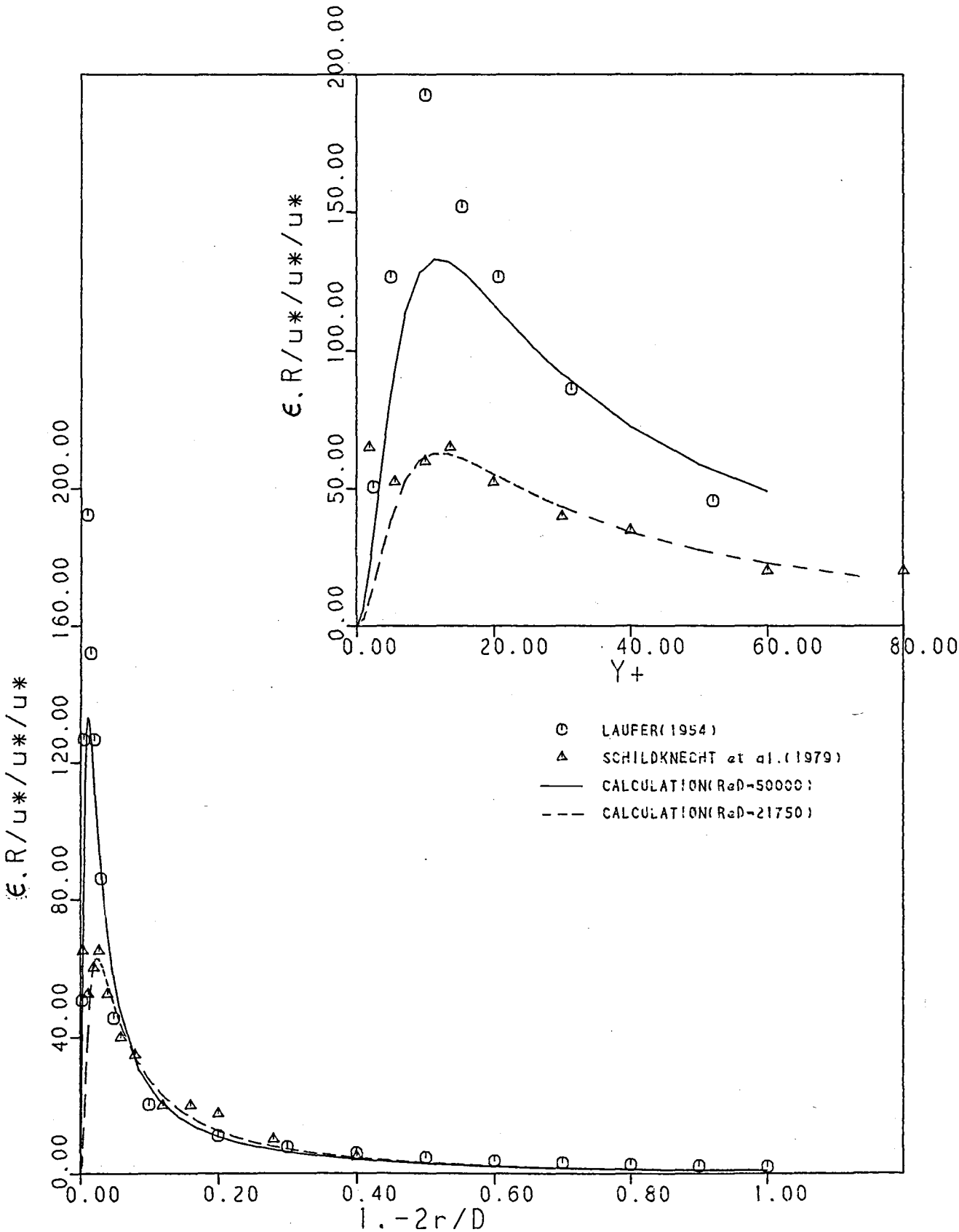
ε.R/u*/u*/u*
200.00
160.00
120.00
80.00
40.00
0.00
0.00
0.20
0.40
0.60
0.80
1.00
1.-2r/D
LAUFER(1954)
SCHILDKNECHT et al.(1979)
CALCULATION(ReD=50000)
CALCULATION(ReD=21750)
ε.R/u*/u*/u*
200.00
150.00
100.00
50.00
0.00
0.00
20.00
40.00
60.00
80.00
Y+

Figure 3e.

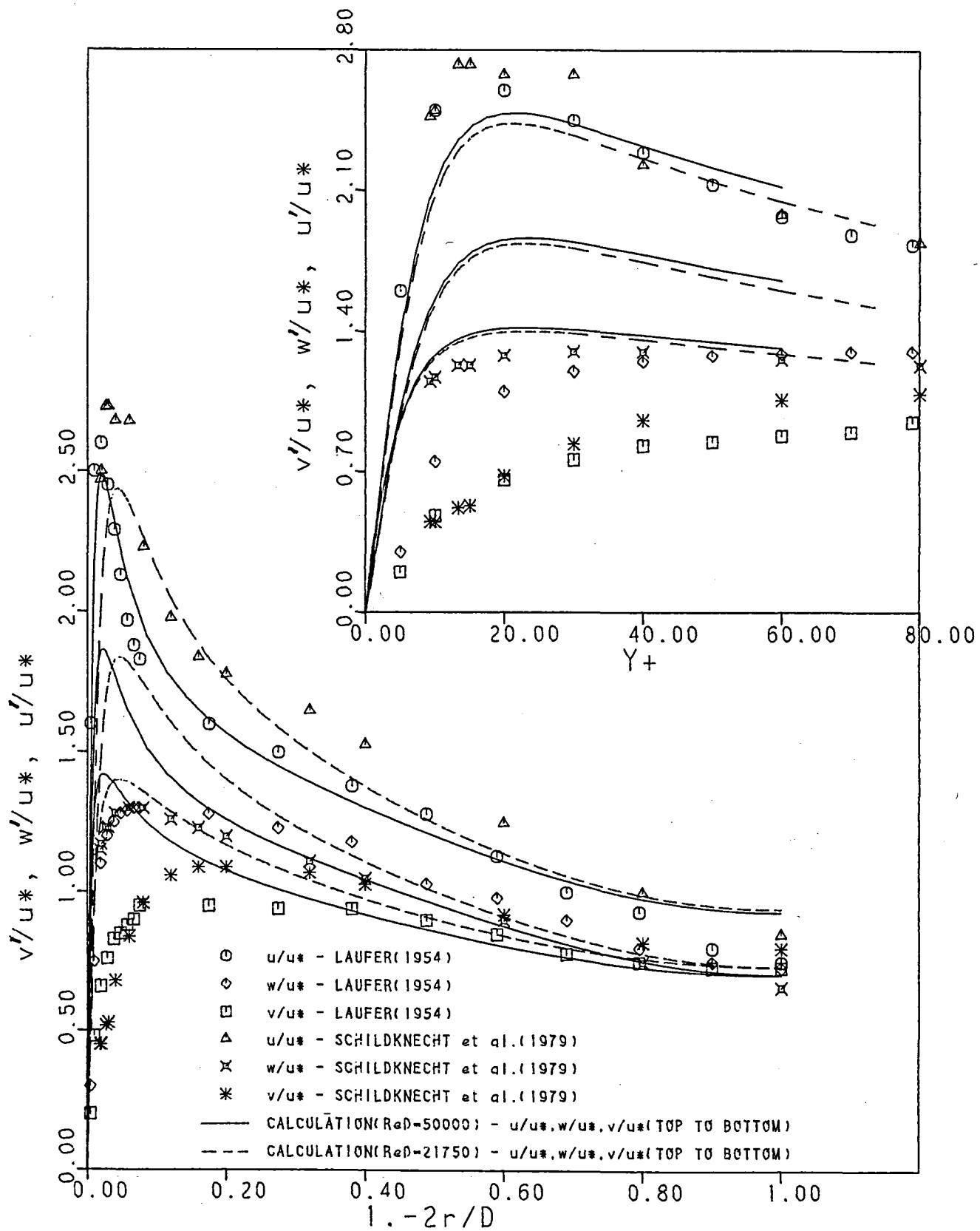
v'/u*, w'/u*, u'/u*
1.-2r/D
0.00
0.20
0.40
0.60
0.80
1.00
0.50
1.00
1.50
2.00
2.50
u/u* - LAUFER(1954)
w/u* - LAUFER(1954)
v/u* - LAUFER(1954)
u/u* - SCHILDKNECHT et al.(1979)
w/u* - SCHILDKNECHT et al.(1979)
v/u* - SCHILDKNECHT et al.(1979)
CALCULATION(ReD=50000) - u/u*, w/u*, v/u* (TOP TO BOTTOM)
CALCULATION(ReD=21750) - u/u*, w/u*, v/u* (TOP TO BOTTOM)
v'/u*, w'/u*, u'/u*
Y+
0.00
20.00
40.00
60.00
80.00
0.00
0.70
1.40
2.10
2.80

Figure 3f.

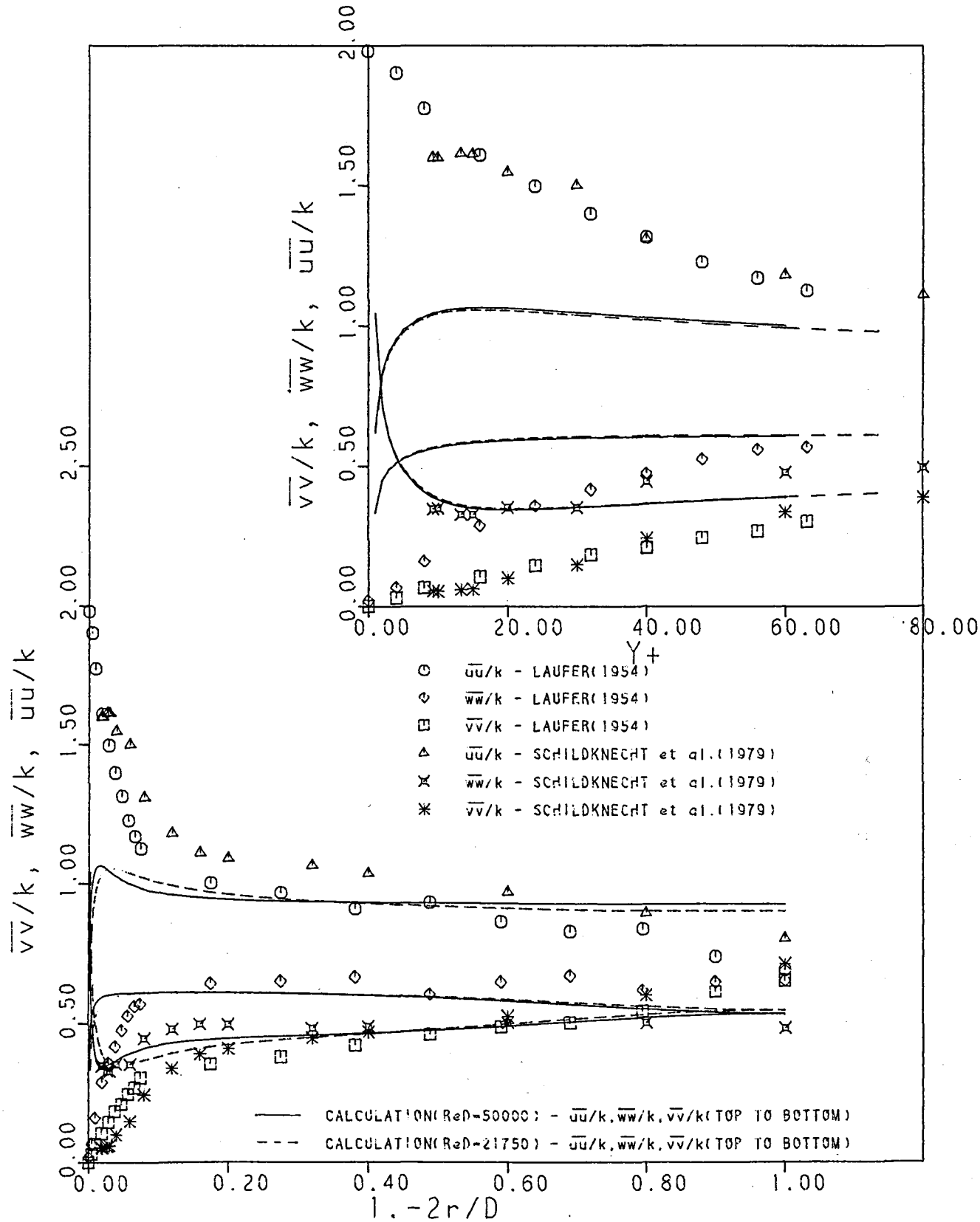
vv/k, ww/k, uu/k
0.00
0.50
1.00
1.50
2.00
2.50
0.00
0.20
0.40
0.60
0.80
1.00
1.-2r/D
vv/k, ww/k, uu/k
0.00
0.50
1.00
1.50
2.00
0.00
20.00
40.00
60.00
80.00
Y+
uu/k - LAUFER(1954)
ww/k - LAUFER(1954)
vv/k - LAUFER(1954)
uu/k - SCHILDKNECHT et al.(1979)
ww/k - SCHILDKNECHT et al.(1979)
vv/k - SCHILDKNECHT et al.(1979)
CALCULATION(ReD=50000) - uu/k,ww/k,vv/k(TOP TO BOTTOM)
CALCULATION(ReD=21750) - uu/k,ww/k,vv/k(TOP TO BOTTOM)

Figure 3g.

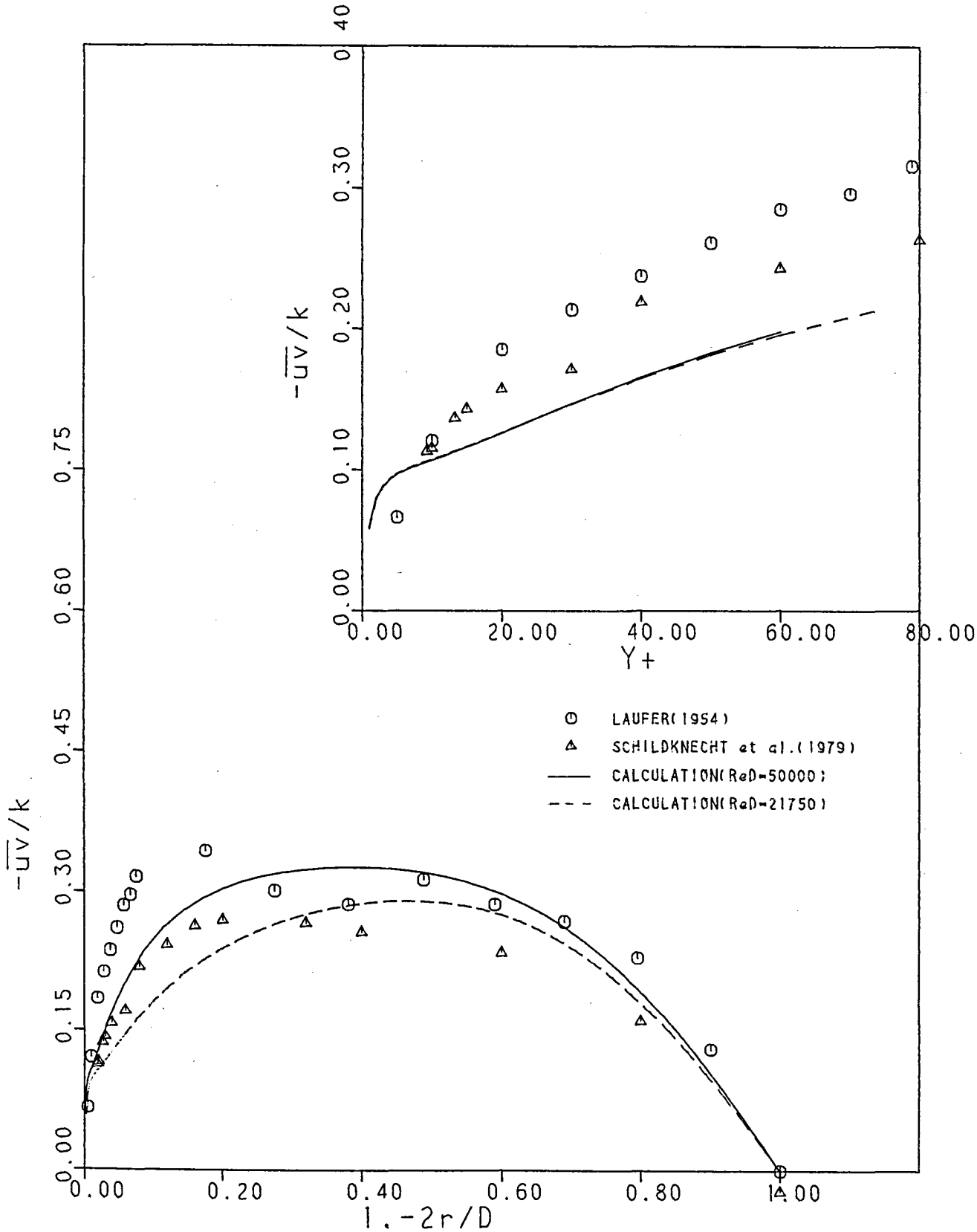
-uv/k
0.00
0.15
0.30
0.45
0.60
0.75
0.00
0.20
0.40
0.60
0.80
1.00
1.-2r/D
LAUFER(1954)
SCHILDKNECHT et al.(1979)
CALCULATION(ReD=50000)
CALCULATION(ReD=21750)
-uv/k
0.00
0.10
0.20
0.30
0.40
0.00
20.00
40.00
60.00
80.00
Y+

Figure 3h.

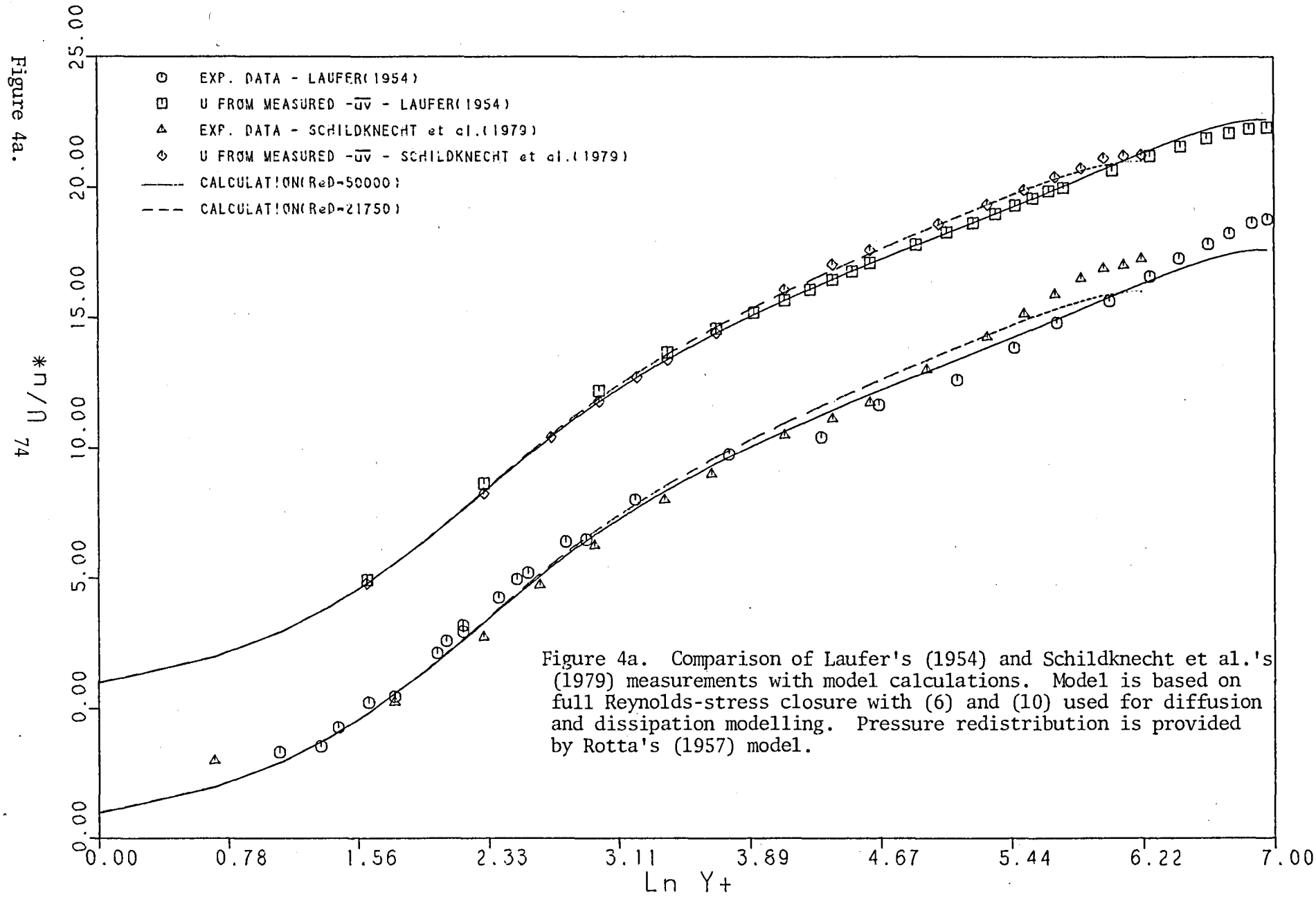

Figure 4a.

Figure 4a. Comparison of Laufer's (1954) and Schildknecht et al.'s (1979) measurements with model calculations. Model is based on full Reynolds-stress closure with (6) and (10) used for diffusion and dissipation modelling. Pressure redistribution is provided by Rotta's (1957) model.

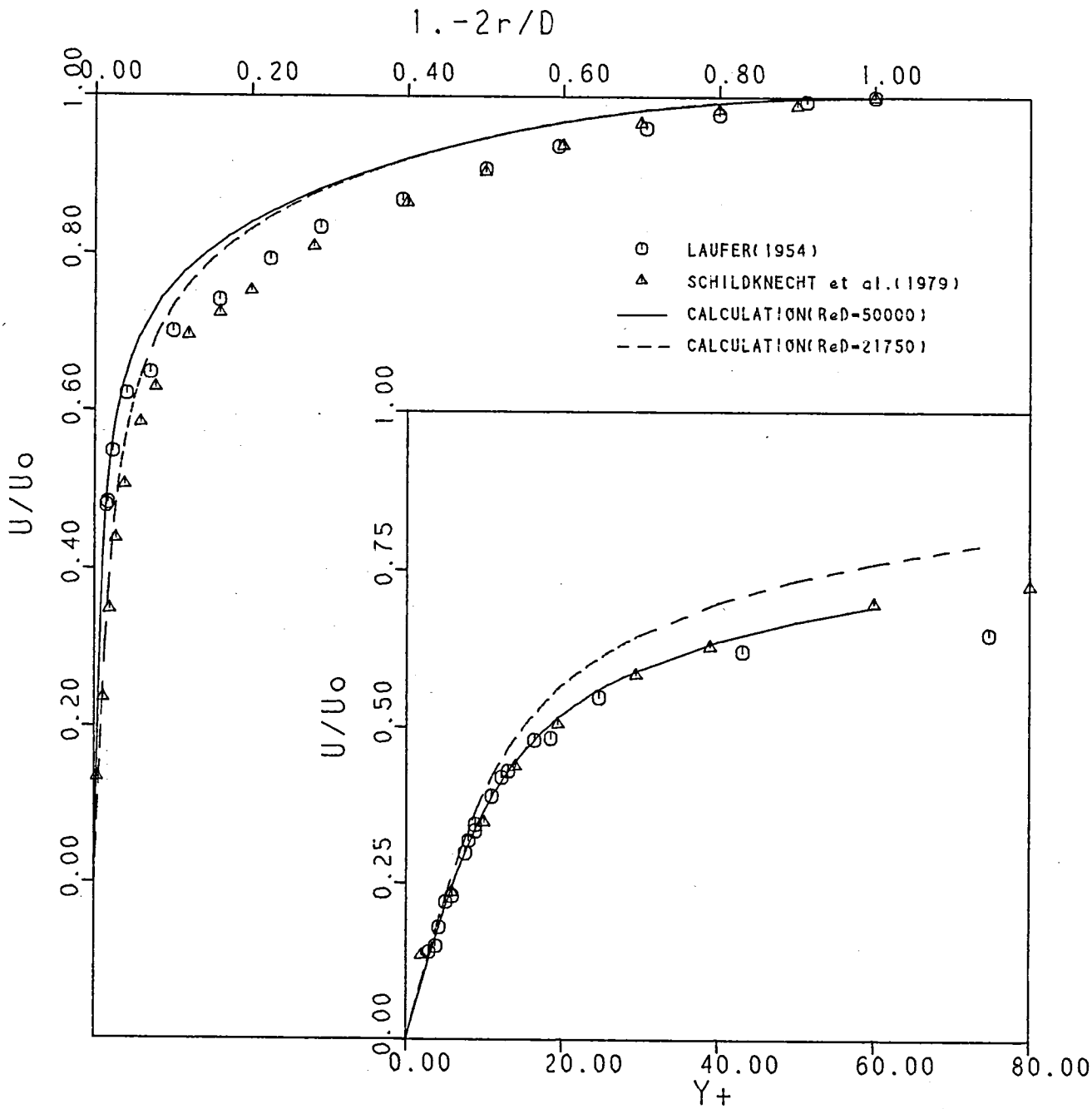
1.-2r/D
0.00
0.20
0.40
0.60
0.80
1.00
U/Uo
LAUFER(1954)
SCHILDKNECHT et al.(1979)
CALCULATION(ReD=50000)
CALCULATION(ReD=21750)
0.00
0.25
0.50
0.75
1.00
20.00
40.00
60.00
80.00
Y+

Figure 4b

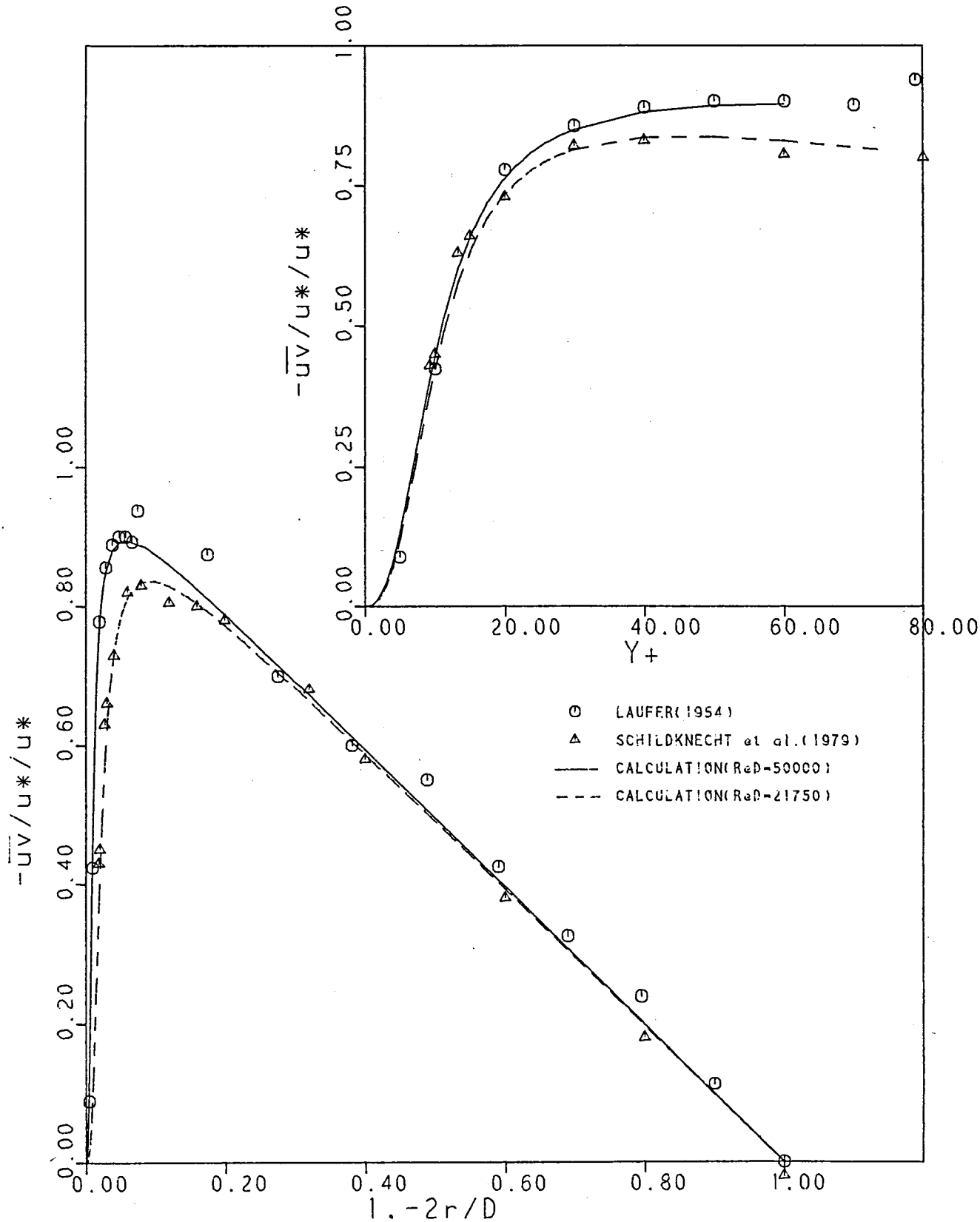
-UV/U*/U*
1.-2r/D
0.00
0.20
0.40
0.60
0.80
1.00
LAUFER(1954)
SCHILDKNECHT et al.(1979)
CALCULATION(ReD=50000)
CALCULATION(ReD=21750)
-UV/U*/U*
Y+
0.00
0.25
0.50
0.75
1.00
0.00
20.00
40.00
60.00
80.00

Figure 4c.

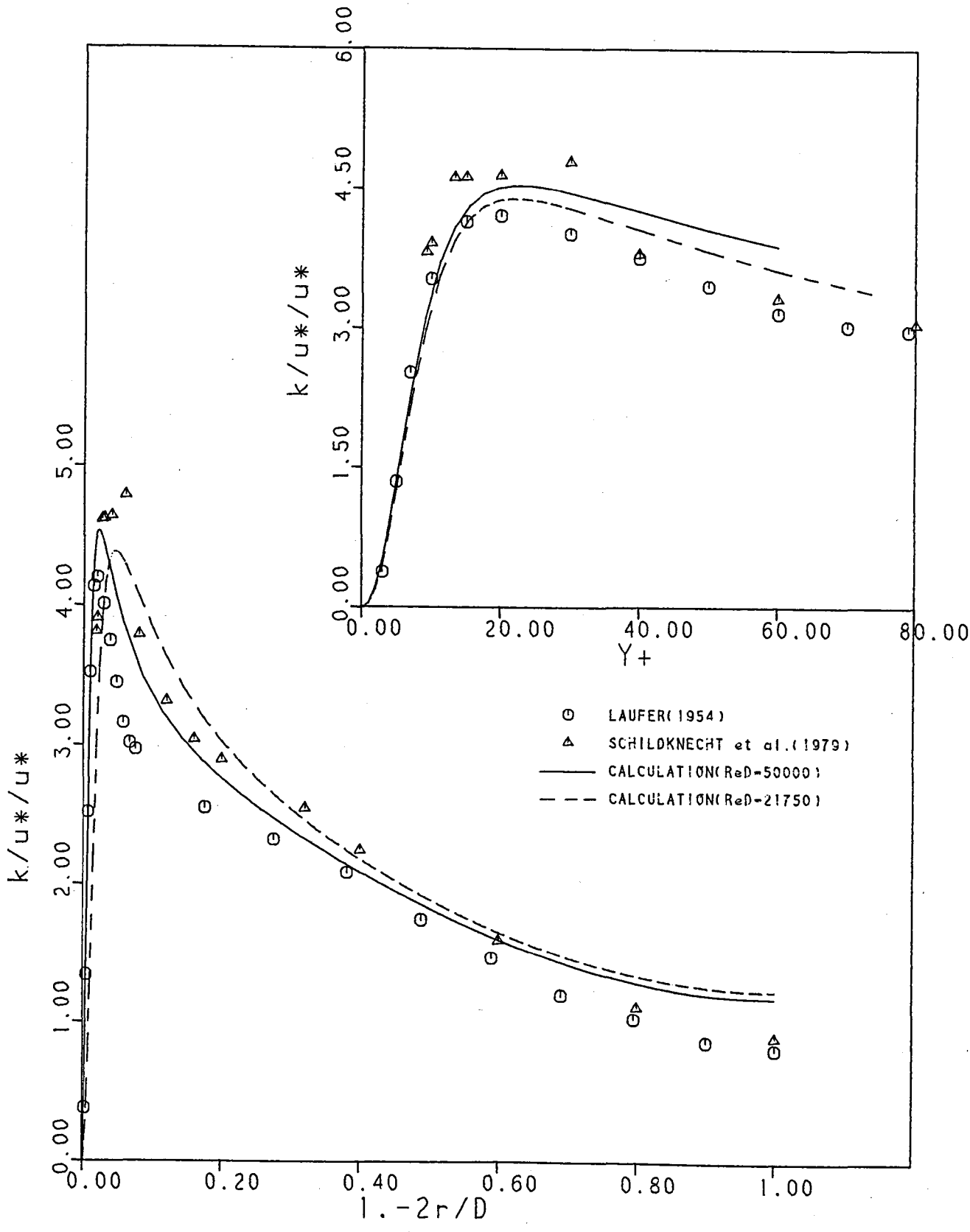
k/u*/u*
1.-2r/D
0.00
1.00
2.00
3.00
4.00
5.00
0.00
0.20
0.40
0.60
0.80
1.00
k/u*/u*
Y+
0.00
1.50
3.00
4.50
6.00
0.00
20.00
40.00
60.00
80.00
LAUFER(1954)
SCHILDKNECHT et al.(1979)
CALCULATION(ReD=50000)
CALCULATION(ReD=21750)

Figure 4d.

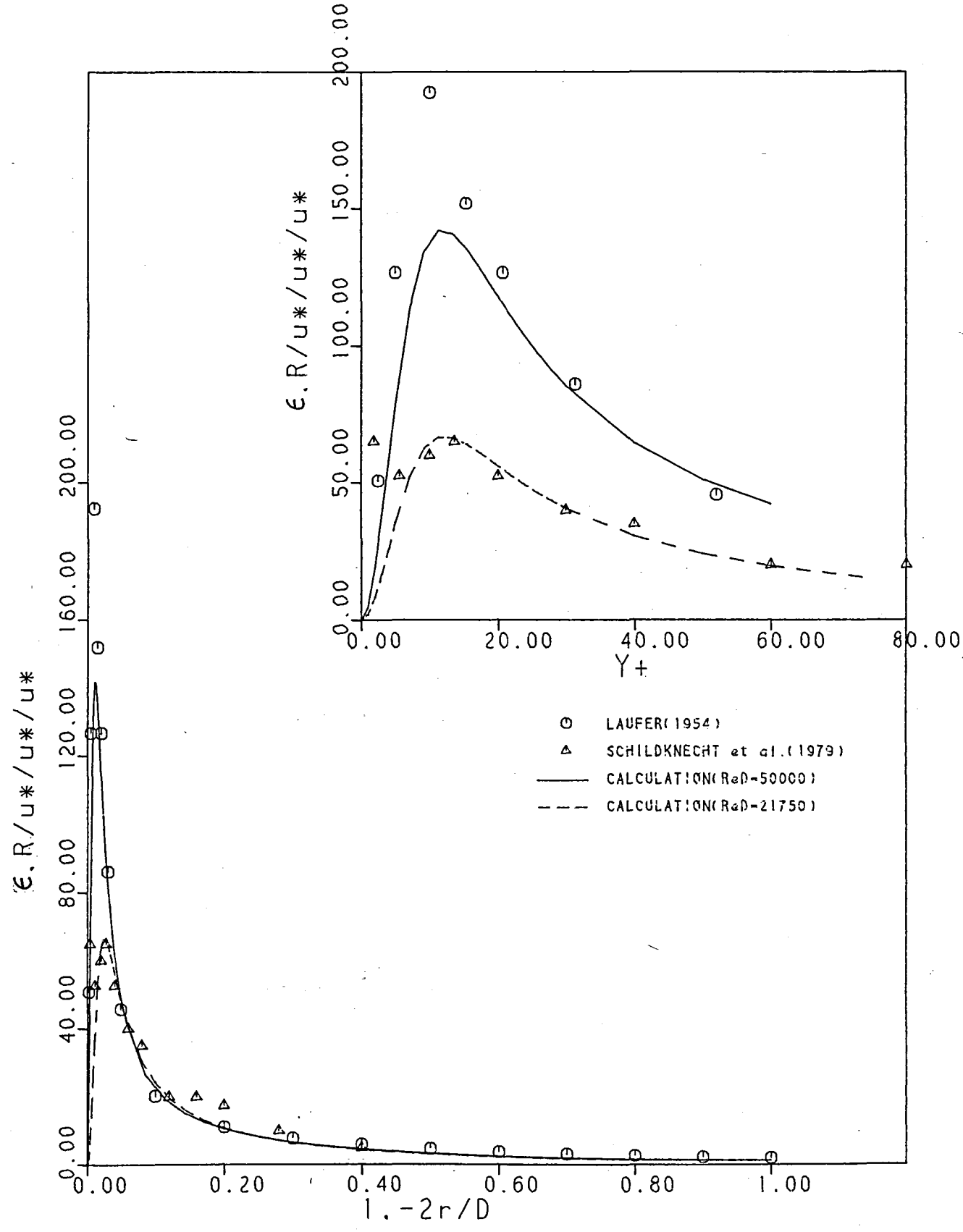
ε.R/u*/u*/u*
0.00
40.00
80.00
120.00
160.00
200.00
0.00
0.20
0.40
0.60
0.80
1.00
1.-2r/D
LAUFER(1954)
SCHILDKNECHT et al.(1979)
CALCULATION(ReD=50000)
CALCULATION(ReD=21750)
ε.R/u*/u*/u*
0.00
50.00
100.00
150.00
200.00
0.00
20.00
40.00
60.00
80.00
Y+

Figure 4e.

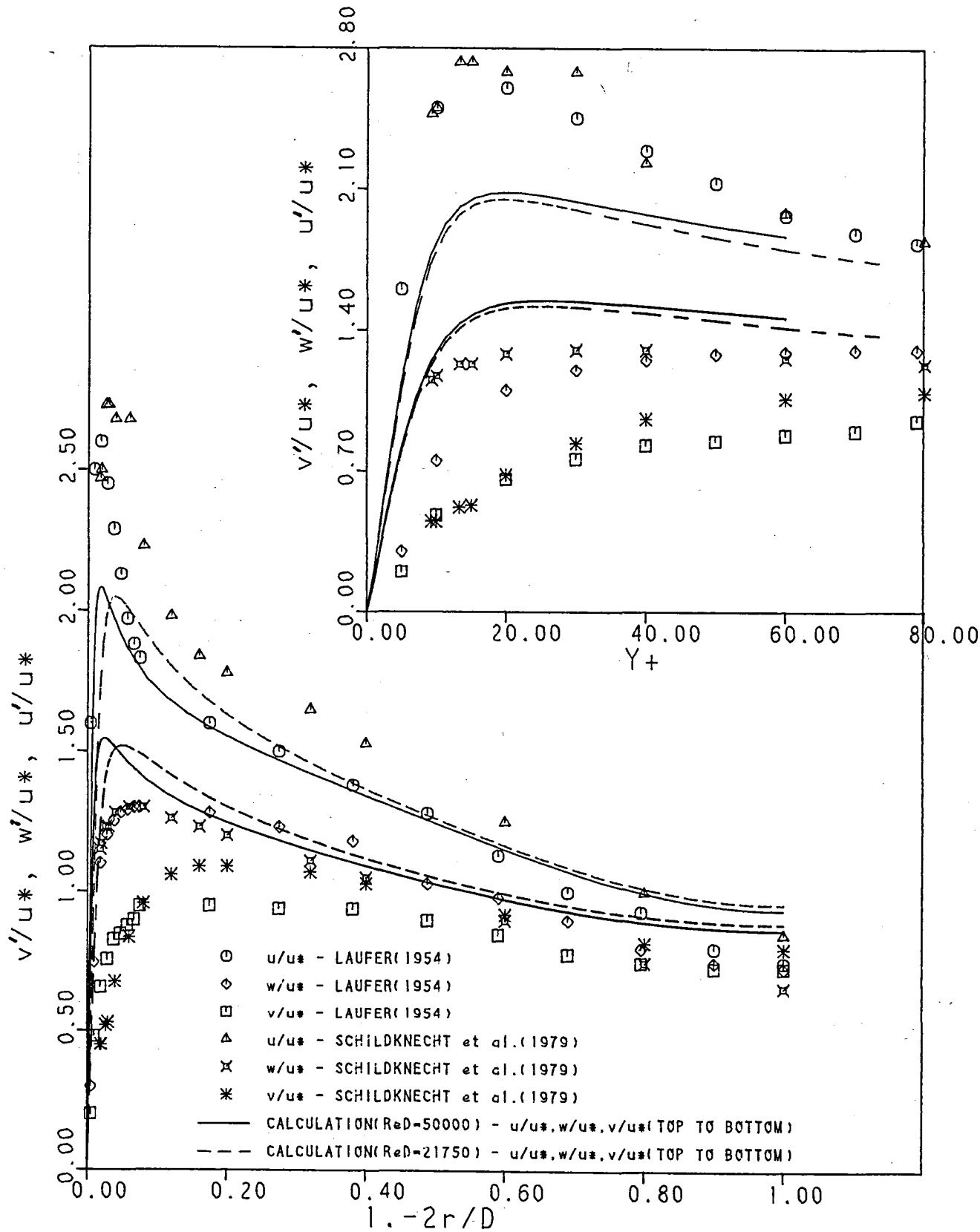
v'/u*, w'/u*, u'/u*
1.-2r/D
0.00
0.20
0.40
0.60
0.80
1.00
0.50
1.00
1.50
2.00
2.50
u/u* - LAUFER(1954)
w/u* - LAUFER(1954)
v/u* - LAUFER(1954)
u/u* - SCHILDKNECHT et al.(1979)
w/u* - SCHILDKNECHT et al.(1979)
v/u* - SCHILDKNECHT et al.(1979)
CALCULATION(ReD=50000) - u/u*,w/u*,v/u*(TOP TO BOTTOM)
CALCULATION(ReD=21750) - u/u*,w/u*,v/u*(TOP TO BOTTOM)
v'/u*, w'/u*, u'/u*
Y+
0.00
20.00
40.00
60.00
80.00
0.70
1.40
2.10
2.80

Figure 4f.

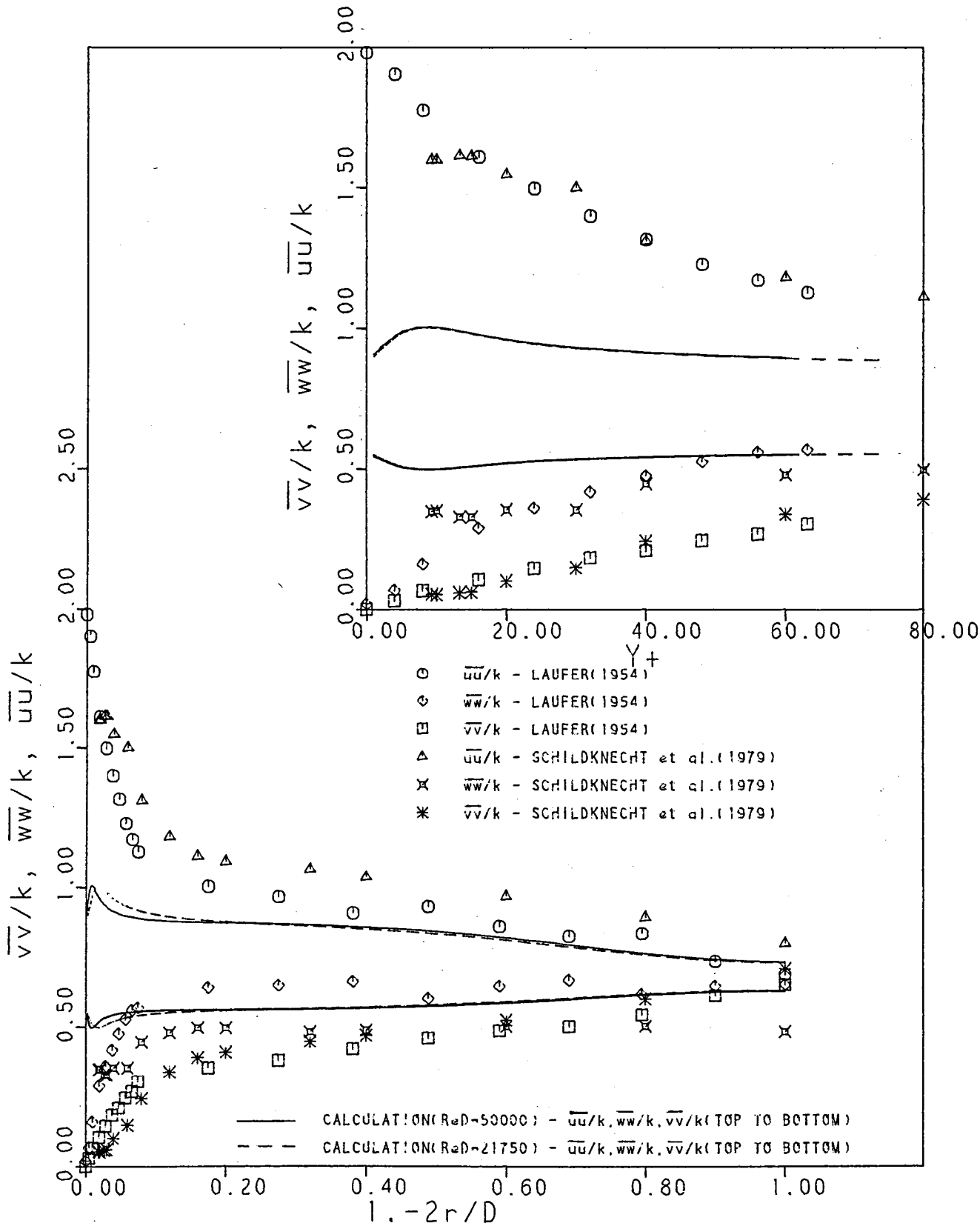
vv/k, ww/k, uu/k
1.-2r/D
0.00
0.20
0.40
0.60
0.80
1.00
0.00
0.50
1.00
1.50
2.00
2.50
vv/k, ww/k, uu/k
Y+
0.00
20.00
40.00
60.00
80.00
0.00
0.50
1.00
1.50
2.00
uu/k - LAUFER(1954)
ww/k - LAUFER(1954)
vv/k - LAUFER(1954)
uu/k - SCHILDKNECHT et al.(1979)
ww/k - SCHILDKNECHT et al.(1979)
vv/k - SCHILDKNECHT et al.(1979)
CALCULATION(ReD=50000) - uu/k,ww/k,vv/k(TOP TO BOTTOM)
CALCULATION(ReD=21750) - uu/k,ww/k,vv/k(TOP TO BOTTOM)

Figure 4g.

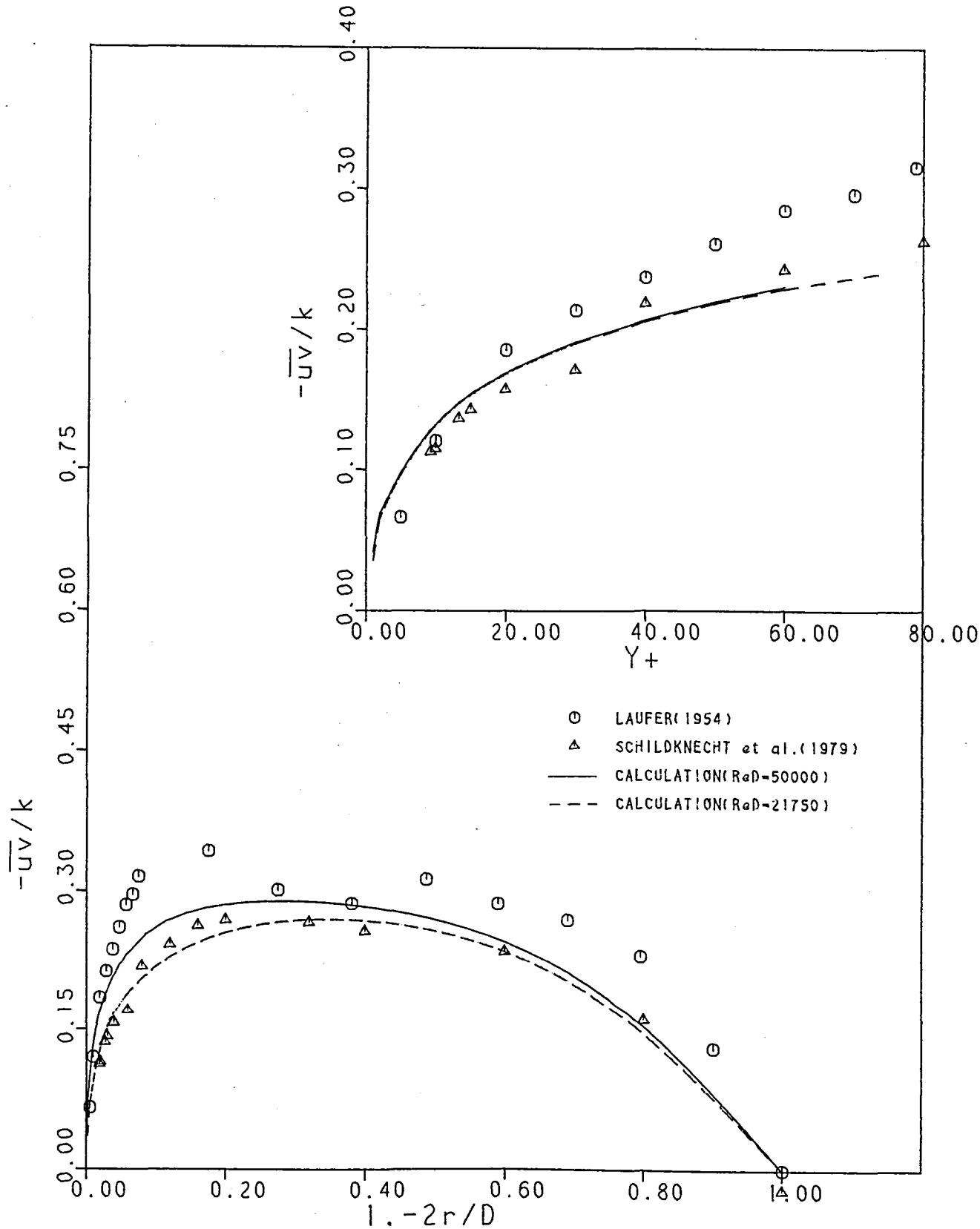
0.00
0.10
0.20
0.30
0.40
-uv/k
0.00
20.00
40.00
60.00
80.00
Y+
0.00
0.15
0.30
0.45
0.60
0.75
-uv/k
0.00
0.20
0.40
0.60
0.80
1.00
1.-2r/D
LAUFER(1954)
SCHILDKNECHT et al.(1979)
CALCULATION(ReD=50000)
CALCULATION(ReD=21750)

Figure 4h.

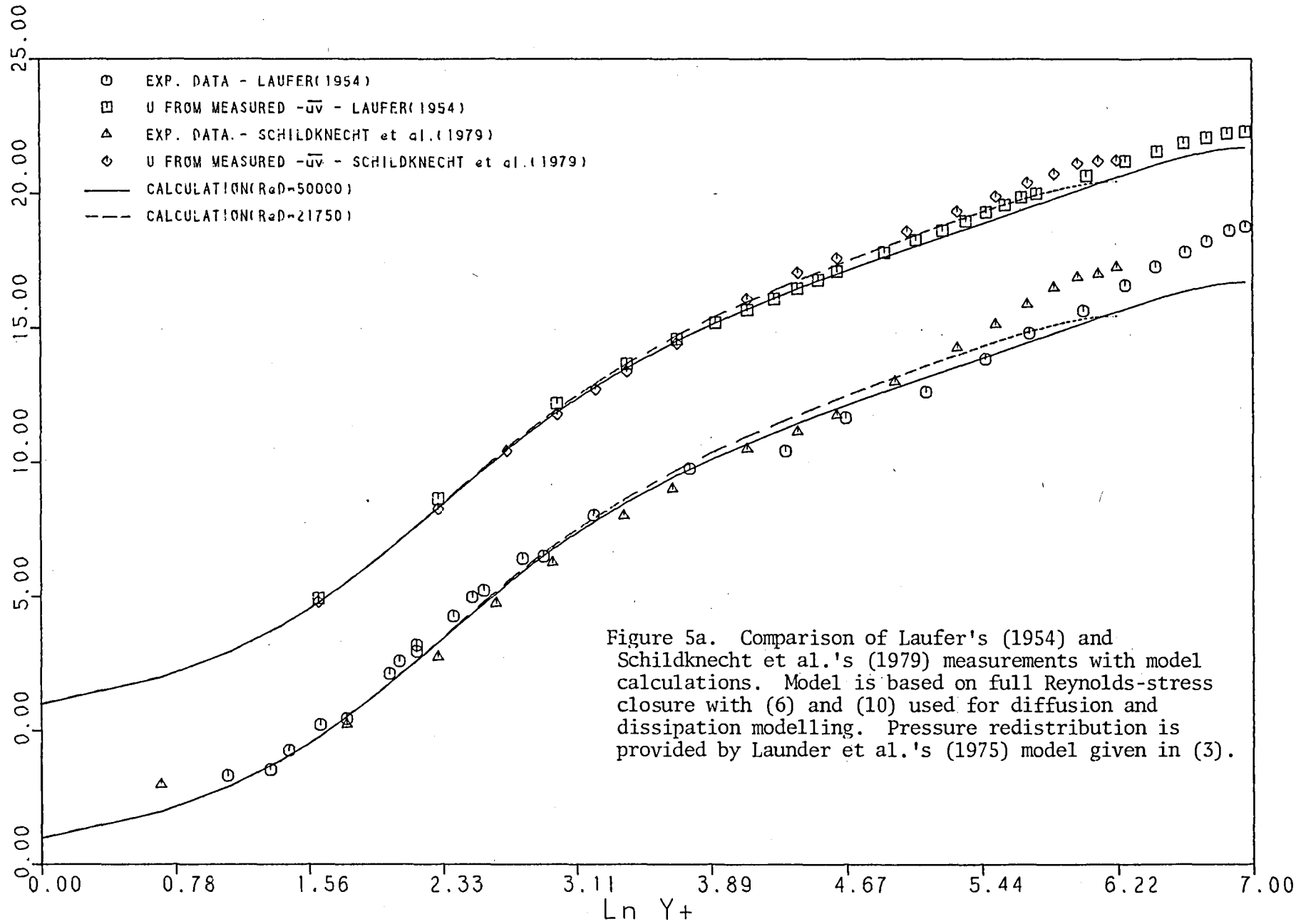

Figure 5a. Comparison of Laufer's (1954) and Schildknecht et al.'s (1979) measurements with model calculations. Model is based on full Reynolds-stress closure with (6) and (10) used for diffusion and dissipation modelling. Pressure redistribution is provided by Launder et al.'s (1975) model given in (3).

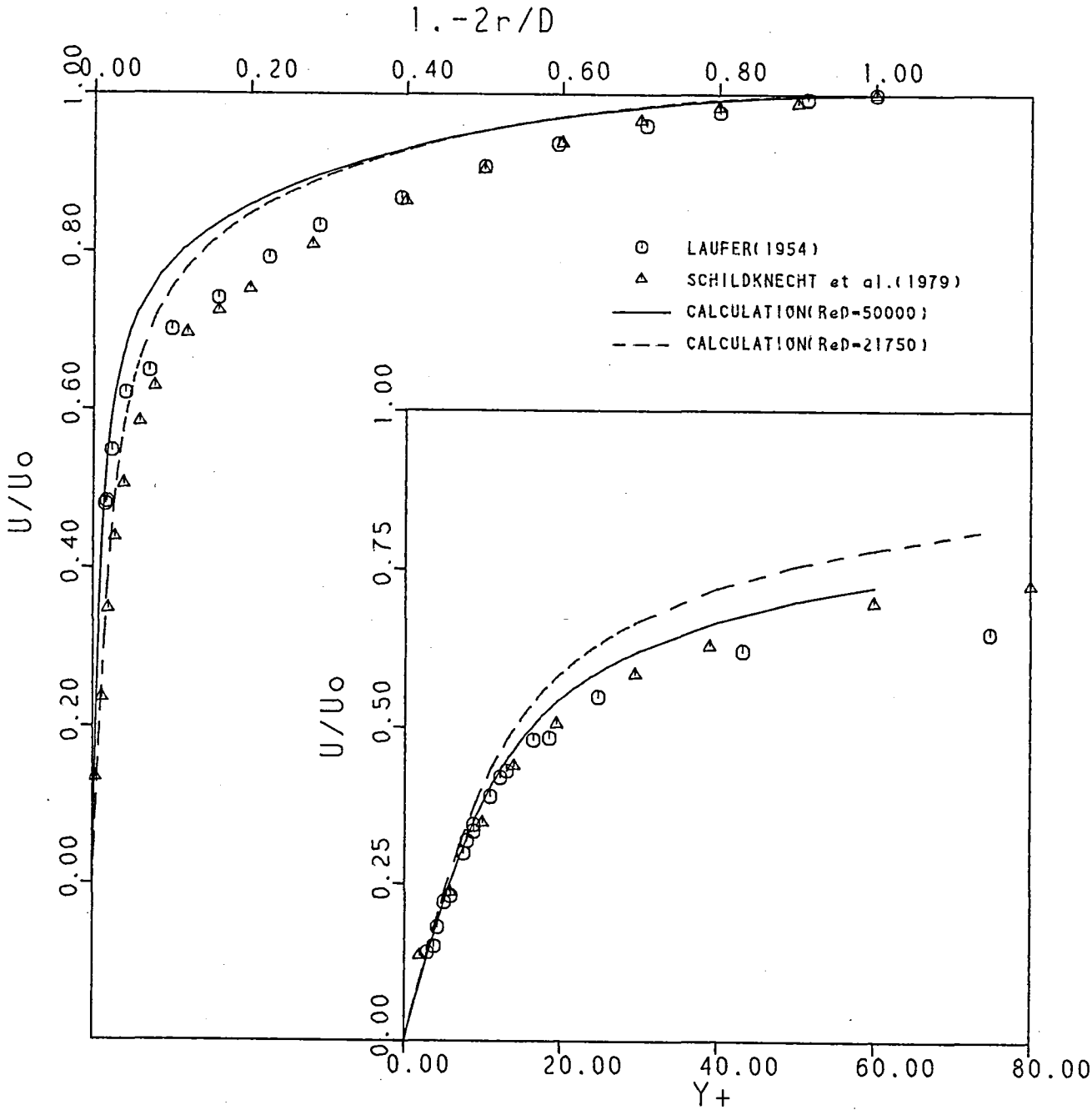
1.-2r/D
0.00
0.20
0.40
0.60
0.80
1.00
U/Uo
LAUFER(1954)
SCHILDKNECHT et al.(1979)
CALCULATION(ReD=50000)
CALCULATION(ReD=21750)
0.00
0.25
0.50
0.75
1.00
20.00
40.00
60.00
80.00
Y+

Figure 5b.

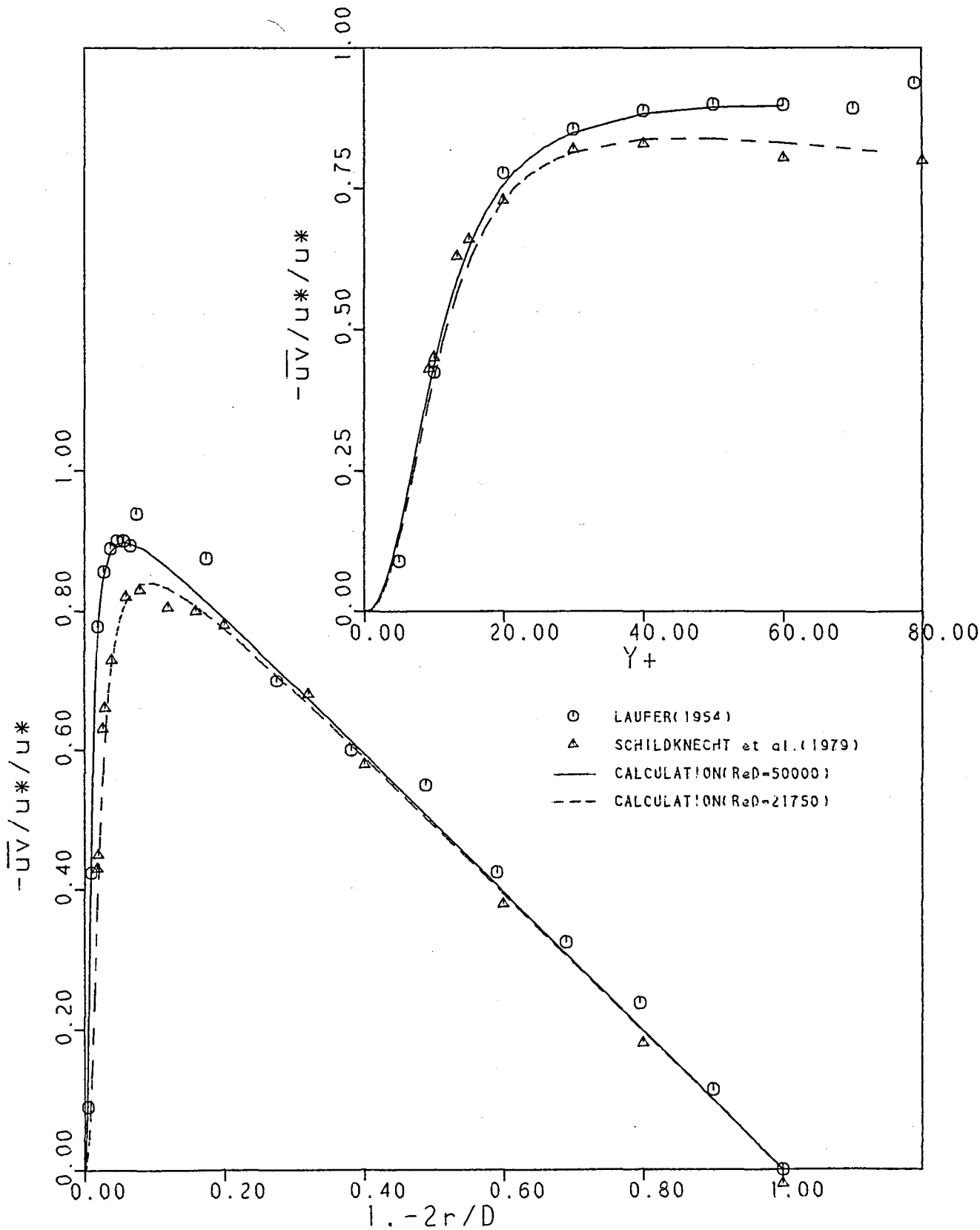
-UV/U*/U*
1.00
0.80
0.60
0.40
0.20
0.00
0.00
0.20
0.40
0.60
0.80
1.00
1.-2r/D
LAUFER(1954)
SCHILDKNECHT et al.(1979)
CALCULATION(ReD=50000)
CALCULATION(ReD=21750)
-UV/U*/U*
1.00
0.75
0.50
0.25
0.00
0.00
20.00
40.00
60.00
80.00
Y+

Figure 5-

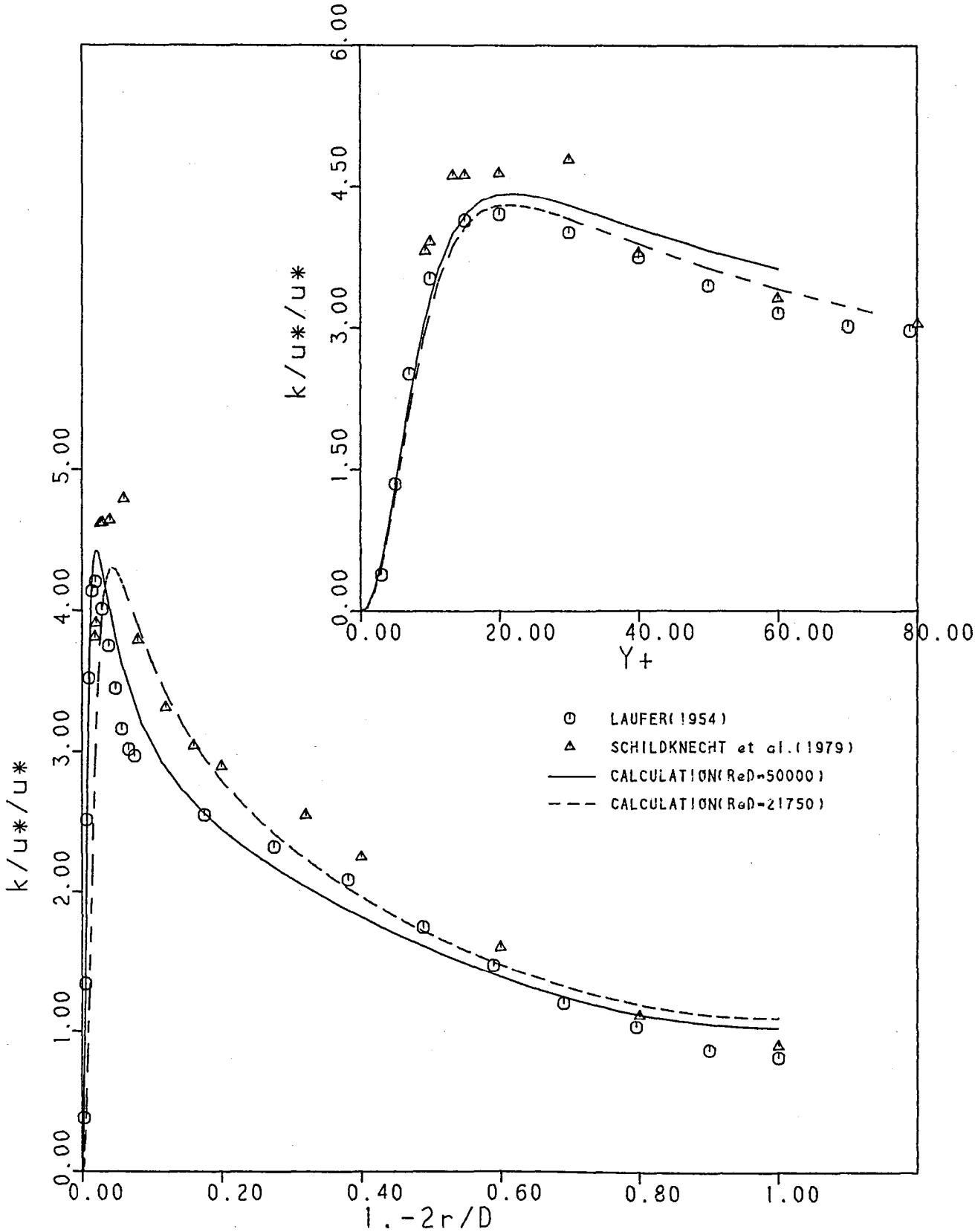
k/u*/u*
1.-2r/D
0.00
1.00
2.00
3.00
4.00
5.00
0.00
0.20
0.40
0.60
0.80
1.00
LAUFER(1954)
SCHILDKNECHT et al.(1979)
CALCULATION(ReD=50000)
CALCULATION(ReD=21750)
k/u*/u*
Y+
0.00
1.50
3.00
4.50
6.00
0.00
20.00
40.00
60.00
80.00

Figure 5d.

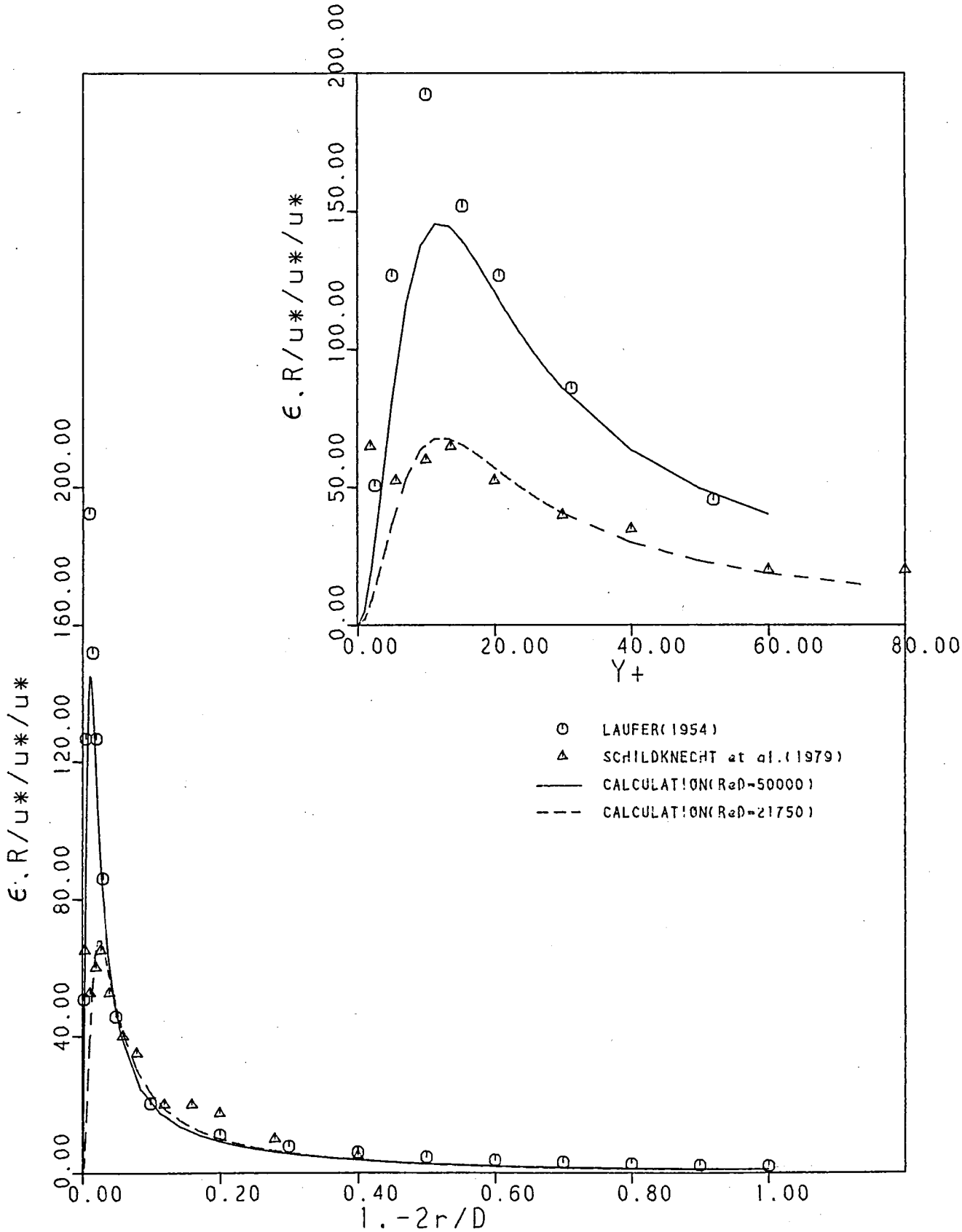
ε. R/u*/u*/u*
1.-2r/D
0.00
40.00
80.00
120.00
160.00
200.00
0.00
0.20
0.40
0.60
0.80
1.00
ε. R/u*/u*/u*
Y+
0.00
50.00
100.00
150.00
200.00
0.00
20.00
40.00
60.00
80.00
LAUFER(1954)
SCHILDKNECHT et al.(1979)
CALCULATION(ReD=50000)
CALCULATION(ReD=21750)

Figure 5e.

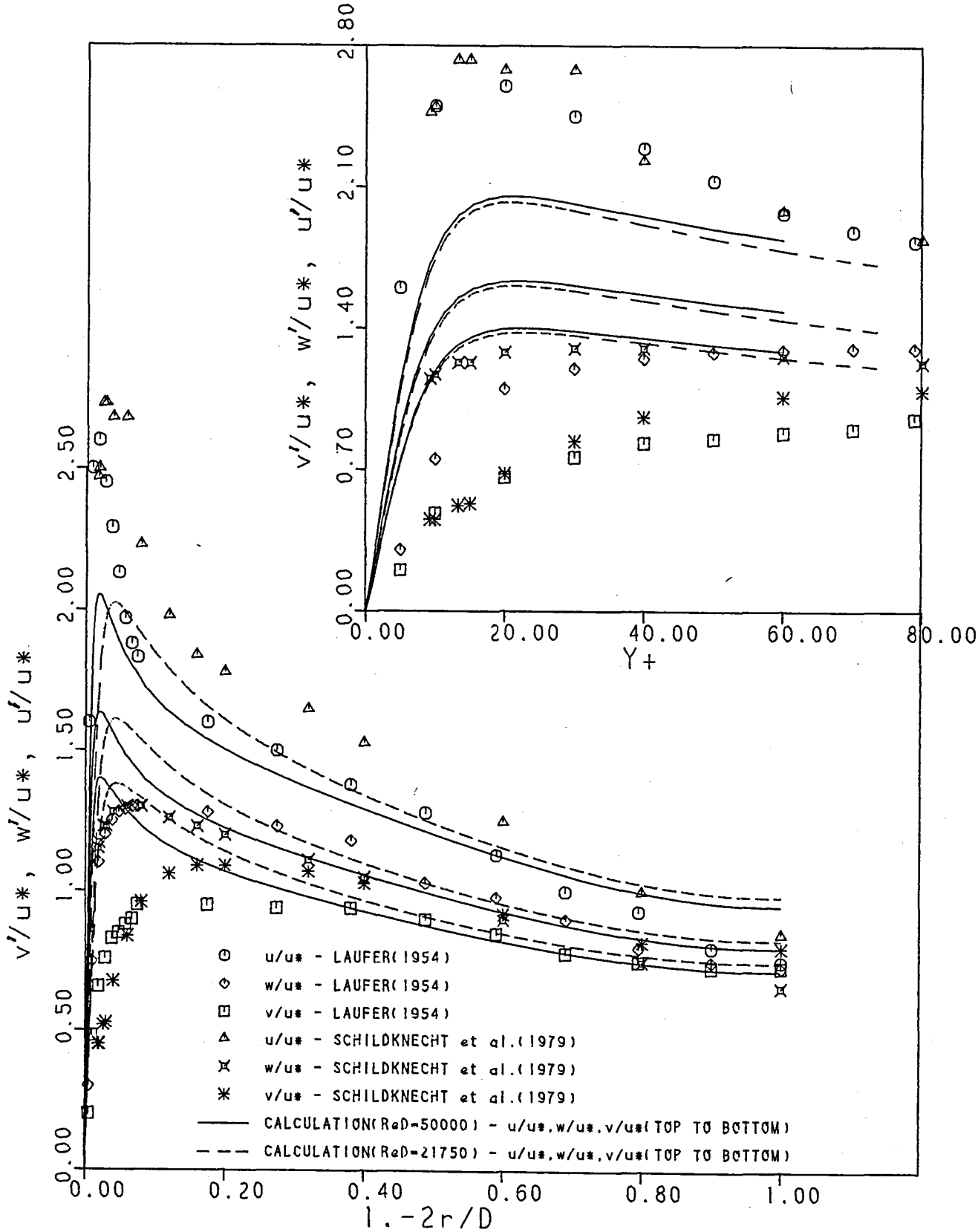
v'/u*, w'/u*, u'/u*
1.-2r/D
0.00
0.50
1.00
1.50
2.00
2.50
0.00
0.20
0.40
0.60
0.80
1.00
u/u* - LAUFER(1954)
w/u* - LAUFER(1954)
v/u* - LAUFER(1954)
u/u* - SCHILDKNECHT et al.(1979)
w/u* - SCHILDKNECHT et al.(1979)
v/u* - SCHILDKNECHT et al.(1979)
CALCULATION(ReD=50000) - u/u*, w/u*, v/u* (TOP TO BOTTOM)
CALCULATION(ReD=21750) - u/u*, w/u*, v/u* (TOP TO BOTTOM)
v'/u*, w'/u*, u'/u*
Y+
0.00
0.70
1.40
2.10
2.80
0.00
20.00
40.00
60.00
80.00

Figure 5f.

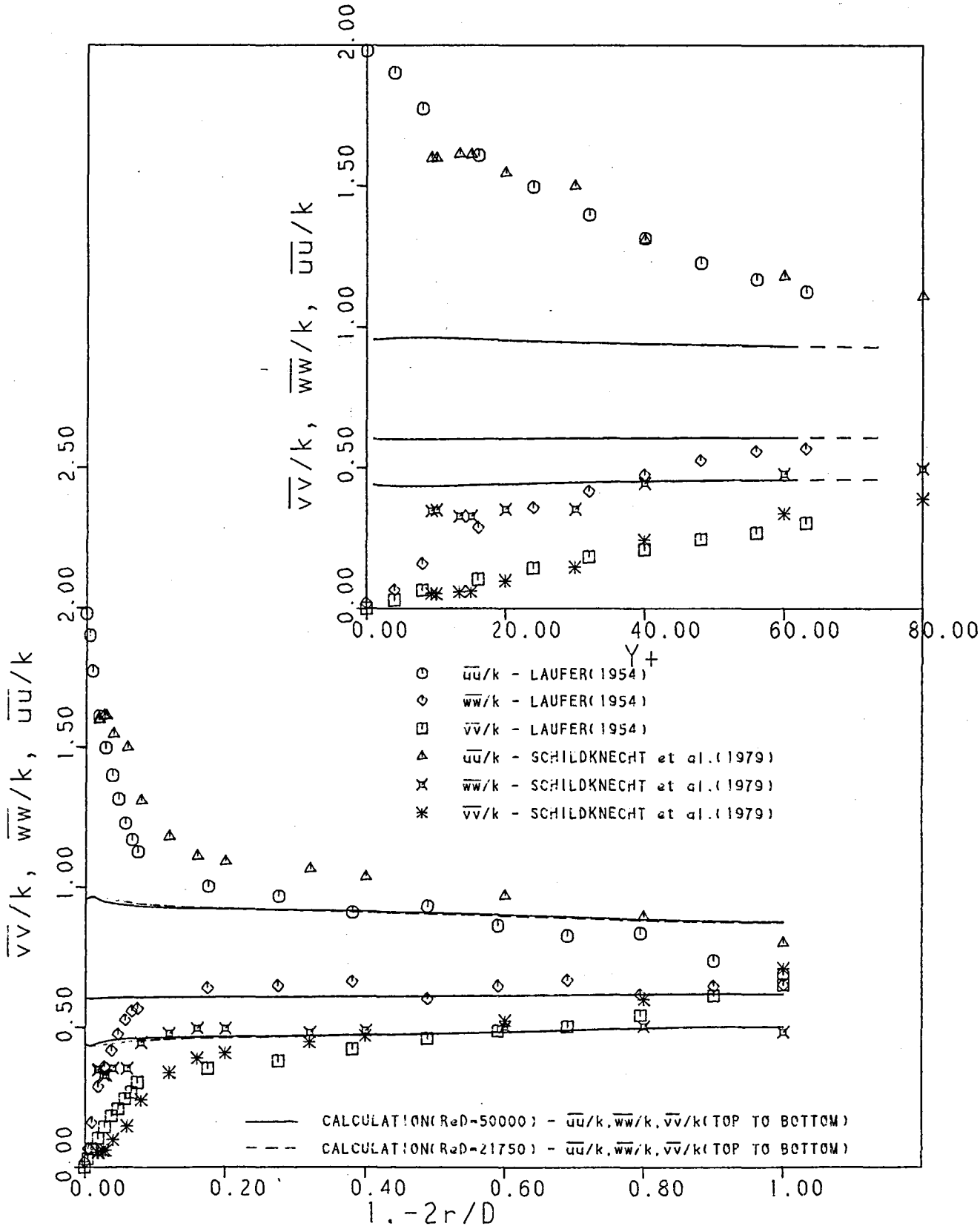
vv/k, ww/k, uu/k
1.-2r/D
0.00
0.20
0.40
0.60
0.80
1.00
0.00
0.50
1.00
1.50
2.00
2.50
uu/k - LAUFER(1954)
ww/k - LAUFER(1954)
vv/k - LAUFER(1954)
uu/k - SCHILDKNECHT et al.(1979)
ww/k - SCHILDKNECHT et al.(1979)
vv/k - SCHILDKNECHT et al.(1979)
CALCULATION(ReD=50000) - uu/k, ww/k, vv/k(TOP TO BOTTOM)
CALCULATION(ReD=21750) - uu/k, ww/k, vv/k(TOP TO BOTTOM)
vv/k, ww/k, uu/k
Y+
0.00
20.00
40.00
60.00
80.00
0.00
0.50
1.00
1.50
2.00

Figure 5g.

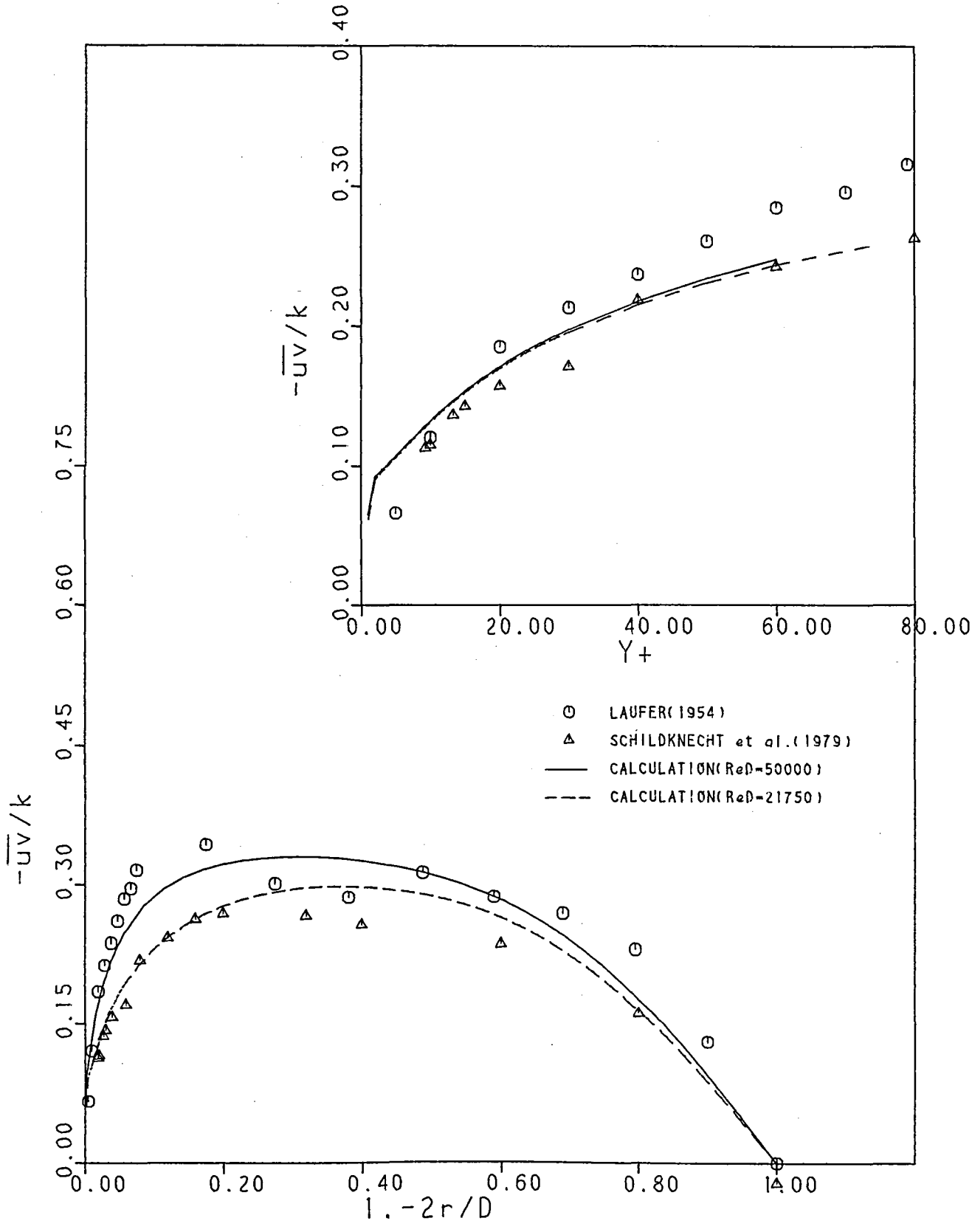
0.00
0.15
0.30
0.45
0.60
0.75
$-\overline{uv}/k$
0.00
0.20
0.40
0.60
0.80
1.00
1.-2r/D
0.00
0.10
0.20
0.30
0.40
$-\overline{uv}/k$
0.00
20.00
40.00
60.00
80.00
Y+
LAUFER(1954)
SCHILDKNECHT et al.(1979)
CALCULATION(ReD=50000)
CALCULATION(ReD=21750)

Figure 5h.

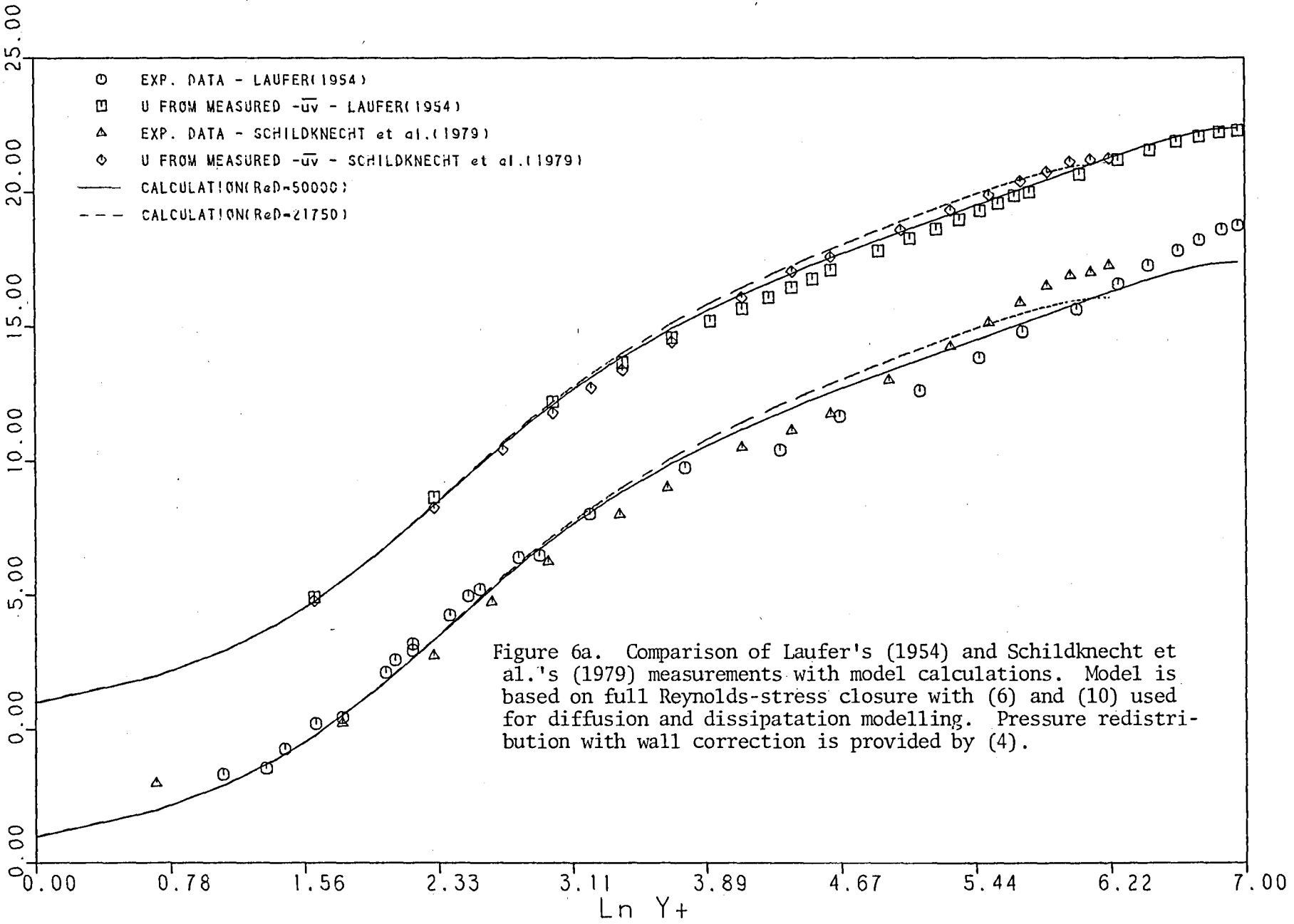

Figure 6a. Comparison of Laufer's (1954) and Schildknecht et al.'s (1979) measurements with model calculations. Model is based on full Reynolds-stress closure with (6) and (10) used for diffusion and dissipatation modelling. Pressure redistribution with wall correction is provided by (4).

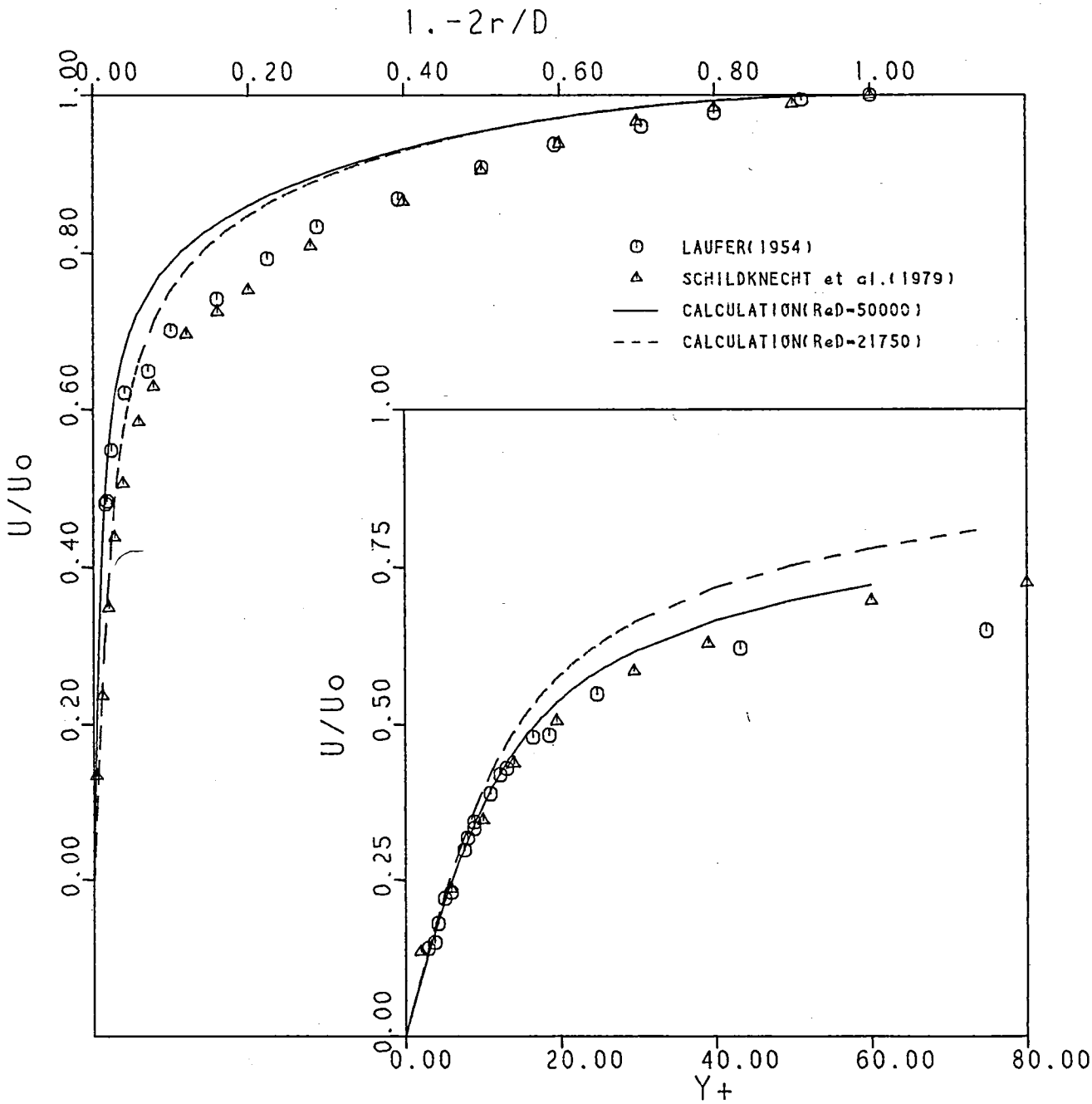
1.-2r/D
0.00
0.20
0.40
0.60
0.80
1.00
U/Uo
LAUFER(1954)
SCHILDKNECHT et al.(1979)
CALCULATION(ReD=50000)
CALCULATION(ReD=21750)
0.00
0.25
0.50
0.75
1.00
20.00
40.00
60.00
80.00
Y+

Figure 6b.

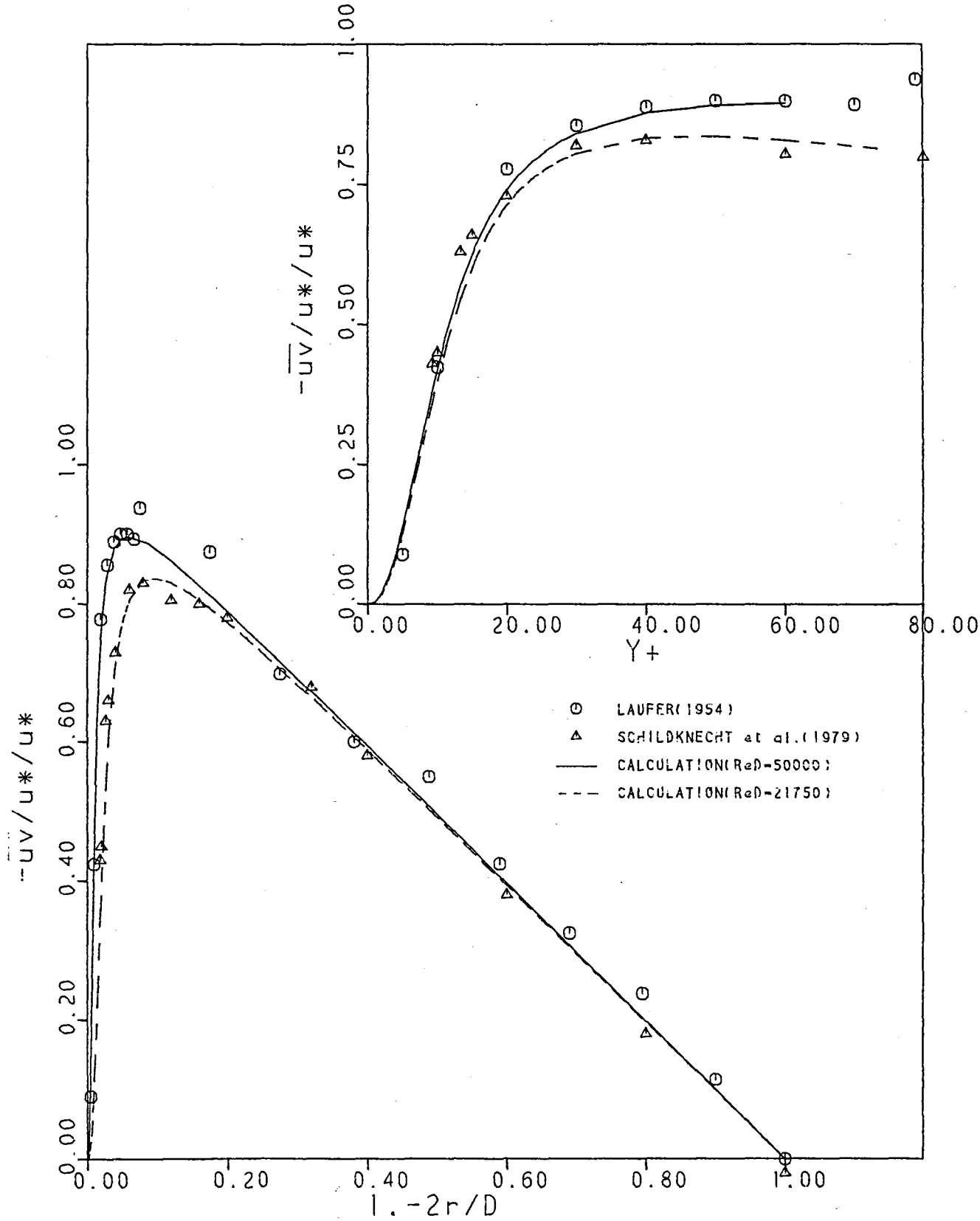
-uv/u*/u*
1.-2r/D
0.00
0.20
0.40
0.60
0.80
1.00
LAUFER(1954)
SCHILDKNECHT et al.(1979)
CALCULATION(ReD=50000)
CALCULATION(ReD=21750)
-uv/u*/u*
Y+
0.00
20.00
40.00
60.00
80.00
0.25
0.50
0.75

Figure 6c.

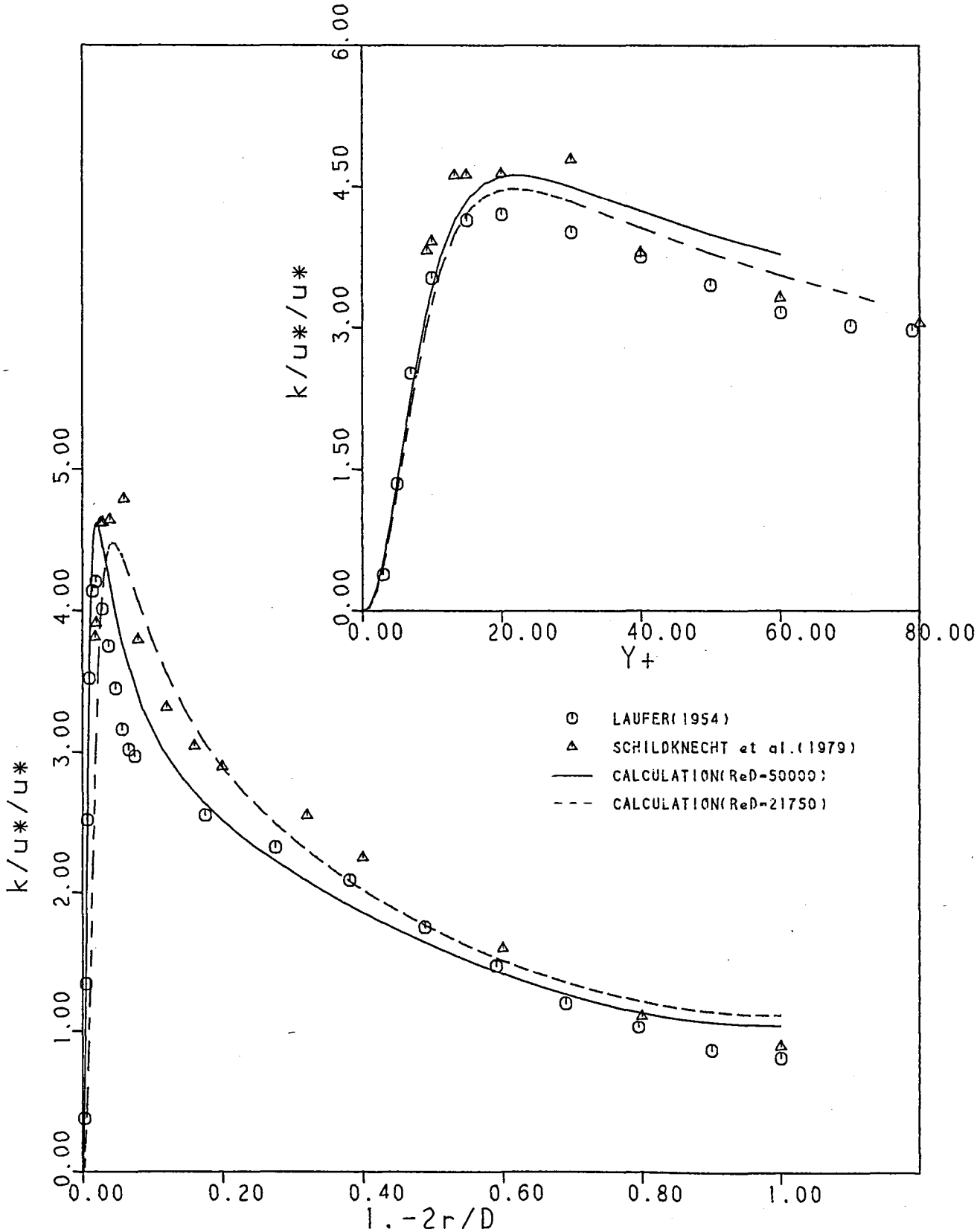
k/u*/u*
1.-2r/D
0.00
1.00
2.00
3.00
4.00
5.00
0.00
0.20
0.40
0.60
0.80
1.00
k/u*/u*
Y+
0.00
1.50
3.00
4.50
6.00
0.00
20.00
40.00
60.00
80.00
LAUFER(1954)
SCHILDKNECHT et al.(1979)
CALCULATION(ReD=50000)
CALCULATION(ReD=21750)

Figure 6d.

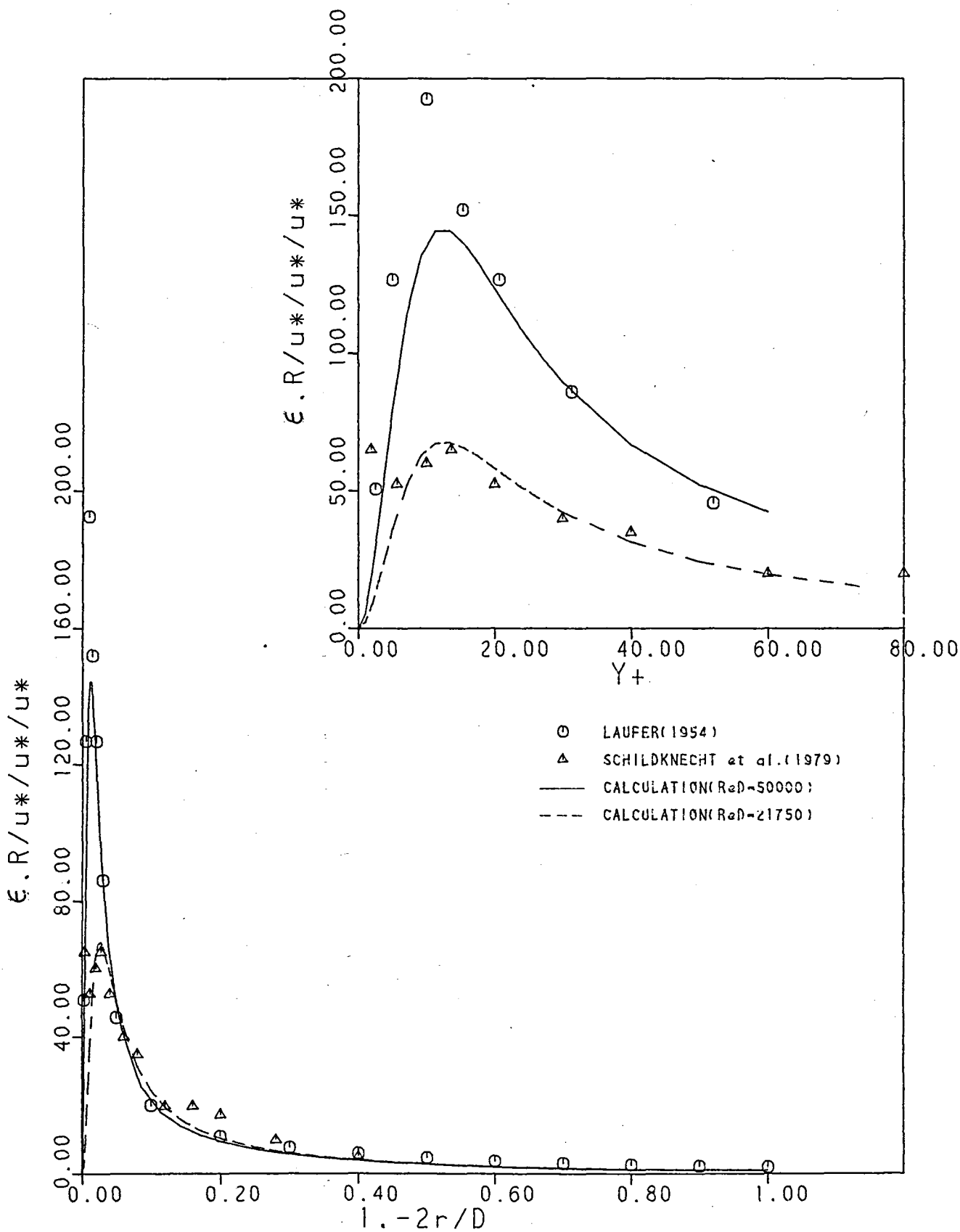
ε.R/u*/u*/u*
1.-2r/D
0.00
40.00
80.00
120.00
160.00
200.00
0.00
0.20
0.40
0.60
0.80
1.00
ε.R/u*/u*
Y+
0.00
50.00
100.00
150.00
200.00
0.00
20.00
40.00
60.00
80.00
LAUFER(1954)
SCHILDKNECHT et al.(1979)
CALCULATION(ReD=50000)
CALCULATION(ReD=21750)

Figure 6e.

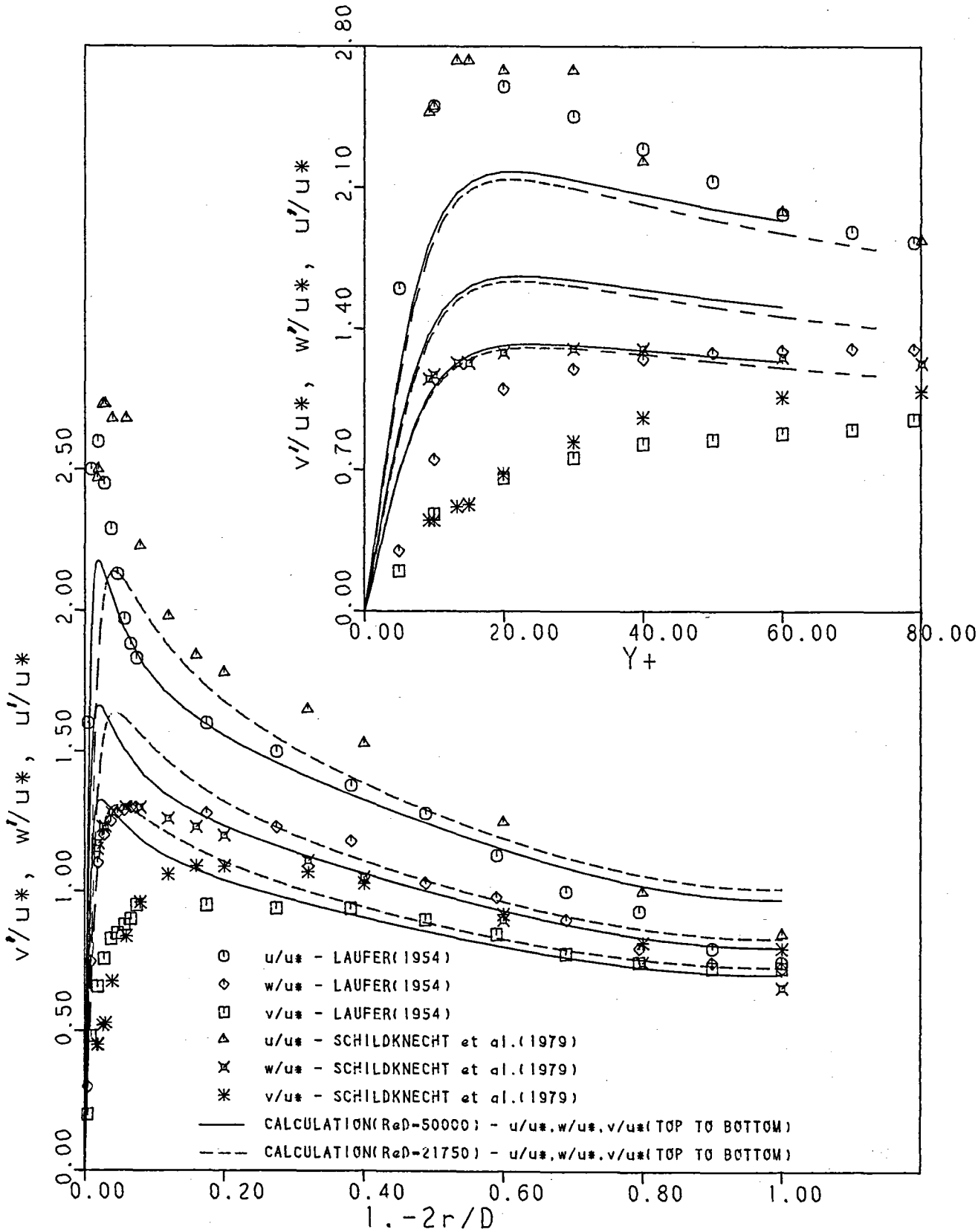
v'/u*, w'/u*, u'/u*
1.-2r/D
u/u* - LAUFER(1954)
w/u* - LAUFER(1954)
v/u* - LAUFER(1954)
u/u* - SCHILDKNECHT et al.(1979)
w/u* - SCHILDKNECHT et al.(1979)
v/u* - SCHILDKNECHT et al.(1979)
CALCULATION(ReD=50000) - u/u*,w/u*,v/u*(TOP TO BOTTOM)
CALCULATION(ReD=21750) - u/u*,w/u*,v/u*(TOP TO BOTTOM)
v'/u*, w'/u*, u'/u*
Y+

Figure 6f.

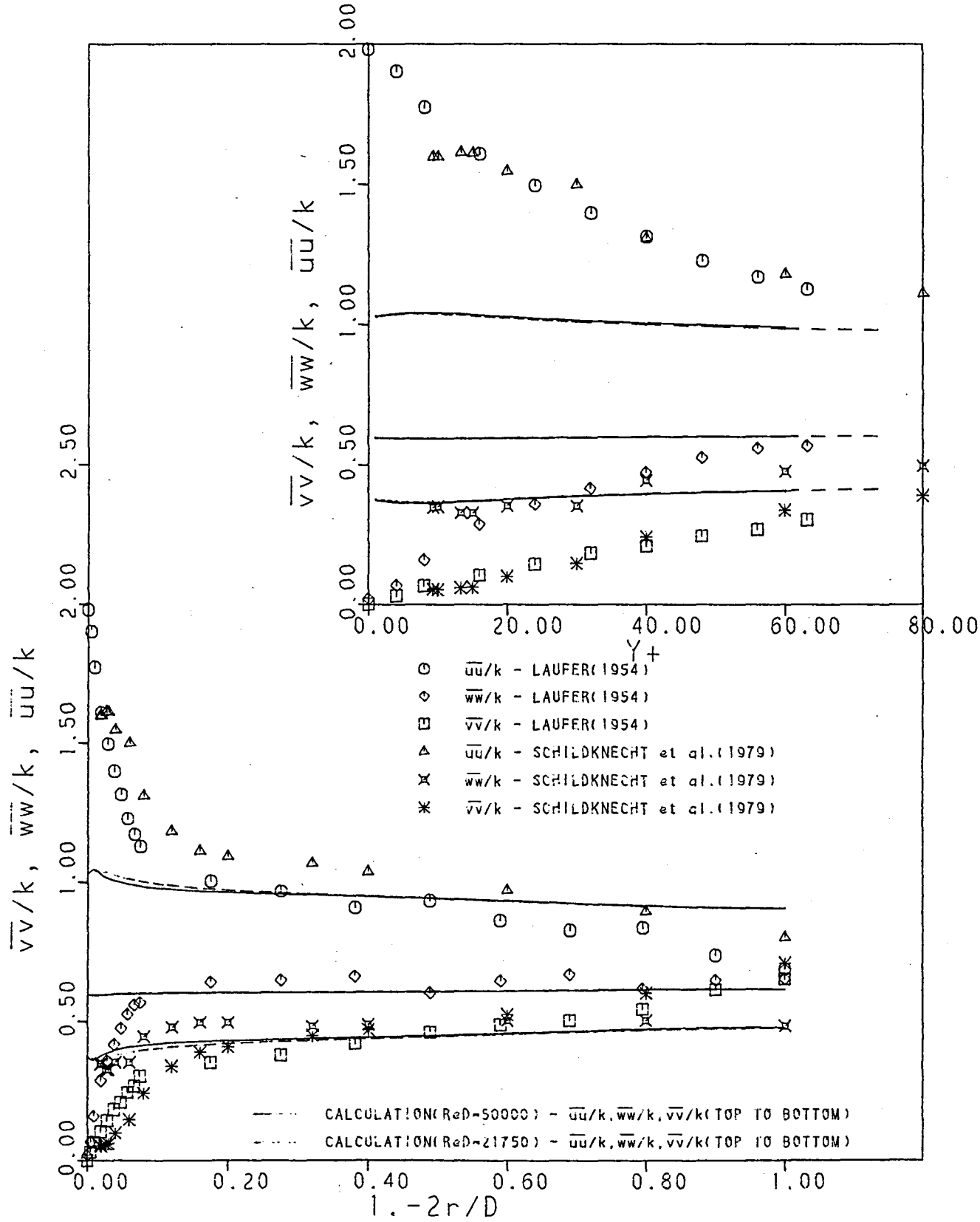
vv/k, ww/k, uu/k
1.-2r/D
0.00
0.20
0.40
0.60
0.80
1.00
0.00
0.50
1.00
1.50
2.00
2.50
uu/k - LAUFER(1954)
ww/k - LAUFER(1954)
vv/k - LAUFER(1954)
uu/k - SCHILDKNECHT et al.(1979)
ww/k - SCHILDKNECHT et al.(1979)
vv/k - SCHILDKNECHT et al.(1979)
CALCULATION(ReD=50000) - uu/k,ww/k,vv/k(TOP TO BOTTOM)
CALCULATION(ReD=21750) - uu/k,ww/k,vv/k(TOP TO BOTTOM)
vv/k, ww/k, uu/k
Y+
0.00
20.00
40.00
60.00
80.00
0.00
0.50
1.00
1.50
2.00

Figure 6g.

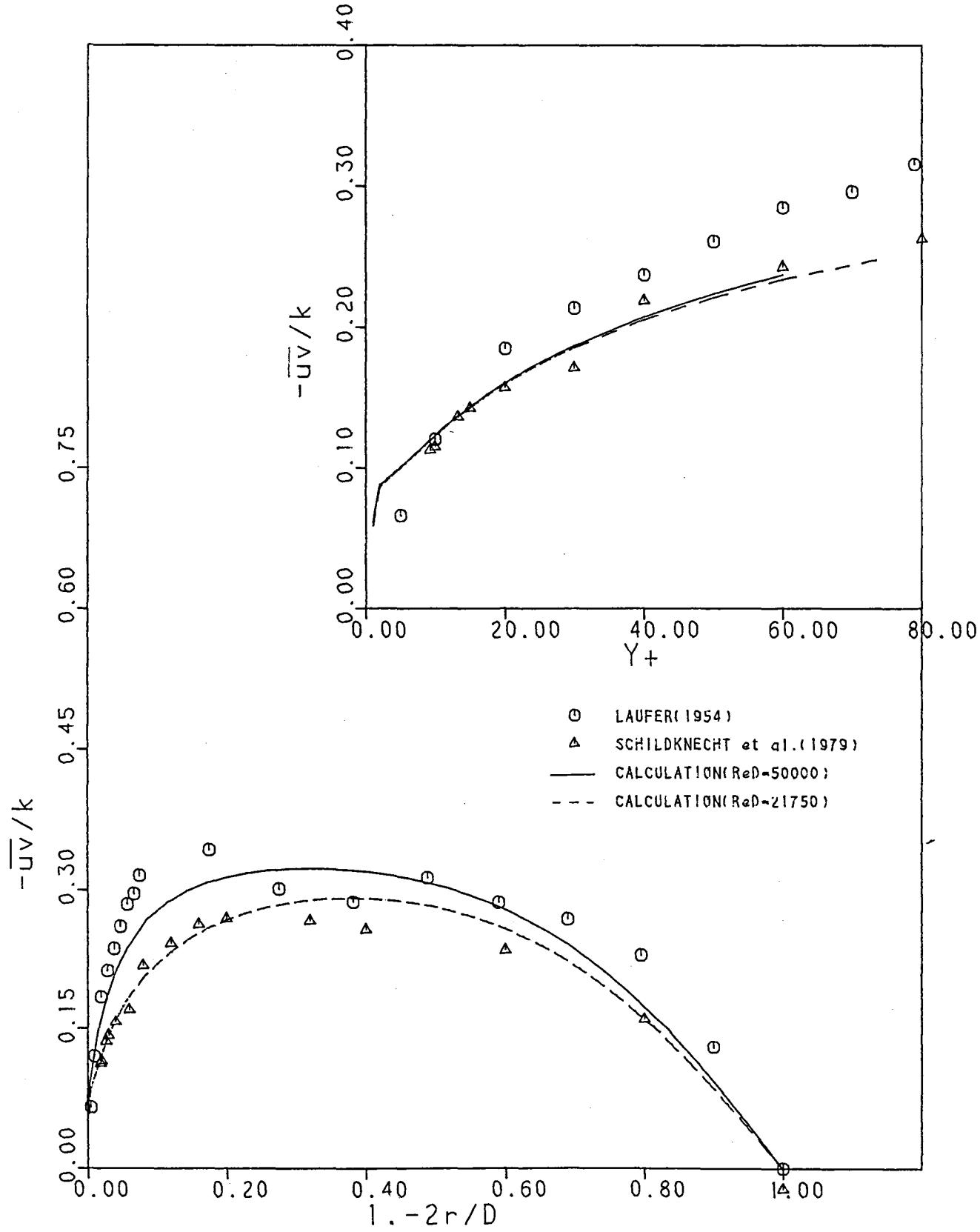
0.00
0.10
0.20
0.30
0.40
-uv/k
0.00
20.00
40.00
60.00
80.00
Y+
0.00
0.15
0.30
0.45
0.60
0.75
-uv/k
LAUFER(1954)
SCHILDKNECHT et al.(1979)
CALCULATION(ReD=50000)
CALCULATION(ReD=21750)
0.00
0.20
0.40
0.60
0.80
1.00
1.-2r/D

Figure 6h.

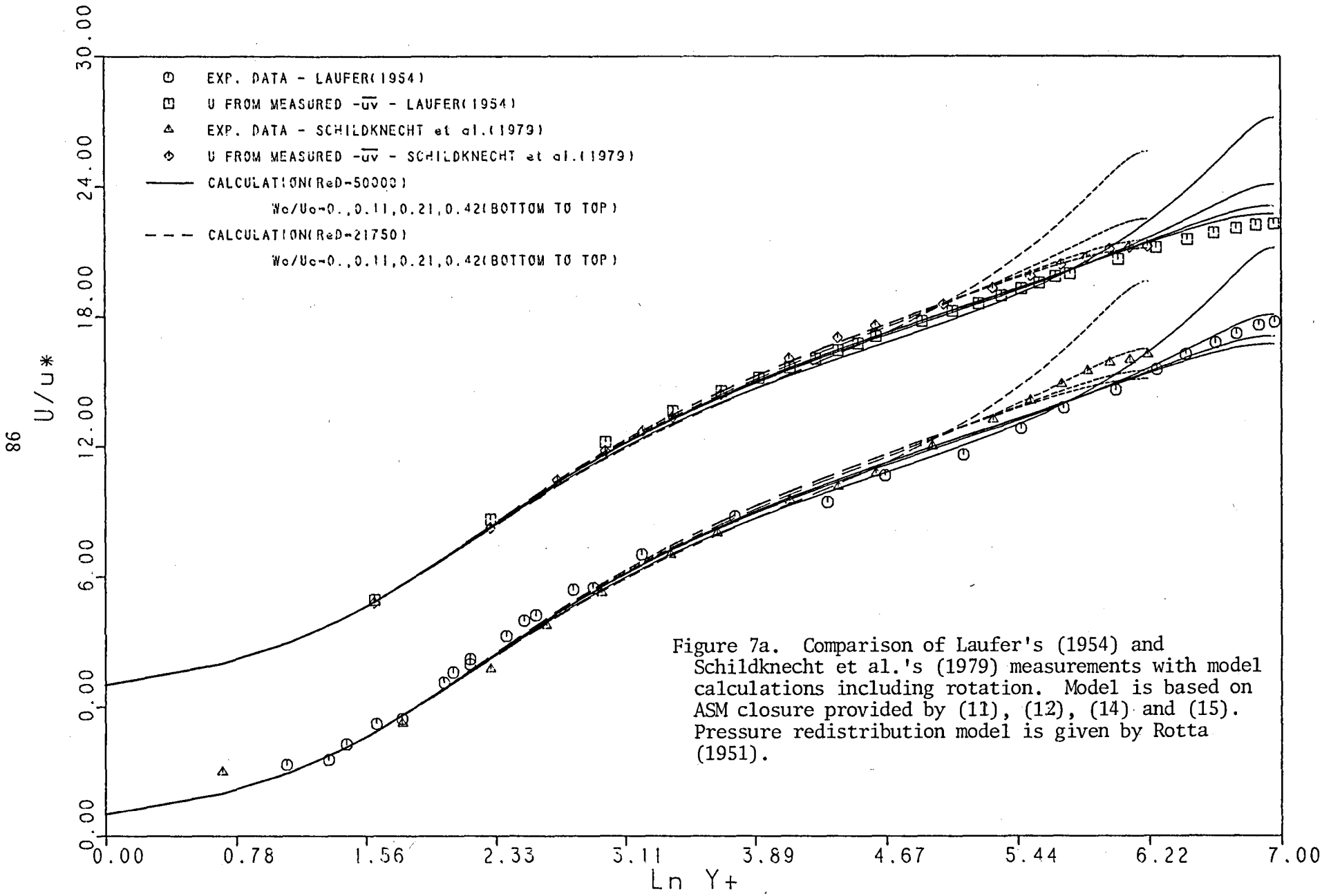

Figure 7a. Comparison of Laufer's (1954) and Schildknecht et al.'s (1979) measurements with model calculations including rotation. Model is based on ASM closure provided by (11), (12), (14) and (15). Pressure redistribution model is given by Rotta (1951).

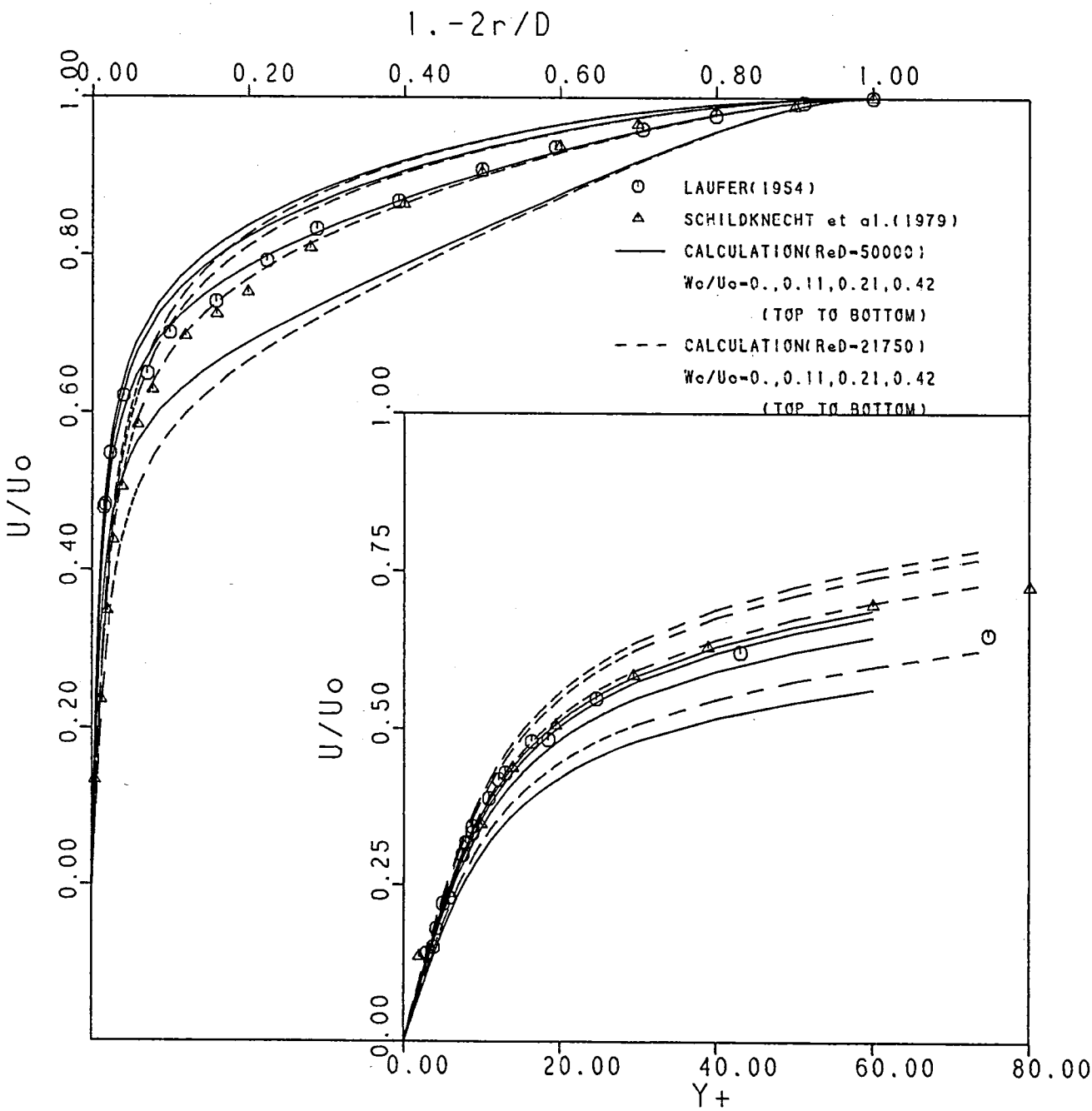
1.-2r/D
0.00
0.20
0.40
0.60
0.80
1.00
U/Uo
LAUFER(1954)
SCHILDKNECHT et al.(1979)
CALCULATION(ReD=50000)
Wo/Uo=0.,0.11,0.21,0.42
(TOP TO BOTTOM)
CALCULATION(ReD=21750)
Wo/Uo=0.,0.11,0.21,0.42
(TOP TO BOTTOM)
0.00
0.25
0.50
0.75
1.00
0.00
20.00
40.00
60.00
80.00
Y+

Figure 7b.

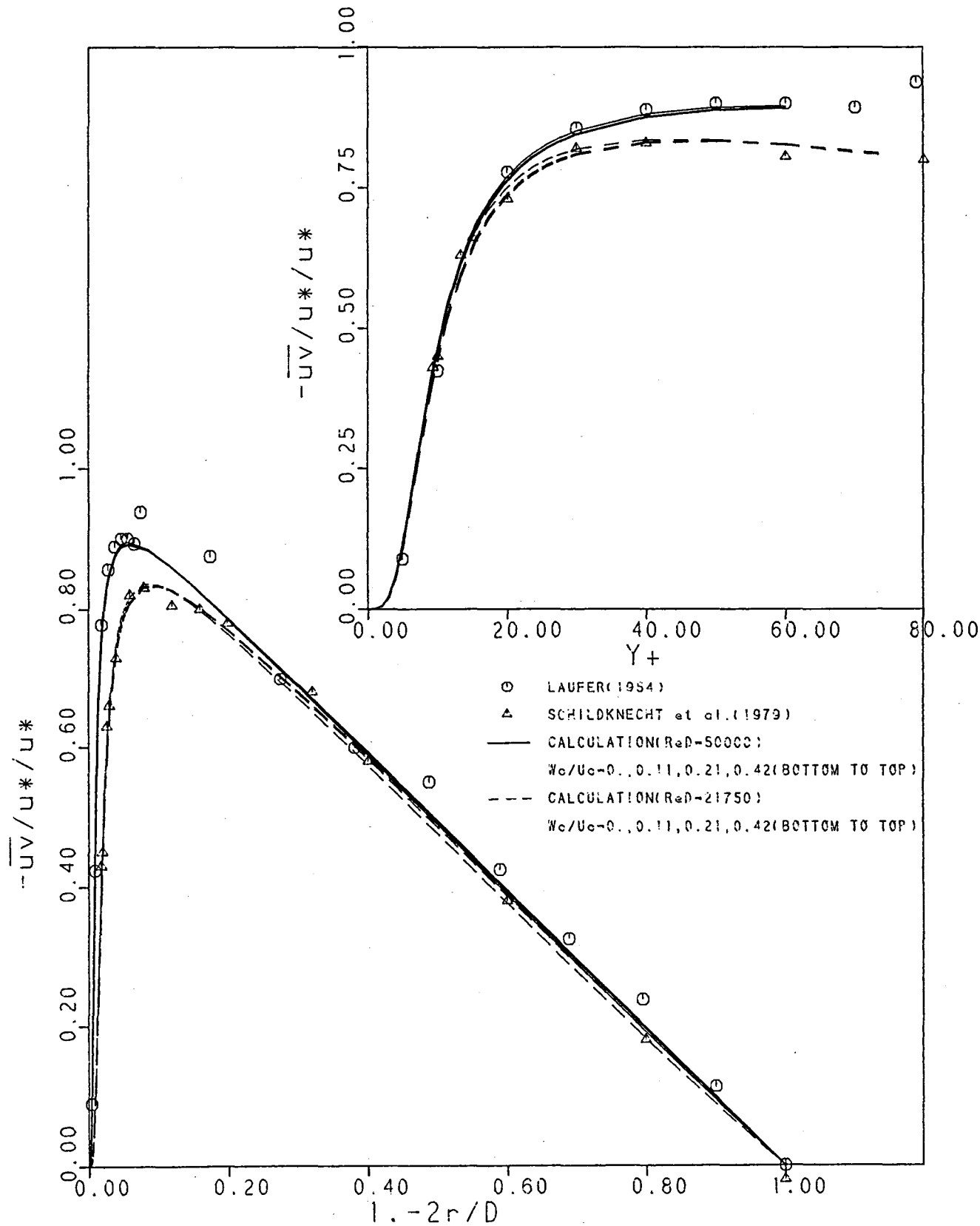
-uv/u*/u*
1.00
0.80
0.60
0.40
0.20
0.00
0.00
0.20
0.40
0.60
0.80
1.00
1.-2r/D
-uv/u*/u*
1.00
0.75
0.50
0.25
0.00
0.00
20.00
40.00
60.00
80.00
Y+
LAUFER(1954)
SCHILDKNECHT et al.(1979)
CALCULATION(ReD=50000)
Wc/Uc=0.,0.11,0.21,0.42(BOTTOM TO TOP)
CALCULATION(ReD=21750)
Wc/Uc=0.,0.11,0.21,0.42(BOTTOM TO TOP)

Figure 7c.

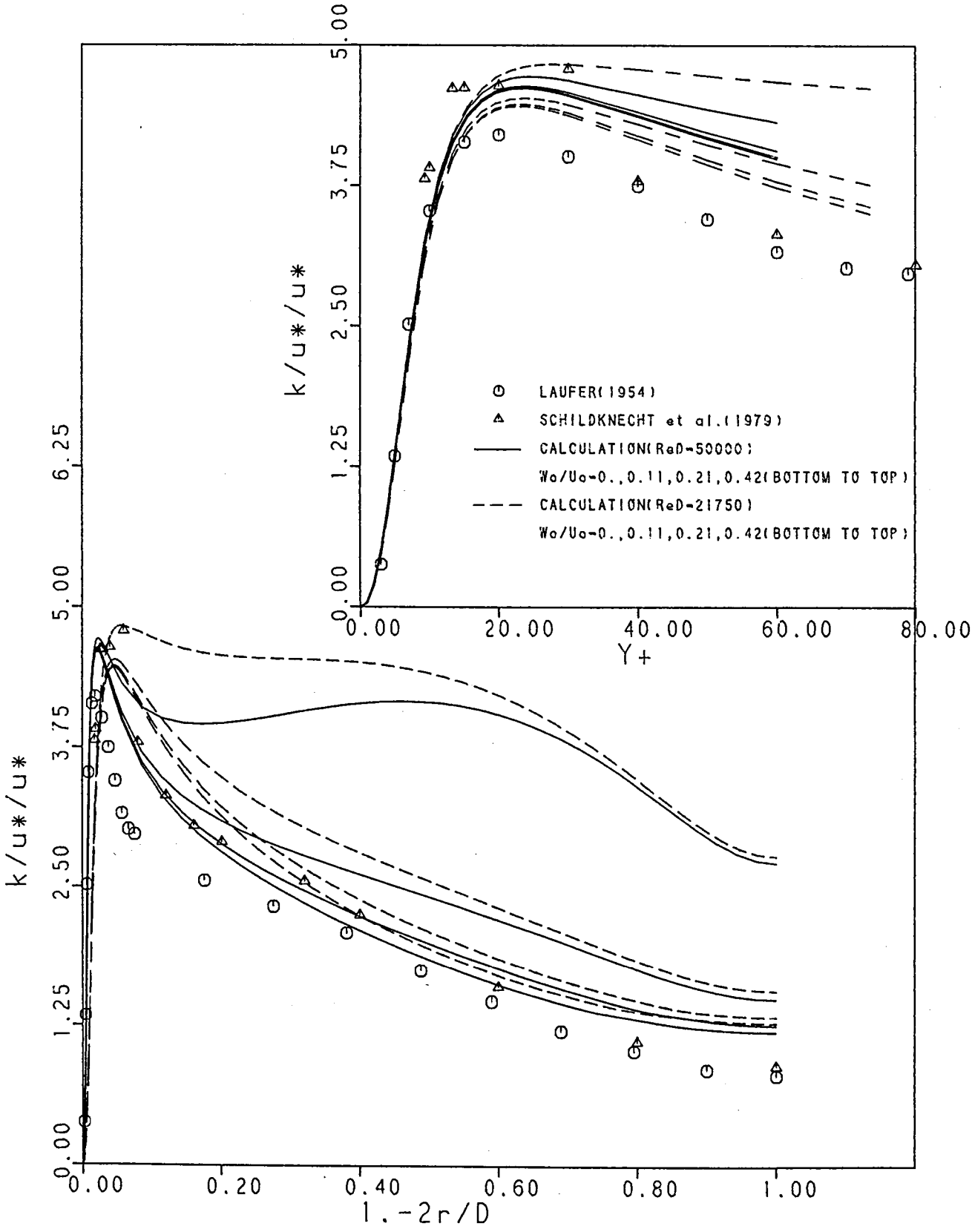
k/u*/u*
1.-2r/D
0.00
1.25
2.50
3.75
5.00
6.25
0.00
0.20
0.40
0.60
0.80
1.00
k/u*/u*
Y+
0.00
1.25
2.50
3.75
5.00
0.00
20.00
40.00
60.00
80.00
LAUFER(1954)
SCHILDKNECHT et al.(1979)
CALCULATION(ReD=50000)
Wo/Uo=0.,0.11,0.21,0.42(BOTTOM TO TOP)
CALCULATION(ReD=21750)
Wo/Uo=0.,0.11,0.21,0.42(BOTTOM TO TOP)

Figure 7d.

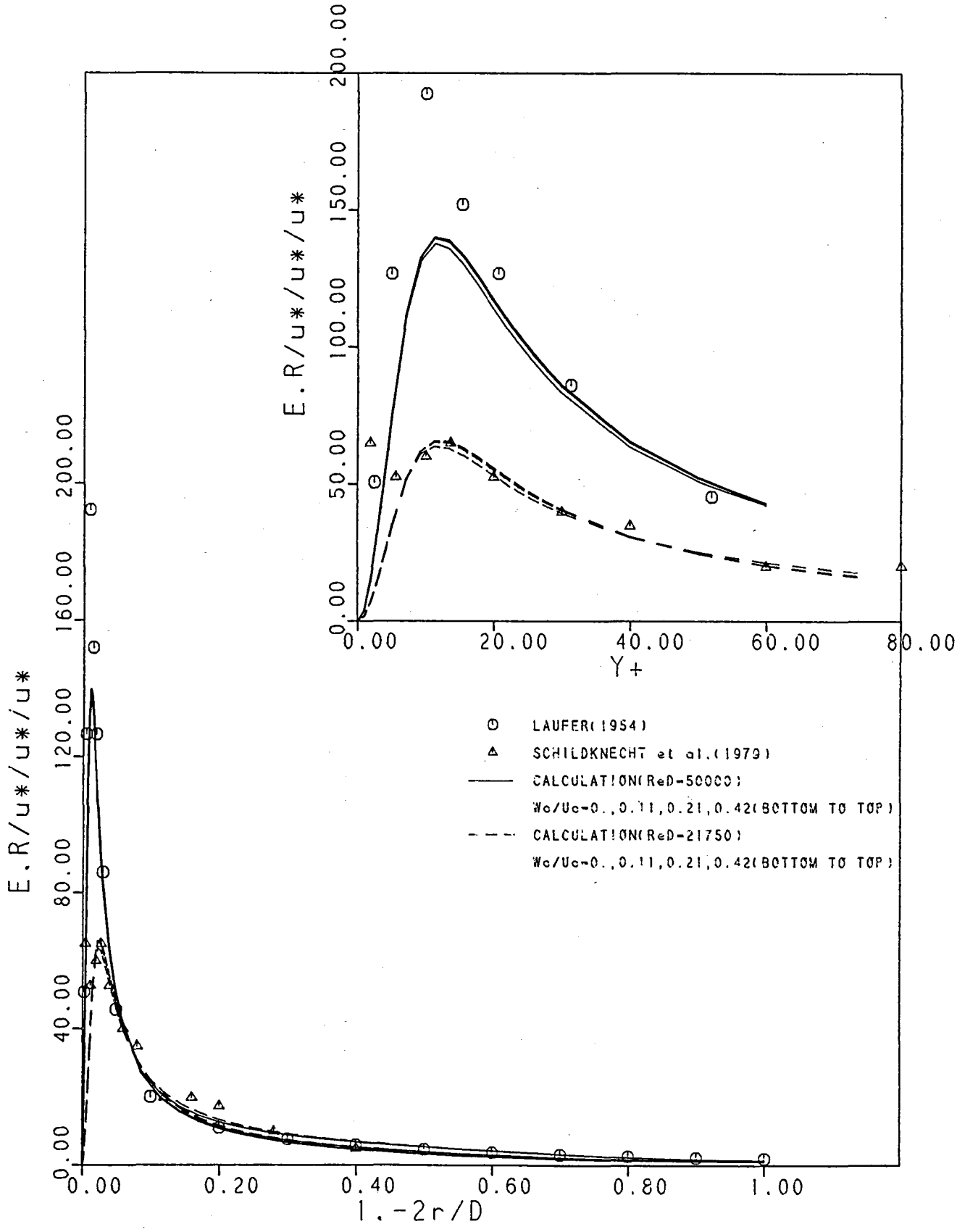
E.R/u*/u*/u*
0.00
40.00
80.00
120.00
160.00
200.00
0.00
0.20
0.40
0.60
0.80
1.00
1.-2r/D
E.R/u*/u*/u*
0.00
50.00
100.00
150.00
200.00
0.00
20.00
40.00
60.00
80.00
Y+
LAUFER(1954)
SCHILDKNECHT et al.(1979)
CALCULATION(ReD=50000)
Wo/Uc=0.,0.11,0.21,0.42(BOTTOM TO TOP)
CALCULATION(ReD=21750)
Wo/Uc=0.,0.11,0.21,0.42(BOTTOM TO TOP)

Figure 7e.

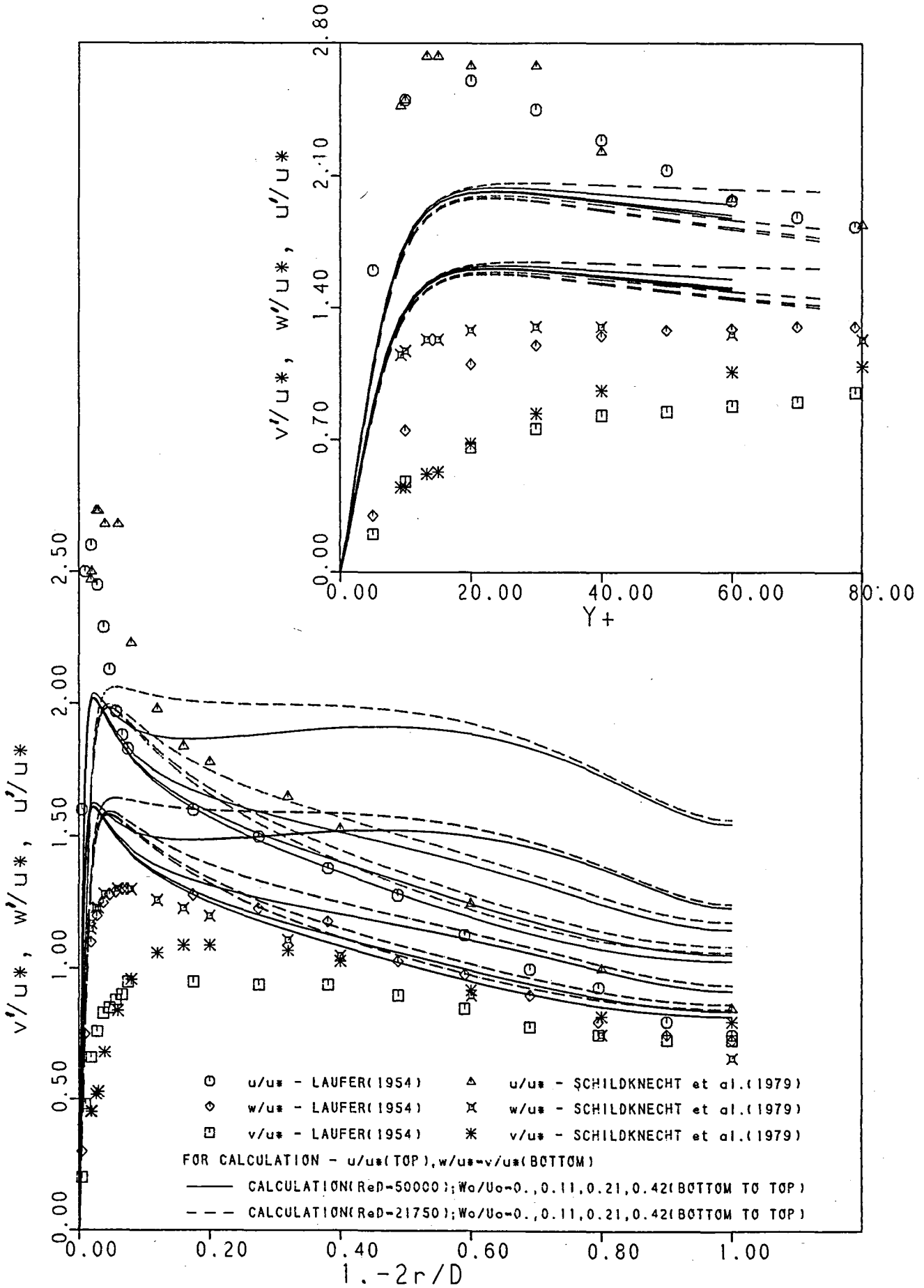
v'/u*, w'/u*, u'/u*
1.-2r/D
0.00
0.20
0.40
0.60
0.80
1.00
0.50
1.00
1.50
2.00
2.50
u/u* - LAUFER(1954)
w/u* - LAUFER(1954)
v/u* - LAUFER(1954)
u/u* - SCHILDKNECHT et al.(1979)
w/u* - SCHILDKNECHT et al.(1979)
v/u* - SCHILDKNECHT et al.(1979)
FOR CALCULATION - u/u*(TOP),w/u*=v/u*(BOTTOM)
CALCULATION(ReD=50000);Wo/Uo=0.,0.11,0.21,0.42(BOTTOM TO TOP)
CALCULATION(ReD=21750);Wo/Uo=0.,0.11,0.21,0.42(BOTTOM TO TOP)
v'/u*, w'/u*, u'/u*
Y+
0.00
20.00
40.00
60.00
80.00
0.70
1.40
2.10
2.80

Figure 7f.

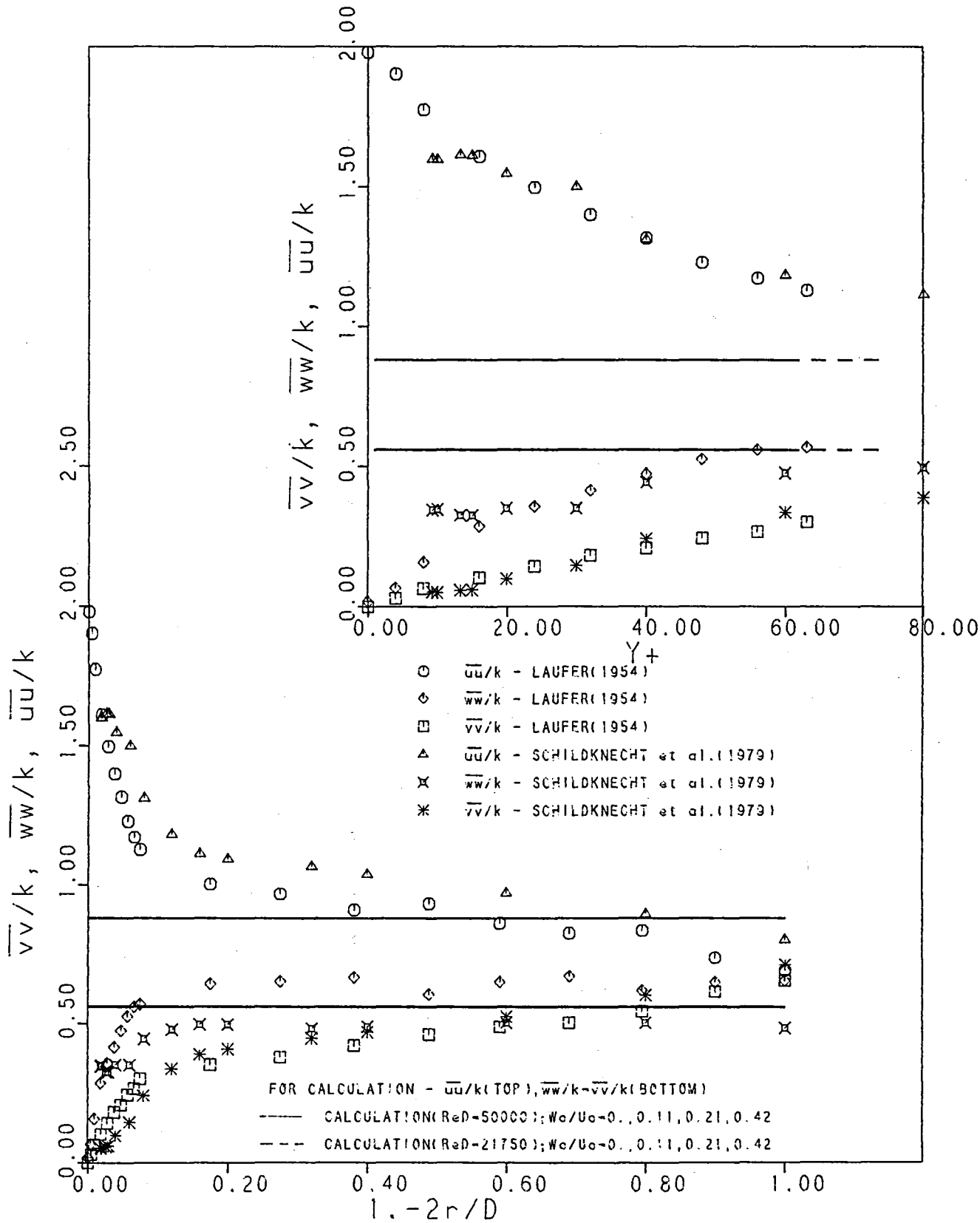
vv/k, ww/k, uu/k
1.-2r/D
Y+
uu/k - LAUFER(1954)
ww/k - LAUFER(1954)
vv/k - LAUFER(1954)
uu/k - SCHILDKNECHT et al.(1979)
ww/k - SCHILDKNECHT et al.(1979)
vv/k - SCHILDKNECHT et al.(1979)
FOR CALCULATION - uu/k(TOP),ww/k-vv/k(BOTTOM)
CALCULATION(ReD=50000);Wo/Uo=0.,0.11,0.21,0.42
CALCULATION(ReD=21750);Wo/Uo=0.,0.11,0.21,0.42

Figure 7g.

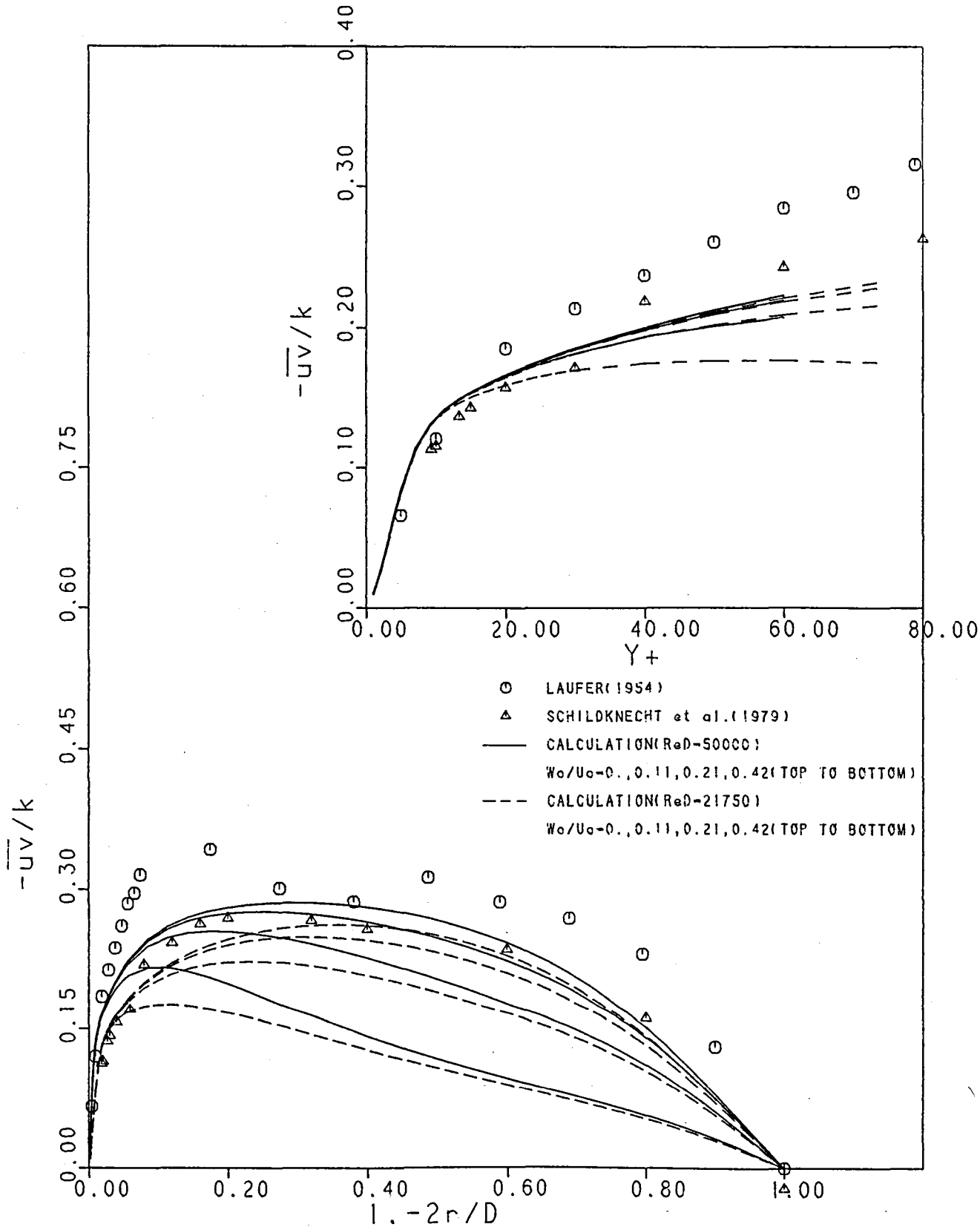
0.40
0.30
0.20
0.10
0.00
$-\overline{uv}/k$
0.00
20.00
40.00
60.00
80.00
Y+
LAUFER(1954)
SCHILDKNECHT et al.(1979)
CALCULATION(ReD=50000)
Wo/Uo=0.,0.11,0.21,0.42(TOP TO BOTTOM)
CALCULATION(ReD=21750)
Wo/Uo=0.,0.11,0.21,0.42(TOP TO BOTTOM)
0.75
0.60
0.45
0.30
0.15
0.00
$-\overline{uv}/k$
0.00
0.20
0.40
0.60
0.80
1.00
1.-2r/D

Figure 7h.

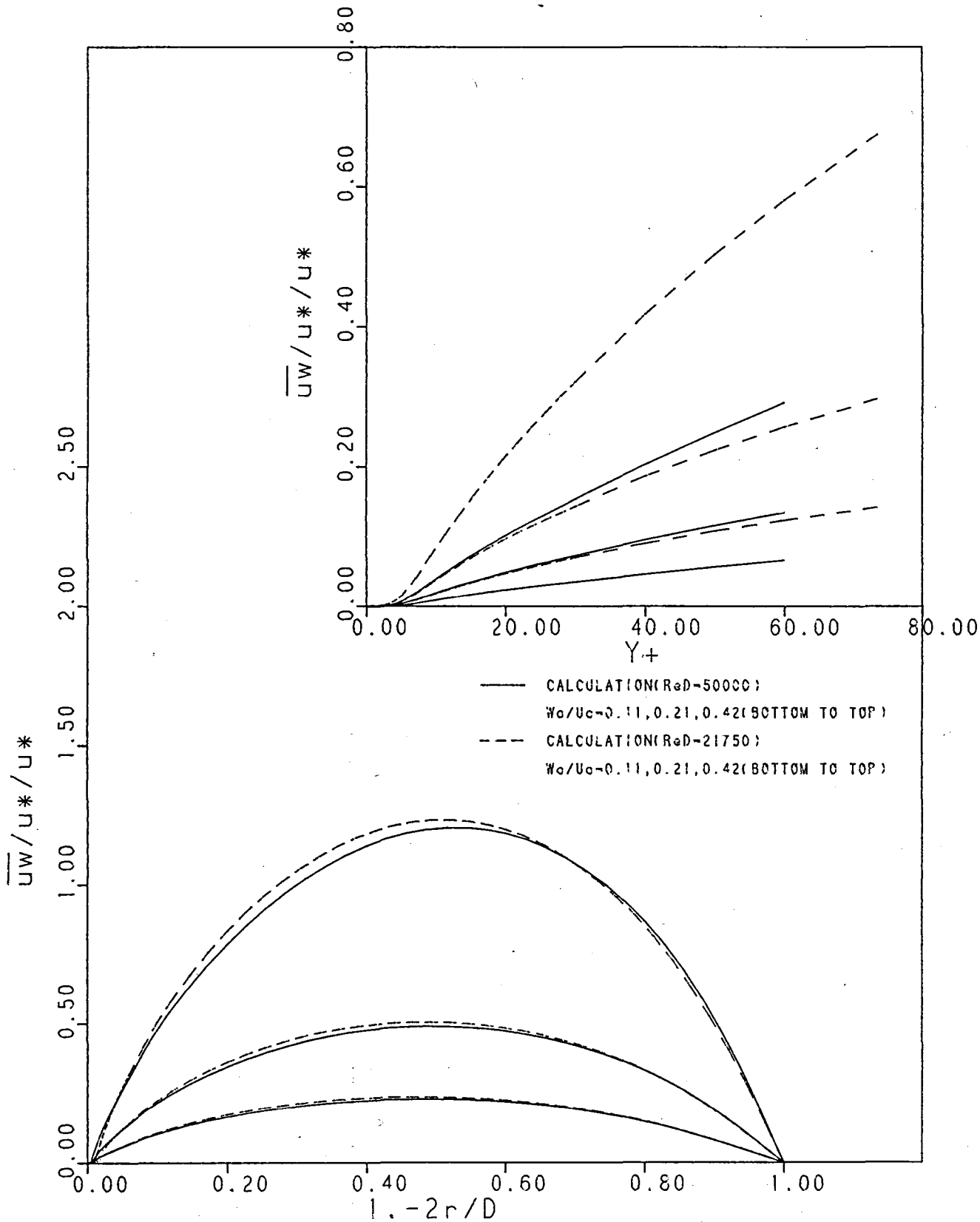
0.80
0.60
0.40
0.20
0.00
$\overline{uw}/u*/u*$
0.00
20.00
40.00
60.00
80.00
Y+
CALCULATION(ReD=50000)
Wo/Uc=0.11,0.21,0.42(BOTTOM TO TOP)
CALCULATION(ReD=21750)
Wo/Uc=0.11,0.21,0.42(BOTTOM TO TOP)
2.50
2.00
1.50
1.00
0.50
0.00
$\overline{uw}/u*/u*$
0.00
0.20
0.40
0.60
0.80
1.00
1.-2r/D

Figure 7i.

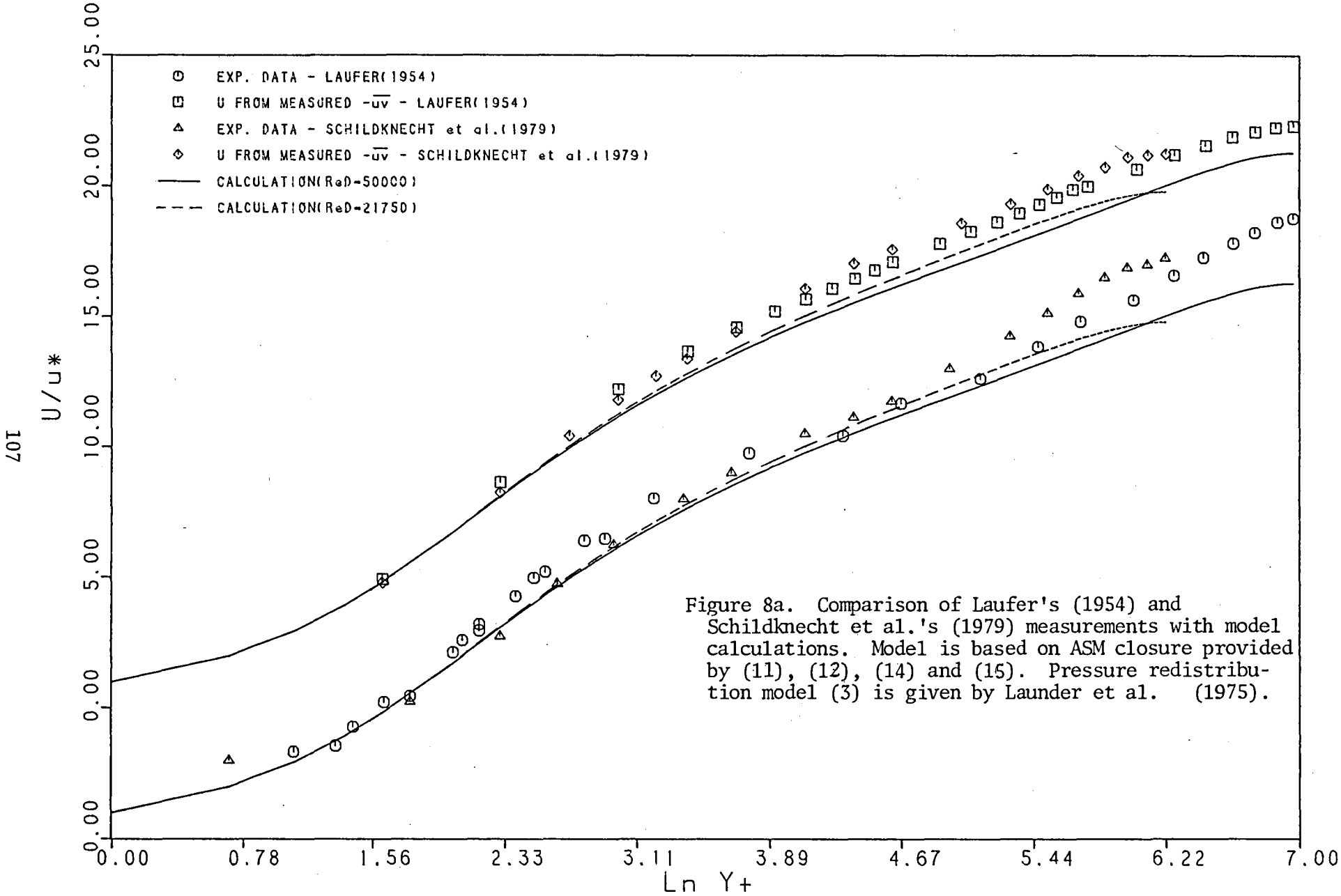

Figure 8a. Comparison of Laufer's (1954) and Schildknecht et al.'s (1979) measurements with model calculations. Model is based on ASM closure provided by (11), (12), (14) and (15). Pressure redistribution model (3) is given by Launder et al. (1975).

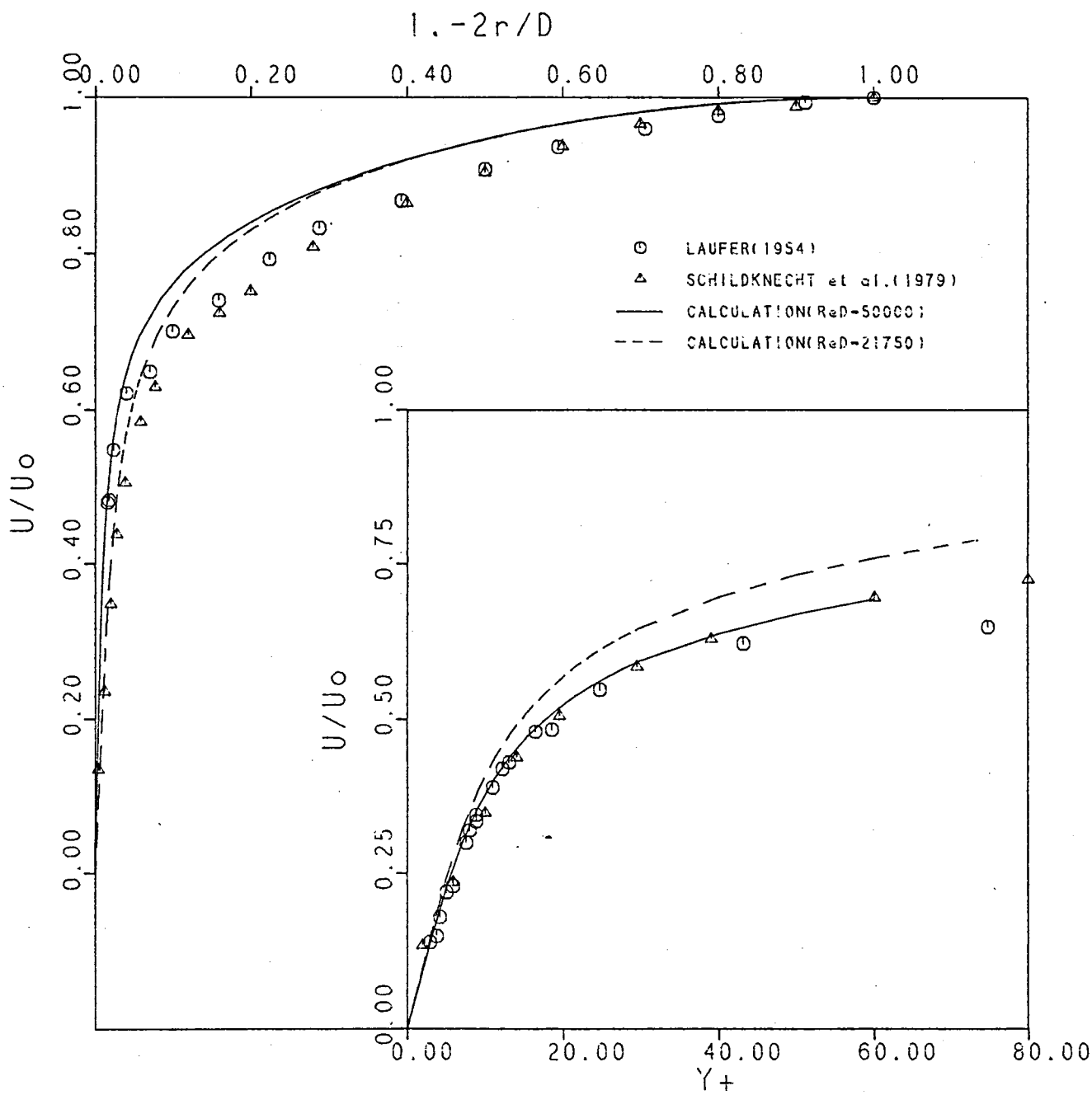
1.-2r/D
0.00
0.20
0.40
0.60
0.80
1.00
U/Uo
LAUFER(1954)
SCHILDKNECHT et al.(1979)
CALCULATION(ReD=50000)
CALCULATION(ReD=21750)
0.00
0.25
0.50
0.75
1.00
20.00
40.00
60.00
80.00
Y+

Figure 8b.

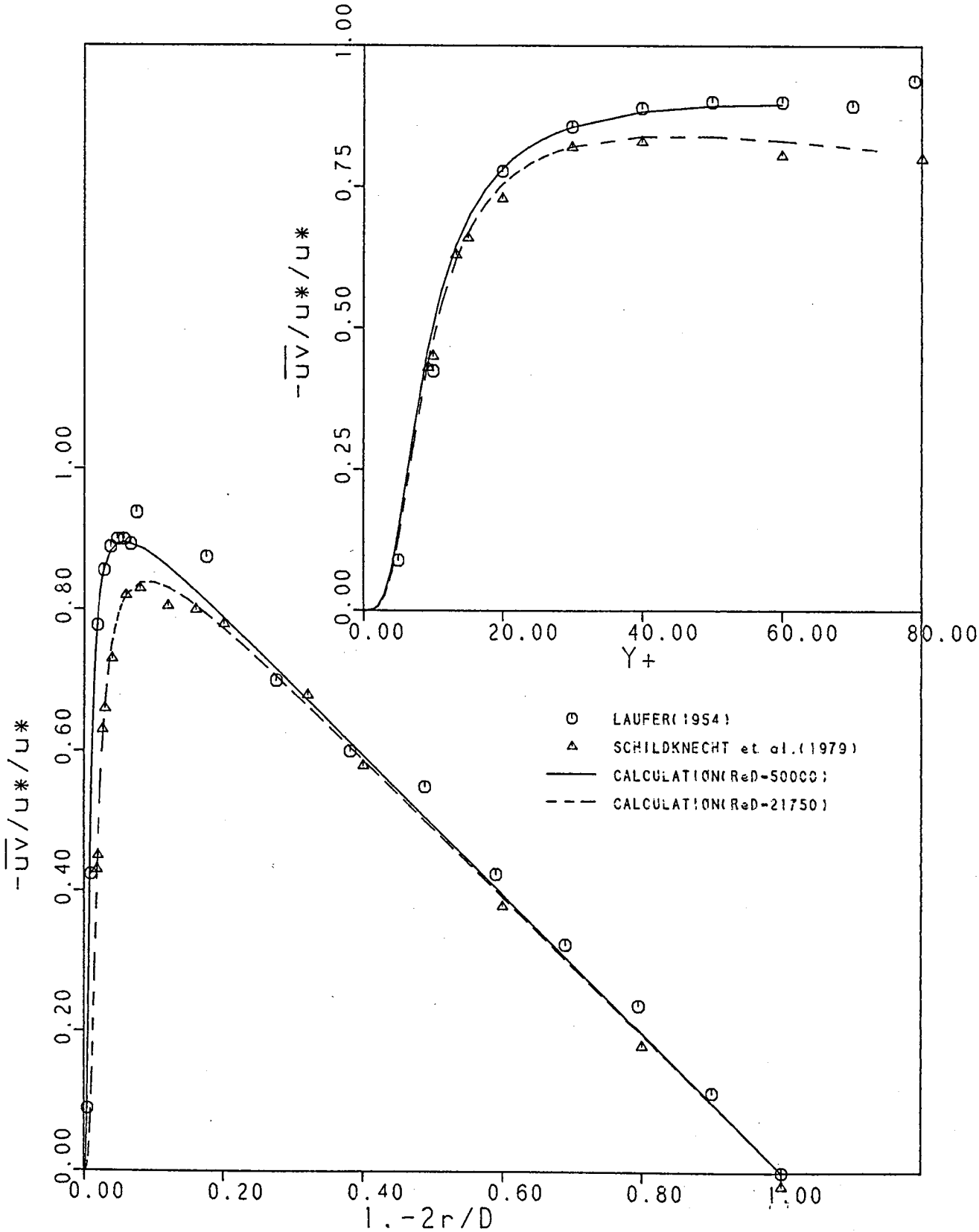
-uv/u*/u*
1.00
0.80
0.60
0.40
0.20
0.00
0.00
0.20
0.40
0.60
0.80
1.00
1.-2r/D
LAUFER(1954)
SCHILDKNECHT et al.(1979)
CALCULATION(ReD=50000)
CALCULATION(ReD=21750)
-uv/u*/u*
1.00
0.75
0.50
0.25
0.00
0.00
20.00
40.00
60.00
80.00
Y+

Figure 8c.

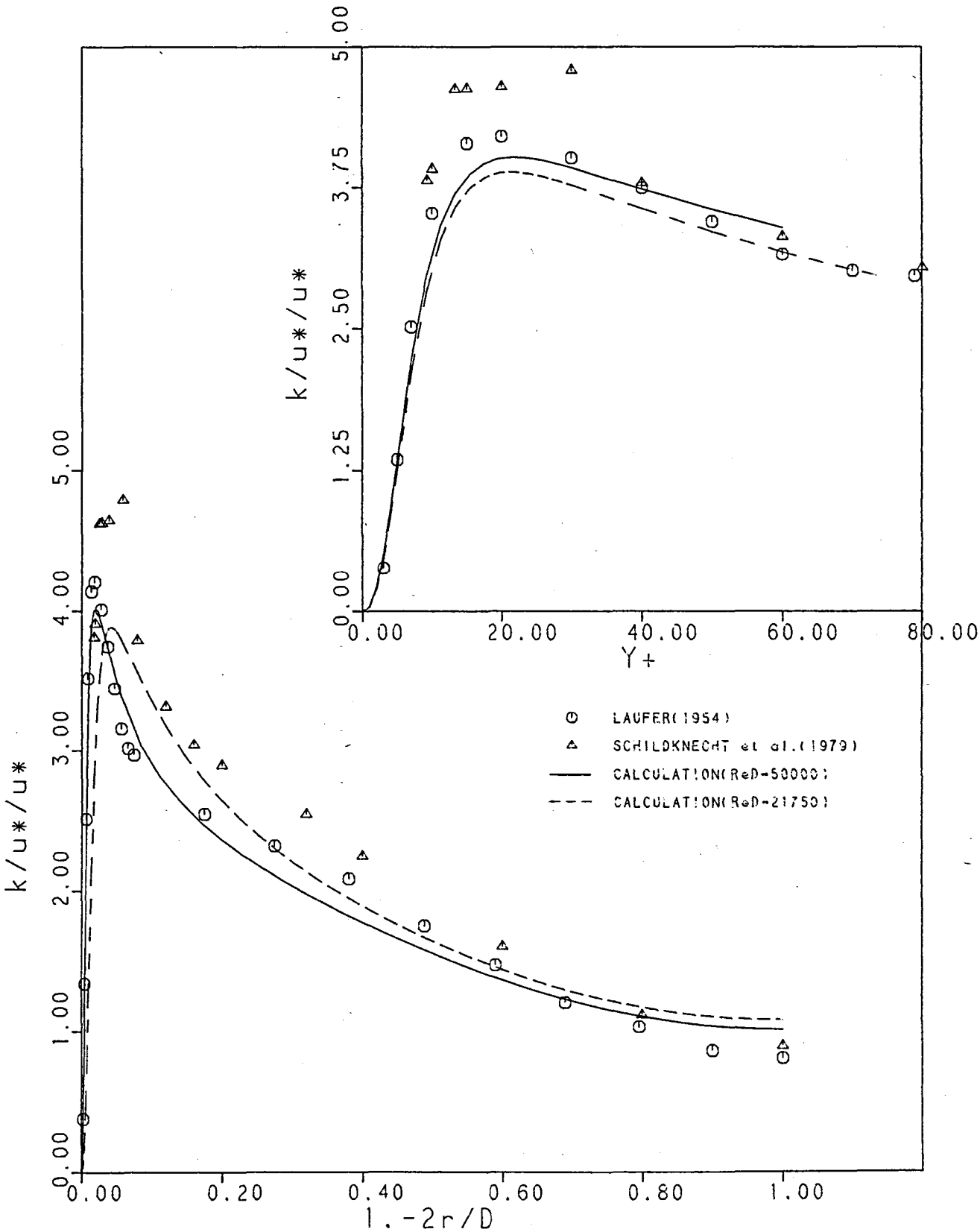
k/u*/u*
1.-2r/D
0.00
0.20
0.40
0.60
0.80
1.00
1.00
2.00
3.00
4.00
5.00
LAUFER(1954)
SCHILDKNECHT et al.(1979)
CALCULATION(ReD=50000)
CALCULATION(ReD=21750)
k/u*/u*
Y+
0.00
20.00
40.00
60.00
80.00
1.25
2.50
3.75
5.00

Figure 8d.

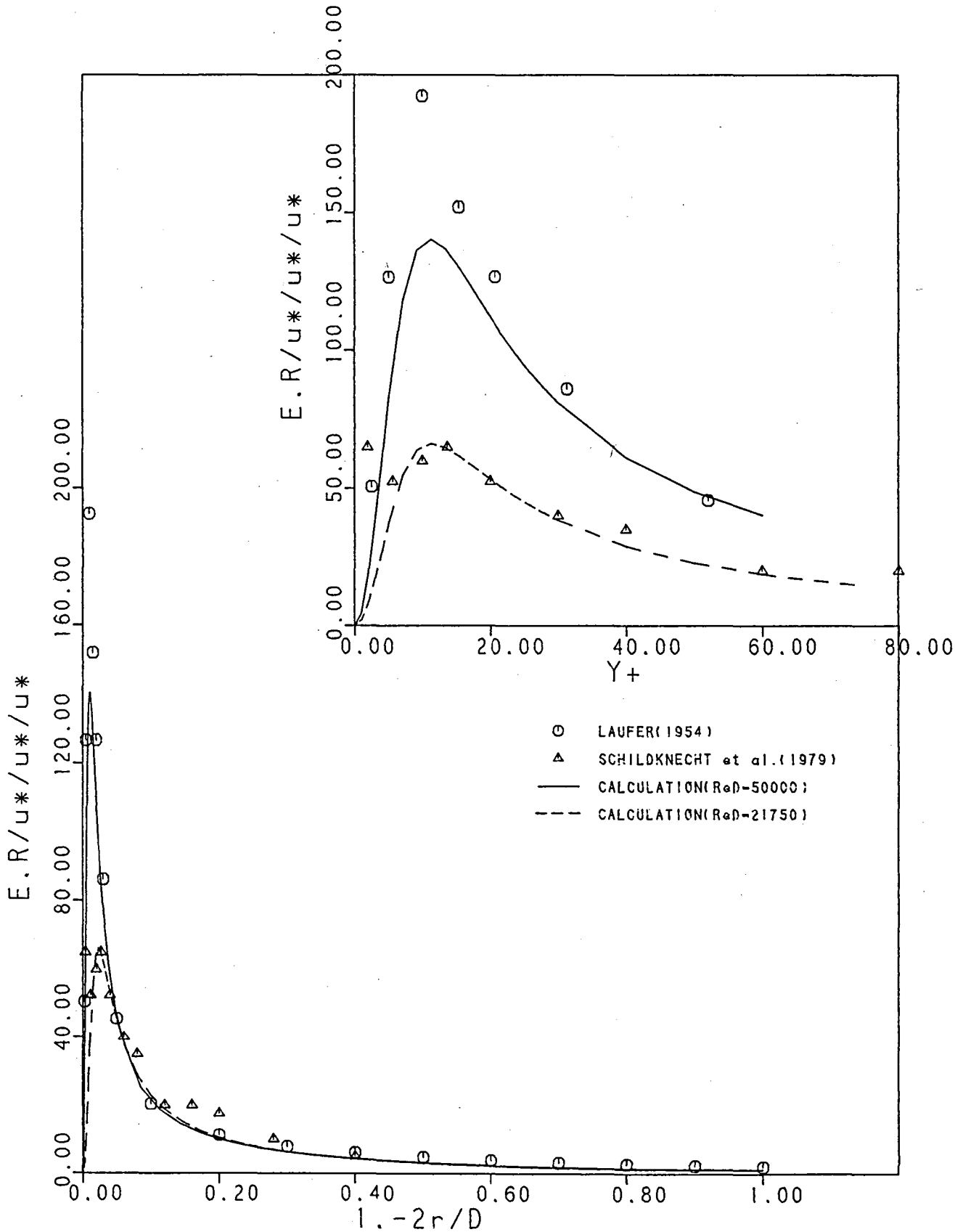
E.R/u*/u*
1.-2r/D
0.00
40.00
80.00
120.00
160.00
200.00
0.00
0.20
0.40
0.60
0.80
1.00
E.R/u*/u*
Y+
0.00
50.00
100.00
150.00
200.00
0.00
20.00
40.00
60.00
80.00
LAUFER(1954)
SCHILDKNECHT et al.(1979)
CALCULATION(ReD=50000)
CALCULATION(ReD=21750)

Figure 8e.

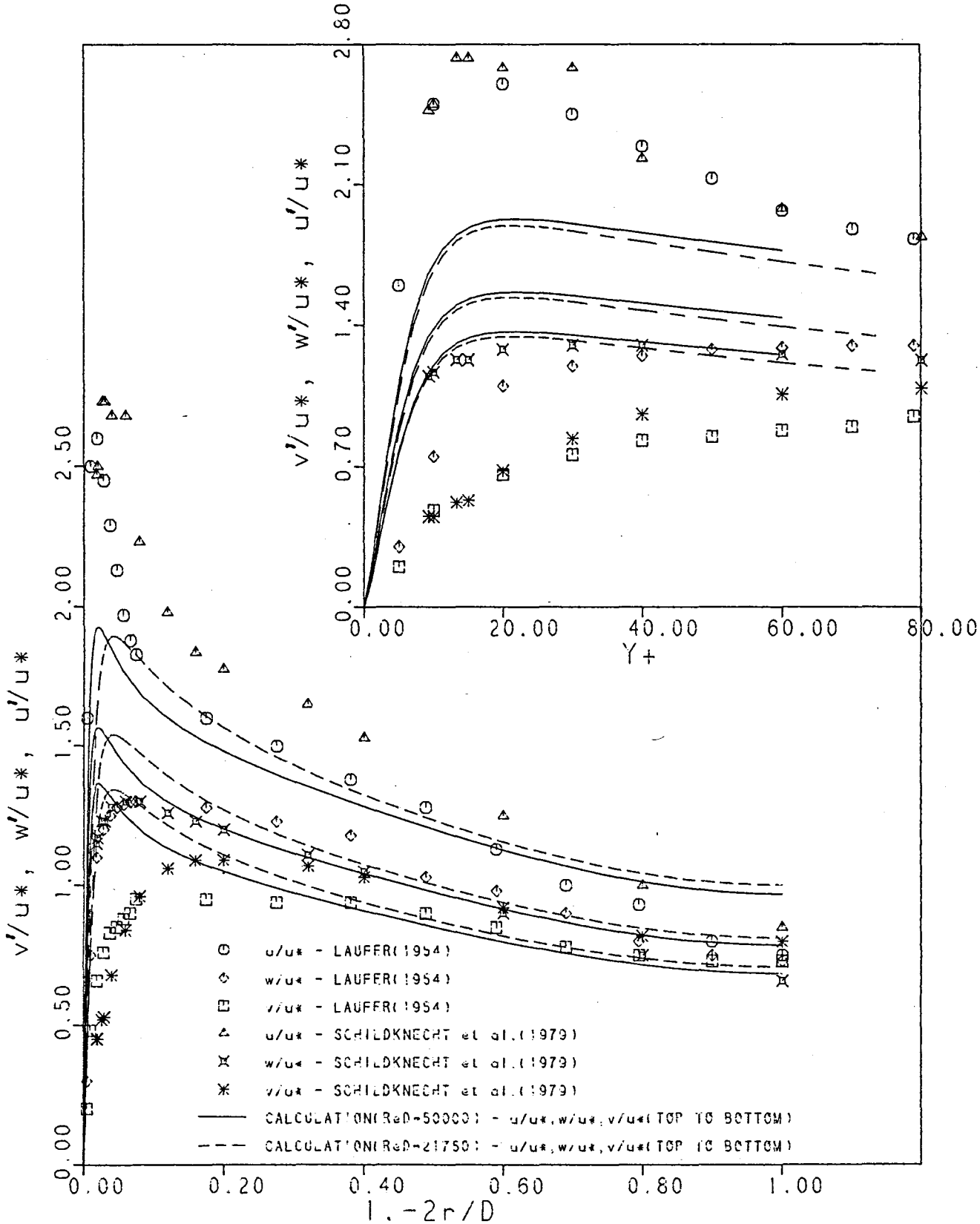
v'/u*, w'/u*, u'/u*
1.-2r/D
0.00
0.20
0.40
0.60
0.80
1.00
0.50
1.00
1.50
2.00
2.50
u/u* - LAUFER(1954)
w/u* - LAUFER(1954)
v/u* - LAUFER(1954)
u/u* - SCHILDKNECHT et al.(1979)
w/u* - SCHILDKNECHT et al.(1979)
v/u* - SCHILDKNECHT et al.(1979)
CALCULATION(ReD=50000) - u/u*,w/u*,v/u*(TOP TO BOTTOM)
CALCULATION(ReD=21750) - u/u*,w/u*,v/u*(TOP TO BOTTOM)
v'/u*, w'/u*, u'/u*
Y+
0.00
20.00
40.00
60.00
80.00
0.00
0.70
1.40
2.10
2.80

Figure 8f.

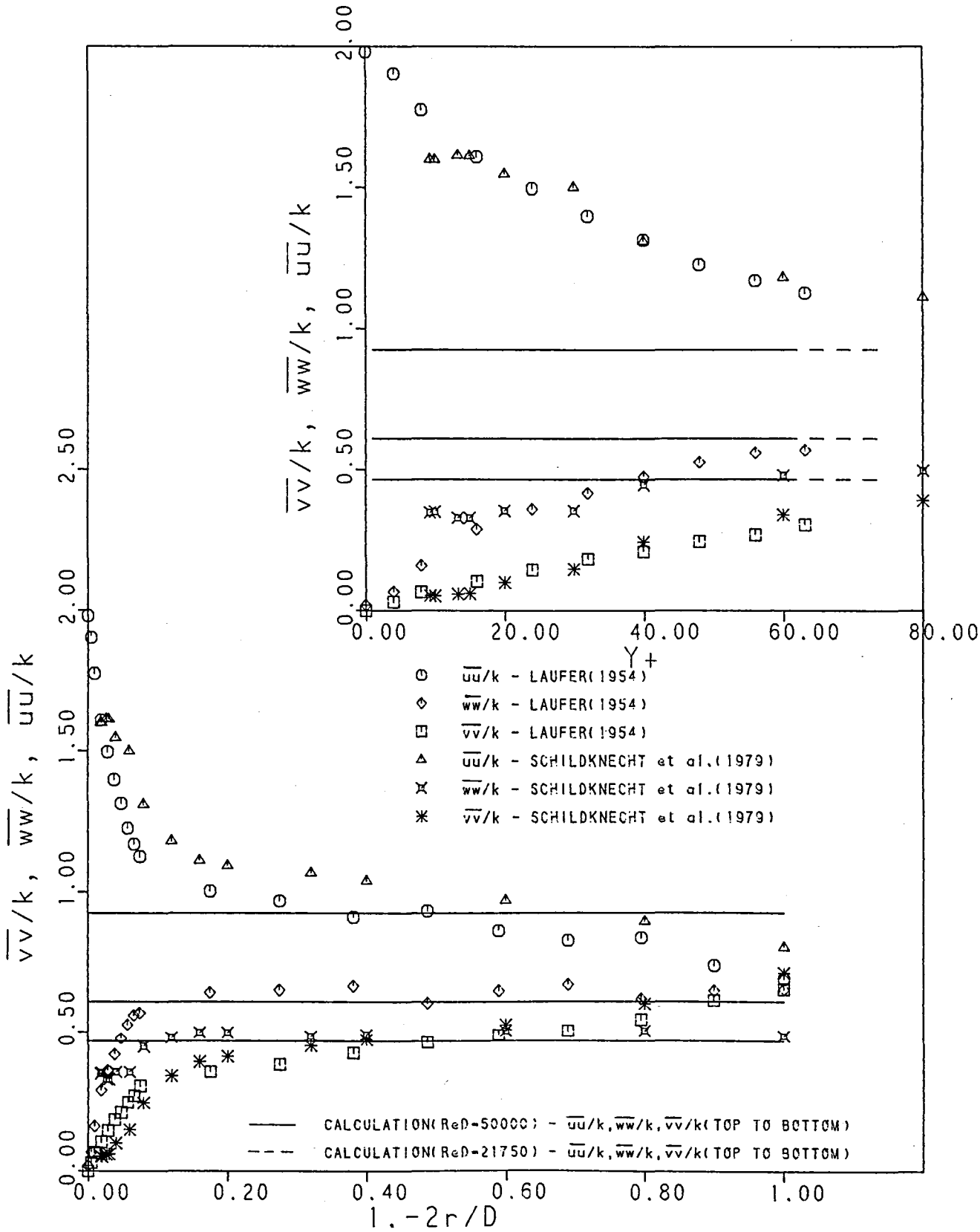
vv/k, ww/k, uu/k
1.-2r/D
0.00
0.20
0.40
0.60
0.80
1.00
0.00
0.50
1.00
1.50
2.00
2.50
uu/k - LAUFER(1954)
ww/k - LAUFER(1954)
vv/k - LAUFER(1954)
uu/k - SCHILDKNECHT et al.(1979)
ww/k - SCHILDKNECHT et al.(1979)
vv/k - SCHILDKNECHT et al.(1979)
CALCULATION(ReD=50000) - uu/k,ww/k,vv/k(TOP TO BOTTOM)
CALCULATION(ReD=21750) - uu/k,ww/k,vv/k(TOP TO BOTTOM)
vv/k, ww/k, uu/k
Y+
0.00
20.00
40.00
60.00
80.00
0.00
0.50
1.00
1.50
2.00

Figure 8g.

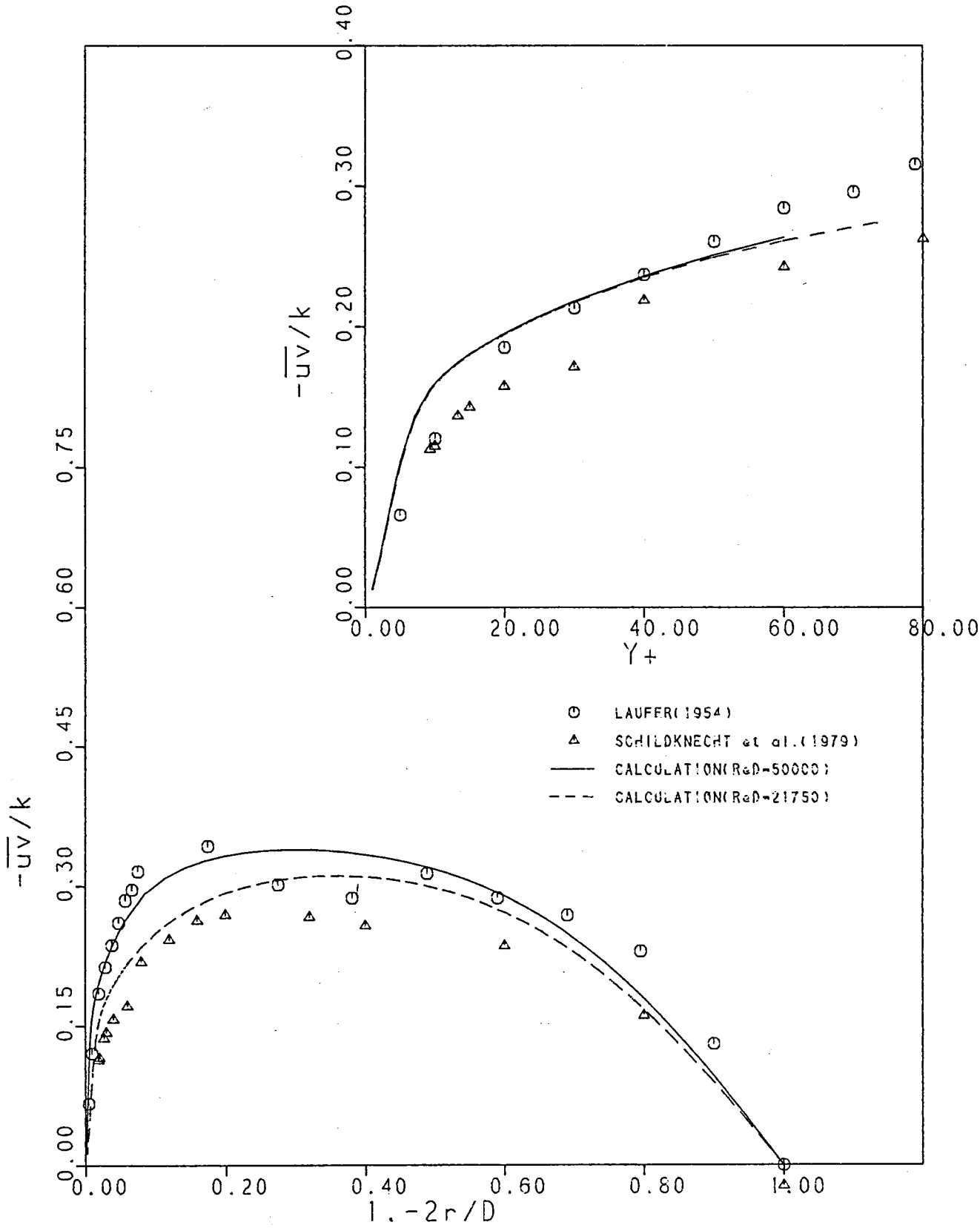
-uv/k
1.-2r/D
0.00
0.15
0.30
0.45
0.60
0.75
0.00
0.20
0.40
0.60
0.80
1.00
LAUFER(1954)
SCHILDKNECHT et al.(1979)
CALCULATION(ReD=50000)
CALCULATION(ReD=21750)
-uv/k
Y+
0.00
0.10
0.20
0.30
0.40
0.00
20.00
40.00
60.00
80.00

Figure 8h.

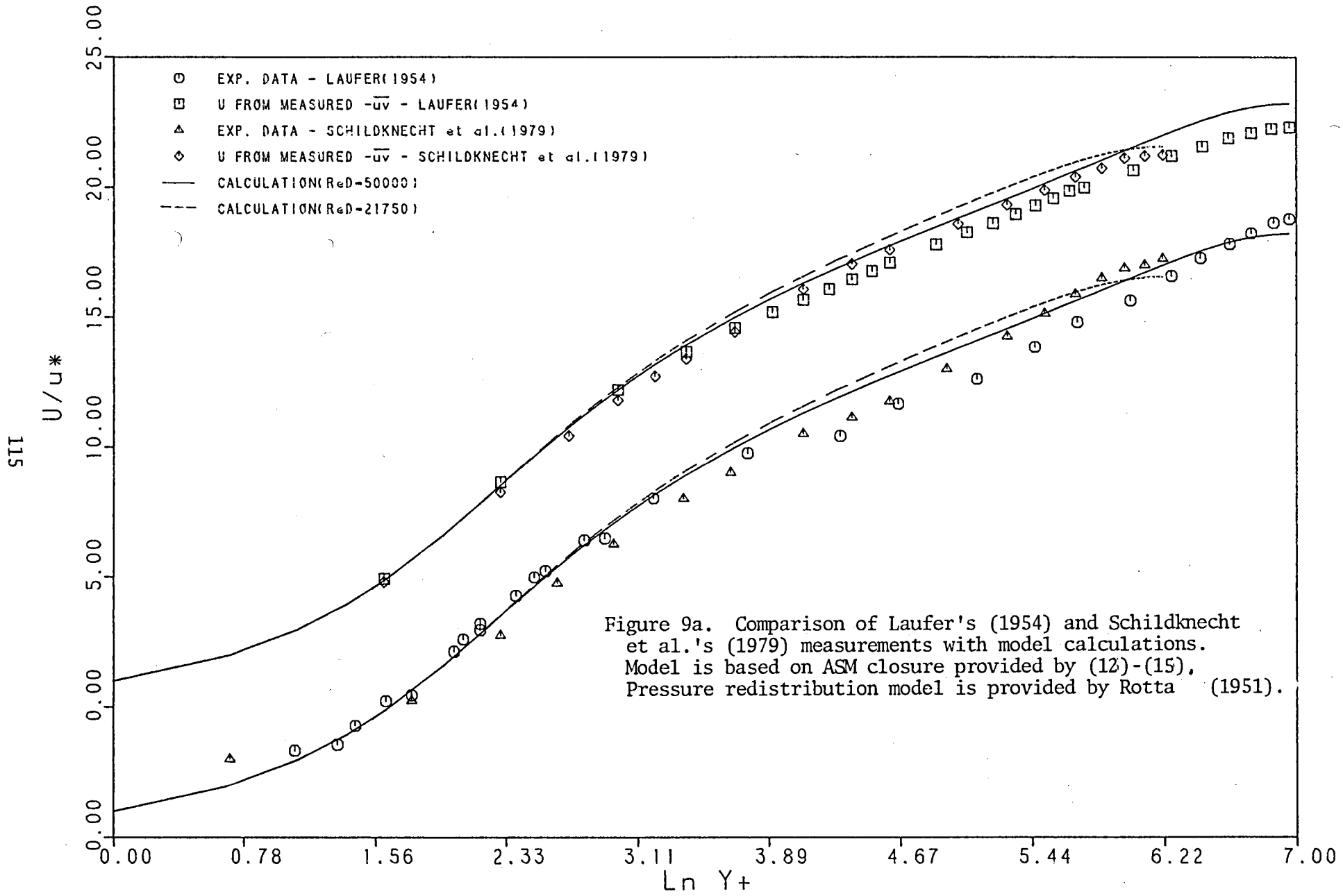

Figure 9a. Comparison of Laufer's (1954) and Schildknecht et al.'s (1979) measurements with model calculations. Model is based on ASM closure provided by (12)-(15), Pressure redistribution model is provided by Rotta (1951).

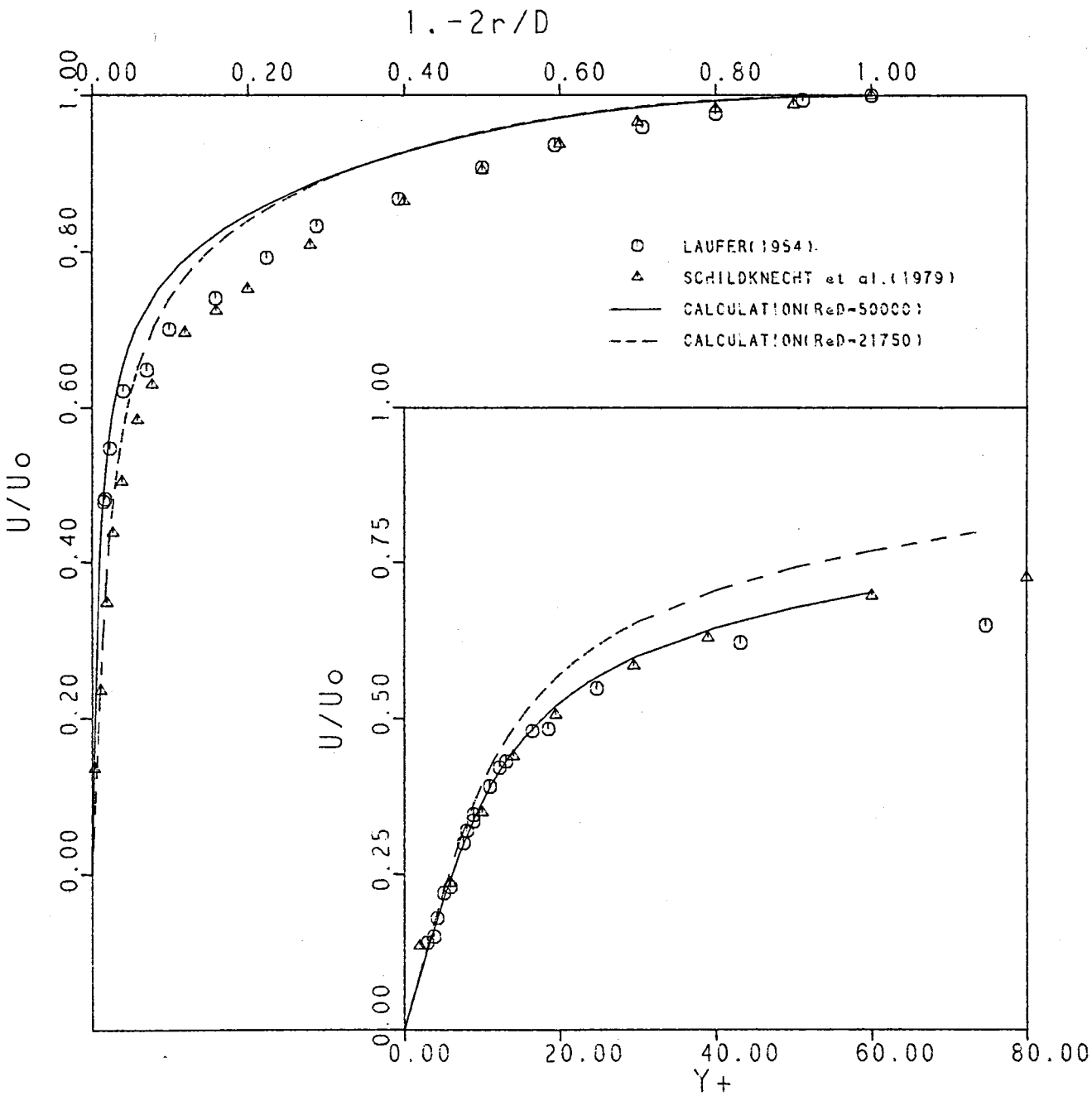
1.-2r/D
0.00
0.20
0.40
0.60
0.80
1.00
U/Uo
0.00
0.20
0.40
0.60
0.80
1.00
LAUFER(1954)
SCHILDKNECHT et al.(1979)
CALCULATION(ReD=50000)
CALCULATION(ReD=21750)
U/Uo
0.00
0.25
0.50
0.75
1.00
0.00
20.00
40.00
60.00
80.00
Y+

Figure 9b.

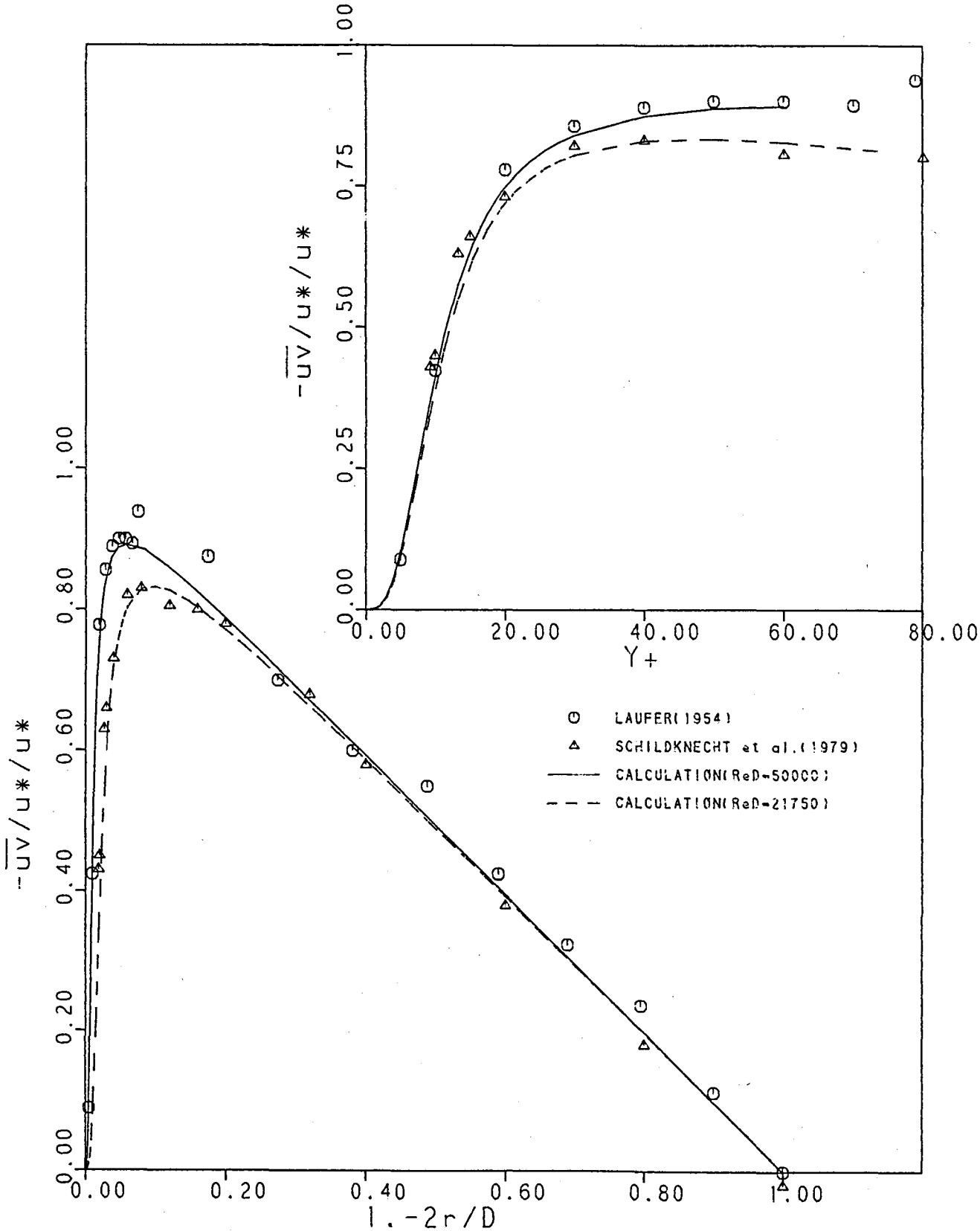
-uv/u*/u*
1.00
0.80
0.60
0.40
0.20
0.00
0.00
0.20
0.40
0.60
0.80
1.00
1.-2r/D
LAUFER(1954)
SCHILDKNECHT et al.(1979)
CALCULATION(ReD=50000)
CALCULATION(ReD=21750)
-uv/u*/u*
1.00
0.75
0.50
0.25
0.00
0.00
20.00
40.00
60.00
80.00
Y+

Figure 9c.

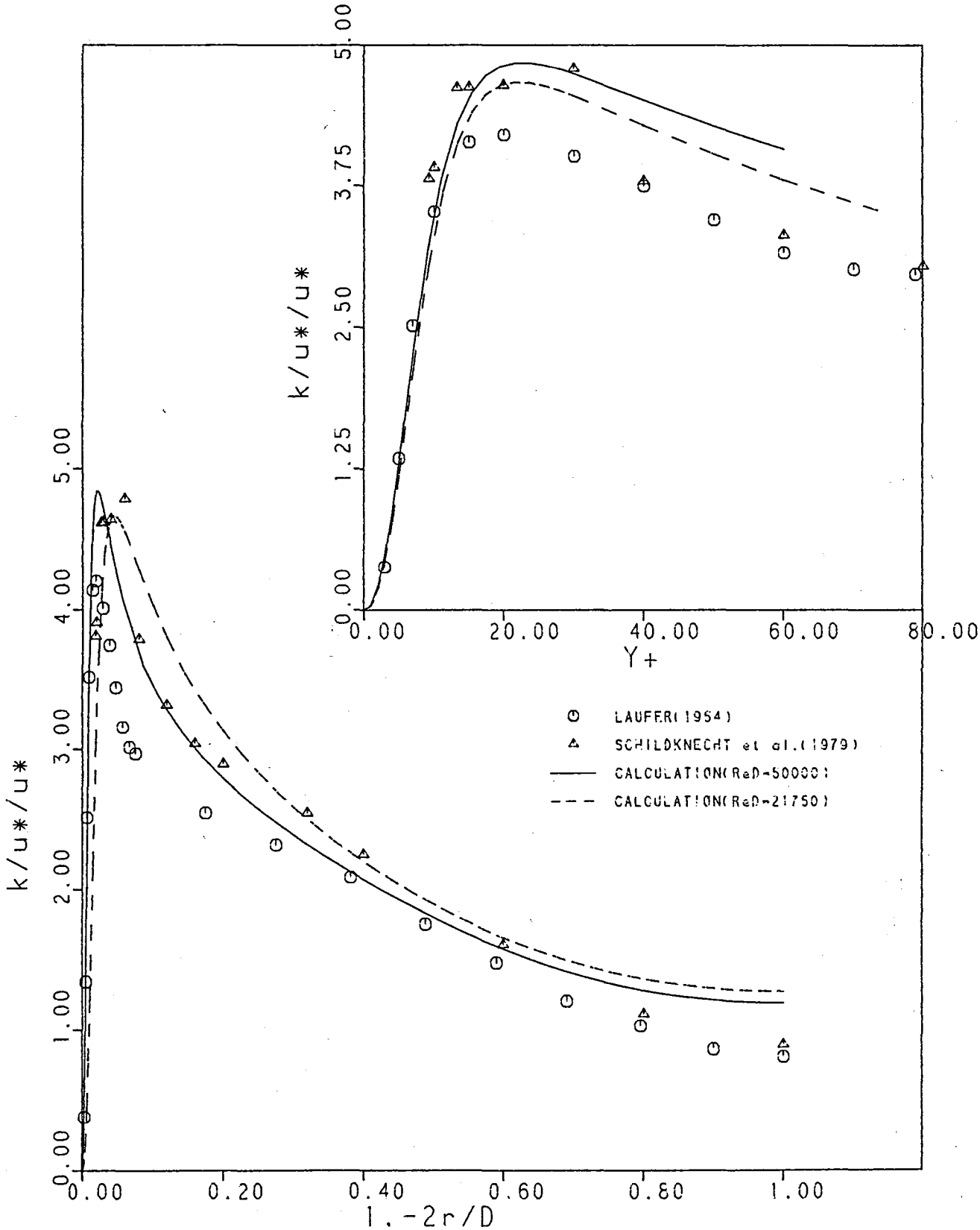
k/u*/u*
1.-2r/D
0.00
1.00
2.00
3.00
4.00
5.00
0.00
0.20
0.40
0.60
0.80
1.00
k/u*/u*
Y+
0.00
1.25
2.50
3.75
5.00
0.00
20.00
40.00
60.00
80.00
LAUFER(1954)
SCHILDKNECHT et al.(1979)
CALCULATION(ReD=50000)
CALCULATION(ReD=21750)

Figure 9d.

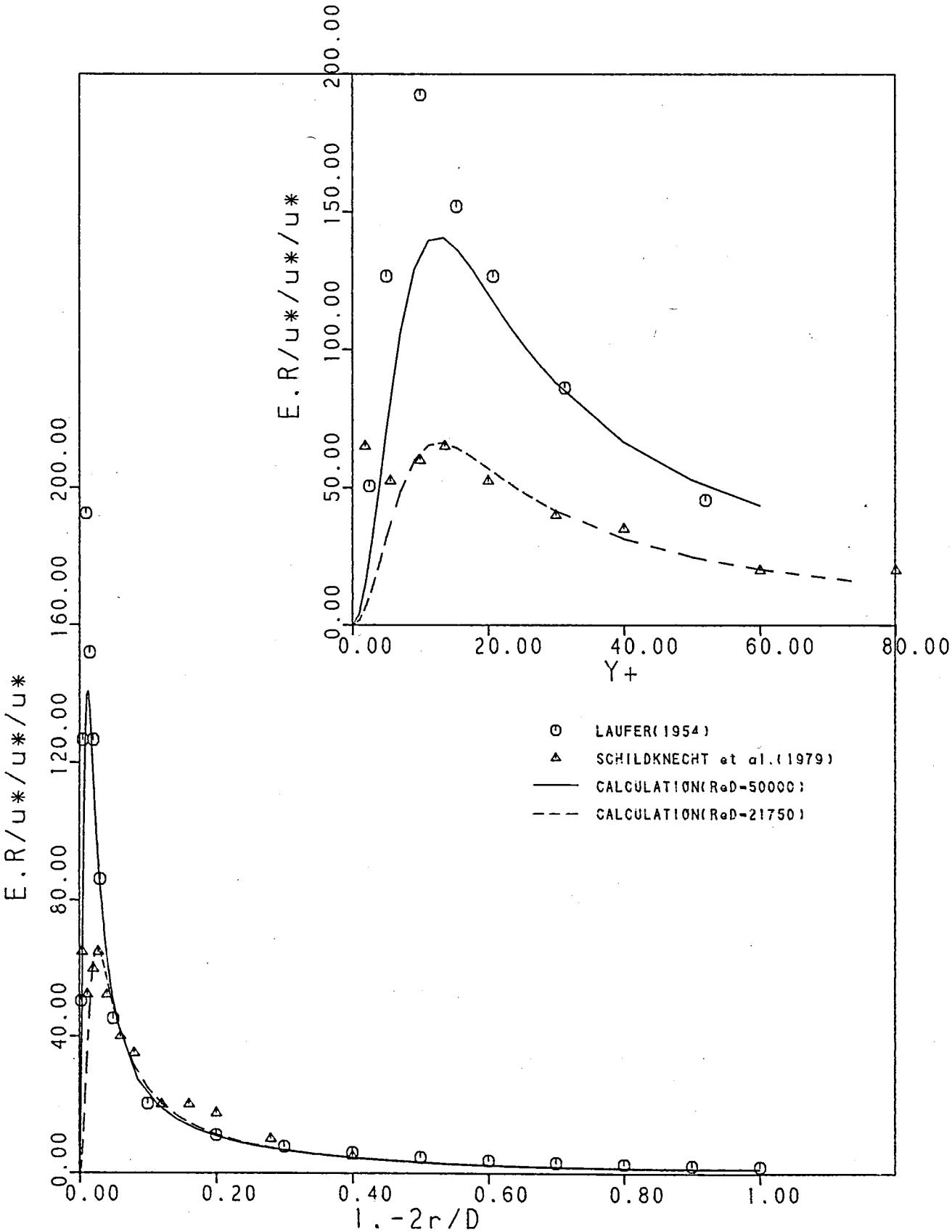
E.R/u*/u*/u*
1.-2r/D
0.00
40.00
80.00
120.00
160.00
200.00
0.00
0.20
0.40
0.60
0.80
1.00
E.R/u*/u*
Y+
0.00
50.00
100.00
150.00
200.00
0.00
20.00
40.00
60.00
80.00
LAUFER(1954)
SCHILDKNECHT et al.(1979)
CALCULATION(ReD=50000)
CALCULATION(ReD=21750)

Figure 9e.

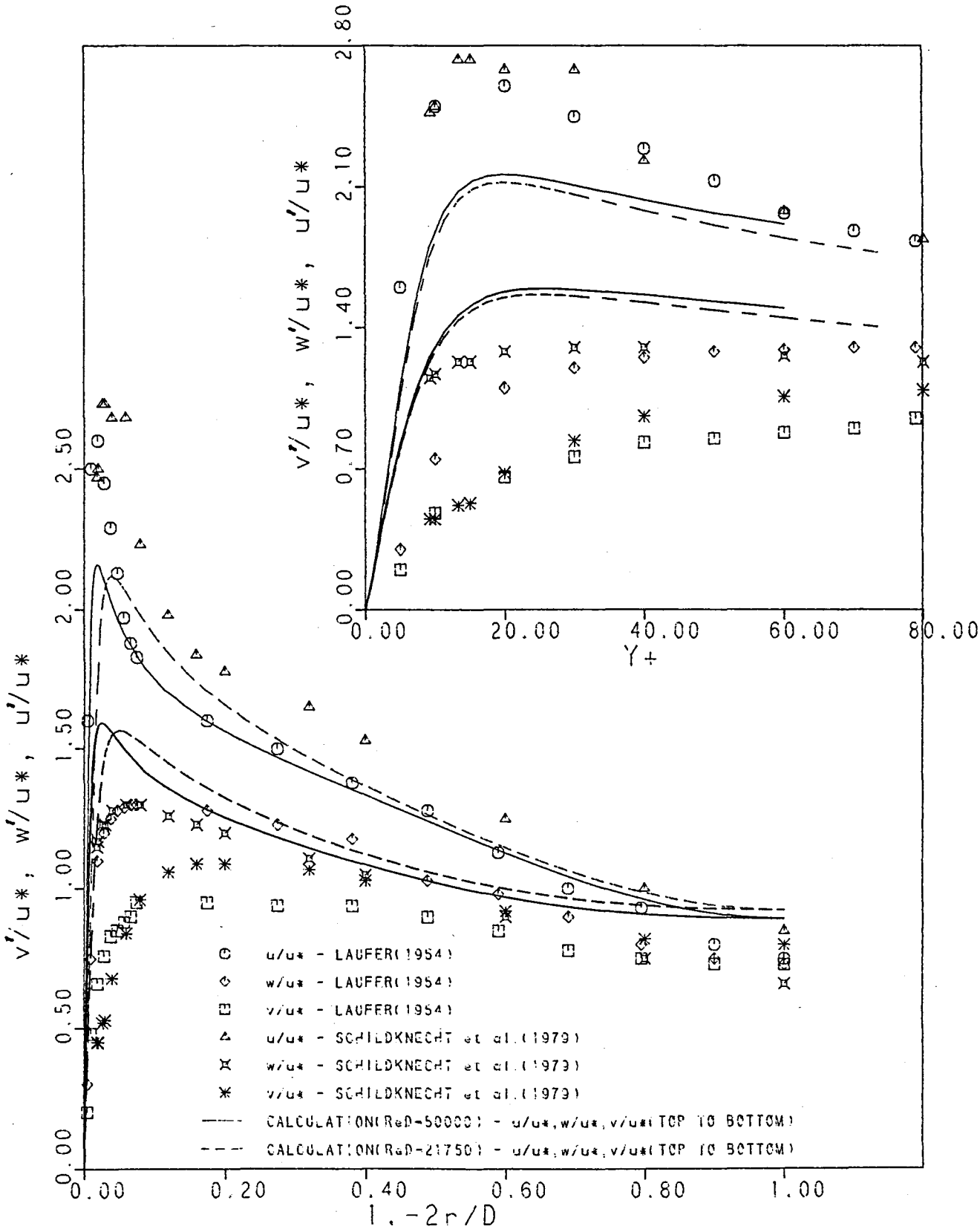
v'/u*, w'/u*, u'/u*
1.-2r/D
0.00
0.20
0.40
0.60
0.80
1.00
0.50
1.50
2.00
2.50
u/u* - LAUFER(1954)
w/u* - LAUFER(1954)
v/u* - LAUFER(1954)
u/u* - SCHILDKNECHT et al.(1979)
w/u* - SCHILDKNECHT et al.(1979)
v/u* - SCHILDKNECHT et al.(1979)
CALCULATION(ReD=50000) - u/u*,w/u*,v/u*(TOP TO BOTTOM)
CALCULATION(ReD=21750) - u/u*,w/u*,v/u*(TOP TO BOTTOM)
v'/u*, w'/u*, u'/u*
Y+
0.00
20.00
40.00
60.00
80.00
0.70
1.40
2.10
2.80

Figure 9f.

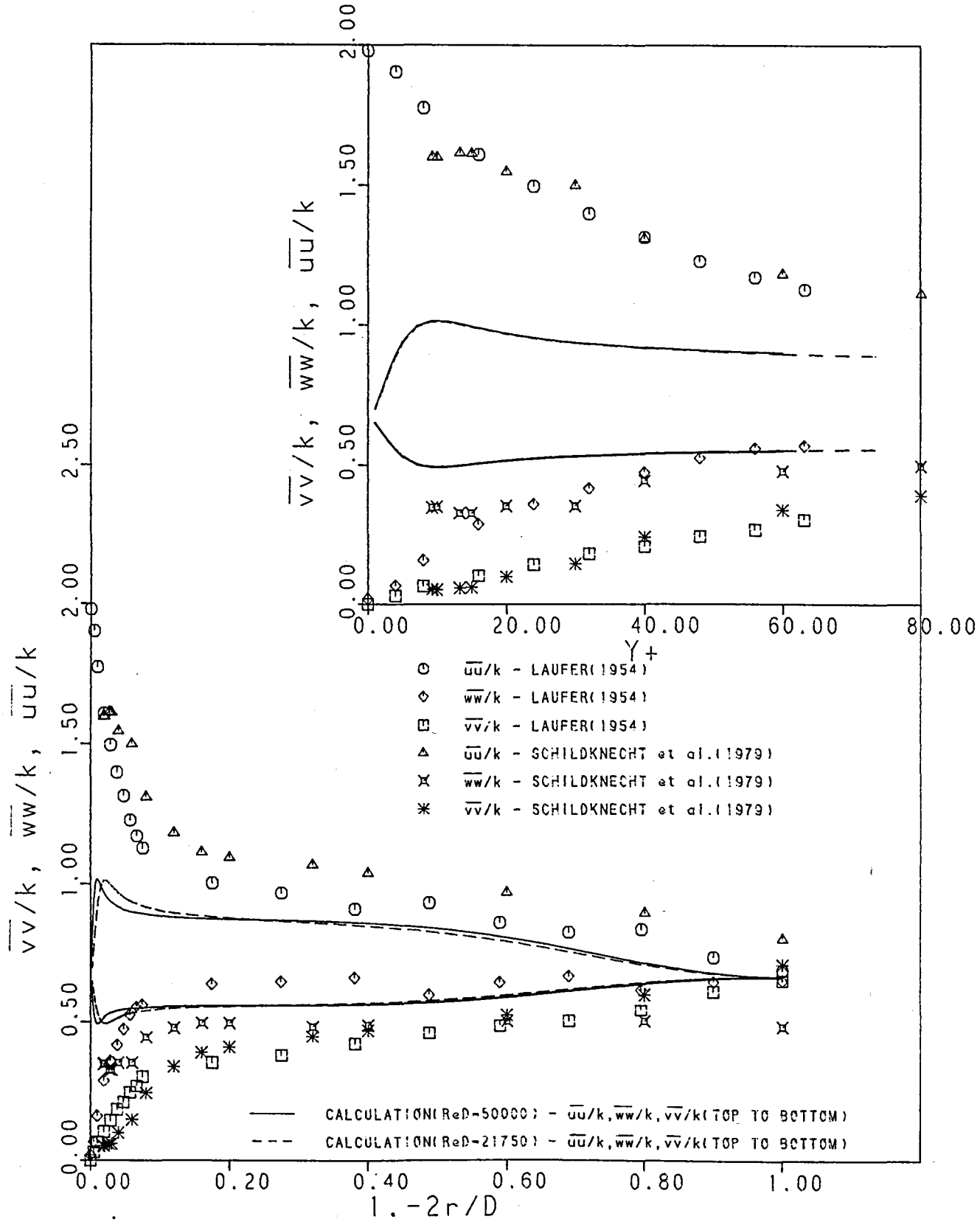
vv/k, ww/k, uu/k
1.-2r/D
0.00
0.20
0.40
0.60
0.80
1.00
0.50
1.00
1.50
2.00
2.50
uu/k - LAUFER(1954)
ww/k - LAUFER(1954)
vv/k - LAUFER(1954)
uu/k - SCHILDKNECHT et al.(1979)
ww/k - SCHILDKNECHT et al.(1979)
vv/k - SCHILDKNECHT et al.(1979)
CALCULATION(ReD=50000) - uu/k,ww/k,vv/k(TOP TO BOTTOM)
CALCULATION(ReD=21750) - uu/k,ww/k,vv/k(TOP TO BOTTOM)
vv/k, ww/k, uu/k
Y+
0.00
20.00
40.00
60.00
80.00
0.00
0.50
1.00
1.50
2.00

Figure 9g.

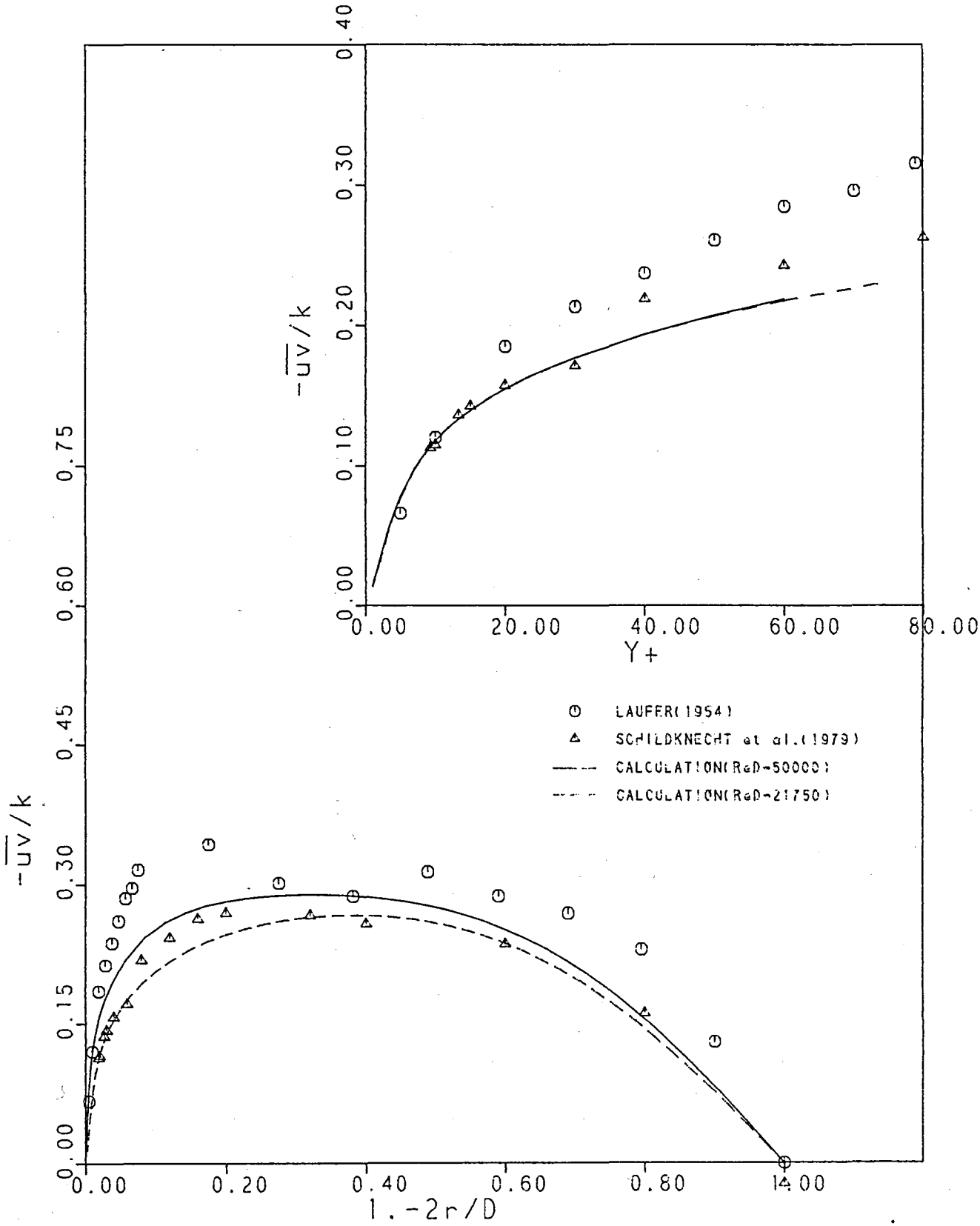
0.40
0.30
0.20
0.10
0.00
$-\overline{uv}/k$
0.00
20.00
40.00
60.00
80.00
Y+
0.75
0.60
0.45
0.30
0.15
0.00
$-\overline{uv}/k$
LAUFER(1954)
SCHILDKNECHT et al.(1979)
CALCULATION(ReD=50000)
CALCULATION(ReD=21750)
0.00
0.20
0.40
0.60
0.80
1.00
1.-2r/D

Figure 9h.

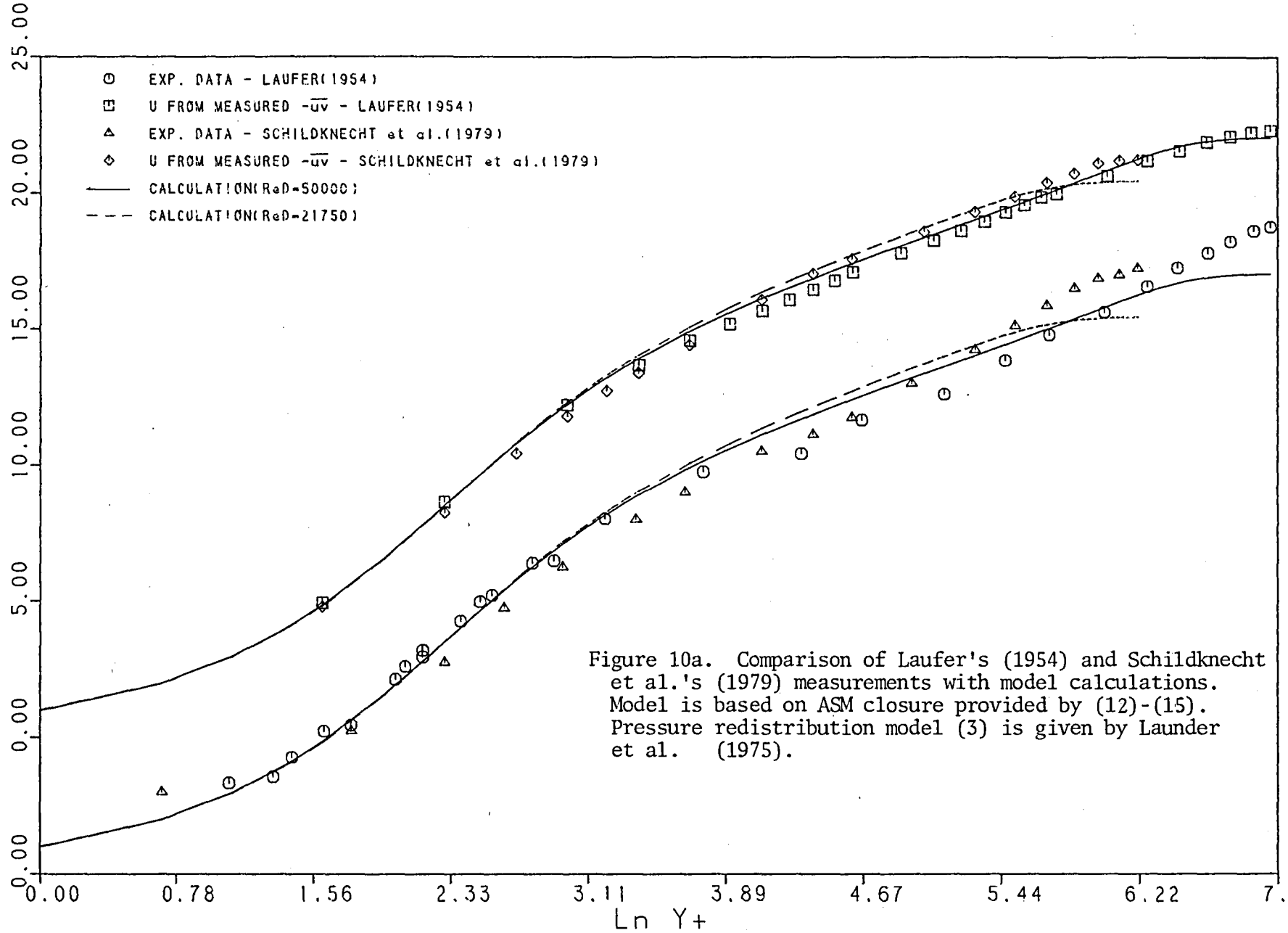

Figure 10a. Comparison of Laufer's (1954) and Schildknecht et al.'s (1979) measurements with model calculations. Model is based on ASM closure provided by (12)-(15). Pressure redistribution model (3) is given by Launder et al. (1975).

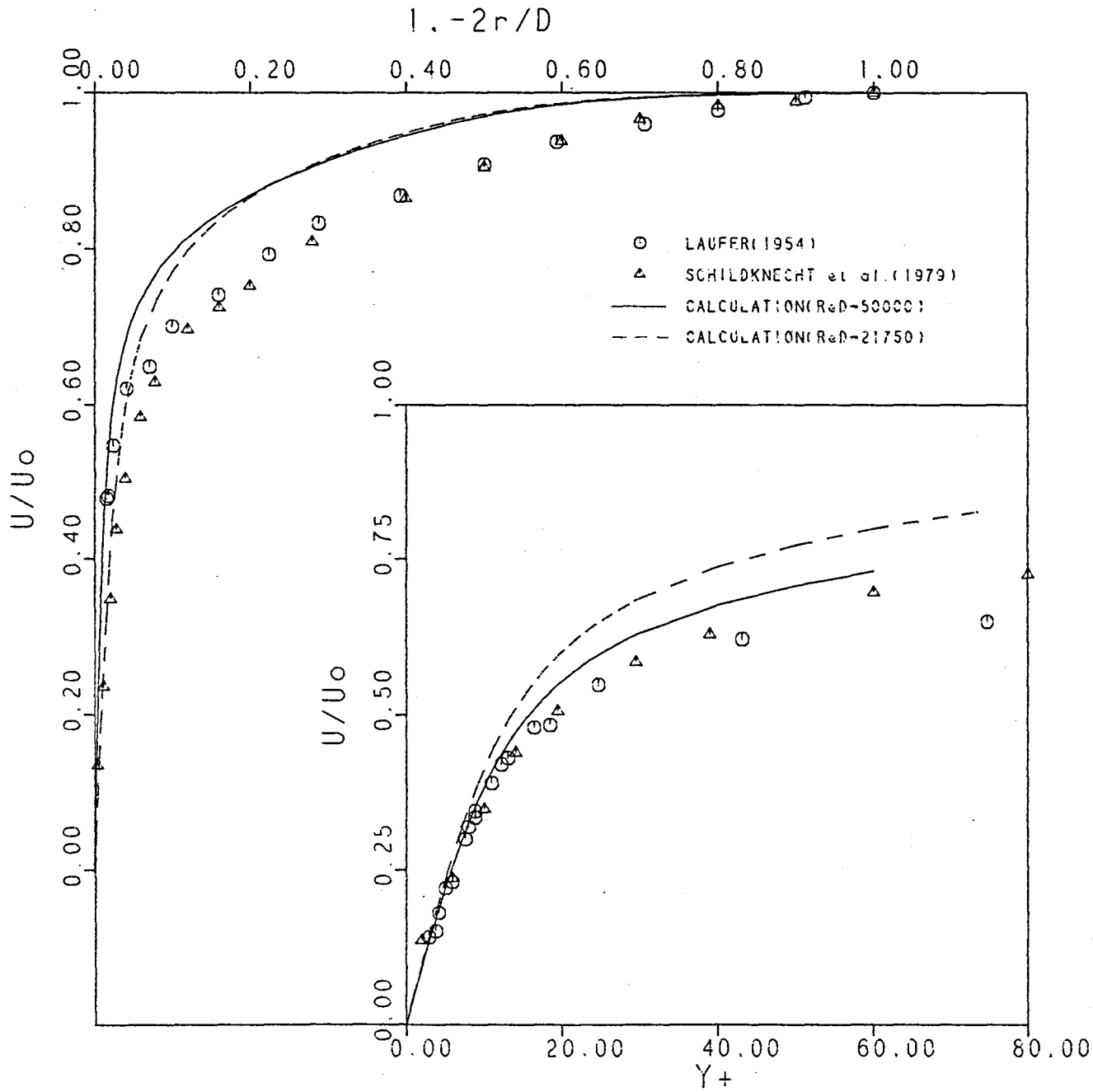
1.-2r/D
0.00
0.20
0.40
0.60
0.80
1.00
U/Uo
LAUFER(1954)
SCHILDKNECHT et al.(1979)
CALCULATION(ReD=50000)
CALCULATION(ReD=21750)
0.00
0.25
0.50
0.75
1.00
20.00
40.00
60.00
80.00
Y+

Figure 10b.

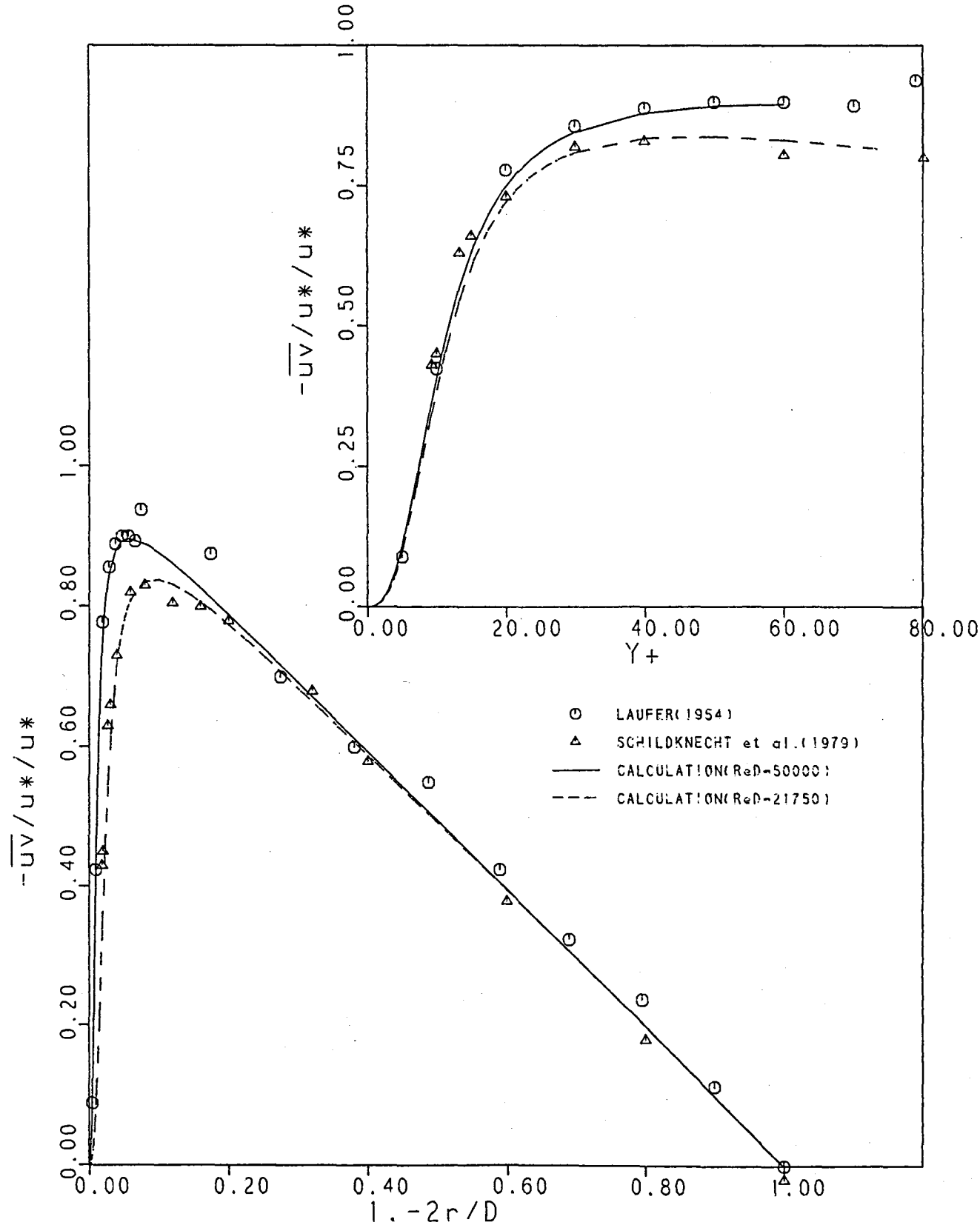
-UV/U*/U*
1.-2r/D
0.00
0.20
0.40
0.60
0.80
1.00
LAUFER(1954)
SCHILDKNECHT et al.(1979)
CALCULATION(ReD=50000)
CALCULATION(ReD=21750)
-UV/U*/U*
Y+
0.00
20.00
40.00
60.00
80.00
0.25
0.50
0.75

Figure 10c.

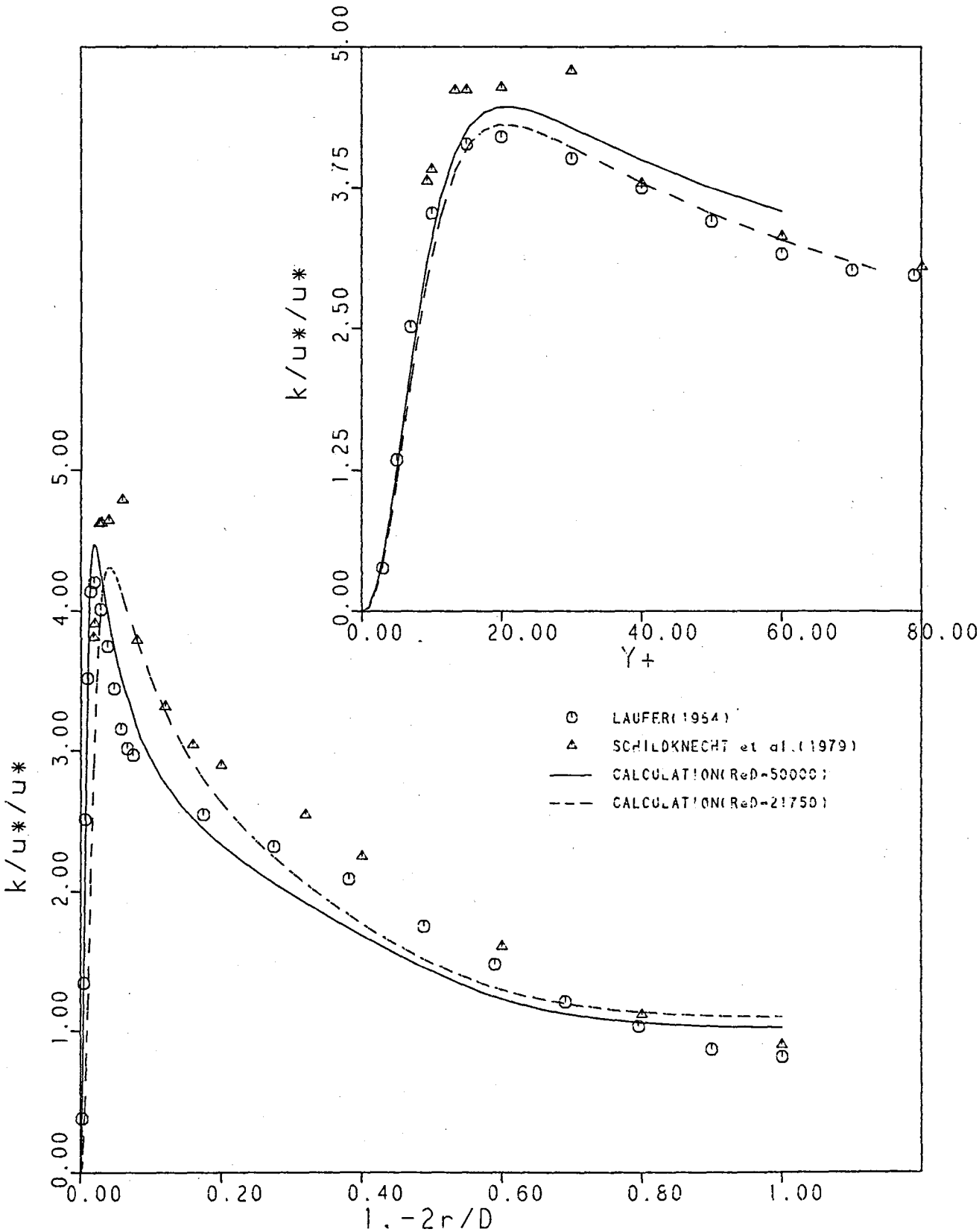
k/u*/u*
1.-2r/D
0.00
1.00
2.00
3.00
4.00
5.00
0.00
0.20
0.40
0.60
0.80
1.00
LAUFER(1954)
SCHILDKNECHT et al.(1979)
CALCULATION(ReD=50000)
CALCULATION(ReD=21750)
k/u*/u*
Y+
0.00
1.25
2.50
3.75
5.00
0.00
20.00
40.00
60.00
80.00

Figure 10d.

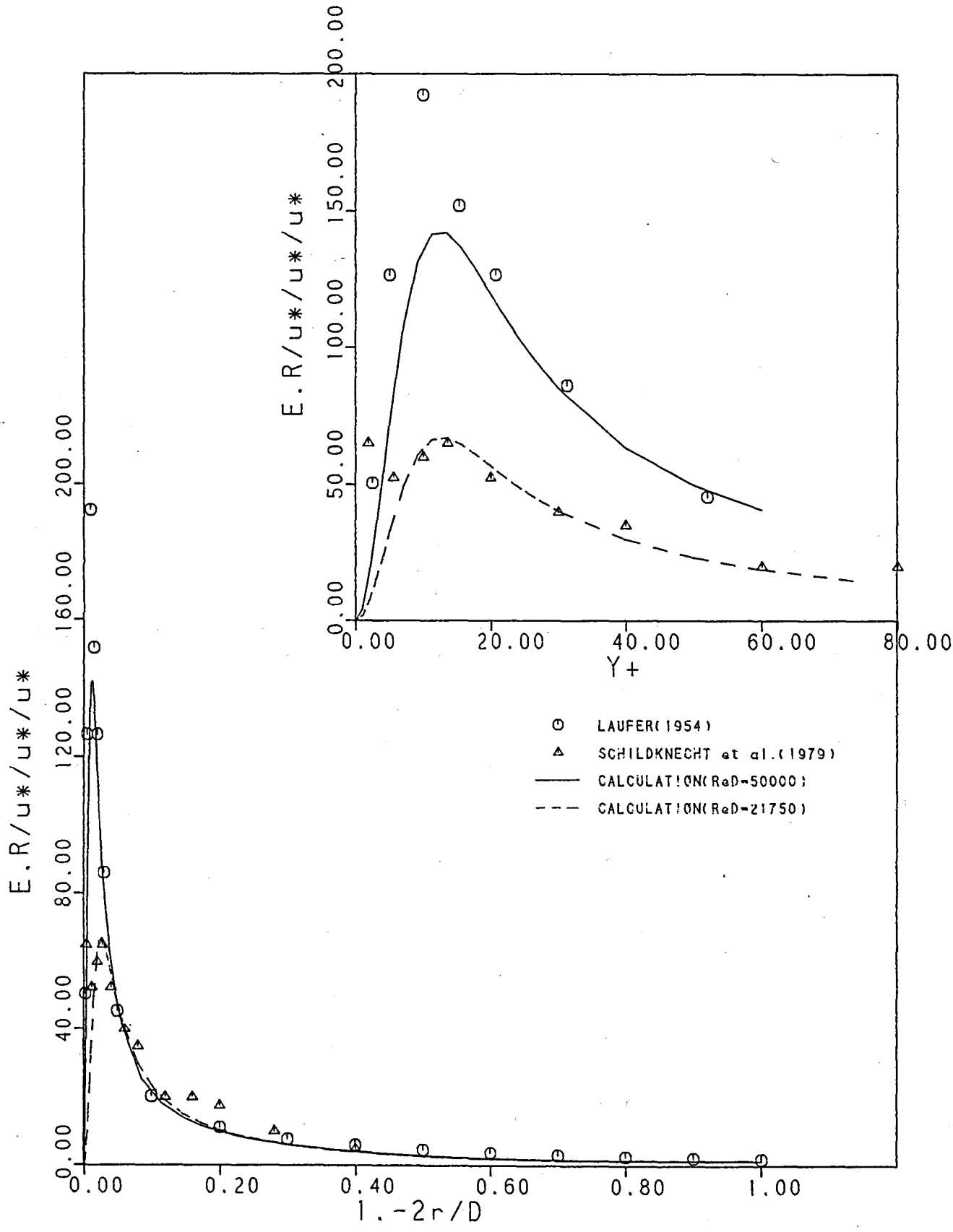
E.R/u*/u*/u*
1.-2r/D
0.00
40.00
80.00
120.00
160.00
200.00
0.00
0.20
0.40
0.60
0.80
1.00
E.R/u*/u*
Y+
0.00
50.00
100.00
150.00
200.00
0.00
20.00
40.00
60.00
80.00
LAUFER(1954)
SCHILDKNECHT et al.(1979)
CALCULATION(ReD=50000)
CALCULATION(ReD=21750)

Figure 10e.

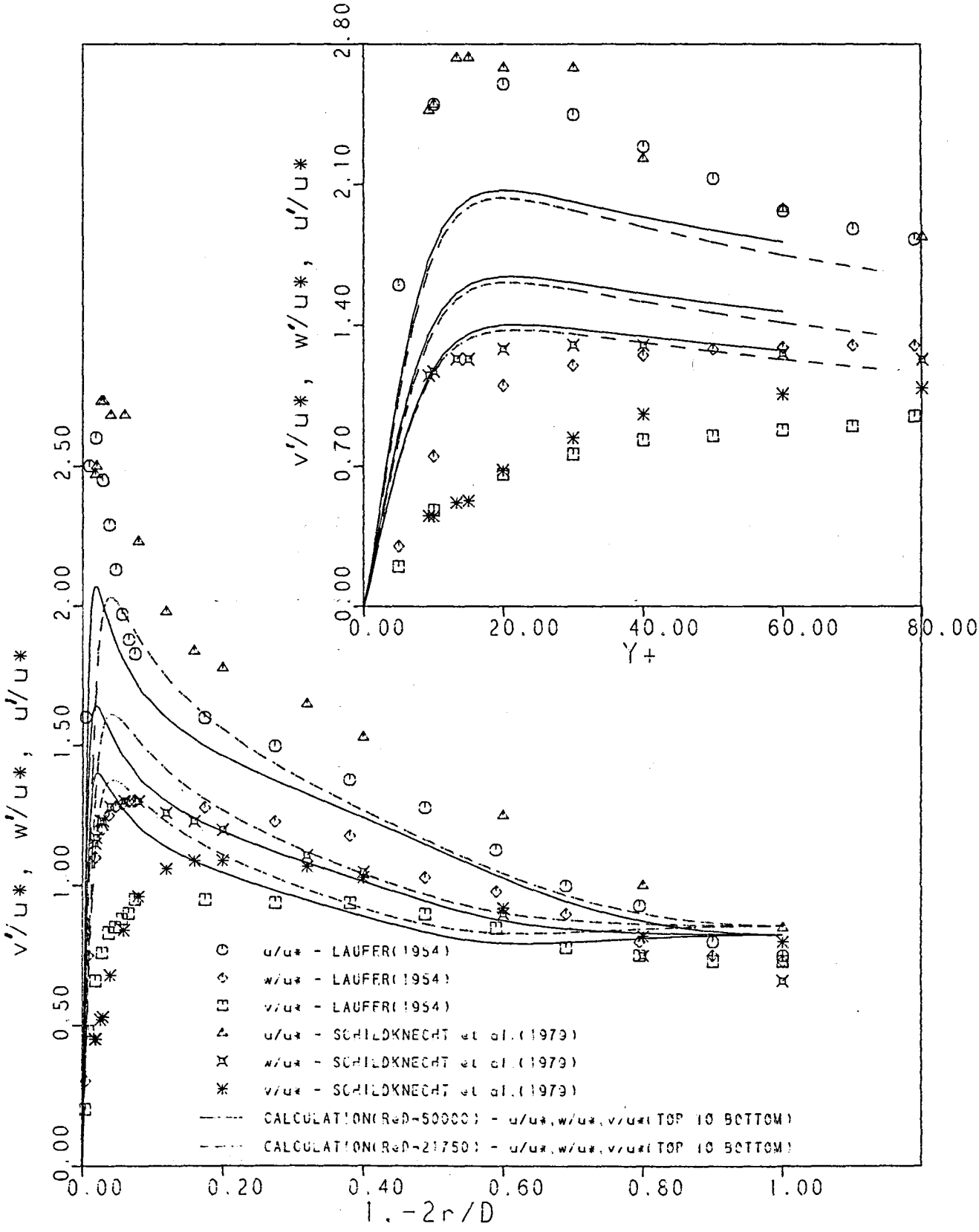
v'/u*, w'/u*, u'/u*
1.-2r/D
0.00
0.50
1.00
1.50
2.00
2.50
0.00
0.20
0.40
0.60
0.80
1.00
u/u* - LAUFER(1954)
w/u* - LAUFER(1954)
v/u* - LAUFER(1954)
u/u* - SCHILDKNECHT et al.(1979)
w/u* - SCHILDKNECHT et al.(1979)
v/u* - SCHILDKNECHT et al.(1979)
CALCULATION(ReD=50000) - u/u*,w/u*,v/u*(TOP TO BOTTOM)
CALCULATION(ReD=21750) - u/u*,w/u*,v/u*(TOP TO BOTTOM)
v'/u*, w'/u*, u'/u*
Y+
0.00
0.70
1.40
2.10
2.80
0.00
20.00
40.00
60.00
80.00

Figure 10f.

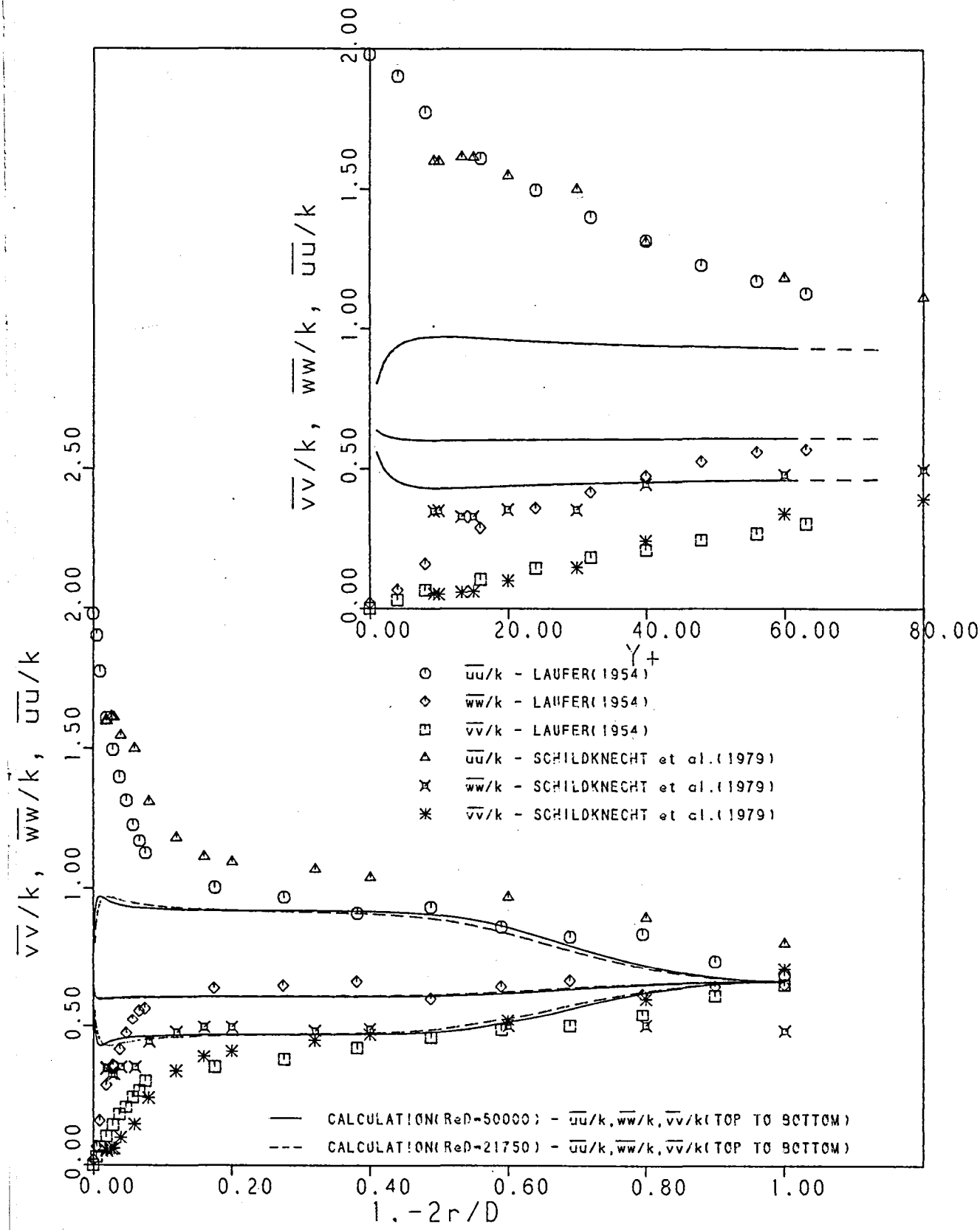
vv/k, ww/k, uu/k
1.-2r/D
0.00
0.20
0.40
0.60
0.80
1.00
0.50
1.00
1.50
2.00
2.50
uu/k - LAUFER(1954)
ww/k - LAUFER(1954)
vv/k - LAUFER(1954)
uu/k - SCHILDKNECHT et al.(1979)
ww/k - SCHILDKNECHT et al.(1979)
vv/k - SCHILDKNECHT et al.(1979)
CALCULATION(ReD=50000) - uu/k,ww/k,vv/k(TOP TO BOTTOM)
CALCULATION(ReD=21750) - uu/k,ww/k,vv/k(TOP TO BOTTOM)
vv/k, ww/k, uu/k
Y+
0.00
20.00
40.00
60.00
80.00
0.00
0.50
1.00
1.50
2.00

Figure 10g.

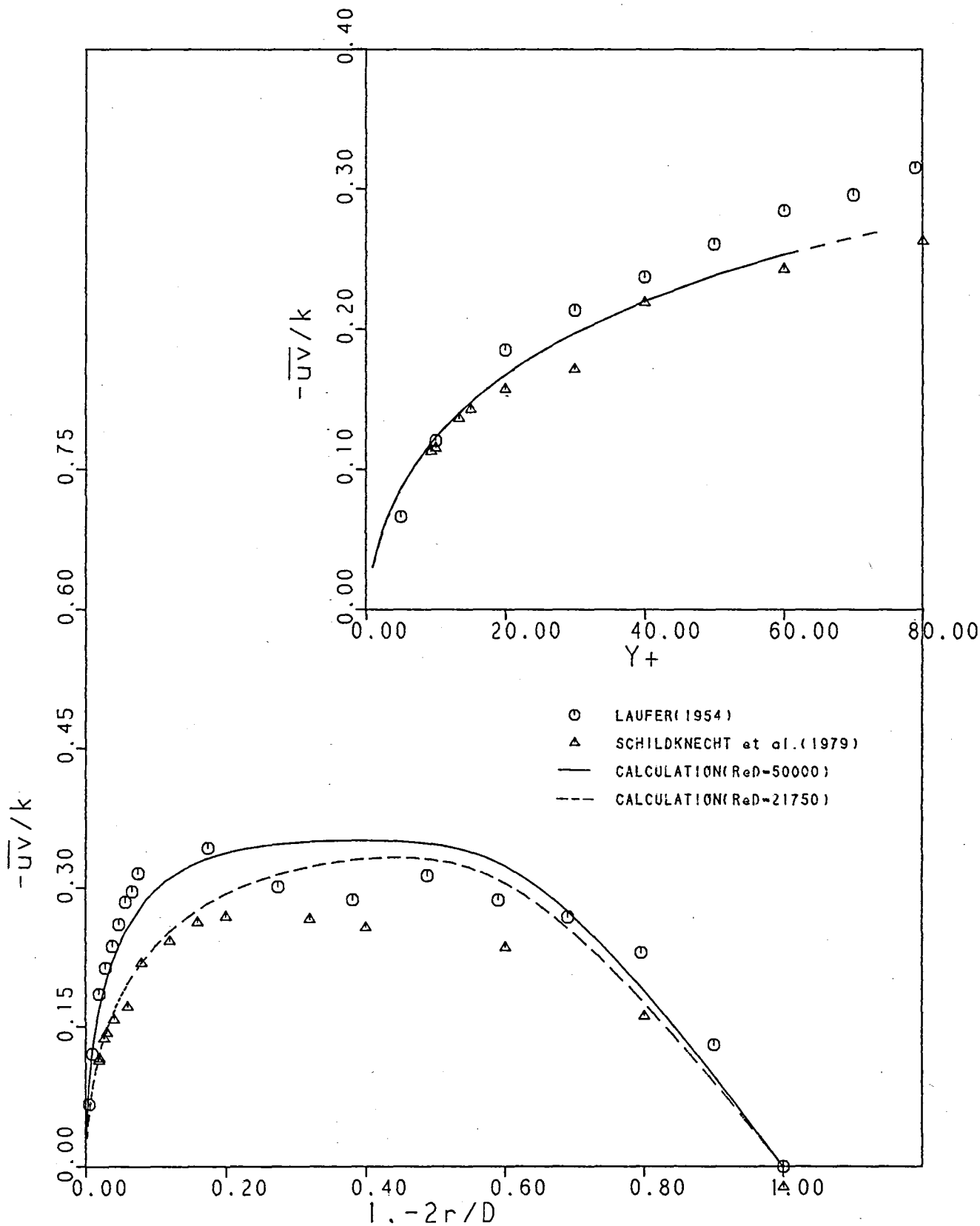
-uv/k
0.00
0.15
0.30
0.45
0.60
0.75
0.00
0.20
0.40
0.60
0.80
1.00
1.-2r/D
LAUFER(1954)
SCHILDKNECHT et al.(1979)
CALCULATION(ReD=50000)
CALCULATION(ReD=21750)
-uv/k
0.00
0.10
0.20
0.30
0.40
0.00
20.00
40.00
60.00
80.00
Y+

Figure 10h.

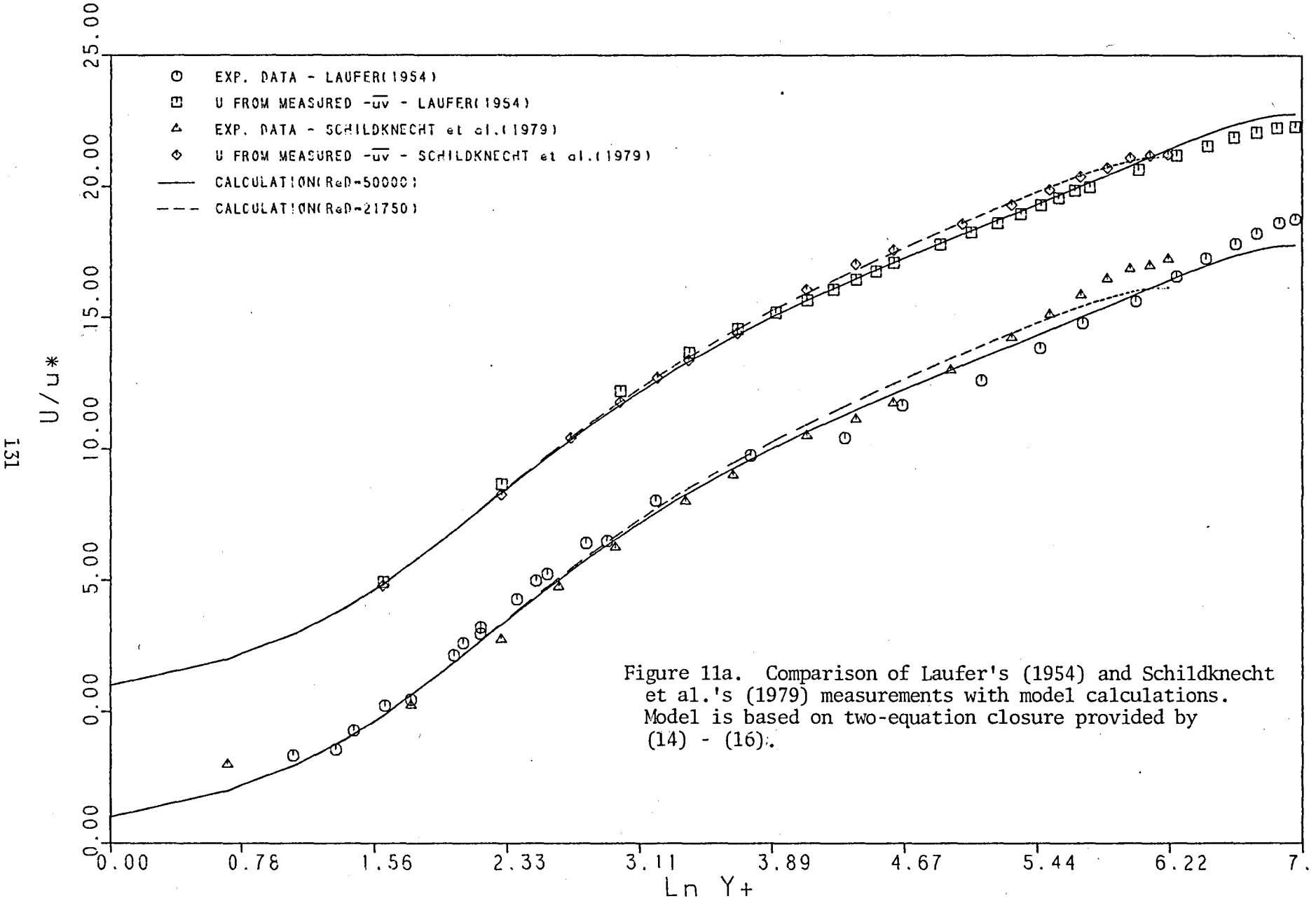

Figure 11a. Comparison of Laufer's (1954) and Schildknecht et al.'s (1979) measurements with model calculations. Model is based on two-equation closure provided by (14) - (16).

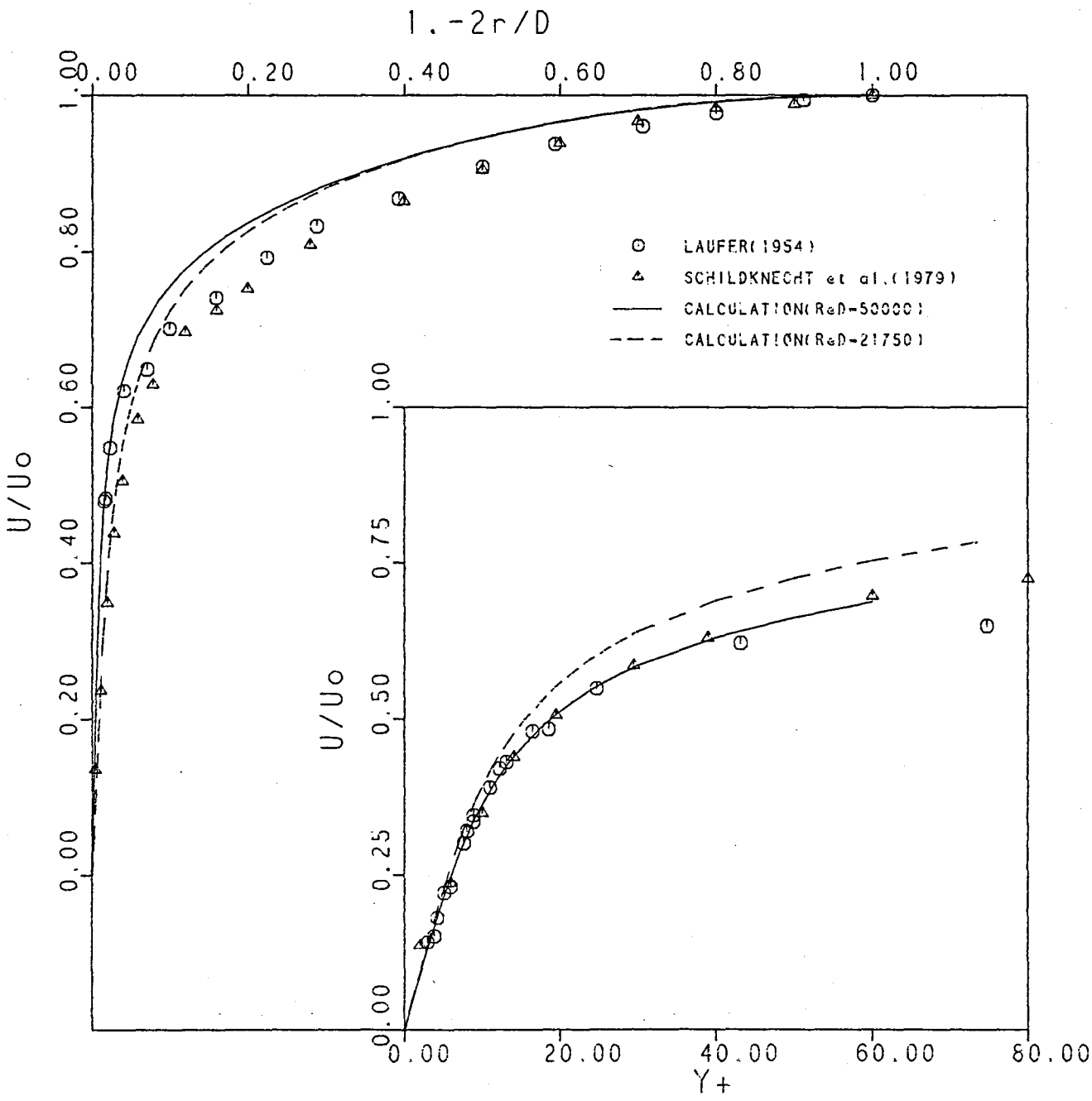
1.-2r/D
0.00
0.20
0.40
0.60
0.80
1.00
U/Uo
LAUFER(1954)
SCHILDKNECHT et al.(1979)
CALCULATION(ReD=50000)
CALCULATION(ReD=21750)
0.00
0.25
0.50
0.75
1.00
20.00
40.00
60.00
80.00
Y+

Figure 11b.

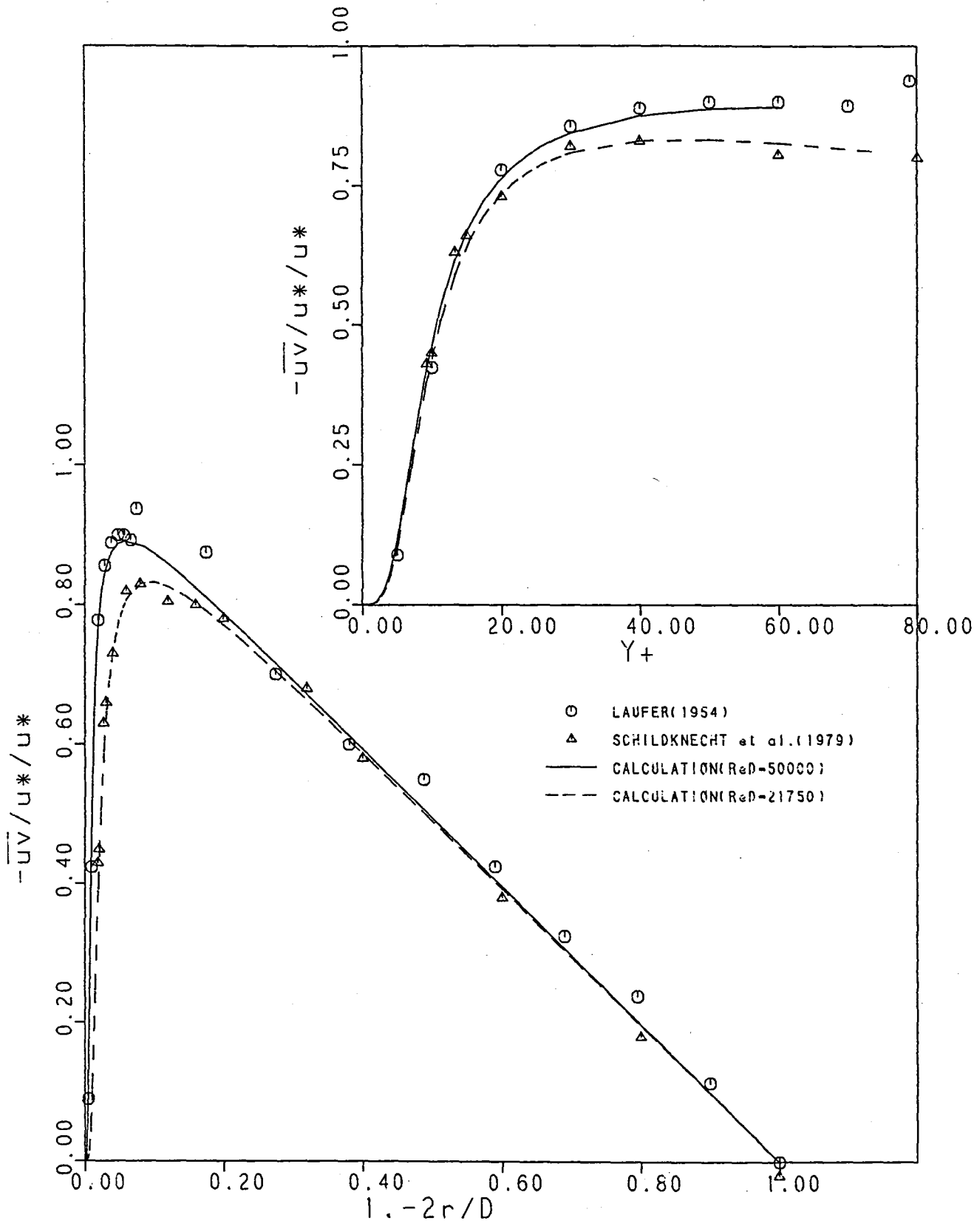
-uv/u*/u*
1.00
0.80
0.60
0.40
0.20
0.00
0.00
0.20
0.40
0.60
0.80
1.00
1.-2r/D
LAUFER(1954)
SCHILDKNECHT et al.(1979)
CALCULATION(ReD=50000)
CALCULATION(ReD=21750)
-uv/u*/u*
1.00
0.75
0.50
0.25
0.00
0.00
20.00
40.00
60.00
80.00
Y+

Figure 11c.

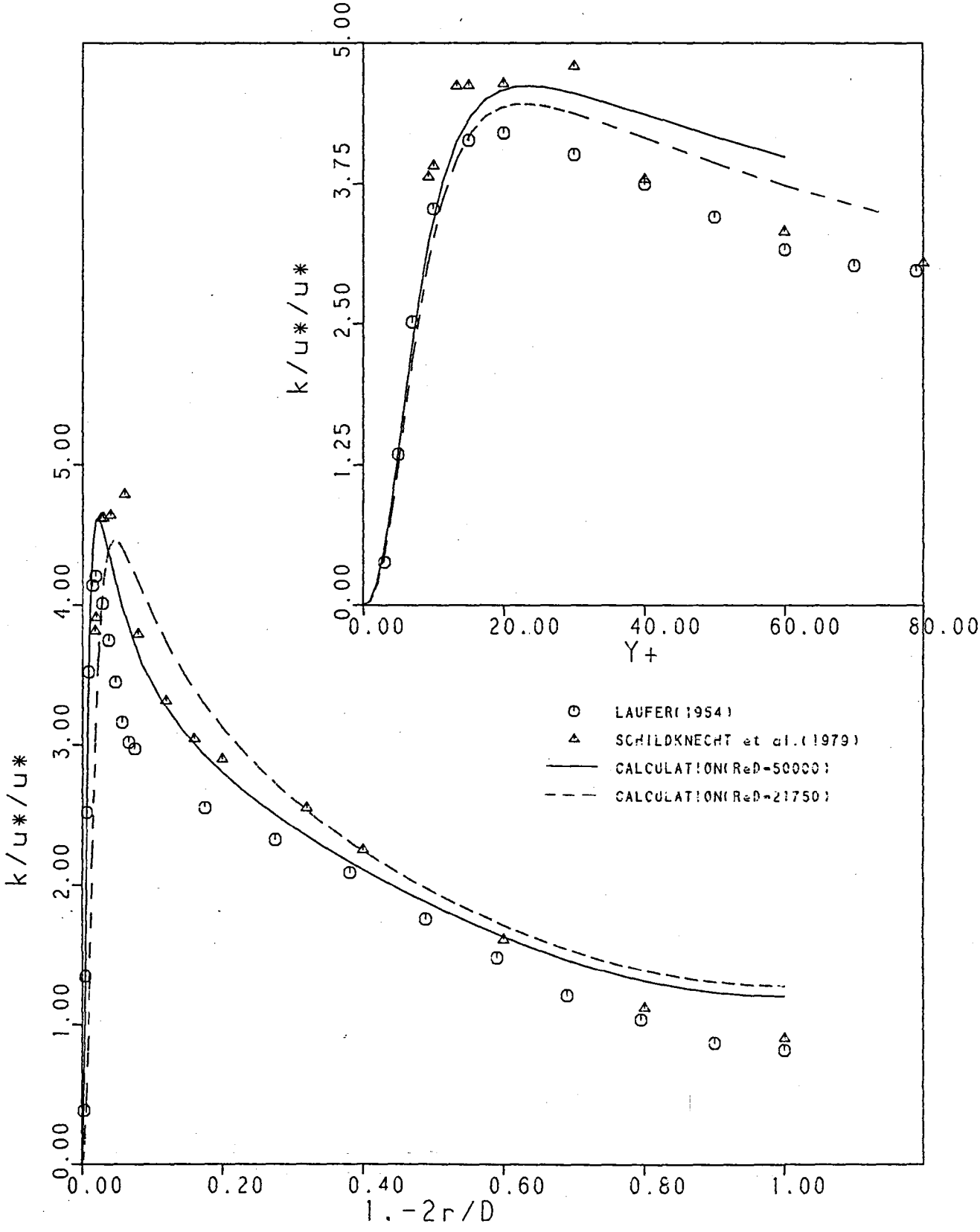
k/u*/u*
1.-2r/D
0.00
0.20
0.40
0.60
0.80
1.00
1.00
2.00
3.00
4.00
5.00
LAUFER(1954)
SCHILDKNECHT et al.(1979)
CALCULATION(ReD=50000)
CALCULATION(ReD=21750)
k/u*/u*
Y+
0.00
20.00
40.00
60.00
80.00
1.25
2.50
3.75
5.00

Figure 11d.

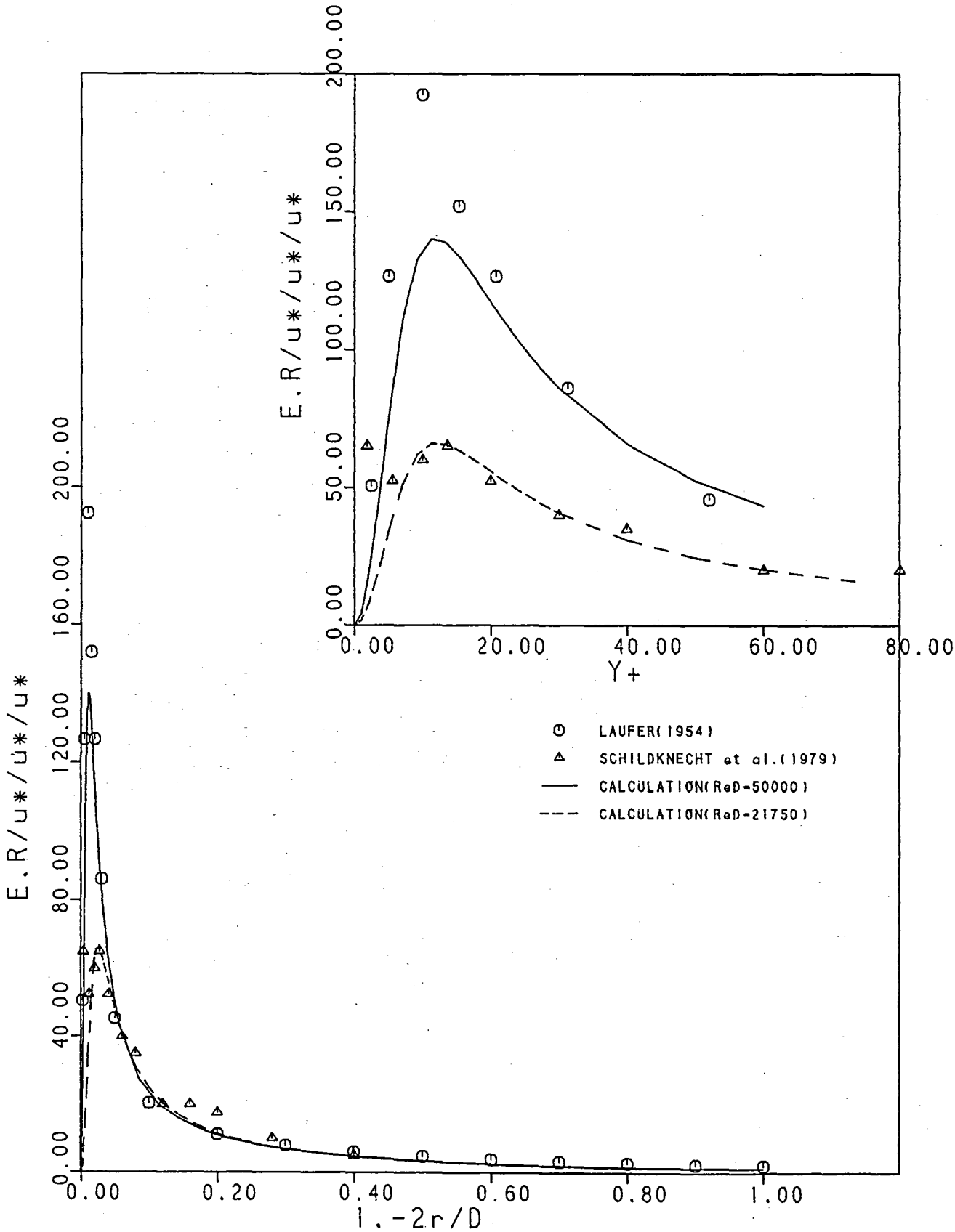
E.R/u*/u*/u*
1.-2r/D
0.00
40.00
80.00
120.00
160.00
200.00
0.00
0.20
0.40
0.60
0.80
1.00
E.R/u*/u*
Y+
0.00
50.00
100.00
150.00
200.00
0.00
20.00
40.00
60.00
80.00
LAUFER(1954)
SCHILDKNECHT et al.(1979)
CALCULATION(ReD=50000)
CALCULATION(ReD=21750)

Figure 11e.

1. Report No.	2. Government Accession No.	3. Recipient's Catalog No.
NASA CR-3994		

4. Title and Subtitle	5. Report Date
On the Modeling of Low-Reynolds-Number Turbulence	July 1986
	6. Performing Organization Code

7. Author(s)	8. Performing Organization Report No.
Ronald M.C. So and G.J. Yoo	CR-R85033
	10. Work Unit No.

9. Performing Organization Name and Address	11. Contract or Grant No.
Arizona State University Mechanical and Aerospace Engineering Tempe, Arizona 85287	NAG3-167
	13. Type of Report and Period Covered
12. Sponsoring Agency Name and Address	Contractor Report
National Aeronautics and Space Administration Washington, D.C. 20546 and Defense Advanced Research Project Agency Arlington, Virginia 22209	14. Sponsoring Agency Code 505-32-32 (E-3059)

15. Supplementary Notes

Final report. Project Manager, James D. Holdeman, Internal Fluid Mechanics Division, NASA Lewis Research Center, Cleveland, Ohio 44135. Work partially funded by DARPA Contracting Agency, Naval Weapons Center, China Lake, California 93555 under Contract No. NG0530-85-C-0191.

16. Abstract

A full Reynolds-stress closure that is capable of describing the flow all the way to the wall has been formulated for turbulent flow through circular pipes. Since viscosity does not appear explicitly in the pressure redistribution terms, conventional high-Reynolds-number models for these terms are found to be applicable. However, the models for turbulent diffusion and viscous dissipation have to be modified to account for viscous diffusion near a wall. Thus modified, viscous dissipation in the flow is no longer isotropic as postulated by Kolmogorov. Two redistribution and two diffusion models are investigated for their effects on the model calculations. Wall correction to pressure redistribution modeling is also examined. Diffusion effects on calculated turbulent properties are further investigated by simplifying the transport equations to algebraic equations for the Reynolds stresses. Two approximations are explored. These are the equilibrium and nonequilibrium turbulence assumptions. Finally, the two-equation closure is also used to calculate the flow in question and the results compared with all the other model calculations. Fully developed pipe flows at two moderate Reynolds numbers are used to validate these model calculations. The calculations show that all closure models give good agreement with measurements of mean velocity, shear stress, turbulent kinetic energy and dissipation rate near a wall. However, the slope of the logarithmic law-of-the-wall recovered from these calculations varies from one closure model to another. Wall correction is found to have little effect on the model calculations. Mean-strain effects on redistribution modeling are found to give rise to an adverse influence on the calculated log-law in the case of nonequilibrium algebraic stress closure. All closure models examined fail to predict the steep rise of turbulence intensities near a wall correctly. Also, they fail to reproduce the isotropic behavior of the normal stresses at the pipe center. Overall, the best model prediction is given by the full Reynolds-stress closure incorporating a nonisotropic gradient diffusion model and the Launder et al. model for pressure redistribution.

17. Key Words (Suggested by Author(s))	18. Distribution Statement
Low-Reynolds-number turbulence Turbulence flow modeling Reynolds-stress closure Algebraic stress closure	Unclassified - unlimited STAR Category 07

19. Security Classif. (of this report)	20. Security Classif. (of this page)	21. No. of pages	22. Price*
Unclassified	Unclassified	141	A07

*For sale by the National Technical Information Service, Springfield, Virginia 22161 NASA-Langley, 1986

End of Document